

**Understanding the RNA-recognition mechanism of
dsRBDs using TAR-RNA Binding Protein (TRBP) as a
model system**

विद्या वाचस्पति की

उपाधि की अपेक्षाओं की आंशिक पूर्ति में प्रस्तुत शोध प्रबंध

A Thesis

Submitted in Partial Fulfillment of Requirements for the Award of Degree of
Doctor of Philosophy

द्वारा / By

फ़िरदौसी परवेज़ / *Firdousi Parvez*

पंजीकरण सं. / Registration No.: २०१७३५१९/ 20173519

शोध प्रबंध पर्यवेक्षक / Thesis Supervisor:

डॉ. जितेन्द्र चुघ / Dr. Jeetender Chugh



भारतीय विज्ञान शिक्षा एवं अनुसंधान संस्थान पुणे

Indian Institute of Science, Education, and Research, Pune

२०२३ / 2023

Dedications...

*My doctoral thesis is dedicated in the loving memory of
my beloved father, **Sk. Pieruddin.***

CERTIFICATE

Certified that the work incorporated in the thesis entitled “Understanding the RNA-recognition mechanism of dsRBDs using TAR-RNA Binding Protein (TRBP) as a model system” submitted by Ms. Firdousi Parvez was carried out by the candidate, under my supervision. The work presented here or any part of it has not been included in any other thesis submitted previously for the award of any degree or diploma from any other University or institution.

Date: 29/08/2023


(Supervisor)

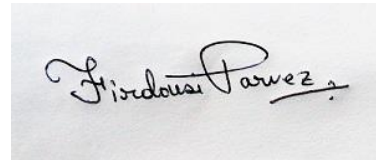
Dr. Jeetender Chugh

DECLARATION

I declare that this written submission represents my idea in my own words and where others' ideas have been included; I have adequately cited and referenced the original sources. I also declare that I have adhered to all principles of academic honesty and integrity and have not misrepresented or fabricated or falsified any idea/data/fact/source in my submission. I understand that violation of the above will be cause for disciplinary action by the Institute and can also evoke penal action from the sources which have thus not been properly cited or from whom proper permission has not been taken when needed.

Place: **Pune**

Date: 29/08/2023

A photograph of a handwritten signature in black ink on a light-colored background. The signature is written in a cursive style and reads "Firdousi Parvez".

Ms. Firdousi Parvez

Acknowledgements

“..... Sometimes I think you believe in me more than I do,” said the boy

“You'll catch up,” said the horse.....”

(A quote from the book The Boy, the Mole, the Fox and the Horse by Charlie Mackesy)

I would like to express my heartfelt gratitude towards my Ph.D. supervisor, Dr. Jeetender Chugh, for his invaluable, incomparable and tremendous support during my Ph.D. journey. He has been an excellent mentor in every way possible and has always pushed me towards excellence and perfection. I will forever be in debt to him for his unwavering trust, motivation, patience, enthusiasm, and guidance. He has been a real inspiration to me. I would also take this opportunity to extend my deepest gratitude towards Dr. Shilpy Sharma, my mentor since my master degree. She has guided me thoroughly and never missed an opportunity to encourage and inspire me through my journey with her. She has given her extremely valuable time and inputs in forming this thesis. She has not only been a guide but also a source of enormous strength to me. The above quote is dedicated to both of them for always believing in me.

I would also like to thank my Research Advisory Committee (RAC) members: Prof. R. V. Hosur, Prof. M. S. Madhusudhan and Dr. Janesh Kumar for tracking the progress of my research over the years and providing valuable insights, suggestions and fruitful discussions during all meetings.

I am thankful to N.L. Prof. Jennifer Doudna (University of California, Berkeley) for providing TRBP plasmid constructs as gift. I would also like to acknowledge IISER-Pune for all the research facilities. This work would not have been complete without generous support by the NMR facility at IISER-Pune (co-funded by DST-FIST and IISER Pune) for access to the 600

MHz NMR spectrometer, NMR facility at IIT-Bombay for access to the 750 MHz NMR spectrometer, and NMR facility at TIFR Bombay for access to the 800 MHz NMR spectrometer. I must also extend my gratitude towards Dr. Radha Chauhan, Ms. Sangeeta Niranjana, and Ms. Jyotsana for the help with measurement and analysis of the SEC-MALS data at NCCS, Pune. I would also like to acknowledge Prof. Gianluigi Veglia (University of Minnesota, Minnesota) and Dr. Fa-An Chao (National Cancer Institute, Maryland) for the active discussions while setting up HARD experiments and data analysis. I also thank DBT India, Govt. of India (Delhi) for providing me fellowship.

I am also thankful to Nitin and Sandeep for maintaining the NMR facility. I am also grateful to Mr. Sachin Kate and Mr. Raghav (Bruker Biospin) for quick support to resolve all technical issues with the NMR spectrometers.

I am grateful to all the past and present members JC lab (Harshad, Santosh, Saleem, Sarita, Guneet, Samrat, Osama, Nikhil, Soumya, Zainab, Ipsita, and many more) for their valuable contribution to my Ph.D. journey. A big thanks to Osama, Nikhil, Ipsita and Soumya for giving their valuable time and energy in helping me with my thesis. You all have been a big loving and caring family away from home. I would miss the lab dearly. A big thank you to my entire Biology & Mathematics batchmates in IISER. My experience at IISER would have not been complete without all of you people. I would specially like to thank Saikat, Rajeshwari, Dilsha, Sandra, Prachi and Mayuresh for being there for me through the thick and thins of my life. A special mention to two of my closest friends Nazia and Ila. I feel extremely lucky to have you guys in my life. You are my strength. I would have been lost without you people.

Lastly and most importantly, my deepest gratitude goes to parents and my sister for their unflagging love, patience and support throughout my life. Their

encouragement and support gave me the strength, dedication, and perseverance to complete my Ph.D. program. Many many thanks for being there always. Everything is meaningless without you people.

Please accept my sincere apology to anyone I have missed an opportunity to acknowledge here.

Thank you,

Firdousi Parvez.

Abbreviations

°C	degree celsius
Å	angstrom
aa	amino acid
ATP	Adenosine triphosphate
BMRB	Biological Magnetic Resonance Bank
bp	base-pair
BSA	Bovine Serum Albumin
cal; kcal	Calorie; kilocalorie
CARA	Computer Aided Resonance Assignment
CPMG	Carr-Purcell-Meiboom-Gill
CSA	Chemical Shift Anisotropy
CSP	Chemical Shift Perturbation
D ₂ O	Deuterium oxide
DGCR8	Di-George syndrome Critical Region 8
DNA	Deoxy-ribonucleic acid
dsRBD	Double-stranded RNA-Binding Domain
dsRNA	Double-stranded RNA
DTT	Dithiothreitol
EDTA	Ethylene diamine tetraacetic acid
HARD	Heteronuclear Adiabatic Relaxation dispersion
h	Hour
HS	Hyperbolic Secant
HSQC	Heteronuclear Single Quantum Coherence
Hz; kHz; MHz	Hertz; kilo-Hertz; mega-Hertz
IPTG	Isopropyl-β-D-1-thiogalactopyranoside
ITC	Isothermal Titration Calorimetry
K	Kelvin
kDa	Kilo-Dalton
M; mM; μM	Mole; milli-mole; micro-mole
MALS	Multi-Angle Light Scattering
MBP	Maltose Binding Protein

miRNA/miR	microRNA
ml; μ l	Milli-liter, micro-liter
NaCl	Sodium chloride
NDB	Nucleic acid Data Bank
nm	nano-meter
NMR	Nuclear Magnetic Resonance
NOE	Nuclear Overhauser Effect
nt	nucleotide
OD	Optical Density
PDB	Protein Data Bank
PKR	Protein kinase R
ppm	Parts per million
RD	Relaxation Dispersion
RISC	RNA Induced Silencing Complex
RMSD	Root-Mean-Square-Deviation
RNA	Ribonucleic acid
RNAi	RNA interference
s; ms; μ s; ps; ns	Second; milli-second; micro-second; pico-second; nano-second
SDS-PAGE	Sodium dodecyl sulfate - Polyacryl Amide Gel Electrophoresis
SEC	Size Exclusion Chromatography
siRNA	Small interfering RNA
TEV	Tobacco Etch Virus
TOCSY	Total correlation Spectroscopy
TRBP	Trans Activation Response RNA Binding Protein
TSP	Total Soluble Protein

Synopsis

Understanding the RNA-recognition mechanism of dsRNA binding domains (dsRBDs)

using TAR RNA binding protein (TRBP) as a model system.

Name: Ms. Firdousi Parvez

Registration No.: 20173519

Thesis Supervisor: Dr. Jeetender Chugh

Department: Department of Biology, IISER Pune

Abstract

TAR RNA binding protein (TRBP) has been known for its involvement in the RNA interference (RNAi) pathway. TRBP aids the Dicer-mediated pre-miRNA cleavage and the recruitment of the RISC complex. While doing so, TRBP binds to various pre-miRNAs and siRNAs having differences in sequence, structure, or both. We proposed that TRBP dynamically adapts to accommodate such diverse RNA structures. Thus, it becomes imperative to understand how intrinsic protein dynamics plays a role in RNA recognition and binding. Previously, we have established the role of intrinsic and RNA-induced conformational exchange in the dsRBD1 of TRBP in shape-dependent RNA recognition. Building further on this, the current study delves into the intrinsic and RNA-induced conformational dynamics of the dsRBD2 of TRBP, juxtaposed with dsRBD1. Remarkably, dsRBD2 exhibits a higher binding affinity to a 12 bp long dsRNA when compared with dsRBD1, which could be attributed to the presence of residues critical to RNA binding and structural plasticity in dsRBD2. Utilizing state-of-the-art NMR spin relaxation and relaxation dispersion experiments, we report that dsRBD2 depicts constrained conformational plasticity when compared to

dsRBD1, as evidenced by the fast (ps-ns) and slower (μ s-ms) conformational dynamics measurements. Although, in the presence of RNA, dsRBD2 undergoes induced conformational exchange within the designated RNA-binding regions and the other residues, the amplitude of the motions remains modest when compared to those observed in dsRBD1. The culmination of our findings leads us to propose a dynamics-driven model of the two tandem domains of TRBP, substantiating their contributions to the versatility of dsRNA recognition and binding.

Chapter 1: Introduction

RNA-binding proteins (RBPs) play a pivotal role in a wide spectrum of RNA biology, including folding, splicing, processing, transport, and localization (Wilkinson & Shyu, 2001; Fu et al., 2016; Dreyfuss et al., 2002; Jiang & Baltimore, 2016; Kim et al., 2009). The RNA-recognition mechanism of these proteins has been studied only recently, and it does not seem to follow a particular rule (Chen & Varani, 2005). A more comprehensive investigation into the RNA-recognition mechanism is still lacking, impeding our capacity to comprehend and manipulate these RNA-binding proteins for the benefit of mankind. There are various RNA-binding domains (RBDs) present in these RBPs. The double-stranded RNA-binding motif/domain (dsRBM/dsRBD) is vital for the dsRBPs (Chen & Varani, 2013; (Saunders & Barber, 2003). This domain is involved in double-stranded RNA (dsRNA)-recognition and binding. In humans, there are at least 30 known dsRBPs (Gleghorn & Maquat, 2014). They work synergistically with several dsRNAs in the cytoplasm to achieve vital bodily functions and maintain homeostasis.

dsRBDs are conserved, 65-68 amino acid long domains with a secondary structure motif of $\alpha\beta\beta\beta\alpha$, where the two α -helices forming a Y shape are packed against the antiparallel β -sheet formed by three β strands (St Johnston et al., 1992). Depending on the homology to the

consensus sequence, dsRBDs can be classified into type A (highly homologous to consensus) and type B (conserved C-terminal α -helix only) (Masliah et al., 2013; Krovat & Jantsch, 1996; Fierro-Monti & Mathews, 2000; St Johnston et al., 1992). dsRBDs across different as well as the same proteins show a lot of variation in terms of binding affinity, stoichiometry, register length of RNA, diffusion ability, dynamics, etc., when it comes to the interaction with the target dsRNAs. They are also known to diffuse/slide over the length of the RNA to achieve the vital function of the complex. It is intriguing to notice that the two type-A dsRBDs originating from the same protein demonstrate a markedly different binding affinity for a variety of target RNAs (Benoit et al., 2013; Yamashita et al., 2011; Daviet et al., 2000). Recent investigations have suggested that the dissimilar behavior of dsRBDs in Dicer (Wostenberg et al., 2012), PKR (Nanduri et al., 2000), and double-stranded-RNA-binding protein 4 (DRB4) (Chiliveri et al., 2017) might be attributed to protein dynamics. We have recently demonstrated the role of dsRBD dynamics in dsRBD-dsRNA interactions using dsRBD1 of human TRBP2 that dsRBD tends to adopt a conformationally dynamic structure (Paithankar et al., 2022).

This thesis has been divided in six chapters, where chapter 1 gives a comprehensive introduction to the world of dsRBDs, followed by a literature summary of category of dsRBDs, canonical fold and interactions of dsRBD with dsRNA, versatility of dsRBD-dsRNA interactions, and lastly a brief introduction of the model dsRBD used in this study. The chapter 2 details the methods used in this thesis along with a brief theory of working of various techniques used. The primary, secondary, and tertiary structure of TRBP2-dsRBD2 has been characterized and then compared with dsRBD1 in Chapter 3. The RNA-binding activity of dsRBD2 has been identified using topologically different dsRNAs using NMR-based titrations. Next, the two binding affinities of the two A-type dsRBDs of TRBP2 with a duplex RNA were compared using an Isothermal Titration Calorimetry-based study in Chapter 4. The motions in the TRBP2-dsRBD2 at ps-ns and μ s-ms timescale dynamics have been measured by nuclear

spin relaxation experiments and relaxation dispersion experiments in apo-state and studied its perturbation in the presence of an A-form duplex RNA in Chapter 5. We have also compared the apo- and RNA-bound conformational dynamics measured in dsRBD2 with that of data measured on dsRBD1 previously. Using this approach, we have finally proposed that the differential binding affinity, protein dynamics, and its perturbation in the presence of RNA in the two dsRBDs enables them to recognize a variety of RNA substrates and diffusion along the length of the RNA in Chapter 6. All the chapters have been individually referenced, and at the end all the measured NMR data has been added in the form of tables in Appendix.

Chapter 2. Methods and Materials

To understand the structure, dynamics and RNA-binding of TRBP2-dsRBD2, we have used various biophysical techniques like Size-exclusion chromatography coupled with Multi-Angle Light Scattering (SEC-MALS) detection, Isothermal Titration Calorimetry (ITC) and NMR spectroscopy. SEC-MALS gives us the molecular mass of the protein in solution. We used ITC to get information on the kinetics and thermodynamics of the protein with RNA. Further, we used solution-state NMR spectroscopy to obtain structure and dynamics of the proteins. Detailed information of the materials, experimental methods used in the study, and their theory have been described here.

Chapter 3. Characterization of TRBP2-dsRBD2 structure

Here, the results of various biophysical techniques were used to characterize TRBP2-dsRBD2 have been described. Both unlabeled- and labeled- TRBP2-dsRBD2 were successfully purified in good NMR-experiment measurable concentrations. SEC-MALS analysis suggested that the protein TRBP2-dsRBD2 was monomeric in nature with a molecular weight of 9.2 kDa. A total of 73 / 84 total residues could be successfully assigned using a series of double and triple resonance NMR experiments (^1H - ^{15}N TOCSY-HSQC, ^1H - ^{15}N NOESY-HSQC, HNC0,

HNCACO, HNCA, HNCOCA, HNN, CBCANH, and CBCA(CO)NH). The CS-ROSETTA structure was calculated from the chemical shifts obtained from the previously mentioned NMR experiments. The structure matched well with the structure reported earlier (2CPN). The comparison of the primary, secondary, and tertiary structure of the two dsRBDs of TRBP2 - dsRBD1 and dsRBD2 has also been described here.

Chapter 4. Characterization of dsRNA binding of TRBP2-dsRBD2

In this chapter, we have characterized the interaction of TRBP2-dsRBD2 with the same set of topologically different dsRNAs (miR-16-1 mutants) used for dsRBD1 through ^1H - ^{15}N HSQC-based NMR titrations in a previous study from our group (Paithankar et al., 2022). In addition to these, a short, perfect duplex A-form RNA (D12 RNA) was also used to investigate the effect of RNA length on TRBP2-dsRBD2 binding. Finally, an ITC experiment was performed with a 12 bp D12 RNA to compare the RNA-binding affinity (K_d) of the dsRBD1 and dsRBD2 of TRBP2 protein. In addition to this, NMR-based studies were carried out on TRBP2-dsRBD2, to measure the structural perturbations upon RNA binding. Line broadening was used to understand the effect of target RNA length in dsRBD-dsRNA interaction.

Chapter 5. Intrinsic and RNA-induced conformational dynamics of TRBP2-dsRBD2

In this chapter, the role of intrinsic protein dynamics in the differential RNA-binding of TRBP2 dsRBDs has been explored. To achieve this, we first deciphered the intrinsic protein dynamics of TRBP2-dsRBD2 at ps-ns (using spin relaxation experiments) and μs -ms timescale (using NMR relaxation dispersion experiments) and then compared it with TRBP2-dsRBD1 (Paithankar et al., 2022). An attempt has been made to gain further insights into the RNA-binding mechanism of TRBP2-dsRBD2, wherein protein dynamics have been probed in the presence of D12 RNA at various timescales. For ps-ns timescales dynamics, nuclear spin relaxation experiments (R_1 , R_2 , and $[^1\text{H}]\text{-}^{15}\text{N}$ -nOe) were recorded. Conformational exchange

processes in the timescale of 0.3-10 ms were studied by recording CPMG RD (Carr-Purcell-Meiboom-Gill relaxation dispersion) experiments. For 10 μ s–10 ms timescale measurements, HARD (heteronuclear adiabatic relaxation dispersion) NMR experiments were performed. The perturbation of conformational dynamics of TRBP2-dsRBD2 in the presence of RNA was then compared to dsRBD1 (Paithankar et al., 2022). During their interaction with the RNA, both dsRBDs experienced enhanced conformational changes on a fast timescale (picoseconds to nanoseconds) and a moderate timescale (microseconds to milliseconds), as observed through nuclear spin relaxation and rotating frame relaxation dispersion measurements. It was observed that dsRBD1 has remarkable flexibility and samples a larger number of conformational states, which allows it to recognize a wide range of structurally and sequentially diverse dsRNAs. On the other hand, dsRBD2 firmly adheres to the RNA ligand due to its conserved RNA-binding stretches and relatively high rigidity in the core domain.

Chapter 6: Conclusion

In this chapter, we conclude the study from the detailed insights obtained from Chapter 3-5, and proposed a model to describe the RNA-recognition mechanism of the two type-A dsRBDs in TRBP2 protein. We believe that dsRBD2, with rigid and conserved RNA-binding regions, binds tightly with the RNA, whereas dsRBD1, with high intrinsic conformational exchange in the RNA-binding regions, is able to recognize different RNA structures (often with bulges and internal loops). Following this, the two dsRBDs, upon contacting the RNA, undergo enhanced conformational exchange to different extents. This enhanced conformational exchange, coupled with a differential binding affinity towards dsRNA, might enable the tandem dsRBDs to move along the backbone of the RNA molecule, leading to the previously reported ATP-independent diffusion.

References

- Benoit, M. P. M. H., Imbert, L., Palencia, A., Pérard, J., Ebel, C., Boisbouvier, J., & Plevin, M. J. (2013). The RNA-binding region of human TRBP interacts with microRNA precursors through two independent domains. *Nucleic Acids Research*, *41*(7), 4241–4252. <https://doi.org/10.1093/nar/gkt086>
- Chen, Y., & Varani, G. (2005). Protein families and RNA recognition. *The FEBS Journal*, *272*(9), 2088–2097. <https://doi.org/10.1111/j.1742-4658.2005.04650.x>
- Chen, Y., & Varani, G. (2013). Engineering RNA-binding proteins for biology. *The FEBS Journal*, *280*(16), 3734–3754. <https://doi.org/10.1111/febs.12375>
- Chiliveri, S. C., Aute, R., Rai, U., & Deshmukh, M. V. (2017). DRB4 dsRBD1 drives dsRNA recognition in Arabidopsis thaliana tasi/siRNA pathway. *Nucleic Acids Research*, *45*(14), 8551–8563. <https://doi.org/10.1093/nar/gkx481>
- Daviet, L., Erard, M., Dorin, D., Duarte, M., Vaquero, C., & Gatignol, A. (2000). Analysis of a binding difference between the two dsRNA-binding domains in TRBP reveals the modular function of a KR-helix motif. *European Journal of Biochemistry*, *267*(8), 2419–2431. <https://doi.org/10.1046/j.1432-1327.2000.01256.x>
- Dreyfuss, G., Kim, V. N., & Kataoka, N. (2002). Messenger-RNA-binding proteins and the messages they carry. *Nature Reviews. Molecular Cell Biology*, *3*(3), 195–205. <https://doi.org/10.1038/nrm760>
- Fierro-Monti, I., & Mathews, M. B. (2000). Proteins binding to duplexed RNA: One motif, multiple functions. *Trends in Biochemical Sciences*, *25*(5), 241–246. [https://doi.org/10.1016/s0968-0004\(00\)01580-2](https://doi.org/10.1016/s0968-0004(00)01580-2)
- Fu, Y., Zhao, X., Li, Z., Wei, J., & Tian, Y. (2016). Splicing variants of ADAR2 and ADAR2-mediated RNA editing in glioma. *Oncology Letters*, *12*(2), 788–792. <https://doi.org/10.3892/ol.2016.4734>
- Gleghorn, M. L., & Maquat, L. E. (2014). “Black sheep” that don’t leave the double-stranded RNA-binding domain fold. *Trends in Biochemical Sciences*, *39*(7), 328–340. <https://doi.org/10.1016/j.tibs.2014.05.003>

- Jiang, S., & Baltimore, D. (2016). RNA-binding protein Lin28 in cancer and immunity. *Cancer Letters*, 375(1), 108–113. <https://doi.org/10.1016/j.canlet.2016.02.050>
- Kim, V. N., Han, J., & Siomi, M. C. (2009). Biogenesis of small RNAs in animals. *Nature Reviews. Molecular Cell Biology*, 10(2), 126–139. <https://doi.org/10.1038/nrm2632>
- Krovat, B. C., & Jantsch, M. F. (1996). Comparative mutational analysis of the double-stranded RNA binding domains of *Xenopus laevis* RNA-binding protein A. *The Journal of Biological Chemistry*, 271(45), 28112–28119. <https://doi.org/10.1074/jbc.271.45.28112>
- Masliyah, G., Barraud, P., & Allain, F. H.-T. (2013). RNA recognition by double-stranded RNA binding domains: A matter of shape and sequence. *Cellular and Molecular Life Sciences: CMLS*, 70(11), 1875–1895. <https://doi.org/10.1007/s00018-012-1119-x>
- Nanduri, S., Rahman, F., Williams, B. R., & Qin, J. (2000). A dynamically tuned double-stranded RNA binding mechanism for the activation of antiviral kinase PKR. *The EMBO Journal*, 19(20), 5567–5574. <https://doi.org/10.1093/emboj/19.20.5567>
- Paithankar, H., Tarang, G. S., Parvez, F., Marathe, A., Joshi, M., & Chugh, J. (2022). Inherent conformational plasticity in dsRBDs enables interaction with topologically distinct RNAs. *Biophysical Journal*, 121(6), 1038–1055. <https://doi.org/10.1016/j.bpj.2022.02.005>
- Saunders, L. R., & Barber, G. N. (2003). The dsRNA binding protein family: Critical roles, diverse cellular functions. *FASEB Journal: Official Publication of the Federation of American Societies for Experimental Biology*, 17(9), 961–983. <https://doi.org/10.1096/fj.02-0958rev>
- St Johnston, D., Brown, N. H., Gall, J. G., & Jantsch, M. (1992). A conserved double-stranded RNA-binding domain. *Proceedings of the National Academy of Sciences of the United States of America*, 89(22), 10979–10983. <https://doi.org/10.1073/pnas.89.22.10979>
- Wilkinson, M. F., & Shyu, A. B. (2001). Multifunctional regulatory proteins that control gene expression in both the nucleus and the cytoplasm. *BioEssays: News and Reviews in Molecular, Cellular and Developmental Biology*, 23(9), 775–787. <https://doi.org/10.1002/bies.1113>
- Wostenberg, C., Lary, J. W., Sahu, D., Acevedo, R., Quarles, K. A., Cole, J. L., & Showalter, S. A. (2012). The role of human Dicer-dsRBD in processing small regulatory RNAs. *PloS One*, 7(12), e51829. <https://doi.org/10.1371/journal.pone.0051829>

Yamashita, S., Nagata, T., Kawazoe, M., Takemoto, C., Kigawa, T., Güntert, P., Kobayashi, N., Terada, T., Shirouzu, M., Wakiyama, M., Muto, Y., & Yokoyama, S. (2011). Structures of the first and second double-stranded RNA-binding domains of human TAR RNA-binding protein. *Protein Science: A Publication of the Protein Society*, 20(1), 118–130. <https://doi.org/10.1002/pro.543>

List of publications

1. Paithankar, H.*, Tarang, G. S.*, **Parvez, F.***, Marathe, A., Joshi, M., & Chugh, J. (2022). Inherent conformational plasticity in dsRBDs enables interaction with topologically distinct RNAs. *Biophysical Journal*, 121(6), 1038–1055. <https://doi.org/10.1016/j.bpj.2022.02.005> (*Authors contributed equally)
2. **Parvez, F.**, Sangpal, D., Paithankar, H., Amin, Z., & Chugh, J. (2023). Differential conformational dynamics in two type-A RNA-binding domains drive the double-stranded RNA recognition and binding [Preprint]. BioRxiv. <https://doi.org/10.1101/2023.08.06.552166>

Table of Contents

Declarations	iv
Acknowledgements	v
Abbreviations	viii
Synopsis	x
List of publications	xx
Chapter 1: Introduction	I
1.1. RNA-binding proteins (RBPs)	2
1.2. Classification of different RNA-binding domains (RBDs)	3
1.3. dsRNA-binding Proteins (dsRBPs)	5
1.4. dsRNA-binding domain (dsRBD)	5
1.5. A broad classification of dsRBDs (Type A & B)	9
1.6. Versatility of dsRBD-dsRNA interaction	11
1.7. The RNA interference pathway (RNAi pathway)	17
1.8. The TAR RNA-binding Protein (TRBP)	20
1.9. Scope of the Thesis	22
References	23
Chapter 2: Materials and Methods	33
2.1. Media, reagents, and buffers	34
2.2. Methodology	41
2.2.1. Competent Cell Preparation	41
2.2.2. Transformation of competent cells	42
2.2.3. TEV Protein overexpression and purification	42
2.2.4. TRBP2-dsRBD2 overexpression and purification	43
2.2.5. Design and preparation of RNA	45
2.2.6. Size-Exclusion Chromatography – Multiple Angle Light Scattering	48
2.2.7. Isothermal titration calorimetric binding assays	48
2.2.8. NMR Spectroscopy Data Collection	52
2.2.8.1 Theory	52
2.2.8.1.1. NMR Spectroscopy	52
2.2.8.1.2. 2D Nuclear magnetic resonance spectroscopy	54
2.2.8.1.3. 3D Nuclear magnetic resonance spectroscopy	55
2.2.8.1.4. NMR relaxation experiments	56
2.2.8.1.5. ps-ns dynamics in proteins probed by Nuclear Spin Relaxation experiments	57
2.2.8.1.6. μ s-ms dynamics by Relaxation Dispersion (RD) experiments	59

2.2.8.2. <i>Experimental Data Collection</i>	61
2.2.9. <i>NMR Relaxation Data Analysis</i>	64
2.2.10. <i>Backbone Assignment and Structure Calculation</i>	66
<i>Reference</i>	68
Chapter 3: <i>Characterization of TRBP2-dsRBD2 structure</i>	76
<i>Introduction</i>	77
<i>Results and Discussion</i>	78
3.1. <i>Purification of TEV protease</i>	78
3.2. <i>Purification of TRBP2-dsRBD2</i>	78
3.3. <i>Estimation of molecular mass of TRBP2-dsRBD2</i>	80
3.4. <i>Backbone resonance assignment of TRBP2-dsRBD2</i>	81
3.5. <i>CS-ROSETTA calculated structure of TRBP2-dsRBD2</i>	85
3.6. <i>Structure of TRBP2-dsRBD2 using POKY Structure Builder</i>	89
<i>Summary</i>	91
<i>References</i>	93
Chapter 4: <i>Characterization of dsRNA binding of TRBP2-dsRBD2</i>	98
<i>Introduction</i>	99
<i>Results and Discussion</i>	99
4.1. <i>NMR-based study of the interaction of TRBP2-dsRBD2 with topologically different dsRNAs</i>	99
4.2. <i>ITC-based study with D12 RNA</i>	107
<i>Summary</i>	109
<i>References</i>	110
Chapter 5: <i>Intrinsic and RNA- induced Conformational dynamics of TRBP2-dsRBD2</i>	113
<i>Introduction</i>	114
<i>Results and Discussion</i>	115
5.1. <i>Intrinsic protein dynamics at ps-ns timescales using nuclear relaxation measurements</i>	115
5.2. <i>Intrinsic protein dynamics at slower ms timescale using CPMG relaxation dispersion measurements</i>	122
5.3. <i>Intrinsic protein dynamics at 10 μs–10 ms timescale using heteronuclear adiabatic relaxation dispersion measurements</i>	123
5.4. <i>Protein Conformational dynamics perturbations of in TRBP2-dsRBD2 at ps-ns timescales in the presence of RNA ligand</i>	127
5.5. <i>Protein dynamics at slower ms timescale (0.3-10 ms) using CPMG relaxation dispersion measurements in presence of RNA</i>	130

5.6. Protein dynamics at the 10 μ s–10 ms timescale using HARD relaxation dispersion measurements	131
5.7. Perturbation of 10 μ s–10 ms timescale protein dynamics in presence of RNA of TRBP2-dsRBD2	133
Summary	135
References	136
Chapter 6: Conclusions	139
Appendix I: Supporting Tables	144
Appendix II: Assignment Report of TRBP2-dsRBD2	174

Chapter 1

Introduction

1.1. RNA-binding proteins (RBPs)

RNA-binding proteins (RBPs) play a crucial role in several aspects of RNA biology, including folding, splicing, processing, transport, and localization (Dreyfuss, Kim, & Kataoka, 2002; Fu, Zhao, Li, Wei, & Tian, 2016; Jiang & Baltimore, 2016; V. N. Kim, Han, & Siomi, 2009; Wilkinson & Shyu, 2001) (Figure 1.1). With the recent advancements in biophysical techniques, including X-ray crystallography, NMR spectroscopy, and Cryo-Electron Microscopy, an enormous number of protein structures have been solved. The first structure of an RBP to be determined was that of U1A complexed with stem-loop II of U1 snRNA in 1994 by Nagai *et al.* (Oubridge, Ito, Evans, Teo, & Nagai, 1994). This RNA-recognition motif (RRM) of U1A was used to enhance the crystallization and determination of different RNAs (Ferre-D'Amare & Doudna, 2000) and RNA-protein complex (Ferre-D'Amare & Doudna, 2000) structures. Hence, a new gate was opened to the field of RNA-centric research. However, out of ~2,08,844 total PDB structures ([rcsb.org](https://www.rcsb.org)) (Berman et al., 2000), there are only 3197 RNA-protein complex structures (as of August 2023) available in the literature. This indicates that a lot of information regarding RNA recognition still remains unexplored. The mode of RNA recognition has been studied only in the last 3 decades, and it does not seem to follow a single-thumb rule (Chen & Varani, 2005). To gain further insights into the process by which RBPs function and modify the process, it is crucial to have an extensive knowledge base of the RNA-recognition and binding mechanism of various RBPs.

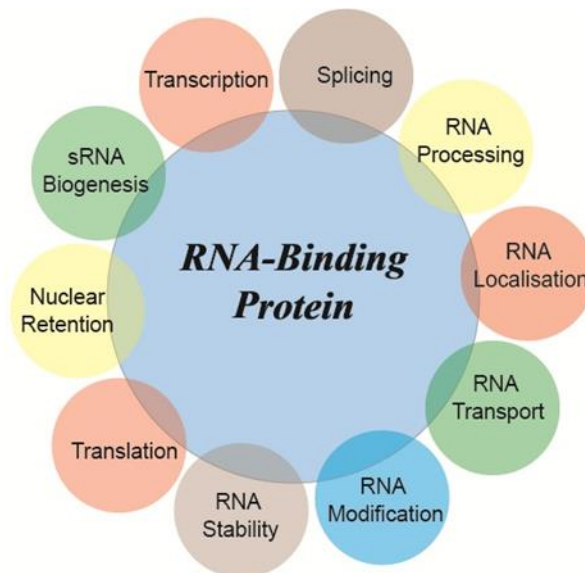


Figure 1.1: The crucial functions of RNA-binding proteins (RBPs) in a cell.

1.2. Classification of different RNA-binding domains (RBDs)

The RBPs can be broadly classified into single-stranded RNA-binding proteins (ssRBPs) and double-stranded RNA-binding proteins (dsRBPs). ssRBPs are generally sequence-specific as the interaction points include exposed nucleobases (Auweter et al., 2006; Daubner, Clery, & Allain, 2013), while dsRBPs tend to target a particular structural fold, especially the A-form RNA duplex via phosphate backbone and sugar hydroxyl protons (Masliah, Barraud, & Allain, 2013). dsRBPs interact with highly structured dsRNAs via their double-stranded RNA-binding motifs/domains (dsRBM/dsRBD). RBPs have a modular structure composed of multiple repetitive domains, giving rise to versatile RNA-binding surfaces. There are various RBDs like the RNA-recognition motif (RRM), the Pumilio/fem-3-binding binding factor (PUF) repeat domains, the hnRNP K homology (KH) domain, the zinc-finger domain, and the dsRBM/dsRBD (Table 1.2) (Chen & Varani, 2013; Kolb, Nail, & Gunderson, 1975). Out of these, the last two domains are involved in dsRNA-recognition and binding (Chen & Varani, 2013; Saunders & Barber, 2003). In the current study, we will focus on the dsRNA binding domain (dsRBD).

Table 1.2: A summary of different RNA-binding motifs targeting various RNA structures. Re-drawn from (Chen & Varani, 2013).

Domain	Amino acid length	Secondary structure Topology	Recognition code	Protein engineering attempts	ssRNA	dsRNA	Stem-loop ^a	Tertiary folded RNA
RRM	80-90	$\beta\alpha\beta\alpha\beta$	No	Yes	PABP (1CVJ) Fox-1(2ERR)		U1A(1URN)	
PUF	36	α -helix	Yes	Yes	Pumilio(1M8Y)			
KH	~ 70	$\beta\alpha\beta\beta\alpha$ $\alpha\beta\beta\alpha\beta$	No	No	Nova-1(1EC6)			
ZF	~30	$\beta\beta\alpha$	No	Yes	TIS11d (1RGO) ZRANB2 (3G9Y)	TIIIA-ZF5 (1UN6) DMATase (3EPH)	HIV-1 NC (1A1T) ^b	TIIIA (1UN6)
dsRBD	~ 65-75	$\alpha\beta\beta\beta\alpha$	No	No		RBP-A (1DI2) RNaseIII (2EZ6)		
Antibodies	~ 215	β -pleated sheet	No	Yes				Fab (2R8S)

^aThe loop, bulge and internal loop regions of the stem-loop may be recognized as ssRNAs in some cases, depending on the dynamics of the local RNA structure. ^bZF domains may recognize both the loop and the phosphate backbone of double-stranded regions of a stem-loop RNA.

1.3. dsRNA-binding Proteins (dsRBPs)

The dsRNA-binding proteins (dsRBPs) consist of an ever-growing family of eukaryotic, prokaryotic, and viral-origin proteins with a characteristic evolutionarily conserved domain, i.e., the dsRBD. dsRBPs have been reported to perform a diverse range of critically important functions in the cell (Fierro-Monti & Mathews, 2000; Saunders & Barber, 2003; Stefl, Skrisovska, & Allain, 2005). For example, the dsRNA-dependent protein kinase (PKR) plays a vital role in dsRNA signaling and host defense against viral infections (Balachandran et al., 2000; Barber, 2001; Dauber & Wolff, 2009). DICER protein helps in mediating gene regulation in RNA interference (RNAi) (Kurzynska-Kokorniak et al., 2015; Reis, Hart-Smith, Eamens, Wilkins, & Waterhouse, 2015; Vergani-Junior, Tonon-da-Silva, Inan, & Mori, 2021). Staufen is an adenosine deaminase acting on RNA (ADAR) that helps in RNA modification (Ren, Veksler-Lublinsky, Morrissey, & Ambros, 2016; Saunders & Barber, 2003). Spermatid Perinuclear RNA-binding protein (SPNR) plays an important role in cell development, protein translation, and RNA-editing (Saunders & Barber, 2003; Schumacher, Lee, Edelhoff, & Braun, 1995). Any disruption in the expression of these proteins leads to various developmental disorders, cancer, embryonic lethality, etc. This implies that the recognition and interaction of dsRNAs with dsRBPs are vital for the normal function in any organism. In humans, at least 30 known proteins harbour a dsRBD (Gleghorn & Maquat, 2014). These human dsRBPs work synergistically with several dsRNAs in the cytoplasm to achieve vital bodily functions and maintain homeostasis.

1.4. dsRNA-binding domain (dsRBD)

A double-stranded RNA-binding domain (dsRBD) exclusively binds double-stranded RNA. dsRBDs are generally 65-68 amino acid long domains (St Johnston, Brown, Gall, & Jantsch, 1992) that contain a highly conserved secondary structure motif ($\alpha\beta\beta\alpha$), where the two α -helices (forming a Y shape) are packed against an antiparallel β -sheet formed by three β strands (Figure 1.4.1) (Bycroft, Grunert, Murzin, Proctor, & St Johnston, 1995; Kharrat, Macias, Gibson, Nilges, & Pastore, 1995). There are 73 reported PDB structures of dsRBDs in apo-form or RNA/protein

complex listed with the accession number SM00358 in the Simple Molecular Architecture Research Tool (SMART) (smart.embl.de).

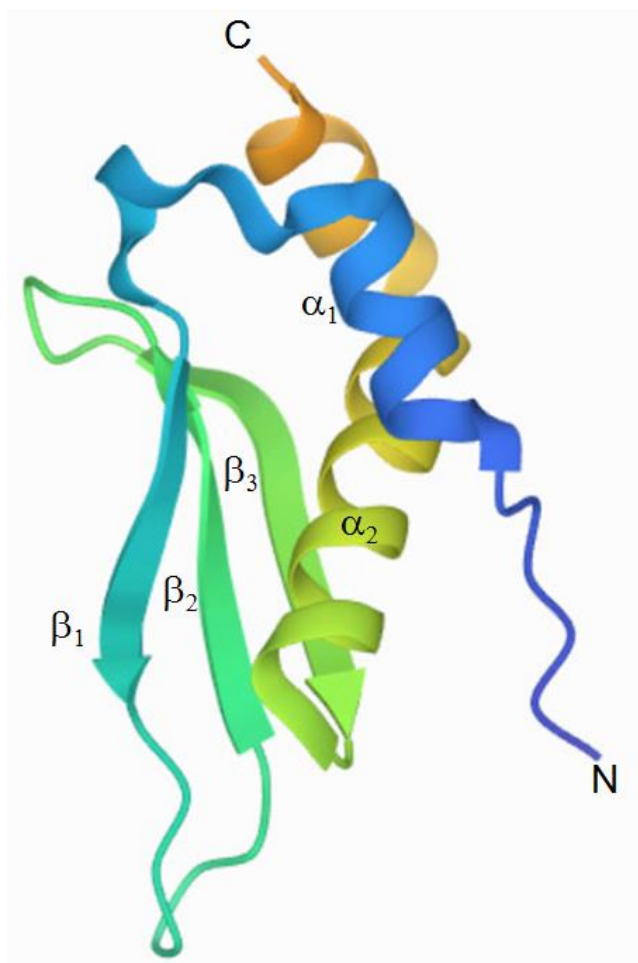


Figure 1.4.1: The conserved dsRBD structural motif ($\alpha\beta\beta\beta$). Representative structure of yeast RNase III (Rnt1p) dsRBD (PDB ID: 1T4O). Adapted from (Leulliot et al., 2004).

All the dsRBDs have three common RNA-binding regions: (1) the middle of helix α_1 (E residue), (2) the N-terminal residues of helix α_2 (KKxAK motif), and (3) the loop between β_1 and β_2 strands (GPxH motif), that form a canonical RNA-binding surface which interacts with the consecutive minor, major, and minor grooves of a dsRNA (Masliah et al., 2013; Tian, Bevilacqua, Diegelman-Parente, & Mathews, 2004). Non-sequence specific interactions of a dsRBD-dsRNA

occur via recognition of the standard features of the A-form dsRNA helix, like (i) the repetitive phosphate oxygens of the phosphodiester backbone, (ii) 2'-hydroxyl groups of the sugar, and (iii) the minor groove (non-polar surface) (Nicholson, 1996). The 2'-hydroxyl groups serve to eliminate any interaction with the A-form DNA, or the RNA-DNA hybrid, first observed by the Bevilacqua and Cech in their study with PKR dsRBDs (Bevilacqua & Cech, 1996). These interactions include hydrogen-bonding, ionic, and stacking interactions either through (i) direct contact of amino acids with the 2'-hydroxyl of the ribose sugar rings, and (ii) direct and/or water-mediated contacts with the non-bridging oxygen of the phosphodiester backbone (Fierro-Monti & Mathews, 2000; Saunders & Barber, 2003; Stefl et al., 2005).

The understanding of the molecular basis of interaction between dsRBD-dsRNA was initially attempted by Ryter and Schultz using the second dsRBD of *Xenopus laevis* RNA-binding protein A (Xlrpba-2) with a GC-rich 10-mer RNA (Ryter & Schultz, 1998) (Figure 1.4.2). Xlrpba-2 interacted with two consecutive minor grooves and the intervening major groove on one side of the dsRNA helix spanning a length of 16 bp (1680 Å). In region 1, the N-terminal α -helix (α_1) interacted with the minor groove of the RNA via glutamine (Q) and glutamate (E). The side chains of Q118 and E119 and a peptide backbone (carbonyl) group of E119 were involved in direct and water-mediated H-bonding with 4 sugar 2'-OH groups and 5 nitrogen-base functional groups of the RNA. In region 2, the β_1 - β_2 loop interacted with the adjacent minor groove via proline (P), histidine (H), and arginine (R). The H141-side chain and 3 peptide backbone groups, CO of P140, CO of H141, and NH of R143, were involved in direct and water-mediated interactions with 2 sugar 2'-OH groups and an N-base functional group. The CO of H141 made contact with 2'-OH groups on one side of the minor groove, and the H141-side chain interacted with the 2'-OH group on the other side. Mutational studies by Krovat and Jantsch further proved that the histidine in the β_1 - β_2 loop is crucial for the dsRNA-dsRBD interaction (Krovat & Jantsch, 1996). Region 3 (N-terminal of the α_2 helix) of the protein interacted with 6 non-bridging oxygens of the phosphodiester backbone either directly or via water-mediated contacts in the major groove of the RNA. The peptide backbone NH groups of K163 and Q164 interacted with non-bridging oxygen of the phosphodiester of the major groove near to the region 2. Additionally, the side-chain of the same K163 made hydrogen-bonds with an adjacent phosphodiester group. The side-chains of Q164 and K167 also interacted with the other side of the major groove closer to region 1. The side chains of lysines like K163 and K167 fold against the aromatic motifs of F145 and Y131. Thus, these

aromatic amino acids indirectly assist in the dsRBD-dsRNA interaction. Mutational analysis confirmed that F145 and the C-terminal α -helix are indeed critical for RNA binding (Krovat & Jantsch, 1996). Leulliot *et al.* demonstrated that *cis-trans* isomerisation of 2 proline residues in β_1 - β_2 loop are important for RNA interaction (Leulliot *et al.*, 2004).

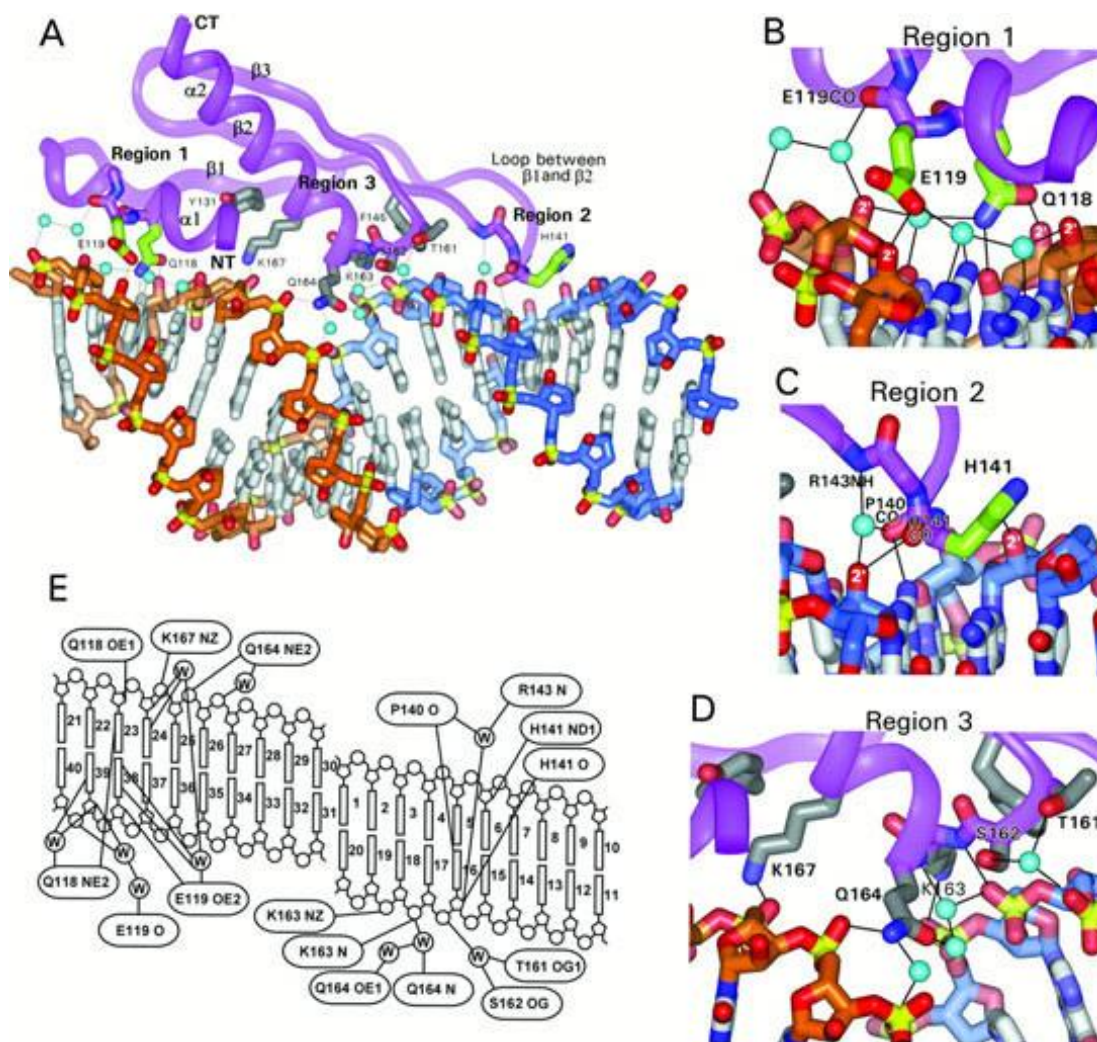


Figure 1.4.2: The molecular basis of interaction between the Xlrpba-2 dsRBD and dsRNA. (A) An overview of the interactions. The protein has been represented in purple. The side-chain residues of regions 1 and 2 have been shown in green, and residues of region 3 in gray. Nitrogen atoms are represented in blue, oxygen atoms in red, and phosphorus in yellow, respectively. The expanded view of (B) region 1 interacting with the minor groove, (C) region 2 - the loop2 interacting with the adjacent minor groove, and (D) region 3 - the N-terminal end of the α_2 helix interacting with the intervening major groove. (E) The schematic detailing of the interactions. The H-bonds have been depicted with black lines. Adapted from (Ryter & Schultz, 1998).

The set of conserved residues matching the sequence consensus (> 40%) of the dsRBD sequence alignment essential for maintaining a stable hydrophobic core (structure with the two α -helices packed on the β -sheet) and for optimal dsRNA binding (Masliah et al., 2013) have been shown in Figure 1.4.3.

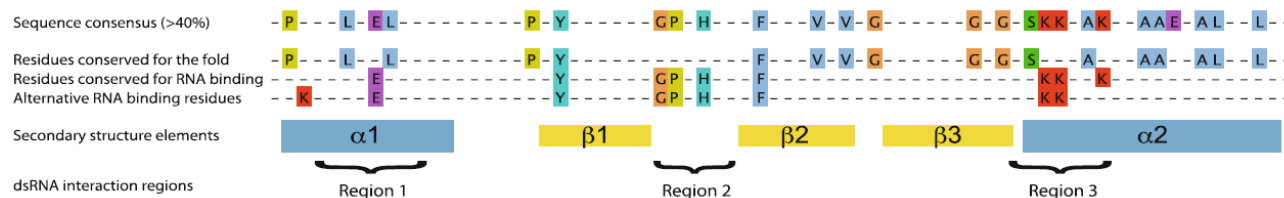


Figure 1.4.3: The conserved residues essential for the fold and/or dsRNA binding in the corresponding canonical secondary structures. The three dsRNA binding regions have been marked as Regions 1-3. Adapted from (Masliah et al., 2013).

1.5. A broad classification of dsRBDs: Type A and B

dsRBDs have been classified into type A and type B (Fierro-Monti & Mathews, 2000; Krovat & Jantsch, 1996; Masliah et al., 2013; St Johnston et al., 1992). Type A dsRBDs are highly homologous (> 59%) (Figure 1.5) to the consensus sequence and are indispensable to RNA-binding, whereas type B has only conserved C-terminal end (the loop₄- α_2 region) that binds weakly to the RNA, and in some cases stabilizes the protein-protein complex (Cosentino et al., 1995; Krovat & Jantsch, 1996; Patel & Sen, 1998; Romano et al., 1998). The type A and type B dsRBDs within and across proteins exhibit significant variations in their binding modes and affinities towards specific RNA targets. For example, *X. laevis* RNA-binding protein A (XlrpA) dsRBD1 and dsRBD2, classified as type A dsRBDs, demonstrate a notably stronger RNA-binding affinity than XlrpA-dsRBD3, which falls under type B category (Krovat & Jantsch, 1996). In Protein Kinase R (PKR), these two types of dsRBDs also demonstrate a differential dynamic behavior, i.e., dsRBD1 (type A) shows plasticity on μ s and ps-ns timescale, while dsRBD2 (type B) predominantly depicts dynamics on the ps-ns timescale (Fierro-Monti & Mathews, 2000),

Nanduri, Rahman, Williams, & Qin, 2000). Furthermore, the average order parameter (S^2) for the individual α -helices and β -sheets is observed to be lower for dsRBD1 than for dsRBD2, suggesting the latter as a more rigid domain (Fierro-Monti & Mathews, 2000), Nanduri et al., 2000).

A

```

DmMALE-1      MDIESFLYQFC---AKSQIEPKYLI-RQTGKKNRQFLCEVVEPNTY----IGVGNSTNKKDAEKNAACRDFVNYLVRV
HsHELIC-1     MGDVKNFLYAWCG--KREM-TPTYEI-RAVGNKKNRQFMCEVOVEGNY----TGMONSTNKKDAQSNAARDPVDNYLVRV
HsTRBP-2     SECNPFVGAQLQELV--QKGNRLPEYITVQESGFAHRKEFTMTQCRVERFIE-----IGSGTSKLLAKRNAAAKMLLRVHTV
XlRSPA-2     MQENPVGSLQELAV--QKGNRLPEYITVAQESGFPFKREFTITCRVETPVE-----TGSQTSKQVAKRVAEEKLLTKPFTI
HsCDNA       NQLNPIGSLQELAI--HHGNRLPEYITLSQEGGFANHKREYTTICRLSPNE-----TGKGAKKQAKRNAAEKFLAKFSNI
DmSTAU-3     DKFSPIQVMEIGI--KRNH-TVMTFVRLREEGFANMKNFITACIVGSIVT-----EGEGNCKKVSKRRAAEKMLVELQKL
EcrNAC       KQKDKPTRLQRYLQG-RMLP-LPTYLVVQVRGEAMDQEFITHCQVSGLSE----PVVGTGSHRKAEQAAAQALKKKLELE
DmSTAU-4     DADNPIITNLIQLQOT-RKEK-EPIFELIAKNGNETARRREFFVMEVSASGS----TAGGTGNKKLAKRNAAQALFELLEAV
MmTIK-1      TPGFYMOKLNKRYQ--MRQV-AITYKELSTSGFPMDRRTTFQVLIIDEKEF----FAKGRSKQEARNAAAKLAVDILDNE
RnTIK-1      TPGFYMOKLNKRYQ--MRQV-AITYKELSTSGFPMDRRTTFQVLIIDEKEF----FAKGRSKQEARNAAAKLAVDILDNE
HsDAI-1      PGKTPISLLQRYGT--RIQK-TPVYDILLKAEQQAQNPFTFRVTVGDTSC----TGQGPSKKAAKHRAAEVALKHLKGG
HsTRBP-1     PGKTPISLLQRYGT--RIQK-TPVYDILLKAEQQAQNPFTFRVTVGDTSC----TGQGPSKKAAKHRAAEVALKHLKGG
XlRSPA-1     PCETPIQLLKEFGT--KTGN-KVYVTLKAEQQAQNPFTFRVTVGDTSC----TGQGPSKKAAKHRAAEVALKHLKGG
HsDRADA-2    SGKSPVITLLECMH--KLGQ-SCEFRLLSKEGFAMHPFQYCVAVGAQTF----PSVSAPEKVKAKQMAAEEAMKALHGE
RnDEAM-2     SGKSPVITLLECMH--KLGQ-SCEFRLLSKEGFAMHPFQYCVAVGAQTF----PSVSAPEKVKAKQMAAEEAMKALHGE
HsDRADA-3    LNTNPFVGLLLEYAR--SHGF-AAETKLVLDQSGFPNEKPFVYQAVGGRWF----FAVCAHKKKQCKQEAADAALRVLIGE
RnDEAM-3     LNTNPFVGLLLEYAR--SHGF-AAETKLVLDQSGFPNEKPFVYQAVGGRWF----FAVCAHKKKQCKQEAADAALRVLIGE
HsDRADA-1    QLKNPIISGLLEYAQFASQT---CEFMIEIQSGFPNEKPFVYQAVGGRWF----FAVCAHKKKQCKQEAADAALRVLIGE
RnDEAM-1     QLKNPIISGLLEYAQFASQT---CEFMIEIQSGFPNEKPFVYQAVGGRWF----FAVCAHKKKQCKQEAADAALRVLIGE
Xl4F1-1      QVMNALMRLNQL---KPG--LQYKLVISQTFVNAHPFTMSFEVDDKTF----EASGPSKKTAKLHVAVKVLQDMGLP
HsNF-1       QANMALMRLNQL---KPG--LQYKLVISQTFVNAHPFTMSFEVDDKTF----EASGPSKKTAKLHVAVKVLQDMGLP
MmSPNR-1     DLMMALMRLNQL---KPG--LQYKLVISQTFVNAHPFTMSFEVDDKTF----EASGPSKKTAKLHVAVKVLQDMGLP
Xl4F1-2      HGKNPVMELENEK---RRG--LKYELISETGGSHDKRFVMEVVDGQKY----QGSGSNKKVAKAYAAALSLEKLPFD
NF-2        HGKNPVMELENEK---RRG--LKYELISETGGSHDKRFVMEVVDGQKY----QGSGSNKKVAKAYAAALSLEKLPFD
MmSPNR-2     SGKNPVMELENEK---RRG--LKYELISETGGSHDKRFVMEVVDGQKY----QGSGSNKKVAKAYAAALSLEKLPFD
HsSONA       SGKNPVMELENEK---RRG--LKYELISETGGSHDKRFVMEVVDGQKY----QGSGSNKKVAKAYAAALSLEKLPFD
VvE3L       KGANPVVINEYCOITRRD---WSPRI-ESVGFNSPTFYACVQIDGRVF----DKADGKRRDANKNAAKLAVDKLLGY
Vae3L       KNANPVVINEYCOITRRD---WSPRI-ESVGFNSPTFYACVQIDGRVF----DKADGKRRDANKNAAKLAVDKLLGY
DmSTAU-1     KDKTSMCLVNEELARYNKIT---HQYRLTEERGFANCKTFTVTLLMLGDDEY----SADGFRKKAQHLAASKAISETHYK
DmMALE-2     TIENAKERLNIYQTNMIR---DDYKY-TPVGFENARSLAELSIYVPALNRTVTARESGSNKKSASKSCALSIVRQLPHL
HsHELIC-2    TLENAKARLIQYFQKEXIQ---GEYRY-TQVGFENARSLAELSIYVPALNRTVTARESGSNKKSASKSCALSIVRQLPHL

```

CONSENSUS NPV LNEYSQ KRG L Y LI GP H F F V V G F P G G SKK AK AA AL L
 L V # RK # F #V M # I # # #
 I I L # L

B

```

Xl4F1-A      TANRPMGAGEAL---REVLECLSSGILNPDGSGGLYDPCEKDAADALEHL-ERQQRREDITQSAQHALLRLAAPGQENHKVLGM
HsNF-A       NTKEPPLSLTIN--LTSPVV--REEMKVLAGESTLSVNDPDPVLDROKCF-----AALASLHNKXNFCARANGLKSCVI
ScmITO       QPEQPTRELAML--CRREGLEKPVSLVAESGRLSKSPVFIHVYVSGRET----LGEYGSLSLKEAKARAATDALNEMVYCY
StROTA       PGPNALVFLNDC--ITKYNL--KIICTFDVNLDDDDGSIHMYICYLKVGSAE----ATGNGCKKKEAKRRAAVSILDQLGM.
SpPAC-1     IDKLAESKLFHKY--STLGH--ISYRW-VDGAGGSAGYVVIACIFNGKEV----ARAWGANCKDAGSRAAMQALEVLAED
CeT20G5-1    LKKTPLMVLLEEA---KA---VYQKTFPTNGTVLPEGFEMTLILNEITV----KQATSKKAARQKAAVEYLKRVVEK
CeYM68      PPRSPRELEMEPEQ--SK---VRESK-MERILESGKVRVTVVNNMRF-----TGMGRNYRIAKATAAKRALKYLHQI
DmSTAU-2     PKFPPSRFALPPP---LGAH--VHGPNPFPSPVPTPPSKITLFWGKQKY----VGIGRTLQCAKHDAARALQVLEKTO
HsTRBP-3     ACCRVLSSELSEEQ---APH---VSYLDIEELSLSGLCQCLVELSTQPATV----HGSATTREAAARGEAAARRALQYLKIM
XlRSPA-3     DYVMEKQVAAEL---DFN---LTYLDIDELVNGQYQCLAELSTNPIITVC----HGTGIECONAHNDAAHNALQYLKIM
DmSTAU-5     AGVHMKEQLLYLS--KLLDFEVNFSY-YPGNHNEFLTIWTLSTHPPQIC----HGVOKESEESQNDAAASNAKILSKL
MmTIK-2     FVGNVYIGLVNSFAQ--KKK-LSVNYEQ-CEPNSHELQRFICKCKYIGQTMV----GTGSGVTQKQAKLAKEAYQKLLS
RnTIK-2     IEGNYIGLVNSFAQ--KEN-LPVNPEL-CDPDSQLPHRFICKCKYIGQTTY----GTGFGANKEAKQLAAKNAYQKLSK
HsDAI-2     SHGNVYIGLVNRIAQ--KER-LTVNYEQ-CASGVHGGPEGFHYKCKMGOKEY----SIGTGSTKQEAQLAAKLAAYLQILSE
CeT20G5-2    PTEMWVGRLOEKSQ--KSK---LQAPVYEDSKNERTERELVICTMNCQKT----RGIRESKDKAKNLAALWLNKALEDG
CeT20G5-3    LEISFRRLVSPDPDLEMGAEHTQTEENKATAREKELRKNMPSDQPLVP----AGMGSAEAKQACKSAIHEWTY
RrCOOP      APCTFACPTGACRQA-DGQVQIVEQRCEIGCKLCLVMVCFQCAITVRSETVVE----QGACTNRGVAKKCDLVDWRASTGK

```

Figure 1.5: Multiple sequence alignments of different type A and type B dsRBDs. The consensus amino acids have been represented in bold and as shaded regions. The consensus sequence has been depicted in the middle. The bold residues indicate predominantly occurring at the corresponding positions, and # indicates hydrophobic residues. Adapted from (Krovat & Jantsch, 1996).

1.6. Versatility of dsRBD-dsRNA interaction

dsRBDs are often arranged in a modular fashion to create highly versatile RNA-binding surfaces (Fierro-Monti & Mathews, 2000). Depending on the function of the double-stranded RNA-binding protein (dsRBP), the dsRBPs can be broadly classified into 9 families (Fierro-Monti & Mathews, 2000). Most of these dsRBPs consist of at least two dsRBDs, except for the RNase III and E3L families, which contain a single dsRBD (Figure 1.6.1).

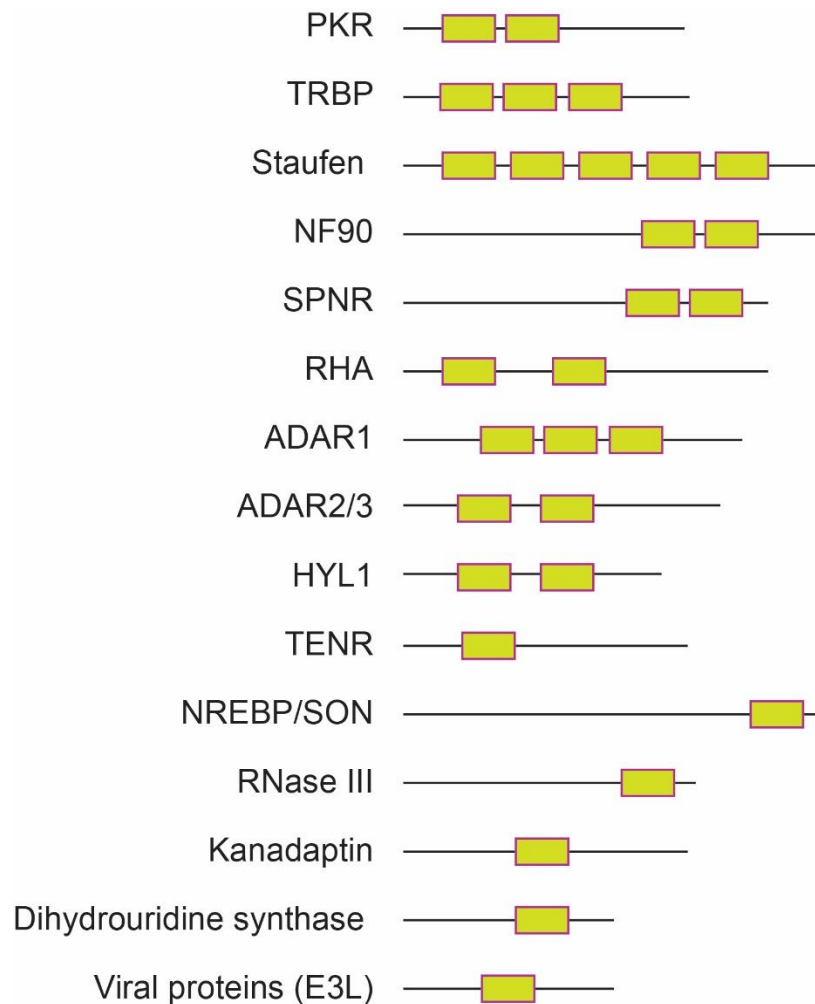


Figure 1.6.1: Representation of the distribution of dsRBDs in various families of dsRBPs. The yellow box represents a single dsRBD. Redrawn from (Fierro-Monti & Mathews, 2000).

There exists a lot of versatility (in terms of binding affinity, stoichiometry, register length of RNA, diffusion ability, dynamics, etc.) when it comes to the interaction of a given dsRBD with the target dsRNA even with the canonical binding surface of dsRBDs. The minimum span of dsRBD over an RNA target varies with different proteins and is also affected by the length and topology of different dsRNAs. Bevilacqua and Cech showed that the minimum register length of PKR-dsRBD1D2 for multiple dsRBD-binding is (11 bp) lower than that for single dsRBD-binding (16 bp), which indicates a role of adjacent dsRBD in RNA binding (Bevilacqua & Cech, 1996). In the case of Xlrbpa-dsRBD2, the dsRBD spans a length of 16 bp (Ryter & Schultz, 1998). On the other hand, a minimum of 8 bp (optimum 12 bp) is shown to be essential for Satufen-dsRBD3 binding to hairpin RNAs (Ucci, Kobayashi, Choi, Alexandrescu, & Cole, 2007). A common stoichiometry for binding a 20 bp RNA of a single dsRBD is 4, and that of two tandem dsRBDs is 2, as observed in PKR (Ucci et al., 2007) TRBP2 (Benoit et al., 2013), and RDE-4 (Chiliveri & Deshmukh, 2014). A study on PKR-dsRBD1 revealed that the binding stoichiometry increases with the increasing length of substrate RNA (Figure 1.6.2) (Ucci et al., 2007).

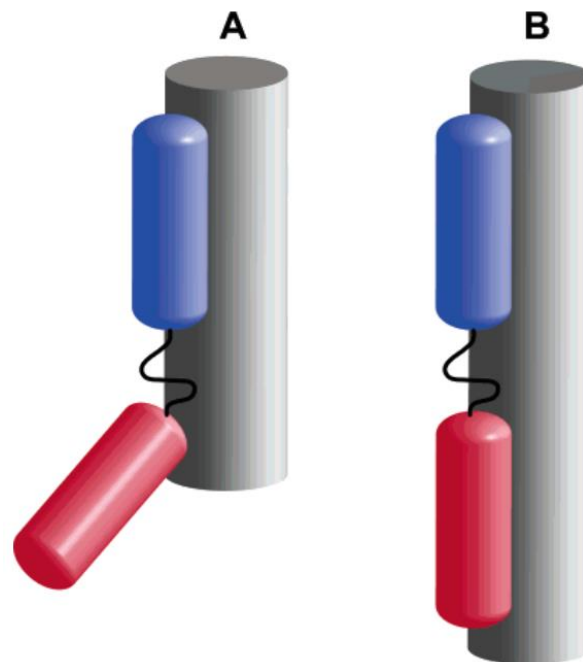


Figure 1.6.2: Models for the binding modes governing interactions of the PKR dsRBD with short (A) and long (B) dsRNA sequences. Adapted from (Ucci et al., 2007).

The linker length between two tandem dsRBDs plays an important role in RNA binding. In the case of DRB4-D1D2, the stoichiometry for 20 bp is 4, which is double of what is generally observed. The short linker length disables the second dsRBD to sit on the same RNA molecule as the first dsRBD (Chiliveri, Aute, Rai, & Deshmukh, 2017).

Although dsRBDs are known to be non-sequence specific, some perform a base-specific readout in the minor groove through sequence-specific contacts made by the α_1 helix and the β_1 - β_2 loop. These include the ADAR dsRBDs (Masliah et al., 2013; Stefl et al., 2010), Barraud & Allain, 2012) and the *Drosophila* Maleless protein (Ankush Jagtap et al., 2019). In both dsRBDs of ADAR2, the side-chain of an equivalent methionine residue in the α_1 helix makes a sequence-specific hydrophobic interaction with the RNA bases (Stefl et al., 2010). In addition to the A-form RNA helix, dsRBDs are able to recognize several other features of RNA, such as the apical loops, base-pair mismatches, bulges, and nucleotide sequences. The interaction between certain dsRBD and stem-loop RNAs shows that the loop acts as the decisive factor in substrate recognition, and α_1 helix plays an important role. Wang *et al.* showed that yeast RNase III dsRBD (Rnt1p) is able to recognize a conserved (A/uGNN or AAGU) tetraloop structure of the hairpin RNA via the α_1 helix (Z. Wang, Hartman, Roy, Chanfreau, & Feigon, 2011). The structural and phylogenetic analysis of Staufen-dsRBD3 by Ramos *et al.* shows that it interacts with the ssRNA of the hairpin loop through the α_1 helix, which can hint toward the sequence specificity of this domain (Ramos et al., 2000). Mutational studies of the Staufen-dsRBD3 indicate that the α_1 helix (Q4, E7, and R12) is critical for RNA-binding (Ramos et al., 2000). Wu *et al.* later solved the solution structure of Rnt1p-dsRBD in complex with a 14 bp RNA hairpin and showed that the interaction between the α_1 and the tetra loop is non-sequence specific in nature (Liang, Lavoie, Comeau, Abou Elela, & Ji, 2014). The NMR-based structural study of ADAR2-dsRBD1 and dsRBD2 with RNA by Stefl *et al.* revealed apical loop contacts with the dsRBD (Masliah et al., 2013; Stefl, Xu, Skrisovska, Emeson, & Allain, 2006).

dsRBDs are also known to diffuse/slide over the length of the RNA. A single molecule fluorescence resonance energy transfer (smFRET)-based study of TRBP dsRBDs showed that it

is involved in the ATP-independent diffusion over the length of the dsRNA, which is critical for accurate cleavage of pre-miRNAs by Dicer (Koh, Kidwell, Raganathan, Doudna, & Myong, 2013). The same study also indicated that PACT and R3D1-L (orthologs of TRBP) are able to diffuse over dsRNAs, whereas Dicer binds to dsRNAs in a static manner without diffusion (Koh et al., 2013). Structural, NMR, and biophysical studies of Loqs-PD with siRNAs (TRBP-homolog in *Drosophila*) indicated that its dsRBDs slide over the length of the RNA (Tants et al., 2017). NMR-based titrations of the MLE dsRBD12 (2 domains joined by a linker) by Jagtap *et al.* showed the presence of extensive line broadening of the protein amide groups, which did not reappear by adding an excess of RNA, confirming the sliding phenomenon over the length of the RNA (Ankush Jagtap et al., 2019). Another NMR-based study by Wostenberg *et al.* showed Dicer binding to a long 33 bp RNA leads to extensive line broadening of the amide peaks in the HSQC spectra (Figure 1.6.3) (Wostenberg et al., 2012). A dynamic profiling study of dsRBDs by Wang *et al.* showed that TRBP and Staufen1 exhibit dynamic sliding, whereas the two deaminases - ADAR1 and ADAR2 remain static when bound (X. Wang, Vukovic, Koh, Schulten, & Myong, 2015). An NMR-based titration by Chiliveri *et al.* with DRB4-D1D2 and 20 bp dsRNA showed that significant line-broadening occurs as a consequence of diffusion over the length of RNA (Chiliveri et al., 2017). The broadened peaks have been mapped to α_1 helix residue of DRB4D1, whereas most of the chemical shift perturbations have been mapped to DRB4D2.

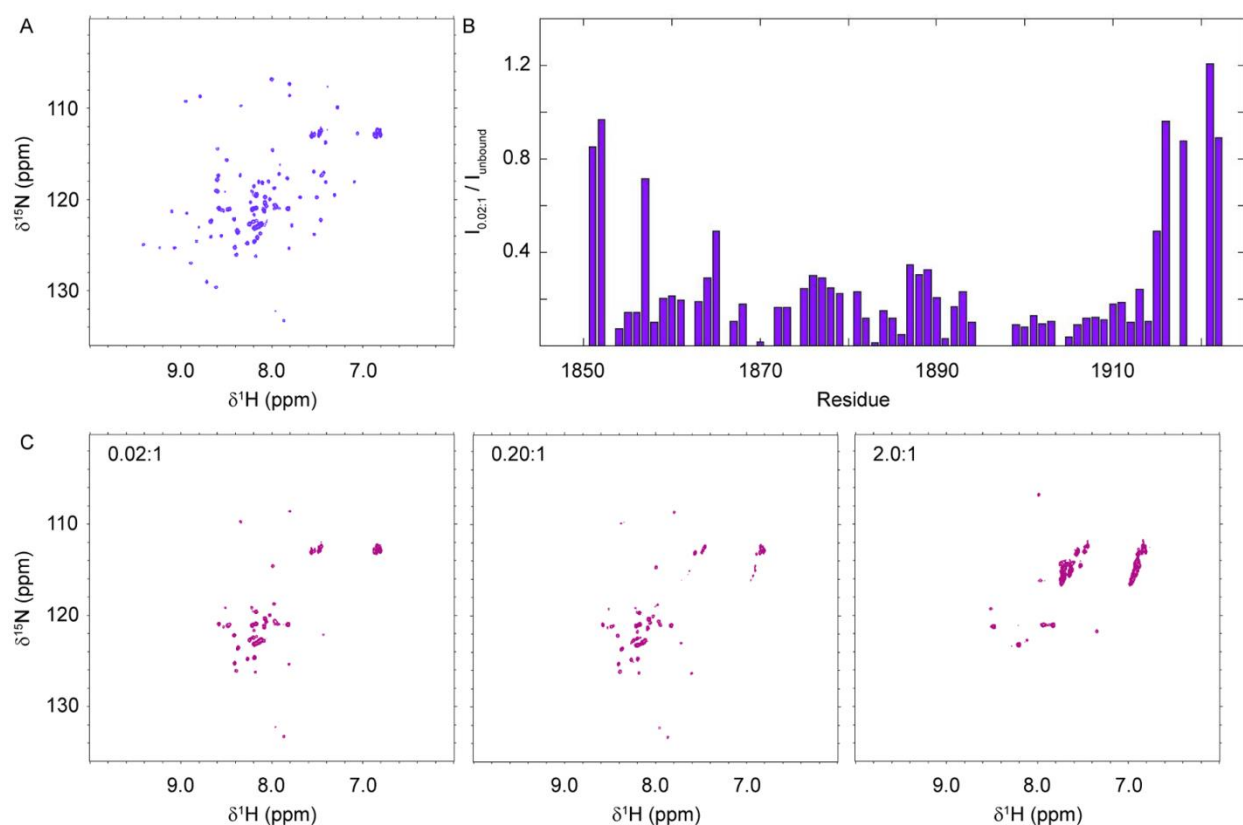


Figure 1.6.3: NMR-based titration of Dicer with a long 33 bp RNA showing extensive line broadening of the amide peaks in the ^1H - ^{15}N HSQC spectra. (A) ^1H - ^{15}N HSQC spectra of apo-Dicer-dsRBD spectra; (B) Peak intensity ratio in the presence of RNA (R:P = 0.02:1). (C) ^1H - ^{15}N HSQC spectra of Dicer-dsRBD in presence RNA (From left to right: R:P = 0.02:1; R:P = 0.20:1, and R:P = 2.0:1). Adapted from (Wostenberg et al., 2012).

dsRBDs across different as well as the same proteins vary strongly in binding mode and affinity towards a specific RNA target. TRBP dsRBD2 shows 4 times stronger binding than dsRBD1 with pre-miR-155 (Benoit et al., 2013). Additionally, studies have reported that dsRBD2 of TBBP displays a higher binding affinity for siRNA and HIV trans-activation response (TAR) RNA (Yamashita et al., 2011; Daviet et al., 2000). NMR-based titration study showed that MLE-dsRBD1 interacts with the SL7 18mer RNA in the fast exchange regime while dsRBD2 interacts in the intermediate exchange regime, leading to a higher affinity of dsRBD2 to the RNA (Ankush Jagtap et al., 2019). Recent investigations have suggested that the dissimilar behaviour of dsRBDs might be attributed to protein dynamics. Nanduri *et al.* showed that the binding affinity of the PKR

first dsRBD (Type A) domain is higher than the second (Type B) (Nanduri, Carpick, Yang, Williams, & Qin, 1998). It was later shown that these two types of domains demonstrate a differential dynamic behavior, i.e., dsRBD1 shows plasticity on μ s- to ps-ns timescale while dsRBD2 depicts only ps-ns timescale dynamics (Nanduri et al., 2000). Moreover, the average order parameter (S^2) for the individual α -helices and β -sheets has been found to be lower for type A (dsRBD1) than for type B (dsRBD2) indicating the latter to be a more rigid domain (Nanduri et al., 2000). The authors proposed that due to the inherent flexibility of PKR dsRBD1, it is able to adapt to a variety of viral dsRNAs with imperfect A-form structures, thereby facilitating the cooperative dsRNA binding of dsRBM2 to achieve an overall high affinity binding.

MD Simulations-based dynamic profiling of DGCR8-dsRBD1 (Wostenberg, Noid, & Showalter, 2010) along with NMR-based dynamics characterization of Dicer (Wostenberg et al., 2012) by Wostenberg *et al.* proved that the dynamics of the dsRBD loops vary across dsRBDs. The β_1 - β_2 loop in Dicer-dsRBD shows limited flexibility. Apart from the canonical RNA-binding regions, dynamics was present all along the backbone of the protein, especially in the L3 and L4 regions, which was not observed in DGCR8-dsRBD1 previously (Wostenberg et al., 2012), Wostenberg et al., 2010). Chiliveri *et al.* demonstrated the presence of ms- μ s dynamics in the RNA-binding region of the first double-stranded-RNA-binding protein 4 (DRB4) dsRBD helps it to establish stronger contacts with the incoming RNA, thereby leading the RNA-recognition phenomenon (Chiliveri et al., 2017). Residues in the α_1 region of dsRBD1 (L14 and H16) depict significant R_{ex} of about 10 Hz, while corresponding residues in dsRBD2 (Q92 and E94) show an absence of any dispersion (Figure 1.6.4). Most of the residues having significant R_{ex} are present in the α_1 region of DRB4D1. A few residues from the non-RNA-binding regions, like F52, L71, and T72 in DRB4D1 and T115, T117, and S147 in DRB4D2, also show the presence of R_{ex} . Hartman *et al.* also showed a loss of slow timescale dynamics in the β_1 - β_2 loop of Rnt1p upon binding to RNA (Hartman et al., 2013). Thus, it is seen that protein dynamics play an important role in the RNA recognition and binding mechanism across several dsRBDs. Dynamics characterization of other dsRBPs might help us get a deeper insight of the RNA-recognition and binding mechanism.

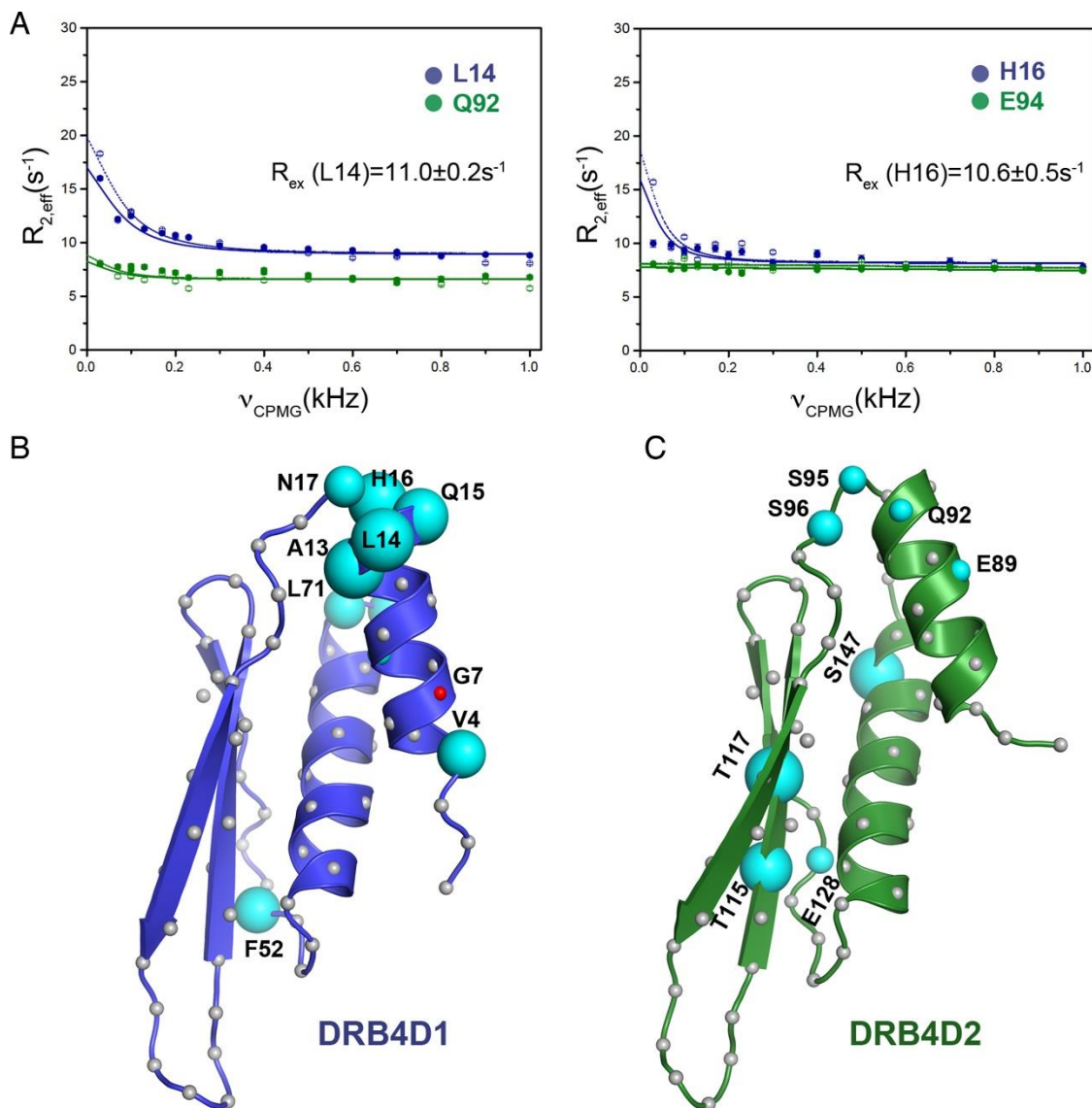


Figure 1.6.4: Differential ms- μ s dynamics of DRB4D1 and DRB4D2. Representative (A) ^{15}N - R_2 relaxation dispersion curves of 2 residues in the $\alpha 1$ region (L14 and H16) of dsRBD1 (shown in blue) and the corresponding residues in dsRBD2 (Q92 and E94) (shown in green). Filled circles represent data from 600 MHz and hollow circles from 700 MHz. The exchange rates are shown as a function of the diameter of the sphere for residues with significant R_{ex} in (B) DRB4D1 and (C) DRB4D2, residues T115, T117 and S147 show R_{ex} without any functional significance. Adapted from (Chiliveri et al., 2017).

1.7. The RNA interference pathway (RNAi pathway)

One of the most interesting cellular pathways involved in post-transcriptional gene regulation is the RNA-interference (RNAi) pathway, which involves many dsRBPs like, Drosha, Di-George Syndrome Critical Region 8 (DGCR8), Smad, Exportin 5, Dicer, TRBP, Ago2 facilitating miRNA/siRNA biogenesis to RISC complex formation (Figure 1.7) (Bhatia, Raina, Chugh, & Sharma, 2015). The roles of the RNAi pathway include defense against viruses, regulation of development, and maintenance of cellular homeostasis. Any imbalance in the cellular miRNA levels results in various diseases and can act as potential disease markers (Bhatia et al., 2015; Condrat et al., 2020; Mi, Zhang, Zhang, & Huang, 2013; H. Wang, Peng, Wang, Qin, & Xue, 2018; Liu et al., 2022; Hermann, Doeppner, & Giebel, 2021; Rupani, Sanchez-Elsner, & Howarth, 2013). Thus, the interaction between the dsRNAs and dsRBDs is very crucial in the RNAi pathway.

In human beings, the dsRBPs in the RNAi pathway interact with at least 1,971 miRNA sequences known from the miRBase (mirbase.org) harboring various helical imperfections like loops, bulges, pseudo-knots, etc. (as of August 2023). Moreover, about 340 known viral-origin miRNAs and perfect A-form duplex pre-siRNAs also use human RNAi machinery to manifest functionally. The canonical miRNA biogenesis pathway initiates with the transcription of the intronic, exonic, or intergenic DNA by RNA polymerase II (Y. Lee et al., 2004). The primary transcript is synthesized as a single ssRNA called the pri-miRNA, which folds on itself to form long hairpin structures (Figure 1.7). This pri-miRNA is then processed by the Drosha and Di-George Syndrome Critical Region 8 (DGCR8) complex. Drosha cleaves the RNA near the dsRNA-ssRNA junction to form a shorter hairpin (~70 nt) precursor-miRNA (pre-miRNA) with 3'-overhang (Y. Lee et al., 2003; Han et al., 2004; Han et al., 2006). The pre-miRNA is exported by nuclear export protein Exportin-5 regulated by RanGTP hydrolysis (X. Wang et al., 2011). On reaching the cytoplasm, the pre-miRNA is acted upon by the Dicer-TRBP complex to form the a ~22-24 bp miRNA duplex (miRNA:miRNA*) (Wilson et al., 2015; H. W. Wang et al., 2009). Initially, TRBP interacts with the pre-miRNA, leading to proper positioning of the RNA, thus ensuring accurate processing by Dicer to generate RNA duplexes (H. Y. Lee & Doudna, 2012). TRBP then recruits the Argonaute protein (Ago) to form the RNA-induced silencing complex (RISC) complex (Chendrimada et al., 2005). The guide strand selection is then mediated by this RISC complex (Noland, Ma, & Doudna, 2011; Noland & Doudna, 2013). The guide miRNA regulates the cellular gene expression either by perfect base-pairing with the mRNA, leading to its

degrading, or by partial base-pairing, leading to sequestering. Thus, TRBP, an indispensable dsRBP to this RNAi pathway, interacts with a lot of sequentially and topologically different RNAs. In summary, it is involved in the Dicer-mediated pre-miRNA/pre-siRNA cleavage (Y. Kim et al., 2014), recruitment of the Ago (Chendrimada et al., 2005), and selection of the guide strand (Noland et al., 2011), Noland & Doudna, 2013). Yamashita *et al.*, after comparing the solution structure of TRBP-dsRBD2 structure with the crystal structure of GC10RNA-bound TRBP-dsRBD2, concluded that the structure of the protein does not get perturbed (Yang et al., 2010; Yamashita et al., 2011). Acevedo *et al.* reported that TRBP dsRBD-dsRNA interaction does not result in any bending of the RNA (Acevedo, Evans, Penrod, & Showalter, 2016). Since the interaction between the TRBP-dsRBD and the dsRNA does not involve any structural perturbations, it becomes crucial to understand how TRBP interacts with such topologically different partners and if at all intrinsic protein dynamics has a role to play in it. Let us have a closer look at the TRBP in the next section.

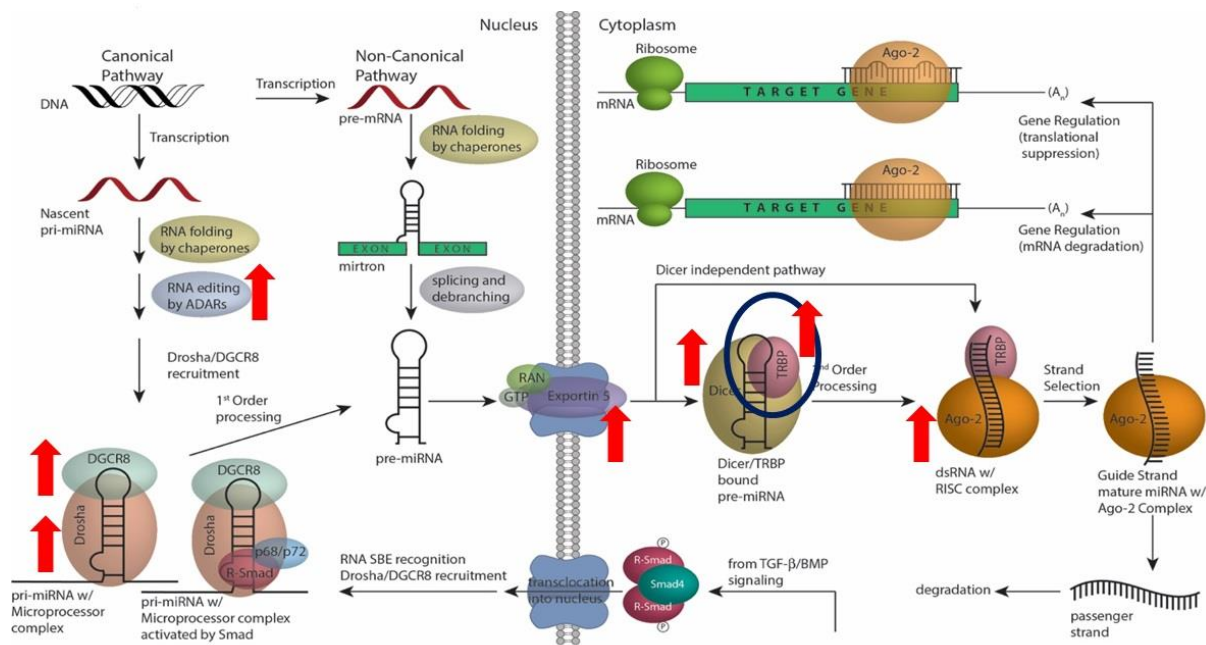


Figure 1.7: The miRNA biogenesis and RNA interference pathway. Red arrows denote dsRBPs involved in the pathway. TRBP, the protein of our interest, has been highlighted by a blue circle. Adapted from (Bhatia et al., 2015).

1.8. The TAR RNA-binding Protein (TRBP)

HIV-1 trans-activating region (TAR) RNA-binding protein (39 kDa) was initially discovered as a protein involved in the HIV-I replication (Gatignol, Buckler-White, Berkhout, & Jeang, 1991). TRBP has two isoforms in humans, TRBP1 and TRBP2. TRBP2 has an additional 21 amino acids at its N terminal when compared to TRBP1 (Daniels & Gatignol, 2012) (Figure 1.8.1). TRBP and its homologs across different species, such as Loquacious (Loqs in *D. melanogaster*), R2D2 (*D. melanogaster*), DRB1-3,5 (*A. thaliana*), RNAi defective 4 (RDE-4 in *C. elegans*), Xlrpba (*X. laevis*) (Eckmann & Jantsch, 1997), and the PKR activator (PACT) protein (mammals) (Peters, Hartmann, Qin, & Sen, 2001) have conserved arrangement of three consecutive dsRBDs; of which, the two N-terminal domains (type A) are known to bind dsRNAs, whereas the third domain is known for protein-protein interactions.

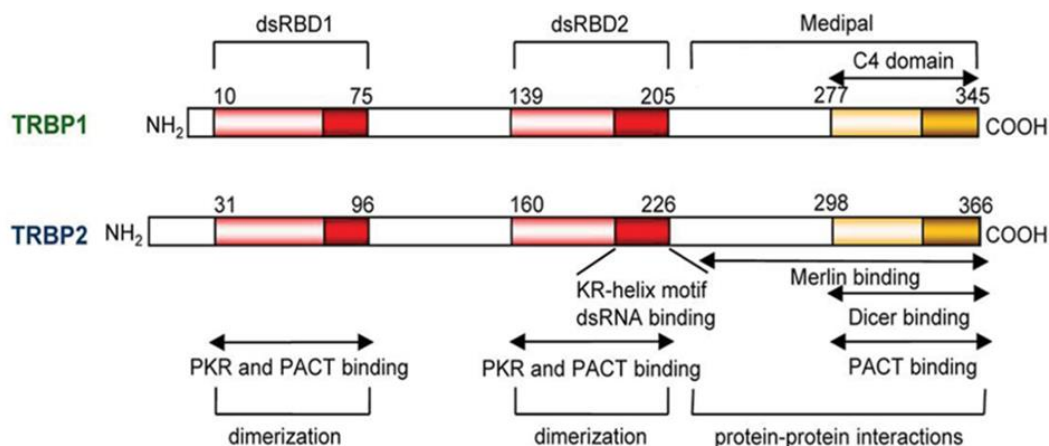


Figure 1.8.1: Domain organization of the two TRBP proteins – TRBP1 and TRBP2. Adapted from (Daniels & Gatignol, 2012).

The RNA processing activity of Dicer gets affected by the diffusion of the dsRBDs of TRBP along the RNA length (Koh et al., 2013) and in the presence of any helical perturbations in the RNA (Koh, Kidwell, Doudna, & Myong, 2017), X. Wang et al., 2015)). Moreover, as discussed previously, TRBP is involved in ATP-independent diffusion over the dsRNA length (Koh et al., 2013).

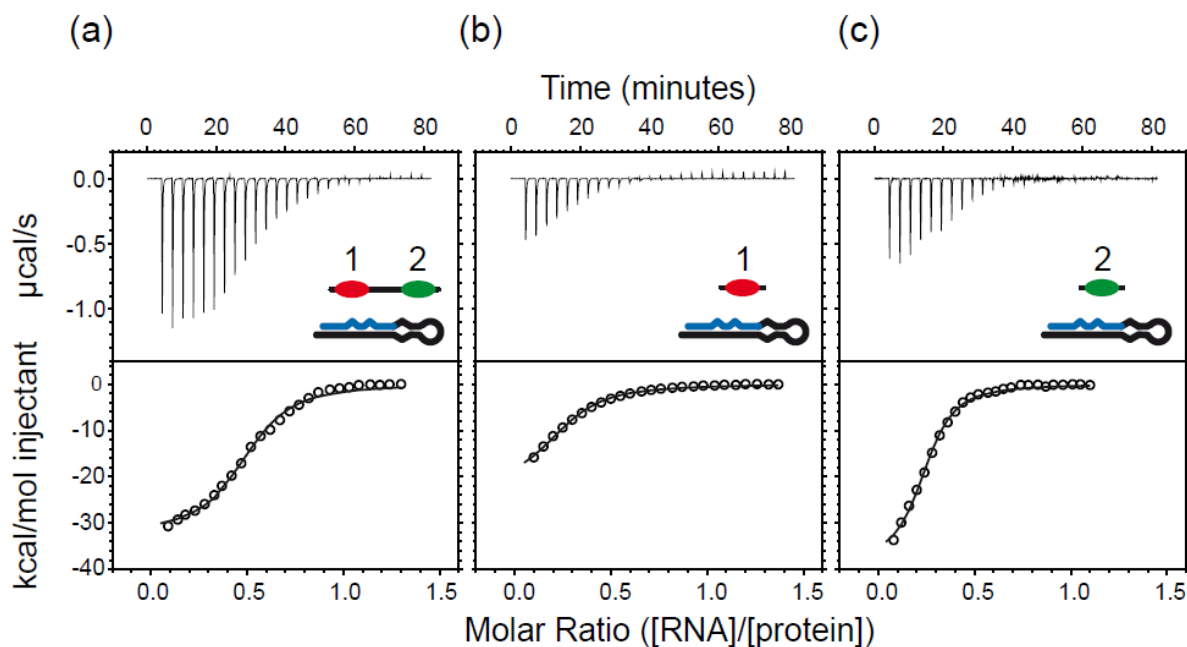


Figure 1.8.2: ITC study of the interaction between pre-miR-155 and (a) TRBP-D12, (b) TRBP-D1 (red), and (c) TRBP-D2 (green). The top panel indicates a plot of raw differential potential against time. The bottom panel indicates the integrated enthalpy per injection plotted against RNA:Protein ratio. Adapted from (Benoit et al., 2013).

TRBP-dsRBD2 shows a significantly stronger binding affinity (4 times) than dsRBD1 for pre-miR-155 (Figure 1.8.2) (Benoit et al., 2013). Additional studies have reported that dsRBD1 and dsRBD2 of TBBP1 display a similar binding affinity for siRNA, whereas, for TAR RNA, dsRBD1 has a higher binding affinity than dsRBD2 (Yamashita et al., 2011; Daviet et al., 2000). It is intriguing to notice that the two type-A dsRBDs originating from the same protein demonstrate a markedly different binding affinity for target RNAs across various cases, as elucidated above. Recent investigations have suggested that the dissimilar behavior of dsRBDs in Dicer (Wostenberg et al., 2012), PKR (Nanduri et al., 2000), and double-stranded-RNA-binding protein 4 (DRB4) (Chiliveri et al., 2017) might be attributed to protein dynamics. Although variations in the binding affinity for the two type-A dsRBDs of TRBP have been documented for several target RNAs, a comprehensive exploration of the differences in the conformational dynamics between these two domains remains to be undertaken. This study is an attempt in this direction and has explored the

role of differential conformational dynamics of the two tandem dsRBD domains of TAR RNA binding protein isoform 1 (TRBP2).

1.9. Scope of the Thesis

We have recently demonstrated the role of dsRBD dynamics in dsRBD-dsRNA interactions using dsRBD1 of human TRBP2 that dsRBD tends to adopt a conformationally dynamic structure (Paithankar et al., 2022). The slower μ s-timescale motions are present along the dsRBD backbone with higher frequency motions ($k_{ex} > 50$ kHz) in the RNA-binding sites. That could enable the dsRBD to dynamically tune itself for targeting topologically distinct dsRNA substrates. In this thesis, TRBP2-dsRBD1 and TRBP2-dsRBD2 have been used to carry out a comparison of the structure, dynamics (intrinsic and RNA-induced), and dsRBD-dsRNA interaction in the two tandem domains. the primary, secondary, and tertiary structure of TRBP2-dsRBD2 has been characterized and then compared with dsRBD1 in Chapter 3. The RNA-binding activity of dsRBD2 has been identified using topologically different dsRNAs using NMR-based titrations. Next, the two binding affinities of the two A-type dsRBDs of TRBP2 with a duplex RNA were compared using an Isothermal Titration Calorimetry-based study in Chapter 4. The motions in the TRBP2-dsRBD2 at ps-ns and μ s-ms timescale dynamics have been measured by nuclear spin relaxation experiments and relaxation dispersion experiments in apo-state and studied its perturbation in the presence of an A-form duplex RNA in Chapter 5. I have also compared the apo- and RNA-bound conformational dynamics measured in dsRBD2 with that of data measured on dsRBD1 previously. Using this approach, we have proposed that the differential binding affinity, protein dynamics, and its perturbation in the presence of RNA in the two dsRBDs enables them to recognize a variety of RNA substrates and diffusion along the length of the RNA in Chapter 6.

References

- Acevedo, R., Evans, D., Penrod, K. A., & Showalter, S. A. (2016). Binding by TRBP-dsRBD2 Does Not Induce Bending of Double-Stranded RNA. *Biophys J*, *110*(12), 2610-2617. doi:10.1016/j.bpj.2016.05.012
- Ankush Jagtap, P. K., Müller, M., Masiewicz, P., von Bülow, S., Hollmann, N. M., Chen, P. C., . . . Hennig, J. (2019). Structure, dynamics and roX2-lncRNA binding of tandem double-stranded RNA binding domains dsRBD1,2 of Drosophila helicase Maleless. *Nucleic Acids Res*, *47*(8), 4319-4333. doi:10.1093/nar/gkz125
- Auweter, S. D., Fasan, R., Reymond, L., Underwood, J. G., Black, D. L., Pitsch, S., & Allain, F. H. (2006). Molecular basis of RNA recognition by the human alternative splicing factor Fox-1. *EMBO J*, *25*(1), 163-173. doi:10.1038/sj.emboj.7600918
- Balachandran, S., Roberts, P. C., Brown, L. E., Truong, H., Pattnaik, A. K., Archer, D. R., & Barber, G. N. (2000). Essential role for the dsRNA-dependent protein kinase PKR in innate immunity to viral infection. *Immunity*, *13*(1), 129-141. doi:10.1016/s1074-7613(00)00014-5
- Barber, G. N. (2001). Host defense, viruses and apoptosis. *Cell Death Differ*, *8*(2), 113-126. doi:10.1038/sj.cdd.4400823
- Barraud, P., & Allain, F. H. (2012). ADAR proteins: double-stranded RNA and Z-DNA binding domains. *Curr Top Microbiol Immunol*, *353*, 35-60. doi:10.1007/82_2011_145
- Benoit, M. P., Imbert, L., Palencia, A., Perard, J., Ebel, C., Boisbouvier, J., & Plevin, M. J. (2013). The RNA-binding region of human TRBP interacts with microRNA precursors through two independent domains. *Nucleic Acids Res*, *41*(7), 4241-4252. doi:10.1093/nar/gkt086
- Berman, H. M., Westbrook, J., Feng, Z., Gilliland, G., Bhat, T. N., Weissig, H., . . . Bourne, P. E. (2000). The Protein Data Bank. *Nucleic Acids Res*, *28*(1), 235-242. doi:10.1093/nar/28.1.235
- Bevilacqua, P. C., & Cech, T. R. (1996). Minor-groove recognition of double-stranded RNA by the double-stranded RNA-binding domain from the RNA-activated protein kinase PKR. *Biochemistry*, *35*(31), 9983-9994. doi:10.1021/bi9607259

- Bhatia, P., Raina, S., Chugh, J., & Sharma, S. (2015). miRNAs: early prognostic biomarkers for Type 2 diabetes mellitus? *Biomark Med*, 9(10), 1025-1040. doi:10.2217/bmm.15.69
- Bycroft, M., Grunert, S., Murzin, A. G., Proctor, M., & St Johnston, D. (1995). NMR solution structure of a dsRNA binding domain from *Drosophila* staufen protein reveals homology to the N-terminal domain of ribosomal protein S5. *EMBO J*, 14(14), 3563-3571. doi:10.1002/j.1460-2075.1995.tb07362.x
- Chen, Y., & Varani, G. (2005). Protein families and RNA recognition. *FEBS J*, 272(9), 2088-2097. doi:10.1111/j.1742-4658.2005.04650.x
- Chen, Y., & Varani, G. (2013). Engineering RNA-binding proteins for biology. *FEBS J*, 280(16), 3734-3754. doi:10.1111/febs.12375
- Chendrimada, T. P., Gregory, R. I., Kumaraswamy, E., Norman, J., Cooch, N., Nishikura, K., & Shiekhattar, R. (2005). TRBP recruits the Dicer complex to Ago2 for microRNA processing and gene silencing. *Nature*, 436(7051), 740-744. doi:10.1038/nature03868
- Chiliveri, S. C., Aute, R., Rai, U., & Deshmukh, M. V. (2017). DRB4 dsRBD1 drives dsRNA recognition in *Arabidopsis thaliana* tasi/siRNA pathway. *Nucleic Acids Res*, 45(14), 8551-8563. doi:10.1093/nar/gkx481
- Chiliveri, S. C., & Deshmukh, M. V. (2014). Structure of RDE-4 dsRBDs and mutational studies provide insights into dsRNA recognition in the *Caenorhabditis elegans* RNAi pathway. *Biochem J*, 458(1), 119-130. doi:10.1042/bj20131347
- Condrat, C. E., Thompson, D. C., Barbu, M. G., Bugnar, O. L., Boboc, A., Cretoiu, D., . . . Voinea, S. C. (2020). miRNAs as Biomarkers in Disease: Latest Findings Regarding Their Role in Diagnosis and Prognosis. *Cells*, 9(2). doi:10.3390/cells9020276
- Cosentino, G. P., Venkatesan, S., Serluca, F. C., Green, S. R., Mathews, M. B., & Sonenberg, N. (1995). Double-stranded-RNA-dependent protein kinase and TAR RNA-binding protein form homo- and heterodimers in vivo. *Proc Natl Acad Sci U S A*, 92(21), 9445-9449. doi:10.1073/pnas.92.21.9445

- Daniels, S. M., & Gatignol, A. (2012). The multiple functions of TRBP, at the hub of cell responses to viruses, stress, and cancer. *Microbiol Mol Biol Rev*, 76(3), 652-666. doi:10.1128/membr.00012-12
- Dauber, B., & Wolff, T. (2009). Activation of the Antiviral Kinase PKR and Viral Countermeasures. *Viruses*, 1(3), 523-544. doi:10.3390/v1030523
- Daubner, G. M., Clery, A., & Allain, F. H. (2013). RRM-RNA recognition: NMR or crystallography...and new findings. *Curr Opin Struct Biol*, 23(1), 100-108. doi:10.1016/j.sbi.2012.11.006
- Daviet, L., Erard, M., Dorin, D., Duarte, M., Vaquero, C., & Gatignol, A. (2000). Analysis of a binding difference between the two dsRNA-binding domains in TRBP reveals the modular function of a KR-helix motif. *Eur J Biochem*, 267(8), 2419-2431. doi:10.1046/j.1432-1327.2000.01256.x
- Dreyfuss, G., Kim, V. N., & Kataoka, N. (2002). Messenger-RNA-binding proteins and the messages they carry. *Nat Rev Mol Cell Biol*, 3(3), 195-205. doi:10.1038/nrm760
- Eckmann, C. R., & Jantsch, M. F. (1997). Xlrpba, a double-stranded RNA-binding protein associated with ribosomes and heterogeneous nuclear RNPs. *J Cell Biol*, 138(2), 239-253. doi:10.1083/jcb.138.2.239
- Ferre-D'Amare, A. R., & Doudna, J. A. (2000). Crystallization and structure determination of a hepatitis delta virus ribozyme: use of the RNA-binding protein U1A as a crystallization module. *J Mol Biol*, 295(3), 541-556. doi:10.1006/jmbi.1999.3398
- Fierro-Monti, I., & Mathews, M. B. (2000). Proteins binding to duplexed RNA: one motif, multiple functions. *Trends Biochem Sci*, 25(5), 241-246. doi:10.1016/s0968-0004(00)01580-2
- Fu, Y., Zhao, X., Li, Z., Wei, J., & Tian, Y. (2016). Splicing variants of ADAR2 and ADAR2-mediated RNA editing in glioma. *Oncol Lett*, 12(2), 788-792. doi:10.3892/ol.2016.4734

- Gatignol, A., Buckler-White, A., Berkhout, B., & Jeang, K. T. (1991). Characterization of a human TAR RNA-binding protein that activates the HIV-1 LTR. *Science*, *251*(5001), 1597-1600. doi:10.1126/science.2011739
- Gleghorn, M. L., & Maquat, L. E. (2014). 'Black sheep' that don't leave the double-stranded RNA-binding domain fold. *Trends Biochem Sci*, *39*(7), 328-340. doi:10.1016/j.tibs.2014.05.003
- Han, J., Lee, Y., Yeom, K. H., Kim, Y. K., Jin, H., & Kim, V. N. (2004). The Drosha-DGCR8 complex in primary microRNA processing. *Genes Dev*, *18*(24), 3016-3027. doi:10.1101/gad.1262504
- Han, J., Lee, Y., Yeom, K. H., Nam, J. W., Heo, I., Rhee, J. K., . . . Kim, V. N. (2006). Molecular basis for the recognition of primary microRNAs by the Drosha-DGCR8 complex. *Cell*, *125*(5), 887-901. doi:10.1016/j.cell.2006.03.043
- Hartman, E., Wang, Z., Zhang, Q., Roy, K., Chanfreau, G., & Feigon, J. (2013). Intrinsic dynamics of an extended hydrophobic core in the *S. cerevisiae* RNase III dsRBD contributes to recognition of specific RNA binding sites. *J Mol Biol*, *425*(3), 546-562. doi:10.1016/j.jmb.2012.11.025
- Hermann, D. M., Doepfner, T. R., & Giebel, B. (2021). Circulating MicroRNAs: Posttranscriptional Regulators and Disease Markers Holding Promise in Stroke Prediction. *Stroke*, *52*(3), 954-956. doi:10.1161/strokeaha.120.033688
- Jiang, S., & Baltimore, D. (2016). RNA-binding protein Lin28 in cancer and immunity. *Cancer Lett*, *375*(1), 108-113. doi:10.1016/j.canlet.2016.02.050
- Kharrat, A., Macias, M. J., Gibson, T. J., Nilges, M., & Pastore, A. (1995). Structure of the dsRNA binding domain of *E. coli* RNase III. *EMBO J*, *14*(14), 3572-3584. doi:10.1002/j.1460-2075.1995.tb07363.x
- Kim, V. N., Han, J., & Siomi, M. C. (2009). Biogenesis of small RNAs in animals. *Nat Rev Mol Cell Biol*, *10*(2), 126-139. doi:10.1038/nrm2632

- Kim, Y., Yeo, J., Lee, J. H., Cho, J., Seo, D., Kim, J. S., & Kim, V. N. (2014). Deletion of human tarbp2 reveals cellular microRNA targets and cell-cycle function of TRBP. *Cell Rep*, 9(3), 1061-1074. doi:10.1016/j.celrep.2014.09.039
- Koh, H. R., Kidwell, M. A., Doudna, J., & Myong, S. (2017). RNA Scanning of a Molecular Machine with a Built-in Ruler. *J Am Chem Soc*, 139(1), 262-268. doi:10.1021/jacs.6b10387
- Koh, H. R., Kidwell, M. A., Raganathan, K., Doudna, J. A., & Myong, S. (2013). ATP-independent diffusion of double-stranded RNA binding proteins. *Proc Natl Acad Sci U S A*, 110(1), 151-156. doi:10.1073/pnas.1212917110
- Kolb, D., Nail, R. L., & Gunderson, E. K. (1975). Pre-service drug abuse as a predictor of in-service drug abuse and military performance. *Mil Med*, 140(2), 104-107.
- Krovat, B. C., & Jantsch, M. F. (1996). Comparative mutational analysis of the double-stranded RNA binding domains of *Xenopus laevis* RNA-binding protein A. *J Biol Chem*, 271(45), 28112-28119. doi:10.1074/jbc.271.45.28112
- Kurzynska-Kokorniak, A., Koralewska, N., Pokornowska, M., Urbanowicz, A., Tworak, A., Mickiewicz, A., & Figlerowicz, M. (2015). The many faces of Dicer: the complexity of the mechanisms regulating Dicer gene expression and enzyme activities. *Nucleic Acids Res*, 43(9), 4365-4380. doi:10.1093/nar/gkv328
- Lee, H. Y., & Doudna, J. A. (2012). TRBP alters human precursor microRNA processing in vitro. *Rna*, 18(11), 2012-2019. doi:10.1261/rna.035501.112
- Lee, Y., Ahn, C., Han, J., Choi, H., Kim, J., Yim, J., . . . Kim, V. N. (2003). The nuclear RNase III Drosha initiates microRNA processing. *Nature*, 425(6956), 415-419. doi:10.1038/nature01957
- Lee, Y., Kim, M., Han, J., Yeom, K. H., Lee, S., Baek, S. H., & Kim, V. N. (2004). MicroRNA genes are transcribed by RNA polymerase II. *Embo j*, 23(20), 4051-4060. doi:10.1038/sj.emboj.7600385

- Leulliot, N., Quevillon-Cheruel, S., Graille, M., van Tilbeurgh, H., Leeper, T. C., Godin, K. S., . . . Varani, G. (2004). A new alpha-helical extension promotes RNA binding by the dsRBD of Rnt1p RNase III. *EMBO J*, *23*(13), 2468-2477. doi:10.1038/sj.emboj.7600260
- Liang, Y. H., Lavoie, M., Comeau, M. A., Abou Elela, S., & Ji, X. (2014). Structure of a eukaryotic RNase III postcleavage complex reveals a double-ruler mechanism for substrate selection. *Mol Cell*, *54*(3), 431-444. doi:10.1016/j.molcel.2014.03.006
- Liu, S., Fan, M., Zheng, Q., Hao, S., Yang, L., Xia, Q., . . . Ge, J. (2022). MicroRNAs in Alzheimer's disease: Potential diagnostic markers and therapeutic targets. *Biomed Pharmacother*, *148*, 112681. doi:10.1016/j.biopha.2022.112681
- Masliyah, G., Barraud, P., & Allain, F. H. (2013). RNA recognition by double-stranded RNA binding domains: a matter of shape and sequence. *Cell Mol Life Sci*, *70*(11), 1875-1895. doi:10.1007/s00018-012-1119-x
- Mi, S., Zhang, J., Zhang, W., & Huang, R. S. (2013). Circulating microRNAs as biomarkers for inflammatory diseases. *Microrna*, *2*(1), 63-71. doi:10.2174/2211536611302010007
- Nanduri, S., Carpick, B. W., Yang, Y., Williams, B. R., & Qin, J. (1998). Structure of the double-stranded RNA-binding domain of the protein kinase PKR reveals the molecular basis of its dsRNA-mediated activation. *Embo j*, *17*(18), 5458-5465. doi:10.1093/emboj/17.18.5458
- Nanduri, S., Rahman, F., Williams, B. R., & Qin, J. (2000). A dynamically tuned double-stranded RNA binding mechanism for the activation of antiviral kinase PKR. *Embo j*, *19*(20), 5567-5574. doi:10.1093/emboj/19.20.5567
- Nicholson, A. W. (1996). Structure, reactivity, and biology of double-stranded RNA. *Prog Nucleic Acid Res Mol Biol*, *52*, 1-65. doi:10.1016/s0079-6603(08)60963-0
- Noland, C. L., & Doudna, J. A. (2013). Multiple sensors ensure guide strand selection in human RNAi pathways. *Rna*, *19*(5), 639-648. doi:10.1261/rna.037424.112
- Noland, C. L., Ma, E., & Doudna, J. A. (2011). siRNA repositioning for guide strand selection by human Dicer complexes. *Mol Cell*, *43*(1), 110-121. doi:10.1016/j.molcel.2011.05.028

Oubridge, C., Ito, N., Evans, P. R., Teo, C. H., & Nagai, K. (1994). Crystal structure at 1.92 Å resolution of the RNA-binding domain of the U1A spliceosomal protein complexed with an RNA hairpin. *Nature*, *372*(6505), 432-438. doi:10.1038/372432a0

Paithankar, H., Tarang, G. S., Parvez, F., Marathe, A., Joshi, M., & Chugh, J. (2022). Inherent conformational plasticity in dsRBDs enables interaction with topologically distinct RNAs. *Biophys J*, *121*(6), 1038-1055. doi:10.1016/j.bpj.2022.02.005

Patel, R. C., & Sen, G. C. (1998). Requirement of PKR dimerization mediated by specific hydrophobic residues for its activation by double-stranded RNA and its antigrowth effects in yeast. *Mol Cell Biol*, *18*(12), 7009-7019. doi:10.1128/MCB.18.12.7009

Peters, G. A., Hartmann, R., Qin, J., & Sen, G. C. (2001). Modular structure of PACT: distinct domains for binding and activating PKR. *Mol Cell Biol*, *21*(6), 1908-1920. doi:10.1128/mcb.21.6.1908-1920.2001

Ramos, A., Grunert, S., Adams, J., Micklem, D. R., Proctor, M. R., Freund, S., . . . Varani, G. (2000). RNA recognition by a Staufen double-stranded RNA-binding domain. *Embo j*, *19*(5), 997-1009. doi:10.1093/emboj/19.5.997

Reis, R. S., Hart-Smith, G., Eamens, A. L., Wilkins, M. R., & Waterhouse, P. M. (2015). Gene regulation by translational inhibition is determined by Dicer partnering proteins. *Nat Plants*, *1*, 14027. doi:10.1038/nplants.2014.27

Ren, Z., Veksler-Lublinsky, I., Morrissey, D., & Ambros, V. (2016). Staufen Negatively Modulates MicroRNA Activity in *Caenorhabditis elegans*. *G3 (Bethesda)*, *6*(5), 1227-1237. doi:10.1534/g3.116.027300

Romano, P. R., Zhang, F., Tan, S. L., Garcia-Barrio, M. T., Katze, M. G., Dever, T. E., & Hinnebusch, A. G. (1998). Inhibition of double-stranded RNA-dependent protein kinase PKR by vaccinia virus E3: role of complex formation and the E3 N-terminal domain. *Mol Cell Biol*, *18*(12), 7304-7316. doi:10.1128/MCB.18.12.7304

Rupani, H., Sanchez-Elsner, T., & Howarth, P. (2013). MicroRNAs and respiratory diseases. *Eur Respir J*, *41*(3), 695-705. doi:10.1183/09031936.00212011

Ryter, J. M., & Schultz, S. C. (1998). Molecular basis of double-stranded RNA-protein interactions: structure of a dsRNA-binding domain complexed with dsRNA. *EMBO J*, *17*(24), 7505-7513. doi:10.1093/emboj/17.24.7505

Saunders, L. R., & Barber, G. N. (2003). The dsRNA binding protein family: critical roles, diverse cellular functions. *FASEB J*, *17*(9), 961-983. doi:10.1096/fj.02-0958rev

Schumacher, J. M., Lee, K., Edelhoff, S., & Braun, R. E. (1995). Spnr, a murine RNA-binding protein that is localized to cytoplasmic microtubules. *J Cell Biol*, *129*(4), 1023-1032. doi:10.1083/jcb.129.4.1023

St Johnston, D., Brown, N. H., Gall, J. G., & Jantsch, M. (1992). A conserved double-stranded RNA-binding domain. *Proc Natl Acad Sci U S A*, *89*(22), 10979-10983. doi:10.1073/pnas.89.22.10979

Stefl, R., Oberstrass, F. C., Hood, J. L., Jourdan, M., Zimmermann, M., Skrisovska, L., . . . Allain, F. H. (2010). The solution structure of the ADAR2 dsRBM-RNA complex reveals a sequence-specific readout of the minor groove. *Cell*, *143*(2), 225-237. doi:10.1016/j.cell.2010.09.026

Stefl, R., Skrisovska, L., & Allain, F. H. (2005). RNA sequence- and shape-dependent recognition by proteins in the ribonucleoprotein particle. *EMBO Rep*, *6*(1), 33-38. doi:10.1038/sj.embor.7400325

Stefl, R., Xu, M., Skrisovska, L., Emeson, R. B., & Allain, F. H. (2006). Structure and specific RNA binding of ADAR2 double-stranded RNA binding motifs. *Structure*, *14*(2), 345-355. doi:10.1016/j.str.2005.11.013

Tants, J. N., Fesser, S., Kern, T., Stehle, R., Geerlof, A., Wunderlich, C., . . . Sattler, M. (2017). Molecular basis for asymmetry sensing of siRNAs by the Drosophila Loqs-PD/Dcr-2 complex in RNA interference. *Nucleic Acids Res*, *45*(21), 12536-12550. doi:10.1093/nar/gkx886

Tian, B., Bevilacqua, P. C., Diegelman-Parente, A., & Mathews, M. B. (2004). The double-stranded-RNA-binding motif: interference and much more. *Nat Rev Mol Cell Biol*, *5*(12), 1013-1023. doi:10.1038/nrm1528

Ucci, J. W., Kobayashi, Y., Choi, G., Alexandrescu, A. T., & Cole, J. L. (2007). Mechanism of interaction of the double-stranded RNA (dsRNA) binding domain of protein kinase R with short dsRNA sequences. *Biochemistry*, *46*(1), 55-65. doi:10.1021/bi061531o

Vergani-Junior, C. A., Tonon-da-Silva, G., Inan, M. D., & Mori, M. A. (2021). DICER: structure, function, and regulation. *Biophys Rev*, *13*(6), 1081-1090. doi:10.1007/s12551-021-00902-w

Wang, H., Peng, R., Wang, J., Qin, Z., & Xue, L. (2018). Circulating microRNAs as potential cancer biomarkers: the advantage and disadvantage. *Clin Epigenetics*, *10*, 59. doi:10.1186/s13148-018-0492-1

Wang, H. W., Noland, C., Siridechadilok, B., Taylor, D. W., Ma, E., Felderer, K., . . . Nogales, E. (2009). Structural insights into RNA processing by the human RISC-loading complex. *Nat Struct Mol Biol*, *16*(11), 1148-1153. doi:10.1038/nsmb.1673

Wang, X., Vukovic, L., Koh, H. R., Schulten, K., & Myong, S. (2015). Dynamic profiling of double-stranded RNA binding proteins. *Nucleic Acids Res*, *43*(15), 7566-7576. doi:10.1093/nar/gkv726

Wang, X., Xu, X., Ma, Z., Huo, Y., Xiao, Z., Li, Y., & Wang, Y. (2011). Dynamic mechanisms for pre-miRNA binding and export by Exportin-5. *Rna*, *17*(8), 1511-1528. doi:10.1261/rna.2732611

Wang, Z., Hartman, E., Roy, K., Chanfreau, G., & Feigon, J. (2011). Structure of a yeast RNase III dsRBD complex with a noncanonical RNA substrate provides new insights into binding specificity of dsRBDs. *Structure*, *19*(7), 999-1010. doi:10.1016/j.str.2011.03.022

Wilkinson, M. F., & Shyu, A. B. (2001). Multifunctional regulatory proteins that control gene expression in both the nucleus and the cytoplasm. *Bioessays*, *23*(9), 775-787. doi:10.1002/bies.1113

Wilson, R. C., Tambe, A., Kidwell, M. A., Noland, C. L., Schneider, C. P., & Doudna, J. A. (2015). Dicer-TRBP complex formation ensures accurate mammalian microRNA biogenesis. *Mol Cell*, *57*(3), 397-407. doi:10.1016/j.molcel.2014.11.030

Wostenberg, C., Lary, J. W., Sahu, D., Acevedo, R., Quarles, K. A., Cole, J. L., & Showalter, S. A. (2012). The role of human Dicer-dsRBD in processing small regulatory RNAs. *PLoS One*, 7(12), e51829. doi:10.1371/journal.pone.0051829

Wostenberg, C., Noid, W. G., & Showalter, S. A. (2010). MD simulations of the dsRBP DGCR8 reveal correlated motions that may aid pri-miRNA binding. *Biophys J*, 99(1), 248-256. doi:10.1016/j.bpj.2010.04.010

Yamashita, S., Nagata, T., Kawazoe, M., Takemoto, C., Kigawa, T., Güntert, P., . . . Yokoyama, S. (2011). Structures of the first and second double-stranded RNA-binding domains of human TAR RNA-binding protein. *Protein Sci*, 20(1), 118-130. doi:10.1002/pro.543

Yang, S. W., Chen, H. Y., Yang, J., Machida, S., Chua, N. H., & Yuan, Y. A. (2010). Structure of Arabidopsis HYPONASTIC LEAVES1 and its molecular implications for miRNA processing. *Structure*, 18(5), 594-605. doi:10.1016/j.str.2010.02.006

Chapter 2

Materials and Methods

2.1. Media, reagents, buffers, fine chemical and plasticware

Fine Chemicals and Plasticware used

All fine chemicals were purchased from HiMedia and all plasticware were purchased from Corning Inc., unless mentioned otherwise. Filters were purchases from Millipore Sigma (Burlington, MA).

Acid salt buffer (Freshly prepared)

Manganese chloride 100 mM

Calcium chloride 70 mM

Sodium acetate 40 mM

The pH was adjusted to 5.5 ± 0.5 (preferably pH 5.1). After pH adjustment, the solution was filter-sterilized through a 0.22 μm membrane filter, autoclaved at 121 °C, 15 psi for 20 mins, and stored at 4 °C.

2X Luria-Bertani (LB) broth

50 g of LB was dissolved in 1000 ml of MilliQ water and autoclaved at 121 °C, 15 psi for 20 mins. Stored at 4 °C until further use.

2X LB Agar plates

50 g of LB and 20 g of agar was dissolved in 1000 ml of MilliQ water and autoclaved at 121 °C, 15 psi for 20 mins. Once cooled to 55°C required, agar plates were poured. Stored at 4 °C until further use.

Luria-Bertani (LB) broth

25 g of LB was dissolved in 1000 ml of MilliQ water and autoclaved at 121 °C, 15 psi for 20 mins. Stored at 4 °C until further use.

LB Agar plates

25 g of LB and 20 g of agar was dissolved in 1000 ml of MilliQ water and autoclaved at 121°C, 15 psi for 20 mins. Once cooled to 55°C, the required antibiotics were added in the required concentration and mixed. Immediately, agar plates were poured. Stored at 4 °C until further use.

Antibiotic used

Ampicillin

Stock concentration 100 mg/ml in MilliQ water

Working concentration 100 µg/ml in MilliQ water

40% Acrylamide/Bis solution, 29:1

Acrylamide 96.67 g

N, N'-Methylenebis (acrylamide) 3.33 g

Mixed in 100 ml autoclaved water. Filter sterilized using a 0.22 µm membrane filter. Stored in amber-coloured bottle at 4 °C until further use.

10% SDS

SDS 10 g

MilliQ water 100 ml

Storage at room temperature until further use.

10% APS (Freshly prepared)

Ammonium persulphate 100 mg

MilliQ water 1 ml

Storage in dark at 4 °C until further use.

1.5 M Tris, pH 8.8 (resolving gel buffer)

Tris-base 18.15 g

Added 60 ml of MilliQ water, pH adjusted to 8.8 using 1 N HCl and volume made up to 100 ml.

The solution was filter sterilized using a 0.22 µm membrane filter and autoclaved. The solution was stored at room temperature until further use.

1 M Tris, pH 6.8 (stacking gel buffer)

Tris-base 12.10 g

Added 60 ml of MilliQ water; pH was adjusted to 6.8 using 1 N HCl and volume was made up to 100 ml. The solution was filter sterilized using a 0.22 μm membrane filter and autoclaved. The solution was stored at room temperature until further use.

10 X Running buffer (pH 8.3)

Tris-base 15 g

Glycine 72 g

SDS 5 g

MilliQ water 500 ml

The pH was adjusted to 8.3. The solution was filter sterilized and stored at room temperature until further use.

5X Sample loading dye

Tris-Cl buffer (1 M, pH 6.8) 2.5 ml

Glycerol 5 ml

SDS 0.8 g

Bromophenol blue 0.1%

Dithiothreitol 1 ml

MilliQ water 1.5 ml

900 μl aliquots were stored at $-20\text{ }^{\circ}\text{C}$, and 100 μl DTT was added freshly at the time of use.

SDS PAGE components:-

Resolving gel (10 ml)

Components	Gel 8%	Gel 10%	Gel 12%	Gel 15%
MilliQ water (ml)	5.275	4.825	4.3	3.55
40% Acrylamide/Bis soln. (ml)	2.025	2.475	3	3.75
1.5 M Tris-HCl, pH 8.8 (ml)	2.5	2.5	2.5	2.5
10% (w/v) SDS (μl)	100	100	100	100
10% APS (μl)	100	100	100	100
TEMED (μl)	20	20	20	20

Stacking gel (5 ml)

Components	Gel 5%
MilliQ water (ml)	3
40% Acrylamide/Bis soln. (ml)	0.630
1 M Tris-HCl, pH 6.8 (ml)	0.630
10% (w/v) SDS (μ l)	50
10% APS (μ l)	50
TEMED (μ l)	10

Gel Staining solution

Staining solution (50 ml)

Coomassie Brilliant Blue-G 250 stain 0.25 g

Methanol:Acetic acid:MilliQ water were mixed in the ratio of 45:10:45 and stored at room temperature until further use.

Gel De-staining solution

Methanol:Acetic acid:MilliQ water were mixed in the ratio of 45:10:45 and were stored at room temperature until further use.

Lysozyme (20 mg/ml)

Lysozyme 100 mg

Volume was made up to 5 ml with MilliQ water. The solution was filter sterilized, 1 ml aliquots were made and stored at -20 °C.

1 M DTT

Dithiothreitol (3.08 g) was dissolved in 20 ml of MilliQ water in a fresh conical tube. The solution was filter sterilized through a syringe filter, 1 ml aliquots were made and stored at -20 °C until further use.

1 M IPTG

2.383 g of IPTG was dissolved in 10 ml of MilliQ water in fresh conical tube. The solution was filter sterilized through a 0.22 μm syringe filter, 1 ml aliquots were made and stored at $-20\text{ }^{\circ}\text{C}$ until further use.

Protease inhibitor cocktail (10X) solution

1 tablet of SigmaFast protease inhibitor cocktail was dissolved in 10 ml of MilliQ water. It was then filter sterilize through a 0.22 μm syringe filter, 1 ml aliquots were made and stored at $-20\text{ }^{\circ}\text{C}$ until further use.

1 M Tris HCl/ Tris base

157.56 g Tris-HCl/ 121.14 g Tris base were dissolved in about 950 ml of water (pH was adjusted wherever necessary). The volume was made up to 1 L using MilliQ water. The solution was filter sterilized using a 0.22 μm membrane filter and autoclaved. Storage was done at room temperature until further use.

5 M Sodium chloride

292.2 g of sodium chloride was dissolved till the volume was about 950 ml of water. The final volume was made up to 1 L using MilliQ water. The solution was filter sterilized using a 0.22 μm membrane filter and autoclaved. The solution was stored at room temperature until further use.

0.5 M EDTA

93.05 g of EDTA-disodium salt dehydrate was dissolved in about 450 ml of MilliQ water. The pH was slowly adjusted to 8 and the volume made up to 500 ml. The solution was filter sterilized using a 0.22 μm membrane filter, autoclaved and stored at room temperature until further use.

3 M Imidazole

51.06 g of imidazole was dissolved in ~ 200 ml of MilliQ water. The volume made up to 250 ml. The solution was filter sterilized using a 0.22 μm membrane filter, autoclaved, and stored at room temperature until further use.

100 mM Phenylmethylsulfonyl fluoride (PMSF)

0.174 g of PMSF was dissolved in 10 ml of 2-propanol (anhydrous). The rotaspin was used to dissolve for about 15-30 mins. The solution was stored at 4°C, in amber colored conical tubes until further use.

3 M Potassium chloride

11.18 g of potassium chloride was dissolved in 40 ml of MilliQ water. The volume was made up to 50 ml, filter sterilized using a 0.22 µm membrane filter and autoclaved. The solution was stored at room temperature until further use.

1 M Sodium phosphate monobasic

5.99 g of Sodium phosphate monobasic was dissolved in 40 ml of MilliQ water. The volume made up to 50 ml. The solution was filter sterilized using a 0.22 µm membrane filter, autoclaved and stored at room temperature until further use.

1 M Sodium phosphate dibasic

7.09 g of Sodium phosphate dibasic was dissolved in about 40 ml of MilliQ water. The volume made up to 50 ml. The solution was filter sterilized using a 0.22 µm membrane filter, autoclaved and stored at room temperature until further use.

5X Minimal media salt mix (pH 7.4) (400 ml)

Na ₂ HPO ₄	12 g
KH ₂ PO ₄	6 g
NaCl	1 g
NH ₄ Cl/ ¹⁵ NH ₄ Cl	2 g

The above-mentioned salts were dissolved in about 300 ml of MilliQ water. The pH was adjusted to 7.4, and the volume was made up to 400 ml. The solution was filter sterilized using a 0.22 µm membrane filter, autoclaved, and stored at room temperature until further use.

1.5% CAS amino acid solution (300 ml)

Casein hydrolysate (4.5 g) was dissolved in about 250 ml of MilliQ water and the volume was made up to 300 ml. The solution was filter sterilized using a 0.22 µm membrane filter, autoclaved and stored at room temperature until further use.

1 M Magnesium chloride

20.33 g of magnesium chloride hexahydrate was dissolved in about 90 ml of MilliQ water and the volume was made up to 100 ml. The solution was filter sterilized using a 0.22 µm membrane filter, autoclaved and stored at room temperature until further use.

1 M Calcium chloride

11.1 g of calcium chloride was dissolved in about 50 ml of MilliQ water and the volume was made up to 100 ml. The solution was filter sterilized using a 0.22 µm membrane filter and stored at room temperature until further use.

20% Glucose solution (40ml, prepared fresh)

8g Glucose/¹³C-glucose was dissolved in autoclaved milliQ water and filter sterilized using Steriflip (Sigma). The solution was prepared fresh each time and was used immediately.

M9 Minimal media

Components	2 L Media
5X Minimal media salt mix (ml)	400
1.5% CAS amino acid solution (ml)	266.5
1 M Magnesium chloride (ml)	4
1 M Calcium chloride (µl)	200
20% Glucose (ml)	40
Ampicillin 100 mg/ml (ml)	2
Autoclaved MilliQ water (ml)	1287.3

The components mentioned were mixed and the volume was made up to 2L with MilliQ water. The media was autoclaved and stored at 4 °C until further use.

2.2. Methodology

The cDNA clones for the protein of interest, i.e., TRBP2-dsRBD2 (154–234 aa), were obtained as a kind gift from N. L. Prof. Jennifer Doudna (University of California, Berkeley, CA, USA). The residue numbers in the construct have been mentioned in reference to the full-length TRBP2 sequence (1–366 aa, Uniprot ID: Q15633-1). The cDNA for TRBP2-dsRBD2 was cloned in pHMGWA vector (AmpR), and was expressed as a fusion protein having N-terminal His₆-Maltose binding protein (MBP) tag-Tobacco Etch virus (TEV) protease cleavage site followed by the protein of interest. As a pre-requisite, TEV protease was overexpressed and purified in-house. Treatment with TEV protease during purification resulted in non-native Ser-Asn-Ala residues at the N-terminal of TRBP2-dsRBD2 (154–234), which were excluded from all the NMR-based dynamics studies. For all protein overexpression and purification, *E. coli* BL21 (DE3) competent cells were used. Unlabeled protein was prepared by growing transformed *E. coli* BL21 (DE3) cells in LB broth. For the NMR experiments, ¹⁵N-labeled and ¹⁵N-¹³C labeled (as required) TRBP2-dsRBD2 protein was prepared using ¹⁵NH₄Cl and ¹³C-glucose (Cambridge Isotope Laboratories) as a sole source of nitrogen and carbon, respectively, in M9 minimal medium. Protein was purified and subjected to NMR and other biophysical studies using the following procedures.

2.2.1. Competent Cell Preparation

Untransformed *E. coli* BL21 (DE3) cells were streaked on a 2X LB agar plate and were incubated for 12 h at 37 °C. A single colony was picked from the agar plate and inoculated in 10 ml 2X LB media (w/o antibiotic), incubated at 37 °C, 225 rpm for 12 h. Next, 0.5 ml of the primary culture was used to inoculate 50 ml 2X LB broth, which was incubated at 37 °C, 225 rpm till OD₆₀₀ reached 1–1.5. The cells were centrifuged at 2700 g for 10 mins, 4 °C to obtain the pellet. The cell pellet was kept on ice for all further procedures and all other solutions were chilled prior to use. The pellet was resuspended in 30 ml of acid salt buffer slowly and incubated on ice for 45 mins. It was again centrifuged at 2700 g for 10 mins, 4 °C. The pellet was resuspended in 3.2 ml of acid salt buffer and 0.8 ml of 80% glycerol. 100 µl aliquots were made in autoclaved microcentrifuge tubes, flash-frozen using liquid N₂, and stored immediately at -80°C until further use.

2.2.2. Transformation of competent cells

For overexpression of recombinant proteins, *E. coli* BL21 (DE3) competent cells were used. Briefly, competent cells were thawed on ice for about 5 mins and 1 µl of plasmid (~100 ng) was added to the cells and the cell suspension was mixed gently with tapping. It was then incubated on ice for 30 mins. Cells were subjected to heat shock for 30 secs at 42 °C, following which they were placed on ice for 10 mins. 800 µl of SOC medium was added to the cells and were incubated at 37 °C, 225 rpm for 45 mins. The microcentrifuge tube was kept in a horizontal position to allow proper shaking. After incubation, 100-200 µl of transformation mix was spread on an LB agar plate containing the selection antibiotic and incubated at 37 °C for 12-16 hours.

2.2.3. TEV Protein overexpression and purification

TEV protease clone 2 (Amp^R) plasmid was transformed into *E. coli* strain BL21 (DE3). A single colony was picked from the transformed plate and grown in 20 ml of LB broth (100 µg/mL ampicillin) overnight at 37 °C, 225 rpm. 1% of this primary culture was inoculated in 2 liters of LB media containing 100 µg/mL ampicillin and further grown at 37 °C till OD₆₀₀ reached 1–1.2. Protein synthesis in cells were then induced by adding 1 mM IPTG and were further allowed to grow at 28 °C, 225 rpm for 12 h. The cells were harvested by centrifuging at 4500 g for 15 minutes at 4 °C. The pellet was resuspended in 20 ml of lysis buffer (20 mM Tris, pH 8.0, 300 mM NaCl, 10 mM imidazole, 10 % glycerol, 1 mM DTT). To the resuspended cells, lysozyme (100 mg/ml) was added to a final concentration of 50 µg/mL and incubated on ice for 30 min. Post incubation, 1% Triton X-100, 100 µl of 1 mM PMSF, and 10 X Protease Inhibitor Cocktail (PIC) (2 mL per 4 g of cell pellet) were added to the cell suspension. The partially lysed cells were sonicated using an ultrasonic sonicator microprobe at 60% amplitude, with 5 s ON and 10 s OFF pulse, for a period of 60 min in an ice bath for complete lysis. The cell lysate was centrifuged at 15,000 x g for 2 h, at 4 °C, to obtain the total soluble protein (TSP). The TSP was circulated through a pre-equilibrated (lysis buffer) Ni-NTA column (HisTrap, 5 ml, GE HealthCare) for 4 h at 4 °C. After equilibrating with the TSP, the column was washed with 40 CVs of wash buffer (lysis buffer containing 20 mM

imidazole) to remove the impurities. The fusion protein was eluted with 5 CV of the elution buffer (buffer A containing 300 mM imidazole). The eluted fractions were checked for purity on a 15 % SDS-PAGE and the fractions containing more than 80% pure protein were pooled together and concentrated. The concentrated sample was then buffer exchanged in gel filtration buffer (20 mM Tris, pH 8.0, 1500 mM NaCl, 10 mM imidazole, 10 % glycerol, 1 mM DTT, 1 mM EDTA) and was subjected to size exclusion chromatography using Sephacryl S-100 HR 16/60 column (GE HealthCare). Absorbance was measured at 280 nm using nanodrop, and the concentration of the protein was calculated using $\epsilon=32290 \text{ M}^{-1}\text{cm}^{-1}$ and Mol wt: 27731 g M^{-1} .

The final purified protein was concentrated to 1 mg/ml of protein mixed with glycerol (50% final conc.). Aliquots of 1 ml were made, flash-frozen in liquid N₂, and stored at -20 °C for further use.

2.2.4. TRBP2-dsRBD2 overexpression and purification

The pHMGWA plasmid containing the cDNA for the TRBP2-dsRBD2 was transformed into *E. coli* BL21 (DE3) cells and plated on an LB agar plate (containing 100 µg/mL ampicillin) and incubated at 37 °C for 12 h. A single isolated colony was inoculated in 20 mL LB broth (containing 100 µg/mL ampicillin) and incubated for 12 h at 37 °C, 225 rpm to initiate a starter culture. This starter culture was eventually used to inoculate 2 L LB broth/ M9 media (containing 100 µg/mL ampicillin) and incubated at 37 °C, 225 rpm till the OD₆₀₀ reached to 1–1.2. For induction, IPTG was added at the final concentration of 1 mM, and the culture was further incubated at 37 °C, 225 rpm for another 10-12 h. The cells were harvested by spinning the culture at 4500 g, 4 °C for 20 min and resuspended in 25 mL of buffer A (20 mM Tris-Cl, pH 7.5, 500 mM NaCl, 10% glycerol, 5 mM DTT, 10 mM Imidazole). To the resuspended cells, lysozyme (Sigma-Aldrich, stock conc. 100 mg/ml) was added to a final concentration of 250 µg/mL and incubated in ice for 30 min. Post-incubation, 1% Triton X-100, 100 µl of 1 mM PMSF, and 10 X Protease Inhibitor Cocktail (PIC) (2 mL per 4 g of cell pellet) were added to the cell suspension. The partially lysed cells were sonicated using an ultrasonic sonicator microprobe at 60% amplitude, with 5 s ON and 10 s OFF pulse, for a period of 60 min in an ice bath for complete lysis. The cell lysate was centrifuged at

15,000 x g for 2 h, at 4°C, to obtain the total soluble protein (TSP). The TSP was circulated through a pre-equilibrated (buffer A) Ni-NTA column (HisTrap, 5 ml, GE HealthCare) for 4-6 h at 4 °C. After equilibrating with the TSP, the column was washed with 40-50 CVs of buffer A containing 30 mM imidazole to remove the impurities. The fusion protein was eluted with the elution buffer B (buffer A containing 300 mM imidazole). Nucleic acids were removed from the eluted protein using polyethyleneimine (PEI) precipitation till the OD_{260/280} reached 0.6-0.7, and on further treatment, no decline in the OD_{260/280} was observed. The protein solution was then concentrated to 50 mg/ml and to it cleavage buffer C was added (20 mM Tris-Cl, pH 7.5, 25 mM NaCl, 10% glycerol, 5 mM DTT) so that the final concentration of protein reached 1 mg/ml. Excess amount of DTT was added at this point to avoid the protein from precipitating. His₆-MBP-tag was cleaved using TEV protease at a final concentration of 1:100 (protease: protein) at 4 °C for 18 h with intermittent mixing. The completion of the cleavage reaction was tested and confirmed by SDS-PAGE analysis. The cleavage mix was then passed through a sulphopropyl sepharose column (HiPrep SP FF 16/10 20ml, GE HealthCare) and washed with buffer C. TRBP2-dsRBD2 protein was eluted from the cation-exchange column using a salt gradient ranging from 25 mM to 1 M NaCl in the buffer C.

To further purify, the protein was subjected to size-exclusion chromatography using sephacryl S-100 HR 16/60 column (GE HealthCare). Absorbance was measured at 280 nm using nanodrop, and the concentration of the protein was calculated using $\epsilon = 6990 \text{ M}^{-1}\text{cm}^{-1}$ and Mol wt: 9381 g M⁻¹. The final purified protein was concentrated to 1 mM using Amicon (3 kDa cutoff, Merck) and exchanged with NMR buffer D (10 mM sodium phosphate, pH 6.4, 100 mM NaCl, 1 mM EDTA, 5 mM DTT) before recording any experiment. The amino acid sequence of the purified protein (numbered according to full length TRBP2 protein with Uniprot ID: Q15633) is given below:

SNA ¹⁵⁴QQSECNP¹⁶⁰ VGALQELVVQ¹⁷⁰ KGWRLPEYTV¹⁸⁰ TQESGPAHRK¹⁹⁰
EFTMTCRVER²⁰⁰ FIEIGSGTSK²¹⁰ KLAKRNAAAK²²⁰ MLLRVHTVPL²³⁰ DARD²³⁴

The 3 N-terminal (bold) amino acids non-native residues left as a consequence of TEV protease cleavage.

2.2.5. Design and preparation of RNA

RNA sequences were designed based on the fact that TRBP interacts with miR-16-1 duplex (miRbase accession no. MI0000070) (Takahashi et al., 2014). The miR-16-1 (wild type or miR-16-1-A) miRNA duplex has a bulge (unpaired uridine) and an internal loop (A:A mismatch), thus producing imperfections in the A-form helical structure of dsRNA (Paithankar et al., 2022). We had introduced mutations (in a previous study) in the wild type to slightly perturb its shape and checked its effect on the binding of TRBP2-dsRBDs. The passenger strand of the wild-type RNA (miR-16-1-A) was mutated to create the following three mutants: (i) miR-16-1-M having only mismatch, (ii) miR-16-1-B having only bulge, and (iii) miR-16-1-D having no bulge or internal loop forming a perfect duplex (Figure 2.2.5.1) (Paithankar et al., 2022). A shorter 12 bp RNA duplex RNA oligo (D12) was designed from miR-16-1-D and procured from either Integrated DNA Technologies (Coralville, IA, USA) or GenScript Biotech Corporation (Piscataway NJ, USA). All the sequences used in this study have been listed in Table 2.2.5.

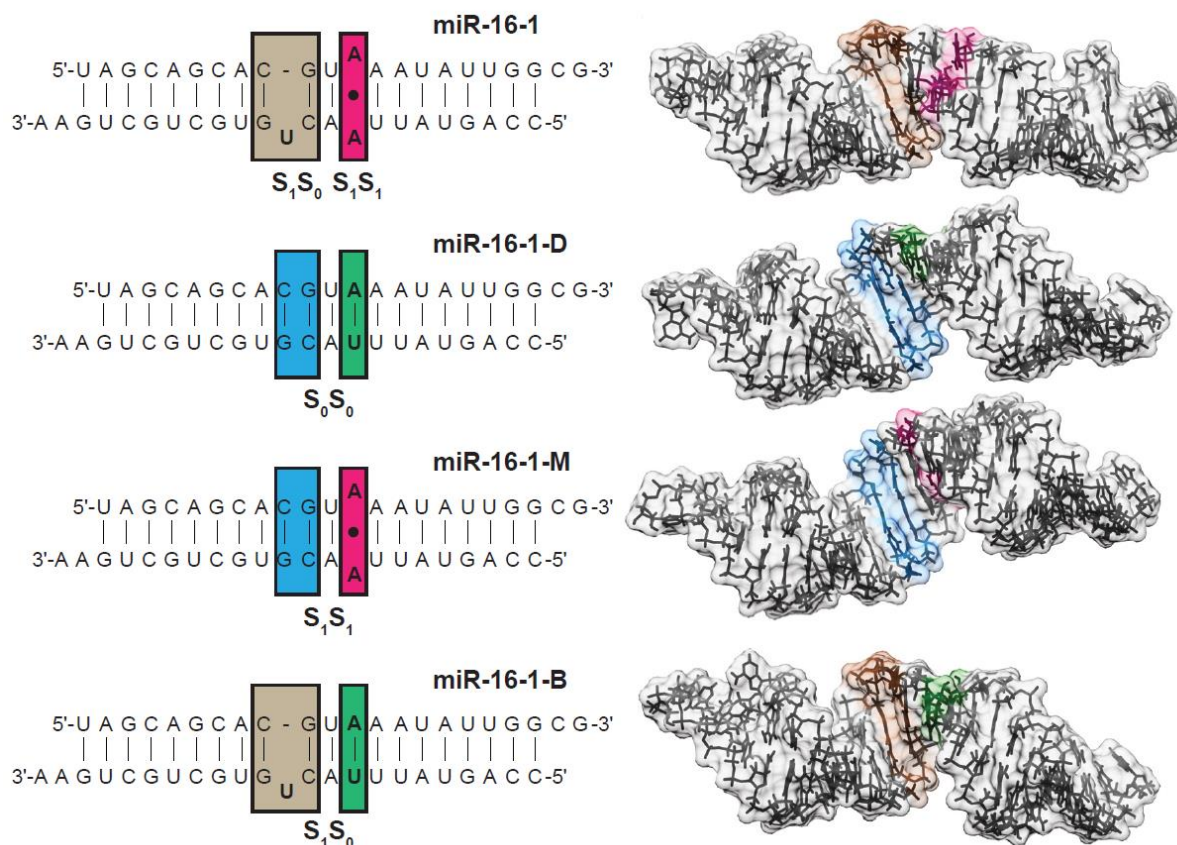


Figure 2.2.5.1: miR-16-1 mutants used in the study. From top to bottom: wild-type RNA (miR-16-1), miR-16-1-D, miR-16-1-M, and miR-16-1-B. Adapted from (Paithankar et al., 2022).

All the RNA oligonucleotides were procured as single strands (guide and passenger separately) and their stock solutions were maintained at 100 μ M. RNA annealing was achieved by mixing the guide and passenger strands in a 1:1 ratio. The mix was denatured by heating at 90 $^{\circ}$ C for 5 min and then allowed to anneal on ice for 10 min. Annealing was confirmed by 1 H NMR by looking at the presence of imino proton peaks (Figure 2.2.5.2). The annealed samples were maintained in buffer D for all data measurements.

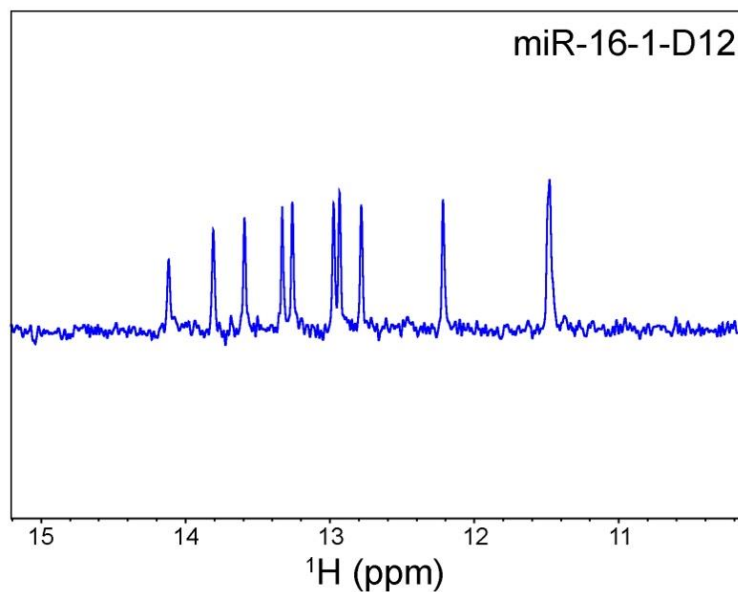


Figure 2.2.5.2: ^1H -NMR spectrum of the imine-region of the annealed D12 RNA. The peak pattern observed indicated the formation of the RNA duplex.

Table 2.2.5: RNA sequences used in this study.

Name	Strand	Sequence (5' → 3')
miR-16-1-A	Guide	UAGCAGCACGUA AAUAUUGGCG
	Passenger	CCAGUAUUAACUGUGCUGCUGAA
miR-16-1-D	Guide	UAGCAGCACGUA AAUAUUGGCG
	Passenger	CCAGUAUUUACGUGCUGCUGAA
miR-16-1-M	Guide	UAGCAGCACGUA AAUAUUGGCG
	Passenger	CCAGUAUUAACGUGCUGCUGAA
miR-16-1-B	Guide	UAGCAGCACGUA AAUAUUGGCG

	Passenger	CCAGUAUUAACGUGCUGCUGAA
D12 RNA	Guide	CGUAAAUAUUCG
	Passenger	CGAGUAUUUACG

2.2.6. Size-Exclusion Chromatography – Multiple Angle Light Scattering

To determine the molar mass and size of protein in solution, - the combination of size-exclusion chromatography coupled with multi-angle light scattering (SEC-MALS) can be used (Folta-Stogniew & Williams, 1999; Wyatt, 1993; Zimm, 1945). In this method, the protein first undergoes a chromatographic separation via SEC, and eventually encounters a MALS detector, followed by probing by a laser beam. A cumulative analysis of the (i) MALS signals, (ii) UV absorbance and (ii) differential refractive index (δ RI) signals is employed to evaluate the physical properties of the protein.

The SEC-MALS experiments were performed using an S75 column (Superdex 75 10/300 GL 24 ml, GE Healthcare), Agilent HPLC system (Wyatt Dawn HELIOs II) and a refractive index detector (Wyatt Optilab T-rEX). The system was first calibrated by injecting 100 μ l of 30 μ M Bovine Serum Albumin (BSA) solution (ThermoScientific). Post calibration, 100 μ l protein samples were injected (in duplicate) at a concentration of 0.8 mM for TRBP2-dsRBD2. The respective molar mass values of the peaks were calculated using the Zimm model in ASTRA software version 7 (Wyatt Technologies).

2.2.7. Isothermal titration calorimetric binding assays

Isothermal Titration Calorimetry (ITC) is a biomolecular interaction quantification technique. It works on the basic principle of thermodynamics where the heat evolved (either endothermic or exothermic) during the interaction between biomolecules is measured. The

instrument has two cells: (i) a reference cell (water) and (ii) a sample cell (Figure 2.2.7.1). The calorimeter, at all times, tends to keep the temperature of these two cells at equilibrium. The heat evolved during the binding event is measured by the energy required to equalize the temperature between the cells. This heat change is monitored as the power or differential potential ($\mu\text{cal}/\text{sec}$) for each injection of the ligand and is plotted against the time (Saponaro, 2018). The integrated area under the curve for each peak gives us the heat change associated with the binding event and is related to the enthalpy of the event. The final plot is between an isotherm of enthalpies against the concentration of the ligand given by molar ratio (Figure 2.2.7.1). The negative and positive dH indicate different kinds of chemical interactions involved during the binding process.

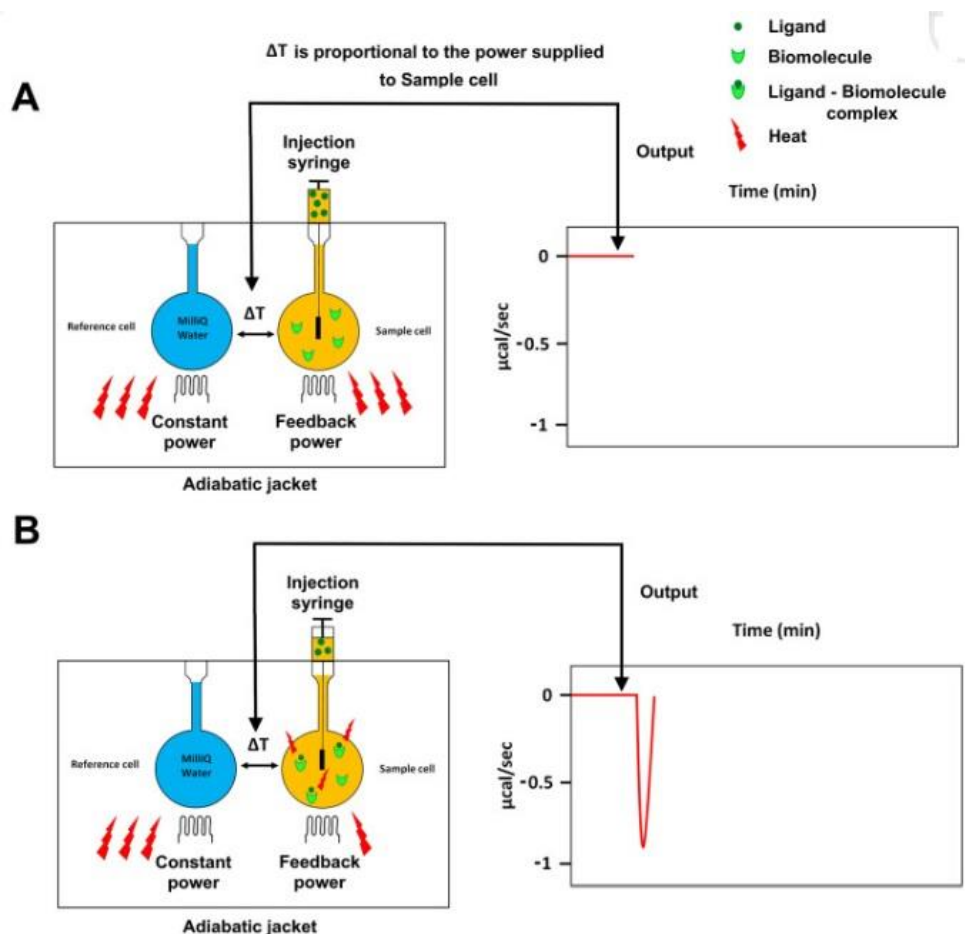


Figure 2.2.7.1: A diagrammatic representation of an isothermal titration calorimetry (ITC) instrument. (A) The temperature difference between the reference and the sample cell, induced by the (B) ligand–biomolecule binding is converted into the power needed to bring the two cells back to the same temperature during the binding reaction. Adapted from (Saponaro, 2018).

The binding isotherm can be fit to various equations depending on the type of binding event to estimate of the binding affinity (K_D), stoichiometry (n), enthalpy (ΔH), and entropy (ΔS) (Freire et al., 1990; Freyer & Lewis, 2008). Equations for fitting data for a single set of Identical Binding Sites have been listed below:

$$K = f / \{(1 - f)[X]\} \quad (2.2.7.1)$$

$$X_t = [X] + n f M t \quad (2.2.7.2)$$

where, K = Binding constant;

n = Number of binding sites;

V = Cell volume;

M_t and $[M]$ are initial and free concentration of macromolecule in V ;

X_t and $[X]$ are initial and free concentration of ligand, and

f = fraction of sites occupied by ligand X .

Combining eq. (2.2.7.1 & 2.2.7.2) above gives

$$f^2 - f \left\{ 1 + \frac{X_t}{nM_t} + \frac{1}{nKM_t} \right\} + \frac{X_t}{nM_t} = 0 \quad (2.2.7.3)$$

The total heat content (Q) of the solution in the cell at fractional saturation (f) is given by

$$Q = n f M t \Delta H V \quad (2.2.7.4)$$

where, ΔH is given by the molar heat of binding. Solving the quadratic equation (2.2.7.3) for “ f ” and substituting in equation (2.2.7.4) gives us:

$$Q = \frac{nM_t\Delta HV}{2} \left(1 + \frac{X_t}{nM_t} + \frac{1}{nKM_t} - \sqrt{\left\{ 1 + \frac{X_t}{nM_t} + \frac{1}{nKM_t} \right\}^2 - \frac{4X_t}{nM_t}} \right) \quad (2.2.7.5)$$

The value of Q for every i^{th} injection can be calculated for a particular value of n, K, and ΔH and is denoted by Q_i . The change of total heat content from the completion of the $i-1$ injection to completion of the i injection after i^{th} injection is given by ΔQ_i :

$$\Delta Q_i = Q(i) + \frac{dV_i}{V} \left[Qi + \frac{Q(i-1)}{2} \right] - Q(i-1) \quad (2.2.7.6)$$

where, dV_i is the injection volume.

The fitting of experimental data involves

- 1) Initial guesses of n, K, and ΔH ,
- 2) Calc. of $\Delta Q(i)$ for each injection and its comparison with measured heat for the corresponding experimental injection,
- 3) Improvement of the initial values of n, K, and ΔH by standard Marquardt methods (Levenberg, 1944; Marquardt, 1963)
- 4) Iterations of 1, 2, and 3 are performed until there is a significant improvement in the fitting.

All ITC experiments were performed using a MicroCal PEAQ-ITC calorimeter (Malvern Panalytical, Malvern, UK) operating at 25°C. The final RNAs and protein solutions used for the assays were prepared in buffer D. The D12 dsRNA was used at a concentration of 10 or 20 μM in the sample cell. TRBP2-dsRBD1 concentration was varied from 5-19 folds of RNA, whereas, in the case of TRBP2-dsRBD2, it varied from 10-18 folds. The first injection was 0.4 μl (discarded for data analysis), which was followed by eighteen 2 μl injections.

The data were fitted with a single-site binding model (as explained above) using the MicroCal PEAQ-ITC analysis software (Malvern Panalytical, Malvern, UK) to extract the binding affinity (K_D), stoichiometry (n), enthalpy (ΔH), and entropy (ΔS). These parameters were used to derive the Gibbs free energy change of binding using the equation:

$$\Delta G = -RT \ln (K_D), \quad (2.2.7.7)$$

and the overall change in the entropy of the system, using the experimental temperature and the relationship:

$$\Delta G = \Delta H - T\Delta S. \quad (2.2.7.8)$$

The final values of the kinetic and thermodynamic parameters are given as the average of triplicate measurements with the standard error of measurement.

2.2.8. NMR Spectroscopy Data Collection

2.2.8.1. Theory

2.2.8.1.1. NMR Spectroscopy

Nuclear magnetic resonance (NMR) uses a large superconductive magnet to probe into the intrinsic spin properties of atomic nuclei. It uses radio frequency waves to manipulate the spins alignment to one's benefit. The basic principle of NMR is based on the quantum property of a nucleus i.e., the spin number, which depends on the distribution of the total protons and neutrons in a particular nucleus. Nucleus with an odd number of protons or an odd number of neutrons have a non-zero spin and are known to be NMR-active, for example, ^1H , ^{13}C , ^{15}N , ^{19}F , and ^{31}P (Levitt, 2008). Solution-state NMR spectroscopy concerns the nuclei having spin quantum number $\frac{1}{2}$. These spin $\frac{1}{2}$ nuclei exist in either parallel (low energy state/ α) or anti-parallel (high energy state/ β) to the direction of an external magnetic field. The distribution of spin in these states generates the bulk magnetization is parallel to the direction of the external magnetic field (B_0) in the z-axis. The bulk magnetization can be perturbed by applying an external oscillatory magnetic field using radio-frequency waves. While returning to its low energy state, energy is released to reach the equilibrium state of distribution. The released energy can be measured using coiled probes placed around the sample where signal is generated as the free induction decay (FID) of current which is later processed via Fourier transform to give an NMR spectrum (absorptive in nature) (Figure 2.2.8.1.1).

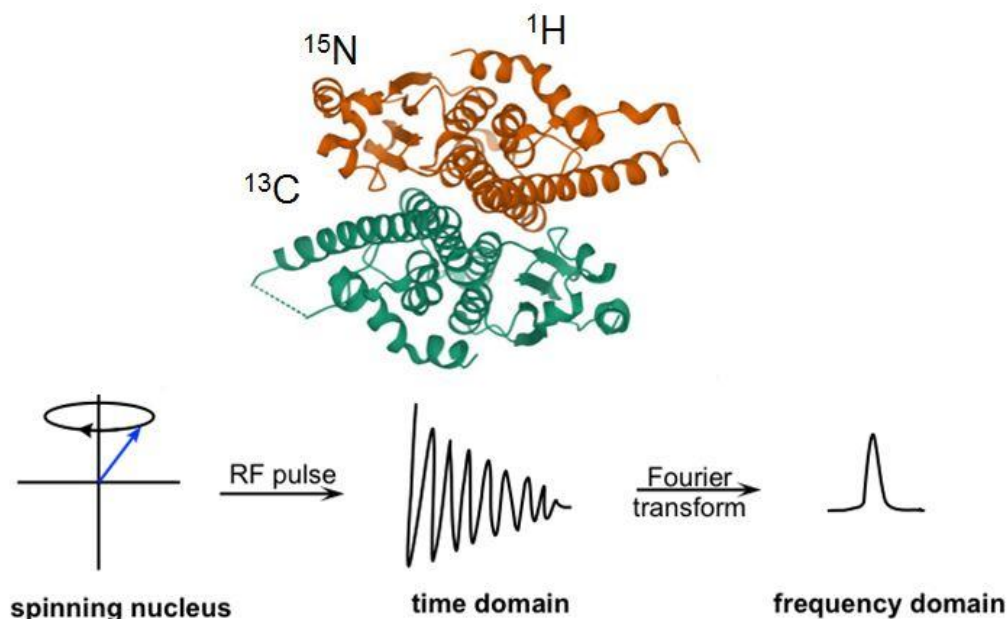


Figure 2.2.8.1.1: Protein labeled with NMR active nuclei ^1H , ^{13}C , and ^{15}N in protein. NMR signal generated by applying an radio frequency (RF) pulse to the spin active nuclei. Time domain signal is detected as a Free Induction Decay of current, which is Fourier transformed to get the frequency domain signal. Redrawn from (Liu, 2021).

Relaxation of bulk magnetization to the equilibrium state is related to its characteristic chemical environment, local interactions, and conformational dynamics. All these factors are manifested into resonance frequency and the line width of the signal. Thus, this resonance frequency acts as a fingerprint of a particular group of nuclei with a distinguishable chemical environment and is measured in parts per million (ppm). There are three important fundamental NMR observables: (1) Resonance frequency/chemical shift (δ), (2) Intensity (I) given by peak height or integrated area under the peak depicts on population of a particular nuclei in a given state, and (3) Linewidth (λ) is the peak width at half of maximum height of a peak, which is proportional to the transverse relaxation rate ($R_2 = 1/T_2$) and is sensitive to the local conformational dynamics/chemical exchange processes in a given timescale. Higher R_2 i.e rapidly relaxing signal of (B) will give shorter and broader line than (A) which has unique conformational dynamics signature in nature (Figure 2.2.8.1.2). The easily discernible differences in the linewidths provides us with site-specific information on protein dynamics.

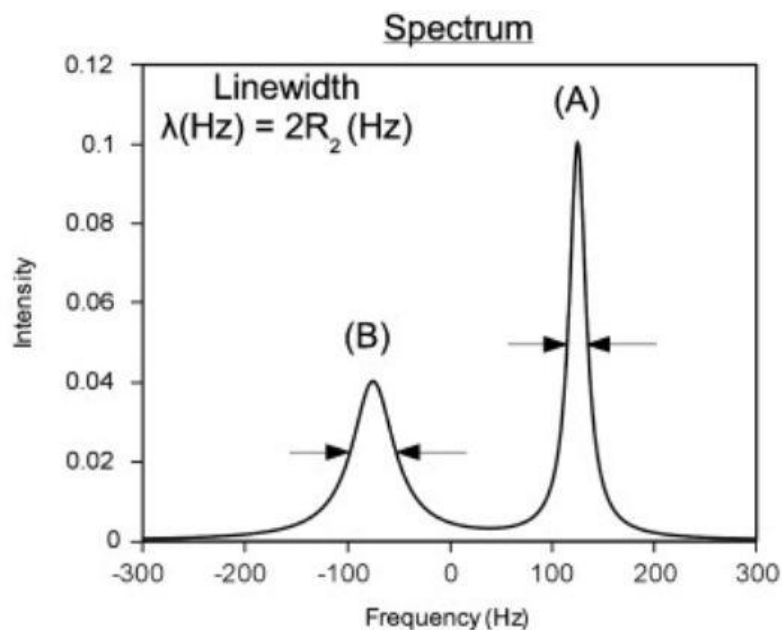


Figure 2.2.8.1.2: Linewidth (λ) differences of two different peak A and B affected by R_2 rates. Adapted from Klecner and Foster., *Biochim Biophys Acta.*, 2011.

NMR spectroscopy is a very powerful tool to get atomistic-level information of structure and dynamics of proteins. Chemical shifts are the most reliable and accurate parameter of NMR which gives us power to differentiate between various conformations of proteins. Structure determination by NMR (Wüthrich, 1989; Wüthrich, 1990; Cavalli et al., 2007) includes NMR spin active isotope labeling of proteins.

2.2.8.1.2. 2D Nuclear magnetic resonance spectroscopy

^1H - ^{15}N HSQC (heteronuclear single quantum coherence) is one of the most preliminary experiments for the study of proteins by NMR. The chemical shift is first evolved on the nitrogen nuclei and then transferred to the proton for detection. An HSQC spectrum gives us a set of peaks (contours) corresponding to a bond vector (backbone and side-chain of protein), correlating the proton and the nitrogen chemical shifts. Here, magnetization is transferred from ^1H to ^{15}N (t_1) and back to ^1H (t_2) nuclei via J-coupling, where t_1 and t_2 indicates chemical shift evolution steps.

2.2.8.1.3. 3D Nuclear magnetic resonance spectroscopy

The resonance assignment of the amide cross-peaks in the ^1H - ^{15}N HSQC spectrum is carried out by using a set of 3D double/triple resonance experiments. In the triple resonance experiments, the transfer of magnetization occurs from one nuclear spin to another via scalar coupling between various NMR active nuclei along the peptide chain (except for the NOE-based experiment, where the transfer of magnetization happens via dipolar coupling). For example, ^1H - ^{15}N -TOCSY-HSQC was recorded to identify a particular type of amino acid. Each of the amino acids has a unique pattern of TOCSY ^1H -correlation peaks in the third dimension corresponding to its side chain protons. Backbone sequential connections can be made by studying various experiments like ^1H - ^{15}N NOESY-HSQC (Fesik et al., 1990), HNC0, HN(CA)CO, HNCA, HN(CO)CA, HNN, CBCANH, and CBCA(CO)NH experiments where in addition to the self-nuclei chemical shift, one also gets information of its neighboring (a list is given in Table 2.2.8.1.3) (in primary sequence) residue nuclei in the third dimension coupled to backbone N-H (K. Chen et al., 2010; Inagaki, 2013; Yamazaki et al., 1994). For example, the HNN experiment gives us information on the sequential connectivity of backbone amide nitrogens of the preceding and succeeding amino acids (Panchal et al., 2001). Another experiment, HN(CA)CO, gives us information on the carbonyl group of the self and preceding residue (Meissner & Sørensen, 2001). A 3D triple resonance experiment can probe the side chain carbons groups as well. Using these experiments sequentially helps us link the backbone NH groups and side-chain carbons and protons.

Table 2.2.8.1.3.: Information acquired from the 3rd dimension for every corresponding NH peak in HSQC in various triple resonance experiments.

Experiment	Peaks in 3 rd Dimension
HNCA	$C\alpha_i, C\alpha_{i-1}$

HN(CO)CA	$C\alpha_{i-1}$
CBCANH	$C\alpha_i, C\alpha_{i-1}, C\beta_i, C\beta_{i-1}$
CBCA(CO)NH	$C\alpha_{i-1}, C\beta_{i-1}$
HNCO	C'_{i-1}
HN(CA)CO	C'_i, C'_{i-1}
HNN	$N_{Hi}, N_{Hi-1}, N_{Hi+1}$

2.2.8.1.4. NMR relaxation experiments

The protein flexibility is directly linked to its activity. Spin relaxation methods of proteins most commonly probe the amide ^{15}N spin, which will elucidate the motion of the protein backbone at atomic resolution (Jarymowycz & Stone, 2006; Kleckner & Foster, 2011; Palmer, 2004). NMR is a very powerful tool for measuring protein dynamics for multiple reasons: (i) Sensitive over a wide range of time scales of movement ranging from picoseconds – hours (Figure 2.2.8.1.4); (ii) Quantifiable under equilibrium conditions; (iii) Quantifiable using multiple probes at the same time.; and (iv) Large selection of experiments for quantification. For example, T_1 relaxation experiments determine the rate at which the bulk magnetization returns to the equilibrium along the z-axis. $T_{1\rho}$ is given by the decay of bulk magnetization spin-locked along the direction of the external magnetic field. $[^1\text{H}]-^{15}\text{N}$ -nOe experiments serve with the information about the motion/flexibility of individual NH bonds.

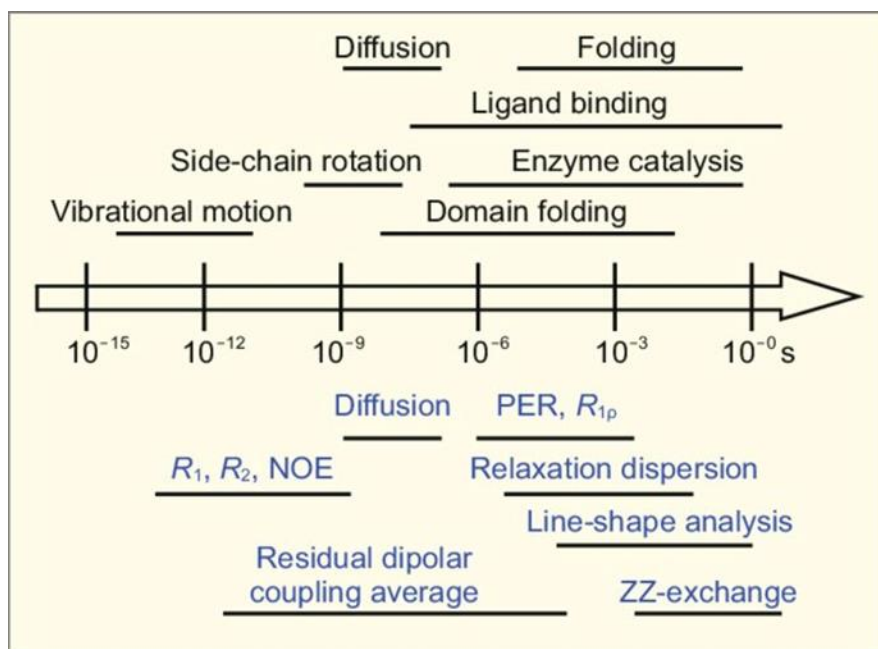


Figure 2.2.8.1.4: Protein dynamics at different timescales probable through different NMR experiments, having functional implications in the protein. Adapted from (Li et al., 2013).

2.2.8.1.5. ps-ns dynamics in proteins probed by Nuclear Spin Relaxation experiments

Nuclear spin relaxation experiments can detect protein motions at the ps–ns timescale by: (1) Longitudinal relaxation rates, R_1 , (2) Transverse relaxation rates R_2 , and (3) heteronuclear nuclear Overhauser effects (*hetNOE*) (Kempf & Loria, 2003; Jarymowycz & Stone, 2006; Igumenova et al., 2006). The physical processes involved in protein in this time frame are bond vibration, librations, side chain rotation/ interconversion, free random coil or loop movement, and rotation of backbone torsional angles (Figure 2.2.8.1.4) (Kleckner & Foster, 2011; Li et al., 2013). R_1 refers to the rate at which the bulk magnetization recovers to the equilibrium along the z-axis. It is determined by an inversion recovery experiment where the bulk magnetization is first inverted in the z-axis and then allowed to relax back using a set of delay periods, followed by detection in the x-y plane. R_2 rates define the loss of coherence of magnetization in the x-y plane and are also sensitive to ms- μ s timescale motions in the biomolecule. *hetNOE* indicates the flexibility of the spin through-space dipolar coupling. Quantifying any motion in this time scale can be achieved by using a time-dependent rotational correlation function/ $C(t)$, or a spectral-density function $J(\omega)$.

The equations for the relation between the spectral density function $J(\omega)$ and the R_1 , R_2 , and *hetNOE* are given by the following equations (Kay et al., 1989):

$$R_1(X) = \frac{d^2}{4} [J(\omega_H - \omega_X) + 3J(\omega_X) + 6J(\omega_H + \omega_X)] + c^2 J(\omega_X) \quad (2.2.8.1.5.1)$$

$$R_2(X) = \frac{d^2}{8} [4J(0) + J(\omega_H - \omega_X) + 3J(\omega_X) + 6J(\omega_H) + 6J(\omega_H + \omega_X)] + \frac{c^2}{6} [4J(0) + 3J(\omega_X)] + R_{ex} \quad (2.2.8.1.5.2)$$

$$hetNOE = 1 + \frac{d^2}{4R_1} \frac{\gamma_H}{\gamma_X} [6J(\omega_H + \omega_X) - J(\omega_H - \omega_X)] \quad (2.2.8.1.5.3)$$

where, X signifies ^{13}C or ^{15}N nucleus attached to the ^1H nucleus, ω_X denotes Larmor frequency of the nucleus X, d is $(\mu_0 h \gamma_H \gamma_X / 8\pi^2) (r_{HX}^{-3})$ indicating the dipolar interaction between H and X directly attached with the distance between them r_{HX} , μ_0 is the permeability of free space, h is the Planck's constant, γ_H and γ_X are the gyromagnetic ratio for the nuclei H and X, c is equal to $(\Delta\sigma_X / \sqrt{3})$ with $\Delta\sigma_X$ as the chemical shift anisotropy (CSA) of the X nucleus.

Model-free analysis of ps-ns timescale relaxation data was developed by Lipari and Szabo (Lipari & Szabo, 1982; Lipari & Szabo, 1982b). Extended model-free analysis developed by Clore *et al.* is now commonly used for the interpretation of the fast dynamics data (Clore et al., 1990). This approach forms an assumption that the internal motion of the spin is independent of the macromolecular rotation and is much faster than it. Since there is no particular pre-described structural model to define the spin motions, it is hence named as model-free. However, the motions are defined by the following 4 parameters: (1) Rotational diffusion tensor “ D ”, describes the three-dimensional motion of the spin and comprises of D_{xx} , D_{yy} , and D_{zz} , (2) Site-specific (atomic) correlation time (τ_e or τ_i) defines the timescale of bond rotation, further classified into fast and slow motions ($\tau_{e,fast}$ and $\tau_{e,slow}$), (3) Squared order parameter S^2 defines motion of a

bond vector in a cone, further classified into fast and slow components (S^2_{fast} and S^2_{slow}), and (4) Exchange broadening/ R_{ex} sensitive to the R_2 rates from μs – ms chemical exchange (Equation 2.2.8.1.5.2). S^2 is related to the semi-cone angle θ as a cosine function, so that

$$S^2 = [(1/2) (\cos \theta) (1 + \cos \theta)]^2 \quad (2.2.8.1.5.4)$$

The larger θ indicates higher flexibility with S^2 value close to 0 and smaller θ indicates rigid NH vector with S^2 value near to 1.

2.2.8.1.6. μs - ms dynamics by Relaxation Dispersion (RD) experiments

Nuclei depicting slow exchange (μs - ms regime) can be thought of as distributed between two states (ground and excited) separated by an energy barrier (assuming a two-state model). The ground (A) and excited state (B) have two different resonance frequencies (chemical ν_A and ν_B) and chemical shifts ($\Delta\nu = |\nu_A - \nu_B|$). The appearance of respective peaks depends on the population of each of these states (P_A and P_B), on the exchange rate ($k_{\text{ex}} = k_A + k_B$), and on their chemical shift difference ($\Delta\nu$). Motions in this time frame are quantified by exchange contribution given by R_{ex} and is related to the R_2 rate as given by the below equation:

$$R_{2,\text{eff}} = R_2^0 + R_{\text{ex}} \quad (2.2.8.1.6.1)$$

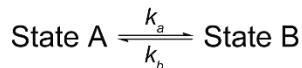
CPMG (Carr-Purcell-Maiboom-Gill) RD experiment is the most common experiment used for the characterization of the slow dynamics in 0.3-10 ms timescale regime (Tollinger et al., 2001). This experiment uses a Spin-Echo scheme ($\tau - 180^\circ - \tau$), where the spins are allowed to dephase in the x-y plane and then again refocused by the 180° pulse. In the presence of any sort of exchange, the exchange between the two states leads to the dephasing of the signal and thus results in line broadening. Each Spin-Echo block refocuses the magnetization during evolution time. The extent of refocusing increases with the increase in the frequency of application of the Spin-Echo block. This frequency of the application of the Spin-Echo block is known as the CPMG frequency ($\nu_{\text{CPMG}} = 1/4\tau$). A set of ^1H - ^{15}N HSQC spectra is recorded with increasing ν_{CPMG} , within a fixed relaxation time (T_{relax}). Effective transverse relaxation rates ($R_{2,\text{eff}}$) for CPMG relaxation

dispersion experiments, at each CPMG frequency, were extracted using the following Equation 2.2.8.1.6.2:

$$R_{2eff} = \frac{1}{T_{relax}} \log\left(\frac{I_0}{I_{vcpmg}}\right) \quad (2.2.8.1.6.2)$$

where, I_0 is the peak intensity in the absence of any CPMG block applied and I_{vcpmg} indicates the peak intensity in presence of a CPMG block with ν frequency.

Heteronuclear Adiabatic Relaxation Dispersion (HARD) exploits a hyperbolic secant family (HSn, n is the stretching factor) of adiabatic pulses (Tannús & Garwood, 1997) that locks the magnetization in the rotating frame (Mangia et al., 2009; Mangia et al., 2010; Traaseth et al., 2012). This method is advantageous over the traditional $R_{1\rho}$ type experiments as the applied spin-lock fields are able to cover the whole range of protein backbone NH spectral width, thus avoiding the need for data collection at multiple fields. The strength of the applied RF field strength is tweaked by modifying the phase and amplitude of the pulse, which is easily achieved by changing the shape of the pulse through the stretching factor (n). Longitudinal/ $R_{1\rho}$ and transverse/ $R_{2\rho}$ relaxation rates in the rotating frame with increasing relaxation delays. The applied magnetic field strength increases with increasing ‘n’. Thus, an increase in $R_{1\rho}$ rate and decrease in $R_{2\rho}$ rate is expected with the increase in ‘n’. The R_1 , $R_{1\rho}$, and $R_{2\rho}$ relaxation rates obtained from the HARD experiments, and the subsequent k_{ex} , and p_A were calculated by fitting the R_1 , $R_{1\rho}$, and $R_{2\rho}$ data to a two-state model using numerical fittings as described (Chao & Byrd, 2016). A grid search by Monte Carlo method from the solution surfaces of the data points generated from the Bloch-McConnell equation (Equation 2.2.8.1.6.3) by geometric approximation method allowed to extract the chemical exchange parameters, which included exchange rate between two states – state A and B – (k_{ex}) (Equation 2.2.8.1.6.4), chemical shift difference between the two states (δ) and populations of the two states (p_B). The errors in different fitted parameters were obtained using 500 Monte-Carlo simulations in addition to the duplicate relaxation data points. The classical model for a two sites exchange can be expressed by the Bloch–McConnell equation (McConnell, 1958), which has been used extensively to describe the evolution of the bulk magnetization (M_z) of a nuclear spin ensemble under chemical exchange in NMR spectroscopy. The equation assuming a two-site exchange model is given by:



$$\frac{d}{dt} \begin{bmatrix} N_{ax} \\ N_{bx} \\ N_{ay} \\ N_{by} \\ N_{az} \\ N_{bz} \end{bmatrix} = \begin{bmatrix} -k_a - R_2 & k_b & -\delta_a & 0 & \omega_1 & 0 \\ k_a & -k_b - R_2 & 0 & -\delta_b & 0 & \omega_1 \\ \delta_a & 0 & -k_a - R_2 & k_b & 0 & 0 \\ 0 & \delta_b & k_a & -k_b - R_2 & 0 & 0 \\ -\omega_1 & 0 & 0 & 0 & -k_a - R_1 & k_b \\ 0 & -\omega_1 & 0 & 0 & k_a & -k_b - R_1 \end{bmatrix} \begin{bmatrix} N_{ax} \\ N_{bx} \\ N_{ay} \\ N_{by} \\ N_{az} \\ N_{bz} \end{bmatrix} + R_1 \begin{bmatrix} 0 \\ 0 \\ 0 \\ 0 \\ N_{a0} \\ N_{b0} \end{bmatrix} \quad (2.2.8.1.6.3)$$

$$k_{\text{ex}} = k_A + k_B \quad (2.2.8.1.6.4)$$

where, k_a and k_b are the forward and reverse reaction rates respectively; δ_a and δ_b is the resonance offset of ground state (A) and excited state (B) w.r.t radiofrequency (RF) pulse; ω_1 is the amplitude of the RF pulse; R_1 and R_2 the longitudinal and transverse relaxation rates; N_{ij} is the nuclear magnetization, where $i = a, b$ denotes state A or B respectively, and $j = x, y, z$ defines bulk magnetization components in x-, y-, and z-direction, respectively. The geometric approximation provides solution surfaces by assuming the $R_{1\rho}$ and $R_{2\rho}$ rates as a linear combination of R_1 , R_2 , and R_{ex} for each pre-defined set of dynamic parameters (k_{ex} , p_A , $\Delta\omega$, and offset). Thus, a rigorous grid search by the Monte Carlo method of these solution surfaces helps us to examine the exchange parameters best fit to the observed dispersion in $R_{1\rho}$ and $R_{2\rho}$ rates. This method can probe into motions over a wider range of 10 μs – 10 ms motions than CPMG RD. Hence, it is very informative in extracting a wide range of slow dynamics in a protein. The slow μs -ms timescale motions are sensitive to the conformational/chemical exchange arising from protein catalysis, ligand-binding, folding-unfolding, etc. (Boehr et al., 2006; Loria et al., 2008; Hansen et al., 2008).

2.2.8.2. Experimental Data Collection

All the NMR experiments were recorded at 298 K either on: 1) AscendTM Bruker AVANCE III HD 14.1 Tesla (600 MHz) NMR spectrometer equipped with a quad-channel ($^1\text{H}/^{13}\text{C}/^{15}\text{N}/^{19}\text{F}$) Cryoprobe (in-house); or on 2) AscendTM Bruker Avance AV 18.89 Tesla (800 MHz) NMR spectrometer equipped with a triple-channel ($^1\text{H}/^{13}\text{C}/^{15}\text{N}$) Cryoprobe and a Broad Band Inverse probe (located at National Facility for High-Field NMR at TIFR, Mumbai). The ^1H -

^{15}N HSQC spectrum was collected with 2048 and 128 points and 12 ppm and 28 ppm spectral width in ^1H and ^{15}N dimensions, respectively, giving an acquisition time of 100 ms in the direct dimension. An inter-scan delay of 1.0 s and 4 scans were used on a 1 mM ^{15}N -labeled TRBP2-dsRBD2 sample in a 5 mm Shigemi tube (Shigemi Co., LTD., Tokyo, Japan) (Takeda et al., 2011). ^1H - ^{15}N TOCSY-HSQC (mixing times = 60, 80, and 120 ms) and ^1H - ^{15}N NOESY-HSQC (mixing times = 150, 300, and 400 ms) were recorded on a 600 MHz NMR spectrometer on ^{15}N -labeled TRBP2-dsRBD2 (Cavanagh, 2007). Further, triple resonance experiments like HNCO, HN(CA)CO, HNCA, HN(CO)CA, HNN, CBCANH, and CBCA(CO)NH were carried out using 1.2 mM of ^{15}N - ^{13}C -labeled TRBP2-dsRBD2 sample in a 5 mm Shigemi tube. All the NMR data were processed via TopSpin/NMRPipe (Delaglio et al., 1995) and were analyzed in SPARKY/CARA (W. Lee et al., 2015; Keller., 2004).

For NMR-based titration assays, ^1H - ^{15}N -HSQCs were measured on TRBP2-dsRBD2 (50 μM) with increasing concentrations of duplex RNAs from 0.05–0.2 (in the case of D12 RNA 0.05–5 equivalents) equivalents of the protein. After every RNA addition, the protein was allowed to equilibrate for 30 mins before acquiring ^1H - ^{15}N HSQC. Peak intensities were plotted against the RNA:protein concentration for each residue and were fit to the one-site binding isotherm using the below equation (Williamson, 2013):

$$\Delta\delta_{obs} = \Delta\delta_{max} \left\{ \frac{([P]_t + [L]_t + K_d) - \sqrt{([P]_t + [L]_t + K_d)^2 - 4[P]_t[L]_t}}{2[P]_t} \right\} \quad (2.2.8.2.1)$$

where, $\Delta\delta_{obs}$ is the change in the observed chemical shift from the apo state, $\Delta\delta_{max}$ is the maximum chemical shift change on saturation with ligand, $[P]_t$ and $[L]_t$ are the total concentration of protein and ligand, respectively, and K_d is the dissociation constant.

Apo-TRBP-dsRBD2 nuclear spin relaxation experiments (R_1 , R_2 , and $[^1\text{H}]\text{-}^{15}\text{N}$ -nOe) were recorded at two different field strengths (600 and 800 MHz NMR spectrometers) on a 1 mM ^{15}N -TRBP2-dsRBD2 sample in a 5 mm Shigemi tube. ^{15}N longitudinal relaxation rates (R_1) were recorded with 8 inversion recovery delays of 10, 30*, 50, 100, 200, 300, 450*, and 600 ms. ^{15}N transverse relaxation rates (R_2) were recorded with 8 CPMG (Carr-Purcell-Meiboom-Gill) delays

of 17, 34*, 51, 68, 85, 102, 136*, and 170 ms. Steady-state $[^1\text{H}]-^{15}\text{N}$ heteronuclear nOe experiments were recorded with and without ^1H saturation with a relaxation delay of 5 s.

All D12-bound TRBP-dsRBD2 nuclear spin relaxation experiments were recorded in a similar fashion as the apo-protein on a 1 mM ^{15}N -TRBP2-dsRBD2 in the presence of 50 μM D12 RNA in a 3 mm NMR tube. The ^{15}N - R_1 rates were measured with 5 inversion recovery delays of 10, 30*, 70, 150, and 600 ms on 600 MHz spectrometer and 10, 70*, 150, 300, and 600* ms on 800 MHz spectrometer. The ^{15}N - R_2 rates were measured with 5 CPMG delays of 17, 51, 85, 136*, and 170 ms on 600 MHz spectrometer and with 4 CPMG delays of 17, 34*, 51, and 68 ms on 800 MHz spectrometer with a CPMG loop length of 17 ms.

For ^{15}N relaxation dispersion measurement, a constant time CPMG (Carr-Purcell-Meiboom-Gill) experiment (Tollinger et al., 2001) was recorded on a 600 MHz NMR spectrometer. CPMG relaxation dispersion experiments for apo- and D12-bound ^{15}N -TRBP2-dsRBD2 were acquired separately, consisting of 15 data points with ν_{cpmg} values of 25, 50, 75, 125*, 175, 275, 375*, 525, 675, 825*, and 1000 Hz at a constant relaxation time – T_{relax} (40 ms).

Heteronuclear Adiabatic Relaxation Dispersion (HARD) experiments (Mangia et al., 2010; Traaseth et al., 2012; Chao & Byrd, 2016) were recorded on apo- and D12-bound ^{15}N -TRBP2-dsRBD2 on the 600 MHz NMR spectrometer. A composite pulse comprised of four hyperbolic secant family of pulse (HSn) with increasing stretching factors ($n = 1,2,4,6,8$). The increasing stretching factors created an increasing effective spin-lock field applied to produce relaxation dispersion in $R_{1\rho}$ and $R_{2\rho}$ experiments. Each pulse delay was of 16 ms and variation of delays were achieved by using multiple sets of these pulses. The relaxation delays used for $R_{1\rho}$ were 0, 16, 32, 64, 96, and 128 ms for apo-; and 0, 16, 32, 64, and 112 ms for D12-bound ^{15}N TRBP2-dsRBD2, respectively. For $R_{2\rho}$ experiments, the relaxation delays used were 0, 16, 32, and 64 ms for apo- and 0, 16, and 32 ms for D12-bound ^{15}N -TRBP2-dsRBD2. R_1 experiments were acquired similarly to $R_{1\rho}$ and $R_{2\rho}$ experiments without using the adiabatic pulse during evolution. The delays used for the R_1 experiment were 16, 48, 96, 160, 224, 320, 480, and 640 ms for both apo- and RNA-bound protein samples.

All relaxation experiments were measured using a single scan interleaving method, and the order of delays was randomized. The time periods marked with an asterisk have been recorded in duplicates for error estimation. An inter-scan delay of 2.5 s was used for all the above-mentioned relaxation experiments (unless mentioned otherwise).

2.2.9. NMR Relaxation Data Analysis

NMR spectra were processed with either TopSpin 3.5pl6 or NMRPipe and visualized through SPARKY (version 3.115).

Different relaxation rates like $R_1/R_2/R_{1\rho}/R_{2\rho}$ were calculated using mono-exponential decay fitting of peak height against the corresponding set of relaxation delays in a Mathematica script employing the equation below (Spyracopoulos, 2006):

$$I(t) = I(0)e^{-R_x t} \quad (2.2.9.1)$$

where, $I(t)$ and $I(0)$ represent peak intensity at delay time t and 0, respectively; R_x represents various relaxation rates, and t represents the delays used in the experiments.

The errors in different fitted parameters were obtained using 500 Monte-Carlo simulations in addition to the duplicate relaxation data points. Steady-state $[^1\text{H}]-^{15}\text{N}$ nOes for individual residues were calculated as a ratio of the corresponding residue peak height in the spectra recorded in the presence and absence of ^1H saturation.

The equations for the relation between the spectral density function $J(\omega)$ and the measured residue-specific relaxation parameters (R_1 , R_2 , and *het*NOE) are given by equations (2.2.8.1.5.1-3) (Kay et al., 1989).

Additional analysis of ^{15}N -relaxation data was conducted using the extended model-free formalism via Relax v4.0.3 software (Bieri et al., 2011). For this analysis, the ^{15}N -relaxation data (R_1 , R_2 , $[^1\text{H}]-^{15}\text{N}$ nOe) measured at two different magnetic fields (600 MHz and 800 MHz) was used. The default parameters of N-H distance and CSA values of 1.02 Å and -172 ppm were used to set the dipole-dipole interactions between ^1H and ^{15}N . The structure of TRBP-dsRBD2 available with PDB ID 2CPN was used for model-free analysis. The initial estimates of global diffusion

tensor values for diffusion models, namely isotropic, axially symmetric, and anisotropic, were obtained by using the quadric_diffusion program (L. K. Lee et al., 1997). The analysis in the Relax program was initiated by the optimization of local t_m models without any global diffusion model defined. Then, using the global diffusion tensor parameters obtained from quadric_diffusion program, internal model-free models were optimized from ten models defined in the Relax. The best model was selected based on Akaike's information criteria. Following this, global diffusion parameters were further optimized by fixing the internal model-free models. This process was iterated until all the parameters were converged. The best global diffusion model was then selected based on chi-squared values. The best model-free and diffusion model parameters were then used for error calculations by the Monte-Carlo method. R_2 rates of a particular spin is sensitive to ps-ns as well as μ s-ms timescale dynamics. From Equation 2.2.8.1.5.2, we see that R_2 rates are influenced by the R_{ex} component. This R_{ex} value represents the μ s-ms timescale dynamics contribution of a particular spin.

Effective transverse relaxation rates (R_{2eff}) for CPMG relaxation dispersion experiments, at each CPMG frequency, were extracted using the following equation:

$$R_{2eff} = \frac{1}{T_{relax}} \log\left(\frac{I_0}{I_{vcpmg}}\right) \quad (2.2.9.5)$$

where, I_0 is the peak intensity in the absence of any CPMG block applied and I_{vcpmg} indicates the peak intensity in presence of a CPMG block with v frequency.

The R_1 , $R_{1\rho}$, and $R_{2\rho}$ relaxation rates obtained from the HARD experiments, and the subsequent k_{ex} , and p_A were calculated by fitting the R_1 , $R_{1\rho}$, and $R_{2\rho}$ data to a two-state model using numerical fittings as described (Chao & Byrd, 2016). A grid search by Monte Carlo method from the solution surfaces of the data points generated from the Bloch-McConnell equation (Equation **Error! No text of specified style in document.**2.9.1) by geometric approximation method allowed to extract the chemical exchange parameters which included exchange rate between two states – state A and state B – (k_{ex}) (Equation **Error! No text of specified style in document.**2.9.7), chemical shift difference between the two states (k_{ex}) and populations of the two states (p_B). The errors in different fitted parameters were obtained using 500 Monte-Carlo simulations in addition to the duplicate relaxation data points. The classical model for a two sites

exchange can be expressed by the Bloch–McConnell equation (McConnell, 1958), which has been used extensively to describe the evolution of the bulk magnetization (M_z) of a nuclear spin ensemble under chemical exchange in NMR spectroscopy. The equation assuming a two-site exchange model is given by:

$$\text{State A} \xrightleftharpoons[k_b]{k_a} \text{State B}$$

$$\frac{d}{dt} \begin{bmatrix} N_{ax} \\ N_{bx} \\ N_{ay} \\ N_{by} \\ N_{az} \\ N_{bz} \end{bmatrix} = \begin{bmatrix} -k_a - R_2 & k_b & -\delta_a & 0 & \omega_1 & 0 \\ k_a & -k_b - R_2 & 0 & -\delta_b & 0 & \omega_1 \\ \delta_a & 0 & -k_a - R_2 & k_b & 0 & 0 \\ 0 & \delta_b & k_a & -k_b - R_2 & 0 & 0 \\ -\omega_1 & 0 & 0 & 0 & -k_a - R_1 & k_b \\ 0 & -\omega_1 & 0 & 0 & k_a & -k_b - R_1 \end{bmatrix} \begin{bmatrix} N_{ax} \\ N_{bx} \\ N_{ay} \\ N_{by} \\ N_{az} \\ N_{bz} \end{bmatrix} + R_1 \begin{bmatrix} 0 \\ 0 \\ 0 \\ 0 \\ N_{a0} \\ N_{b0} \end{bmatrix} \quad (\text{Error! No text of specified style in document..2.9.2})$$

$$k_{\text{ex}} = k_A + k_B \quad (2.2.9.7)$$

where, k_a and k_b are the forward and reverse reaction rates respectively; δ_a and δ_b is the resonance offset of ground state (A) and excited state (B) w.r.t radiofrequency (RF) pulse; ω_1 is the amplitude of the RF pulse; R_1 and R_2 the longitudinal and transverse relaxation rates; N_{ij} is the nuclear magnetization, where $i = a, b$ denotes state A or B respectively, and $j = x, y, z$ defines bulk magnetization components in x-, y-, and z-direction, respectively.

2.2.10. Backbone Assignment and Structure Calculation

For the backbone resonance assignment, CARA (Computer Aided Resonance Assignment) was used (Keller., 2004). A project was created for TRBP2-dsRBD2. The sequence of the protein was fed as a .seq file to the project. All the input NMR spectra were fed in the form of either ucsf or 3rrr file formats. Manual peak picking was done for double and triple-resonance NMR experiments using a synchroscope in CARA. Further identification, confirmation, and assignment of residues were done in a stripscope mode following the CARA manual. TALOS-N (Shen & Bax, 2013) was used to predict the backbone and sidechain torsion angles from chemical shifts assigned

from CARA. The input to the TALOS-N server (spin.niddk.nih.gov/bax/nmrserver/talosn) was a .tab file. This .tab file was exported from CARA executing the “WriteTalosFiile” LUA script as directed by the CARA wiki. TALOS-N gave out several output files which were visualized in jRAMA java viewer (spin.niddk.nih.gov/bax/software/TALOS-N/JRAMA) to check the quality of torsion angle predictions. jRAMA only runs on the latest JAVA update. “Tools” option in jRAMA was used to export a .aco angle restraint file from the prediction.

For structure calculation using CS-Rosetta (Shen et al., 2009; Shen et al., 2008, Bowers et al., 2000; Shen et al., 2010; Lange et al., 2012) program, the assigned residues were used as inputs as .tab file (TALOS format) in the BMRB CS-Rosetta program server (csrosetta.bmrwisc.edu/csrosetta/) to get an ensemble of the 10 lowest energy structures (.pdb file) out of total 3000 calculated.

Further, to incorporate NOE-based distance constraints to the structure of TRBP2-dsRBD2, POKY software was used (W. Lee et al., 2021). All the 3D NOESY spectra were processed in TopSpin 3.5pl6 and then converted into .ucsf files. A work folder was created with all the inputs (.seq, .prot, .pdb, .ucsf, and .aco) files required for the structure calculation. In the POKY Builder window, all the input files were imported from the respective work folder. After uploading all the raw files, they were preprocessed using AUDANA/AUDASA (W. Lee et al., 2016) automated with PACSY (W. Lee et al., 2012) boost on POKY servers (computing option). On completion of preprocessing, the job was submitted for Xplore-NIH-based (Schwieters et al., 2018) structure calculation. The results of the calculation were further refined and validated using various tools like Ramachandran plots (Ramachandran et al., 1963), Contact Maps, MolProbity Score (Chen et al., 2010; Williams et al., 2018), no. of distance, angle violations, etc in the POKY Analyzer window. The final ensemble of 20 lowest energy structure (.pdb file) was exported from the POKY Analyzer and visualized and compared to the other reported structures using UCSF Chimera and PyMOL.

References

- Bieri, M., d'Auvergne, E. J., & Gooley, P. R. (2011). relaxGUI: A new software for fast and simple NMR relaxation data analysis and calculation of ps-ns and μ s motion of proteins. *Journal of Biomolecular NMR*, *50*(2), 147–155. <https://doi.org/10.1007/s10858-011-9509-1>
- Boehr, D. D., McElheny, D., Dyson, H. J., & Wright, P. E. (2006). The dynamic energy landscape of dihydrofolate reductase catalysis. *Science (New York, N.Y.)*, *313*(5793), 1638–1642. <https://doi.org/10.1126/science.1130258>
- Bowers, P. M., Strauss, C. E., & Baker, D. (2000). De novo protein structure determination using sparse NMR data. *Journal of Biomolecular NMR*, *18*(4), 311–318. <https://doi.org/10.1023/a:1026744431105>
- Cavalli, A., Salvatella, X., Dobson, C. M., & Vendruscolo, M. (2007). Protein structure determination from NMR chemical shifts. *Proceedings of the National Academy of Sciences*, *104*(23), 9615–9620. <https://doi.org/10.1073/pnas.0610313104>
- Cavanagh, J. (2007). *Protein NMR spectroscopy: Principles and practice* (2nd ed.). Academic Press.
- Chao, F.-A., & Byrd, R. A. (2016). Geometric Approximation: A New Computational Approach To Characterize Protein Dynamics from NMR Adiabatic Relaxation Dispersion Experiments. *Journal of the American Chemical Society*, *138*(23), 7337–7345. <https://doi.org/10.1021/jacs.6b02786>
- Chen, K., Delaglio, F., & Tjandra, N. (2010). A practical implementation of cross-spectrum in protein backbone resonance assignment. *Journal of Magnetic Resonance (San Diego, Calif.: 1997)*, *203*(2), 208–212. <https://doi.org/10.1016/j.jmr.2009.12.018>
- Chen, V. B., Arendall, W. B., Headd, J. J., Keedy, D. A., Immormino, R. M., Kapral, G. J., Murray, L. W., Richardson, J. S., & Richardson, D. C. (2010). MolProbity: All-atom structure validation for macromolecular crystallography. *Acta Crystallographica. Section D, Biological Crystallography*, *66*(Pt 1), 12–21. <https://doi.org/10.1107/S0907444909042073>

Clore, G. M., Szabo, A., Bax, A., Kay, L. E., Driscoll, P. C., & Gronenborn, A. M. (1990). Deviations from the simple two-parameter model-free approach to the interpretation of nitrogen-15 nuclear magnetic relaxation of proteins. *Journal of the American Chemical Society*, *112*(12), 4989–4991. <https://doi.org/10.1021/ja00168a070>

Delaglio, F., Grzesiek, S., Vuister, G. W., Zhu, G., Pfeifer, J., & Bax, A. (1995). NMRPipe: A multidimensional spectral processing system based on UNIX pipes. *Journal of Biomolecular NMR*, *6*(3), 277–293. <https://doi.org/10.1007/BF00197809>

Fesik, S. W., Zuiderweg, E. R., Olejniczak, E. T., & Gampe, R. T. (1990). NMR methods for determining the structures of enzyme/inhibitor complexes as an aid in drug design. *Biochemical Pharmacology*, *40*(1), 161–167. [https://doi.org/10.1016/0006-2952\(90\)90191-m](https://doi.org/10.1016/0006-2952(90)90191-m)

Folta-Stogniew, E., & Williams, K. R. (1999). Determination of molecular masses of proteins in solution: Implementation of an HPLC size exclusion chromatography and laser light scattering service in a core laboratory. *Journal of Biomolecular Techniques: JBT*, *10*(2), 51–63.

Freire, E., Mayorga, O. L., & Straume, M. (1990). Isothermal titration calorimetry. *Analytical Chemistry*, *62*(18), 950A-959A. <https://doi.org/10.1021/ac00217a002>

Freyer, M. W., & Lewis, E. A. (2008). Isothermal titration calorimetry: Experimental design, data analysis, and probing macromolecule/ligand binding and kinetic interactions. *Methods in Cell Biology*, *84*, 79–113. [https://doi.org/10.1016/S0091-679X\(07\)84004-0](https://doi.org/10.1016/S0091-679X(07)84004-0)

Hansen, D. F., Vallurupalli, P., Lundström, P., Neudecker, P., & Kay, L. E. (2008). Probing chemical shifts of invisible states of proteins with relaxation dispersion NMR spectroscopy: How well can we do? *Journal of the American Chemical Society*, *130*(8), 2667–2675. <https://doi.org/10.1021/ja078337p>

Igumenova, T. I., Frederick, K. K., & Wand, A. J. (2006). Characterization of the fast dynamics of protein amino acid side chains using NMR relaxation in solution. *Chemical Reviews*, *106*(5), 1672–1699. <https://doi.org/10.1021/cr040422h>

Inagaki, F. (2013). Protein NMR Resonance Assignment. In G. C. K. Roberts (Ed.), *Encyclopedia of Biophysics* (pp. 2033–2037). Springer Berlin Heidelberg. https://doi.org/10.1007/978-3-642-16712-6_312

Jarymowycz, V. A., & Stone, M. J. (2006). Fast time scale dynamics of protein backbones: NMR relaxation methods, applications, and functional consequences. *Chemical Reviews*, *106*(5), 1624–1671. <https://doi.org/10.1021/cr040421p>

Kay, L. E., Torchia, D. A., & Bax, A. (1989). Backbone dynamics of proteins as studied by ¹⁵N inverse detected heteronuclear NMR spectroscopy: Application to staphylococcal nuclease. *Biochemistry*, *28*(23), 8972–8979. <https://doi.org/10.1021/bi00449a003>

Kempf, J. G., & Loria, J. P. (2003). Protein dynamics from solution NMR: Theory and applications. *Cell Biochemistry and Biophysics*, *37*(3), 187–211. <https://doi.org/10.1385/cbb:37:3:187>

Kleckner, I. R., & Foster, M. P. (2011). An introduction to NMR-based approaches for measuring protein dynamics. *Biochimica Et Biophysica Acta*, *1814*(8), 942–968. <https://doi.org/10.1016/j.bbapap.2010.10.012>

Lange, O. F., Rossi, P., Sgourakis, N. G., Song, Y., Lee, H.-W., Aramini, J. M., Ertekin, A., Xiao, R., Acton, T. B., Montelione, G. T., & Baker, D. (2012). Determination of solution structures of proteins up to 40 kDa using CS-Rosetta with sparse NMR data from deuterated samples. *Proceedings of the National Academy of Sciences of the United States of America*, *109*(27), 10873–10878. <https://doi.org/10.1073/pnas.1203013109>

Lee, L. K., Rance, M., Chazin, W. J., & Palmer, A. G. (1997). Rotational diffusion anisotropy of proteins from simultaneous analysis of ¹⁵N and ¹³C alpha nuclear spin relaxation. *Journal of Biomolecular NMR*, *9*(3), 287–298. <https://doi.org/10.1023/a:1018631009583>

Lee, W., Petit, C. M., Cornilescu, G., Stark, J. L., & Markley, J. L. (2016). The AUDANA algorithm for automated protein 3D structure determination from NMR NOE data. *Journal of Biomolecular NMR*, *65*(2), 51–57. <https://doi.org/10.1007/s10858-016-0036-y>

Lee, W., Rahimi, M., Lee, Y., & Chiu, A. (2021). POKY: A software suite for multidimensional NMR and 3D structure calculation of biomolecules. *Bioinformatics (Oxford, England)*, *37*(18), 3041–3042. <https://doi.org/10.1093/bioinformatics/btab180>

Lee, W., Tonelli, M., & Markley, J. L. (2015). NMRFAM-SPARKY: Enhanced software for biomolecular NMR spectroscopy. *Bioinformatics (Oxford, England)*, *31*(8), 1325–1327. <https://doi.org/10.1093/bioinformatics/btu830>

Lee, W., Yu, W., Kim, S., Chang, I., Lee, W., & Markley, J. L. (2012). PACSY, a relational database management system for protein structure and chemical shift analysis. *Journal of Biomolecular NMR*, *54*(2), 169–179. <https://doi.org/10.1007/s10858-012-9660-3>

Levenberg, K. (1944). A method for the solution of certain non-linear problems in least squares. *Quarterly of Applied Mathematics*, *2*(2), 164–168. <https://doi.org/10.1090/qam/10666>

Levitt, M. H. (2008). *Spin dynamics: Basics of nuclear magnetic resonance* (2nd ed). John Wiley & Sons.

Li, C., Tang, C., & Liu, M. (2013). Protein dynamics elucidated by NMR technique. *Protein & Cell*, *4*(10), 726–730. <https://doi.org/10.1007/s13238-013-3912-1>

Lipari, G., & Szabo, A. (1982a). Model-free approach to the interpretation of nuclear magnetic resonance relaxation in macromolecules. 1. Theory and range of validity. *Journal of the American Chemical Society*, *104*(17), 4546–4559. <https://doi.org/10.1021/ja00381a009>

Lipari, G., & Szabo, A. (1982b). Model-free approach to the interpretation of nuclear magnetic resonance relaxation in macromolecules. 2. Analysis of experimental results. *Journal of the American Chemical Society*, *104*(17), 4559–4570. <https://doi.org/10.1021/ja00381a010>

Liu, X. (2021, December 9). Organic Chemistry I. Pressbooks. <https://kpu.pressbooks.pub/organicchemistry>

Loria, J. P., Berlow, R. B., & Watt, E. D. (2008). Characterization of enzyme motions by solution NMR relaxation dispersion. *Accounts of Chemical Research*, *41*(2), 214–221. <https://doi.org/10.1021/ar700132n>

Mangia, S., Liimatainen, T., Garwood, M., & Michaeli, S. (2009). Rotating frame relaxation during adiabatic pulses vs. conventional spin lock: Simulations and experimental results at 4 T. *Magnetic Resonance Imaging*, 27(8), 1074–1087. <https://doi.org/10.1016/j.mri.2009.05.023>

Mangia, S., Traaseth, N. J., Veglia, G., Garwood, M., & Michaeli, S. (2010). Probing slow protein dynamics by adiabatic R(1rho) and R(2rho) NMR experiments. *Journal of the American Chemical Society*, 132(29), 9979–9981. <https://doi.org/10.1021/ja1038787>

Marquardt, D. W. (1963). An Algorithm for Least-Squares Estimation of Nonlinear Parameters. *Journal of the Society for Industrial and Applied Mathematics*, 11(2), 431–441. <https://doi.org/10.1137/0111030>

McConnell, H. M. (1958). Reaction Rates by Nuclear Magnetic Resonance. *The Journal of Chemical Physics*, 28(3), 430–431. <https://doi.org/10.1063/1.1744152>

Meissner, A., & Sørensen, O. W. (2001). Sequential HNCACB and CBCANH protein NMR pulse sequences. *Journal of Magnetic Resonance (San Diego, Calif.: 1997)*, 151(2), 328–331. <https://doi.org/10.1006/jmre.2001.2374>

Paithankar, H., Tarang, G. S., Parvez, F., Marathe, A., Joshi, M., & Chugh, J. (2022). Inherent conformational plasticity in dsRBDs enables interaction with topologically distinct RNAs. *Biophysical Journal*, 121(6), 1038–1055. <https://doi.org/10.1016/j.bpj.2022.02.005>

Palmer, A. G. (2004). NMR characterization of the dynamics of biomacromolecules. *Chemical Reviews*, 104(8), 3623–3640. <https://doi.org/10.1021/cr030413t>

Panchal, S. C., Bhavesh, N. S., & Hosur, R. V. (2001). Improved 3D triple resonance experiments, HNN and HN(C)N, for HN and ¹⁵N sequential correlations in (¹³C, ¹⁵N) labeled proteins: Application to unfolded proteins. *Journal of Biomolecular NMR*, 20(2), 135–147. <https://doi.org/10.1023/a:1011239023422>

R. Keller, *The computer aided resonance assignment tutorial*, 1st edn., 2004.

Ramachandran, G. N., Ramakrishnan, C., & Sasisekharan, V. (1963). Stereochemistry of polypeptide chain configurations. *Journal of Molecular Biology*, 7, 95–99. [https://doi.org/10.1016/s0022-2836\(63\)80023-6](https://doi.org/10.1016/s0022-2836(63)80023-6)

Saponaro, A. (2018). Isothermal Titration Calorimetry: A Biophysical Method to Characterize the Interaction between Label-free Biomolecules in Solution. *Bio-Protocol*, 8(15), e2957. <https://doi.org/10.21769/BioProtoc.2957>

Schwieters, C. D., Bermejo, G. A., & Clore, G. M. (2018). Xplor-NIH for molecular structure determination from NMR and other data sources. *Protein Science: A Publication of the Protein Society*, 27(1), 26–40. <https://doi.org/10.1002/pro.3248>

Shen, Y., & Bax, A. (2013). Protein backbone and sidechain torsion angles predicted from NMR chemical shifts using artificial neural networks. *Journal of Biomolecular NMR*, 56(3), 227–241. <https://doi.org/10.1007/s10858-013-9741-y>

Shen, Y., Bryan, P. N., He, Y., Orban, J., Baker, D., & Bax, A. (2010). De novo structure generation using chemical shifts for proteins with high-sequence identity but different folds. *Protein Science: A Publication of the Protein Society*, 19(2), 349–356. <https://doi.org/10.1002/pro.303>

Shen, Y., Lange, O., Delaglio, F., Rossi, P., Aramini, J. M., Liu, G., Eletsky, A., Wu, Y., Singarapu, K. K., Lemak, A., Ignatchenko, A., Arrowsmith, C. H., Szyperski, T., Montelione, G. T., Baker, D., & Bax, A. (2008). Consistent blind protein structure generation from NMR chemical shift data. *Proceedings of the National Academy of Sciences of the United States of America*, 105(12), 4685–4690. <https://doi.org/10.1073/pnas.0800256105>

Shen, Y., Vernon, R., Baker, D., & Bax, A. (2009). De novo protein structure generation from incomplete chemical shift assignments. *Journal of Biomolecular NMR*, 43(2), 63–78. <https://doi.org/10.1007/s10858-008-9288-5>

Spyracopoulos, L. (2006). A suite of Mathematica notebooks for the analysis of protein main chain ¹⁵N NMR relaxation data. *Journal of Biomolecular NMR*, 36(4), 215–224. <https://doi.org/10.1007/s10858-006-9083-0>

Takahashi, T., Zenno, S., Ishibashi, O., Takizawa, T., Saigo, K., & Ui-Tei, K. (2014). Interactions between the non-seed region of siRNA and RNA-binding RLC/RISC proteins, Ago and TRBP, in mammalian cells. *Nucleic Acids Research*, 42(8), 5256–5269. <https://doi.org/10.1093/nar/gku153>

Takeda, M., Hallenga, K., Shigezane, M., Waelchli, M., Löhr, F., Markley, J. L., & Kainosho, M. (2011). Construction and performance of an NMR tube with a sample cavity formed within magnetic susceptibility-matched glass. *Journal of Magnetic Resonance (San Diego, Calif.: 1997)*, 209(2), 167–173. <https://doi.org/10.1016/j.jmr.2011.01.005>

Tannús, A., & Garwood, M. (1997). Adiabatic pulses. *NMR in Biomedicine*, 10(8), 423–434. [https://doi.org/10.1002/\(sici\)1099-1492\(199712\)10:8<423::aid-nbm488>3.0.co;2-x](https://doi.org/10.1002/(sici)1099-1492(199712)10:8<423::aid-nbm488>3.0.co;2-x)

Tollinger, M., Skrynnikov, N. R., Mulder, F. A., Forman-Kay, J. D., & Kay, L. E. (2001). Slow dynamics in folded and unfolded states of an SH3 domain. *Journal of the American Chemical Society*, 123(46), 11341–11352. <https://doi.org/10.1021/ja011300z>

Traaseth, N. J., Chao, F.-A., Masterson, L. R., Mangia, S., Garwood, M., Michaeli, S., Seelig, B., & Veglia, G. (2012). Heteronuclear Adiabatic Relaxation Dispersion (HARD) for quantitative analysis of conformational dynamics in proteins. *Journal of Magnetic Resonance (San Diego, Calif.: 1997)*, 219, 75–82. <https://doi.org/10.1016/j.jmr.2012.03.024>

Williams, C. J., Headd, J. J., Moriarty, N. W., Prisant, M. G., Videau, L. L., Deis, L. N., Verma, V., Keedy, D. A., Hintze, B. J., Chen, V. B., Jain, S., Lewis, S. M., Arendall, W. B., Snoeyink, J., Adams, P. D., Lovell, S. C., Richardson, J. S., & Richardson, D. C. (2018). MolProbity: More and better reference data for improved all-atom structure validation. *Protein Science: A Publication of the Protein Society*, 27(1), 293–315. <https://doi.org/10.1002/pro.3330>

Williamson, M. P. (2013). Using chemical shift perturbation to characterise ligand binding. *Progress in Nuclear Magnetic Resonance Spectroscopy*, 73, 1–16. <https://doi.org/10.1016/j.pnmrs.2013.02.001>

Wüthrich, K. (1989). Protein structure determination in solution by nuclear magnetic resonance spectroscopy. *Science (New York, N.Y.)*, 243(4887), 45–50. <https://doi.org/10.1126/science.2911719>

Wüthrich, K. (1990). Protein structure determination in solution by NMR spectroscopy. *The Journal of Biological Chemistry*, 265(36), 22059–22062.

Wyatt, P. J. (1993). Light scattering and the absolute characterization of macromolecules. *Analytica Chimica Acta*, 272(1), 1–40. [https://doi.org/10.1016/0003-2670\(93\)80373-S](https://doi.org/10.1016/0003-2670(93)80373-S)

Yamazaki, T., Lee, W., Arrowsmith, C. H., Muhandiram, D. R., & Kay, L. E. (1994). A Suite of Triple Resonance NMR Experiments for the Backbone Assignment of ¹⁵N, ¹³C, ²H Labeled Proteins with High Sensitivity. *Journal of the American Chemical Society*, 116(26), 11655–11666. <https://doi.org/10.1021/ja00105a005>

Zimm, B. H. (1945). Molecular Theory of the Scattering of Light in Fluids. *The Journal of Chemical Physics*, 13(4), 141–145. <https://doi.org/10.1063/1.1724013>

Chapter 3

**Characterization of TRBP2-
dsRBD2 structure**

Introduction

TRBP2-dsRBD2 is a double-stranded RNA-binding domain (dsRBD). dsRBDs, in general, have a characteristic $\alpha\beta\beta\beta\alpha$ secondary structure motif, where the two α -helices fold onto the surface of the anti-parallel β -sheet formed by the three β -strands. Here, a combination of biophysical techniques was used to characterize TRBP2-dsRBD2. First, the protein was overexpressed in *E. coli* BL21 (DE3) cells and purified by performing a series of affinity and size exclusion chromatography steps. The purified protein was subjected to SEC-MALS (Folta-Stogniew & Williams, 1999, Wyatt, 1993, Zimm, 2004) analysis to determine the exact molecular mass of the protein in solution. To characterize the protein using solution-state NMR, ^{15}N - and/or ^{13}C -labeled protein was purified, and a battery of double and triple-resonance NMR experiments were recorded. These experiments helped determine the resonance assignment of various atoms of the protein. We started with recording the ^1H - ^{15}N -HSQC spectrum, where every peak in the 2D spectrum represented an N-H bond vector (backbone amide and side chain NHs). The ^1H - ^{15}N HSQC of TRBP2dsRBD2 (154–234 aa) was compared to previously assigned spectra of TRBP2-D1D2 construct (19–228 aa) (Benoit et al., 2013) and TRBP2-dsRBD2 construct (157–228 aa) (Yamashita et al., 2011) to transfer the backbone amide resonance assignments. The remaining resonance assignments were confirmed using the double and triple-resonance NMR experiments, as mentioned previously in the Materials and Methods (Ref. Section 2.2.8). For structure calculation, all the assigned chemical shifts were fed to the CS-ROSETTA (Shen, Vernon, Baker, & Bax, 2009, Shen et al., 2008, Bowers, Strauss, & Baker, 2000, Shen et al., 2010, Lange et al., 2012) server to get an ensemble of the 10 lowest energy structures out of a total of 3000 calculated. The primary, secondary, and tertiary structure of the two N-terminal dsRBDs of TRBP2: dsRBD1 and dsRBD2, were then compared with each other to identify their unique differences. Further, the AUDANA/AUDASA-assisted (Lee, Petit, Cornilescu, Stark, & Markley, 2016) Xplore-NIH-based structure calculation (Schwieters, Bermejo, & Clore, 2018) was used with the NOESY-based distance constraints in addition to the chemical shift information in the POKY Structure Builder (Lee, Rahimi, Lee, & Chiu, 2021). The resultant structure was further refined and validated using an integrated POKY Analyzer. The final ensemble of the 20 lowest energy structures was obtained.

Results and Discussion

3.1. Purification of TEV protease

The overexpression and purity of TEV protease was analyzed on SDS-PAGE by testing samples from various stages of the purification protocol. The induced TEV protease protein band was visible at ~45 kDa rather than 27 kDa (theoretically calculated mol. wt. of TEV protease) in SDS-PAGE (Figure 3.1A). Final purified TEV Protease (27 kDa) was obtained from a two-step purification process, i.e., Ni-NTA affinity chromatography, followed by size-exclusion chromatography (SEC) (Figure 3.1). The chromatogram obtained after SEC showed three prominent peaks. Among them, peak 2 and peak 3 (Figure 3.1B) corresponded to active TEV protease. On an average, a 2 L secondary culture yielded ~15 mg of TEV-protease. The final purified protein (Figure 3.1C) was stored as 50% glycerol stock at a concentration of 0.6 mg/ml at -20°C. TEV protease was required for performing cleavage of TRBP2-dsRBD2 overexpressed protein.

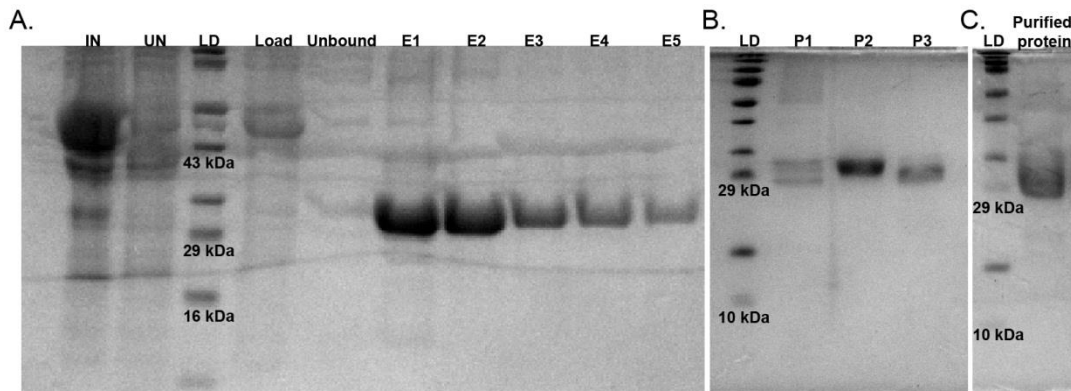


Figure 3.1: Overexpression and purification of TEV protease as seen in SDS PAGE. (A) Ni-NTA affinity chromatography (From LtoR: Induced (IN), Uninduced (UN), Ladder (LD), Total Soluble Protein (Load), Flow-through (Unbound), Elutions 1-5 (E1 to E5)). (B) Size exclusion chromatography protein profile (From LtoR: Ladder (LD), SEC peaks 1-3 (P1 to P3)). (C) Final purified TEV protease (27 kDa) (from L to R: Ladder (LD), Purified TEV protease)

3.2. Purification of TRBP2-dsRBD2

The cDNA for TRBP2-dsRBD2 was cloned in pHMGWA vector (Amp^R), and was expressed as a fusion protein having N-terminal His₆-Maltose binding protein (MBP) tag-TEV protease cleavage site followed by the protein of interest. The band for the overexpressed fusion

protein was observed at ~54 kDa (Figure 3.2.1A). Relatively pure protein was obtained after performing Ni-NTA chromatography (Figure 3.2.1B). Following this, it was subjected to TEV-protease cleavage of the MBP tag (~ 44 kDa) from TRBP2-dsRBD2 (~10 kDa) (Figure 3.2.1C). The theoretical isoelectric point (pI) of TRBP2-dsRBD2 is 9.5, whereas the pI of the MBP tag is 6. Thus, at the working pH 7.5, TRBP2-dsRBD2 will be positively charged, and the MBP tag will be negatively charged. Thus, cation exchange chromatography was performed to remove the MBP tag (negatively charged and remains in the flow-through) (Figure 3.2.1D). Size-exclusion chromatography (Figure 3.2.1E) was done to further purify the protein.

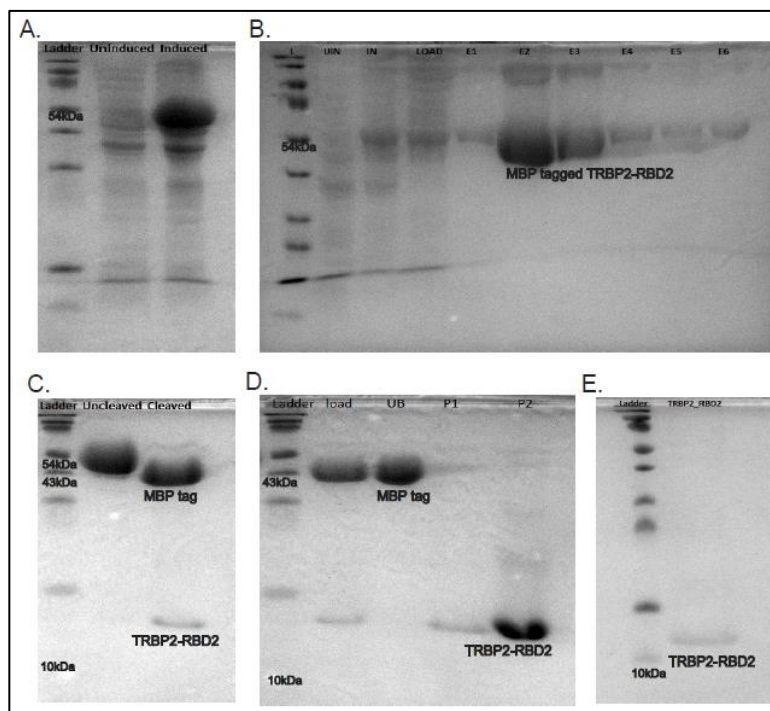


Figure 3.2.1: Overexpression and purification of TRBP2-dsRBD2. (A) Overexpression of TRBP2-dsRBD2 in *E. coli* BL21 (DE3) cells (from L to R: Ladder, Uninduced and Induced); (B) Ni-NTA affinity chromatography of the purified protein (from L to R: Ladder (L), Uninduced (UN), Induced (IN), Total soluble protein (Load), and Elutions 1 to 6 (E1 to E6) (C) MBP tag cleavage using TEV protease (from L to R: Ladder, Uncleaved protein, Cleaved protein); (D) Separation of MBP tag and TRBP2-dsRBD2 using cation-exchange chromatography (from L to R: Ladder, Total soluble protein (Load), Unbound protein (UB), and purified protein fractions (P1-P2); and (E) Size-exclusion chromatography of the final purified TRBP2-dsRBD2 (from L to R: Ladder and Purified TRBP2-dsRBD2).

The final yield of pure protein (Figure 3.2.2) was ~2 mM for the unlabeled protein and ~1 mM for the labeled protein (^{15}N or ^{15}N - ^{13}C , as required) in 350 μl from a 2 L prep.

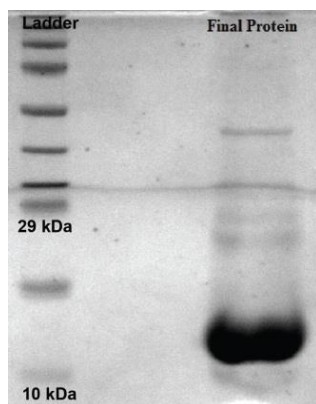


Figure 3.2.2.: Final purified TRBP2-dsRBD2 domain (From L-R: Ladder, empty well, Final concentrated purified TRBP2-dsRBD2).

3.3. Estimation of molecular mass of TRBP2-dsRBD2

A single overlapping peak of the UV absorbance and Rayleigh ratio curves indicated the presence of only one species of protein with a particular molecular weight (Figure 3.3). The size exclusion column was calibrated with bovine serum albumin (BSA) and the molecular mass of the protein was found to be 9.2 kDa. Thus, from the SEC-MALS analysis, it was concluded that the protein TRBP2-dsRBD2 was monomeric in nature with a molecular weight of 9.2 kDa.

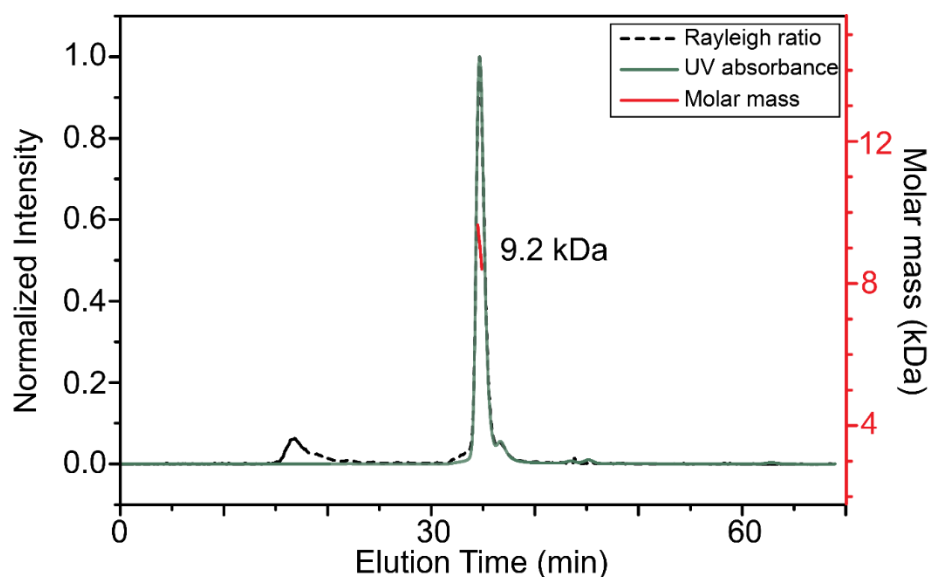


Figure 3.3: SEC-MALS elution profile for TRBP2-dsRBD2 showing that the protein remains monomeric (9.2 kDa) at the conditions used for NMR studies.

3.4. Backbone resonance assignment of TRBP2-dsRBD2

The ^1H - ^{15}N HSQC spectrum of TRBP2-dsRBD2 indicated a well-folded protein with the backbone amide chemical shift ranging from 6.5-9.5 ppm (Figure 3.4.1). ^1H - ^{15}N HSQC spectrum was recorded on the TRBP2-dsRBD2 (aa 154-234) and was compared with previously assigned spectra of TRBP2-D1D2 construct (aa 19-228) (Benoit et al., 2013) and TRBP2-dsRBD2 construct (aa 157-228) (Yamashita et al., 2011) to transfer the backbone amide resonance assignments. A few chemical shift perturbations were observed between the spectrum recorded in this study and the ones from the literature (Benoit et al., 2013), owing to different buffer conditions used to study the system.

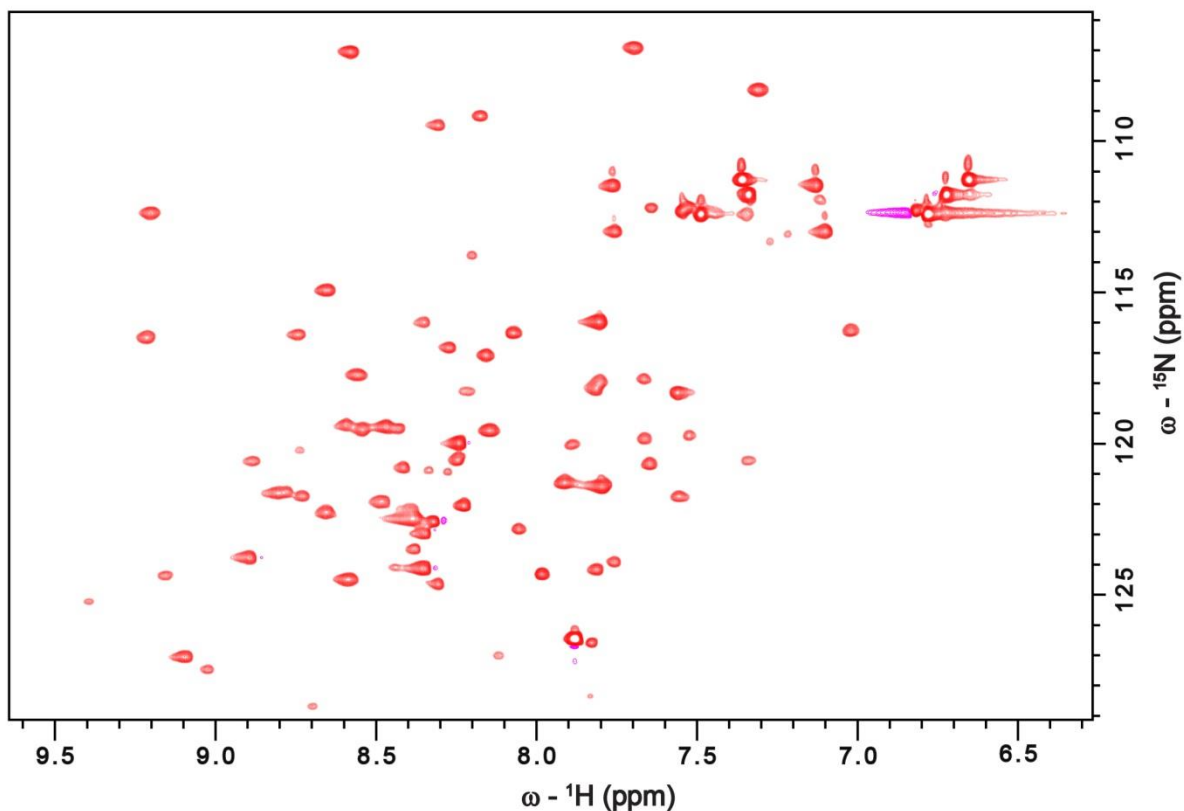


Figure 3.4.1: ^1H - ^{15}N HSQC spectrum of ^{15}N -TRBP2-dsRBD2 measured on 600 MHz NMR spectrometer at room temperature.

Chemical shift assignments were confirmed and further extended using experiments like ^1H - ^{15}N TOCSY-HSQC, ^1H - ^{15}N NOESY-HSQC, HNC0, HN(CA)CO, HNCA, HN(CO)CA, HNN, CBCANH, and CBCA(CO)NH. For example, ^1H - ^{15}N -TOCSY-HSQC was recorded to

identify a particular type of amino acid. Each of the amino acids has a unique pattern of TOCSY ^1H -correlation peaks in the third dimension corresponding to its backbone N-H. Backbone sequential connections were made by studying the ^1H - ^{15}N NOESY-HSQC (Fesik, Zuiderweg, Olejniczak, & Gampe, 1990), HNN (Panchal, Bhavesh, & Hosur, 2001), HNCO, HN(CA)CO, HNCA, HN(CO)CA, CBCANH (Meissner & Sørensen, 2001), and CBCA(CO)NH experiments where in addition to the self-nuclei chemical shift, one also gets information of its neighboring residue nuclei in the third dimension coupled to backbone N-H. In these experiments, the transfer of magnetization occurs from one nuclear spin to another via scalar coupling between various NMR active nuclei along the peptide chain (except for the NOE-based experiment, where the transfer of magnetization happens via dipolar coupling). Two examples of backbone sequential walk have been shown below for HNCA (Figure 3.4.2) and CBCANH (Figure 3.4.3).

For the HNCA experiment, correlations between $^{13}\text{C}_\alpha$, $^{15}\text{N}_\text{H}$, and $^1\text{H}_\text{N}$ were obtained. Each $^{15}\text{N}_\text{H}$ - $^1\text{H}_\text{N}$ peak correlated with two C_α peaks in the third (^{13}C -dimension) – one from self $\text{C}_{\alpha,i}$ and another from preceding residue $\text{C}_{\alpha,i-1}$ (Figure 3.4.2). Self and sequential peaks in the third dimension can be distinguished by their relative intensities. Self-peaks are more intense than the neighboring ones owing to differences in the scalar coupling constants between $^{15}\text{N}_{\text{H},i}$ and $\text{C}_{\alpha,i}$, and $^{15}\text{N}_{\text{H},i}$ and $\text{C}_{\alpha,i-1}$.

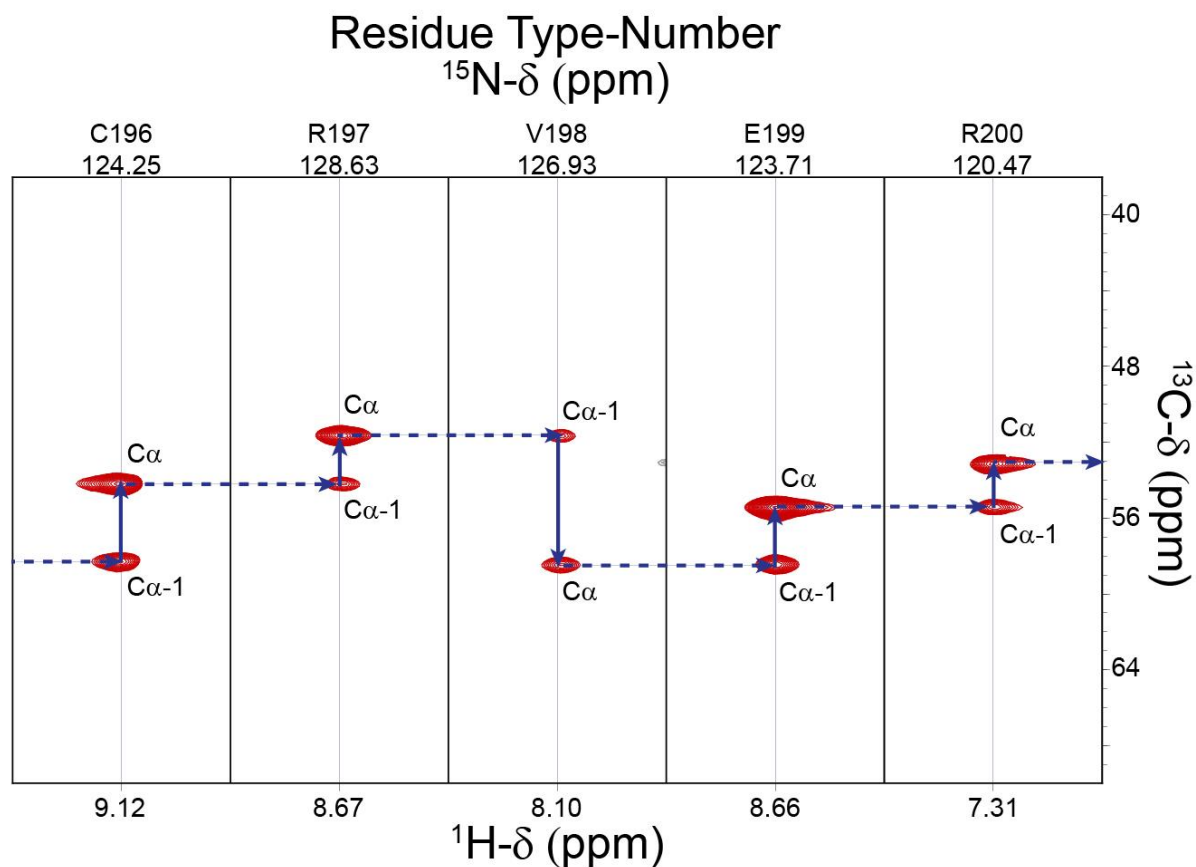


Figure 3.4.2: Chemical shift correlations between $^{13}\text{C}_\alpha$, $^{15}\text{N}_\text{H}$, and $^1\text{H}_\text{N}$ of residues C196-R200 of TRBP2-dsRBD2 observed in the HNCA experiment. More intense peaks represent self $\text{C}_{\alpha,i}$, and lesser ones represent the preceding $\text{C}_{\alpha,i-1}$. The arrows indicate the sequential connectivities.

The CBCANH experiment shows correlations between $^{13}\text{C}_\alpha$, $^3\text{C}_\beta$, $^{15}\text{N}_\text{H}$, and $^1\text{H}_\text{N}$. Each $^{15}\text{N}_\text{H}-^1\text{H}_\text{N}$ peak correlated with four peaks in the third (^{13}C -dimension): two C_α peaks – one from self $\text{C}_{\alpha,i}$ and another from preceding residue $\text{C}_{\alpha,i-1}$ and two C_β peaks – one from self $\text{C}_{\beta,i}$ and the other from preceding residue $\text{C}_{\beta,i-1}$ (Figure 3.4.3). The C_β peaks appear oppositely phased compared to C_α peaks. The CBCANH experiment also helps in identifying residues like Alanine whose C_β chemical shift is the most up-field (10-20 ppm); and Serine, and Threonine, whose C_β chemical shifts are the most down-field than even their corresponding C_α (60-80 ppm). Similar to HNCA experiment, self-peaks are more intense than the neighbouring ones.

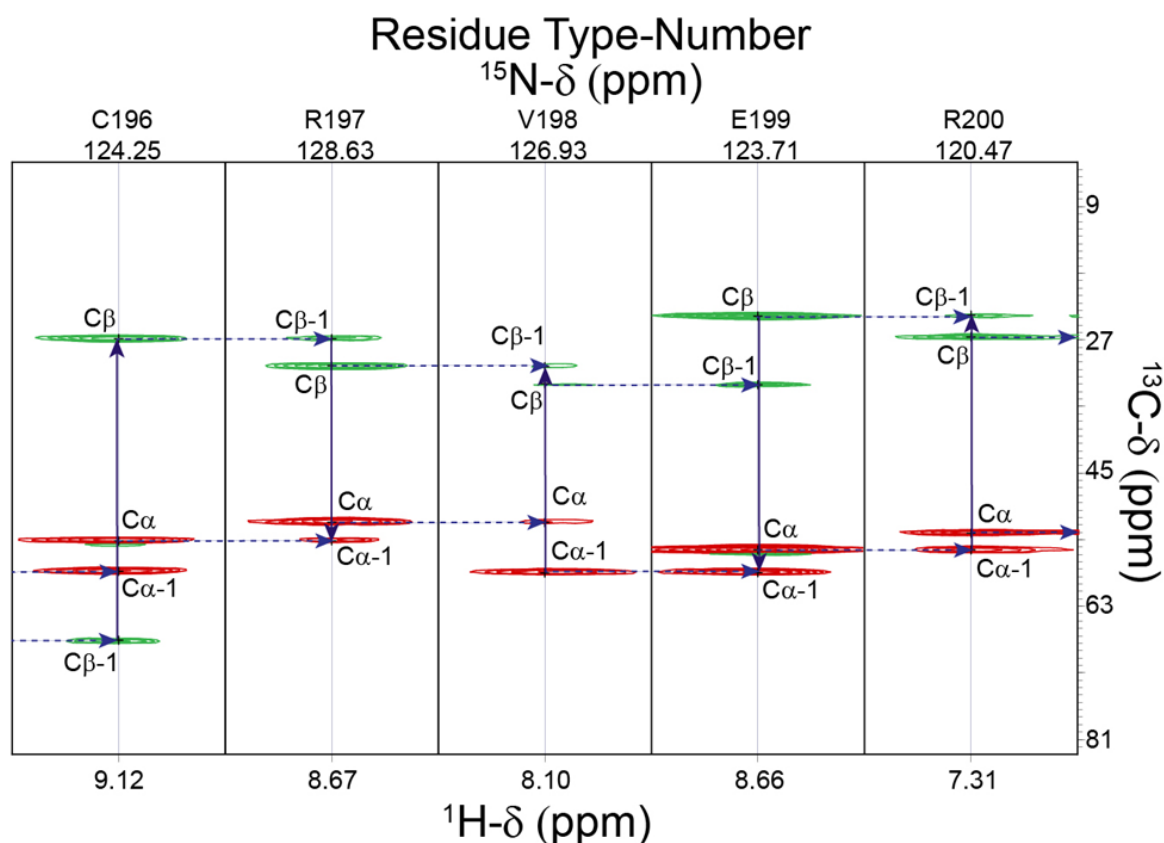


Figure 3.4.3: Chemical shift correlations between $^{13}\text{C}_\alpha$, $^{15}\text{N}_\text{H}$, and $^1\text{H}_\text{N}$ of residues 196-200 of TRBP2-dsRBD2 observed in the CBCANH experiment. The red colour represents C_α and green represents C_β . More intense peaks represent self-peaks, and lesser ones represent the peaks from preceding residues. The arrows indicate the sequential connectivities.

Likewise, chemical shift information of various nuclei and sequential connections along the protein backbone were obtained from these experiments: $^1\text{H}-^{15}\text{N}$ NOESY-HSQC, HNCOC, HNCACO, HNCA, HNCOCA, HNN, CBCANH, and CBCA(CO). Overall, 89% ^1H (151/169), 74% ^{13}C (124/168), and 87% ^{15}N (73/84) resonances from the backbone, and 43% ^1H (174/402) and 25% ^{13}C (59/238) from the side chains were assigned. A total of 73 non-proline residues out of 84 residues could be successfully assigned, as depicted in the figure below (Figure 3.4.4).

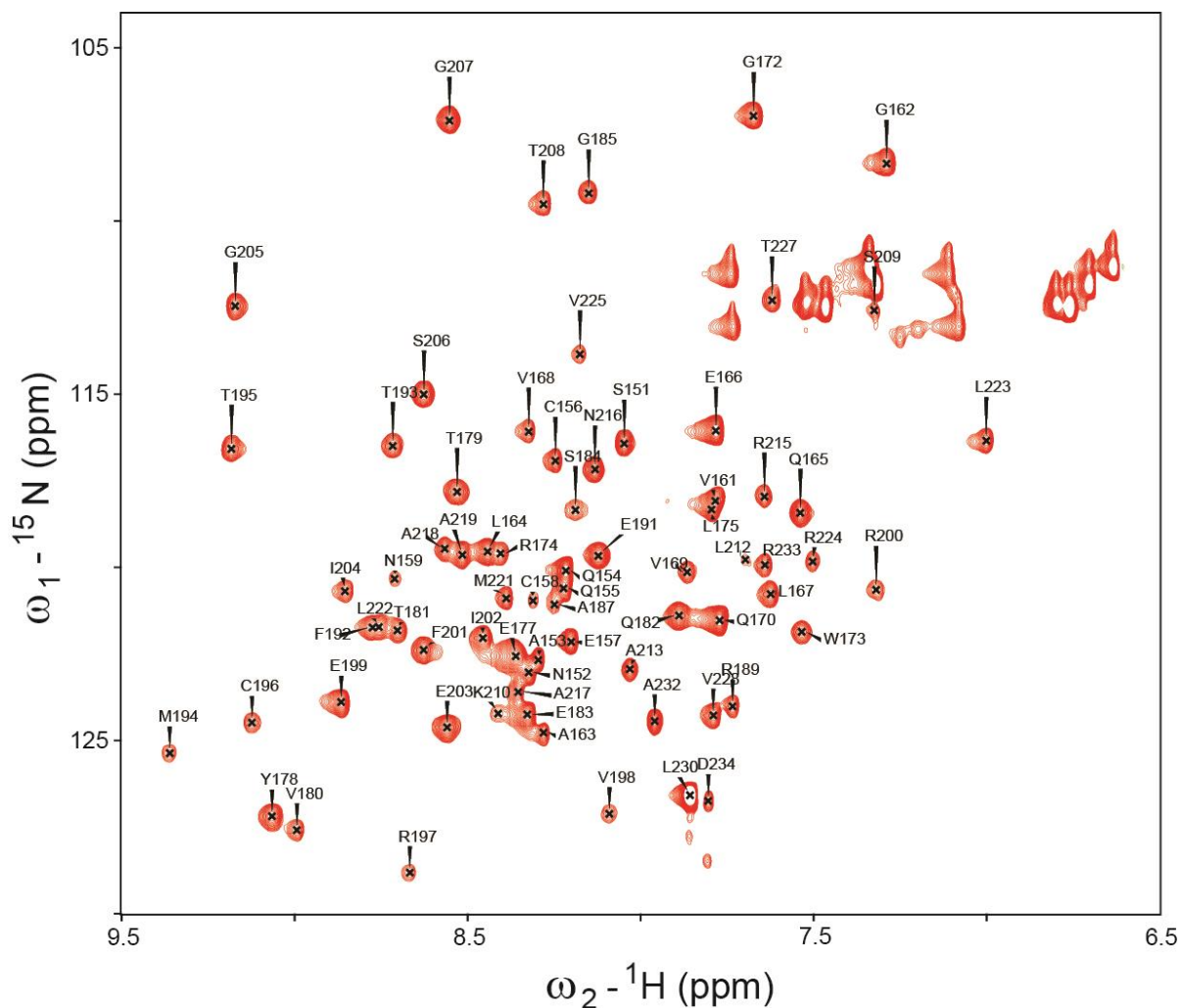


Figure 3.4.4: Backbone resonance assignments for TRBP2-dsRBD2 marked on ^1H - ^{15}N HSQC measured on 600 MHz NMR spectrometer at room temperature.

3.5. CS-ROSETTA calculated structure of TRBP2-dsRBD2

The CS-Rosetta structure was calculated for TRBP2-dsRBD2 using a total of 581 (325 ^1H , 183 ^{13}C , and 73 ^{15}N) backbone and side-chain chemical shifts (Figure 3.5.1). TRBP2-dsRBD2 was found to adapt the characteristic $\alpha\beta\beta\alpha$ fold of a dsRBD (Masliah, Barraud, & Allain, 2013; St Johnston, Brown, Gall, & Jantsch, 1992; Tian, Bevilacqua, Diegelman-Parente, & Mathews, 2004).

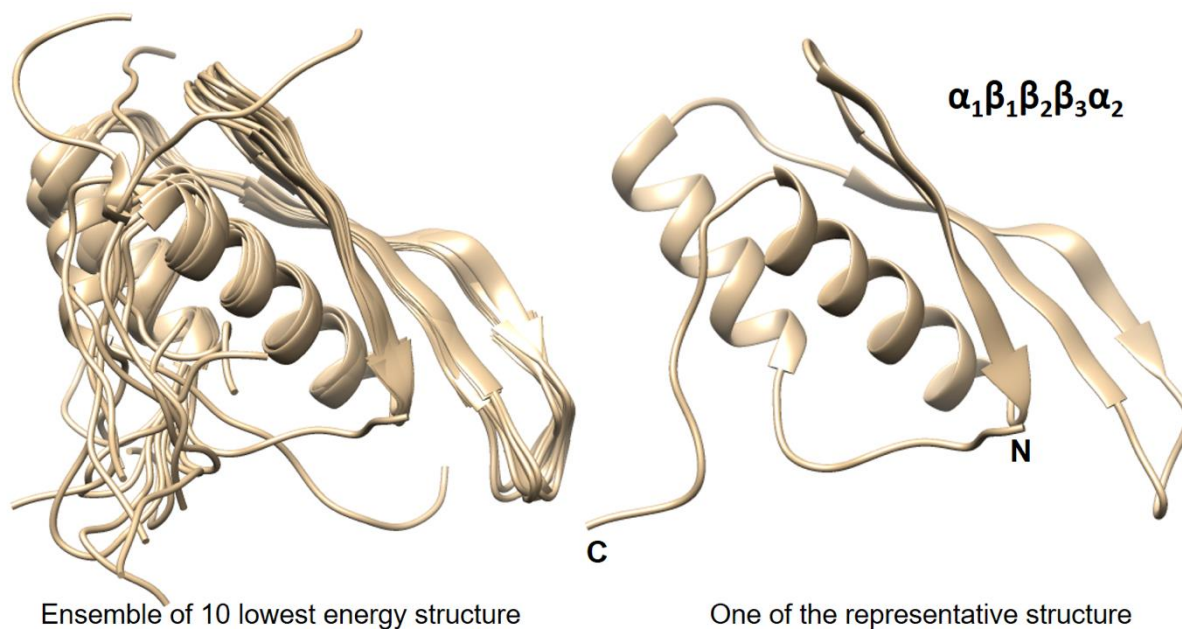


Figure 3.5.1: CS-ROSETTA structures of TRBP2-dsRBD2 (Left - an Ensemble of 10 lowest energy structures; Right – one of the representative structures of TRBP2-dsRBD2).

The structure of TRBP2-dsRBD2 was then aligned with the previously reported structure – 2CPN (www.rcsb.org/structure/2CPN), and the core RMSD was found to be 1.284 Å, which indicates a good agreement between the two structures (Figure 3.5.2).

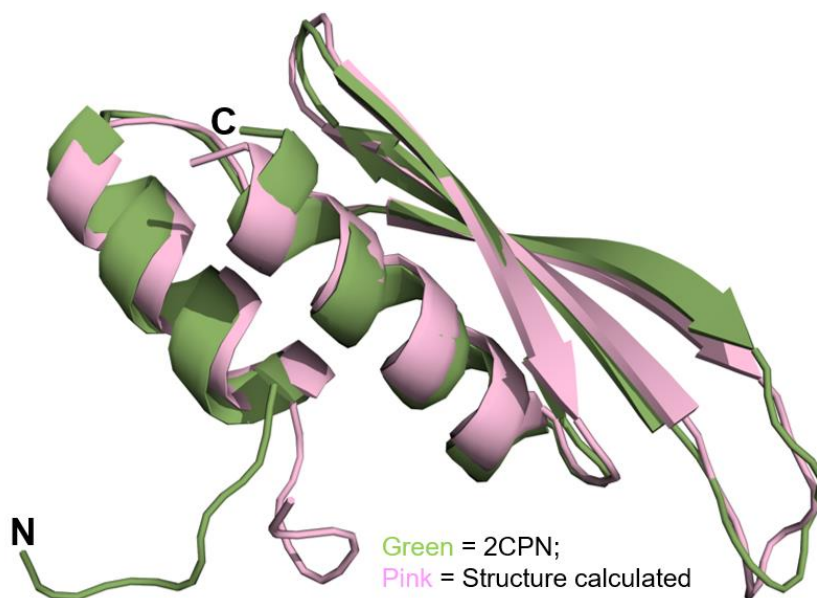


Figure 3.5.2: Structure alignment of TRBP2-dsRBD2 (pink) and 2CPN (green; previously reported structure).

Primary sequence comparison of TRBP2-dsRBD1 and TRBP2-dsRBD2 domain constructs (Figure 3.5.3) revealed 30% identity and 38% similarity. The consensus for dsRNA-binding has been marked in red. The grey highlighted areas refer to the reported RNA binding regions. The two reported RNA-binding regions 1 (E) and 3 (KKxAK) of both the domains were well matched to the consensus (Figure 3.5.3B). While region 2 (GPxH) of TRBP2-dsRBD2 was found to match the consensus, dsRBD1 harbored a mutation in region 2 (P56Q). Proline is a rigid amino acid with one less dihedral angle; it imparts flexibility to the backbone by causing secondary structure breaks (Imai & Mitaku, 2005; Krieger, Moglich, & Kiefhaber, 2005). Thus, the presence of Pro186 in the β_1 - β_2 loop of dsRBD2 may perturb the β_1 - β_2 loop region plasticity, thereby affecting its accessibility to the incoming RNA partner (Krieger et al., 2005; Leulliot et al., 2004). Additionally, dsRBD2 also contains a KR-helix motif (Daviet et al., 2000) in α_2 -helix, which is also known to increase its binding affinity. Due to the tightly conserved RNA-binding regions and the KR-helix motif, dsRBD2 could make stronger contact with the RNA. An alignment of core CS-ROSETTA structures between TRBP2-dsRBD1 (Paithankar, Jadhav, Naglekar, Sharma, & Chugh, 2018) and TRBP2-dsRBD2 yielded an RMSD of 0.894 Å, indicating a close match between the two domains (Figure 3.5.3).

Despite their core length being identical (69 aa), the individual secondary structure spans were found to be different for TRBP2-dsRBD1 and TRBP2-dsRBD2 domains (Table 3.3.1). The flexible regions, like loops 1 and 2, are longer in dsRBD2, whereas the structured regions β_2 , β_3 , and α_2 are longer in dsRBD1. Most importantly, loop 2 (β_1 - β_2 loop) — critical for RNA-binding (Masliah et al., 2013) — is equal to the canonical length in dsRBD2, while in dsRBD1, it is shorter by 1 residue.

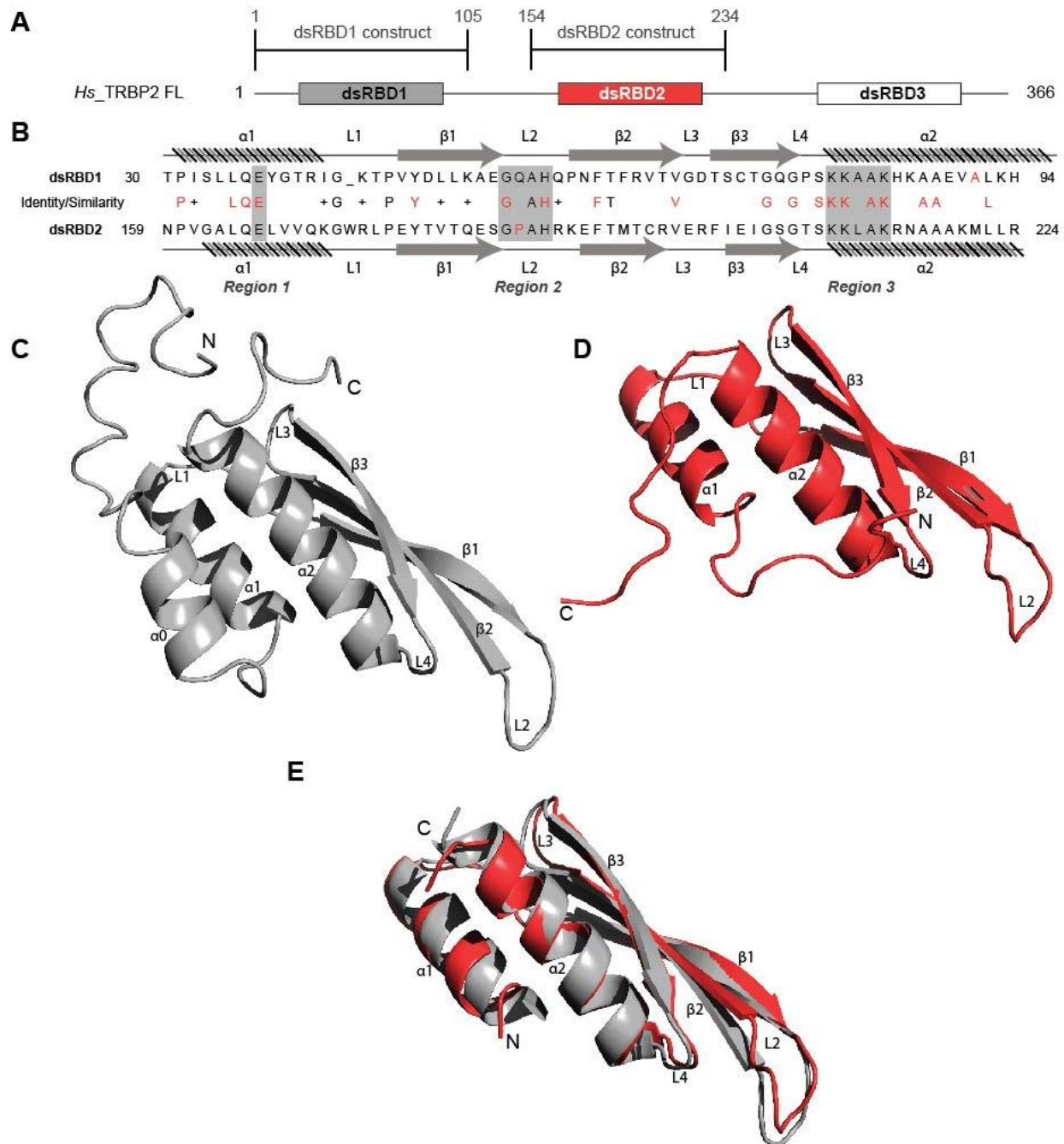


Figure 3.5.3: Comparison of TRBP2-dsRBD1 and TRBP2-dsRBD2 domains (A) dsRBD constructs [TRBP2-dsRBD1 (1–105 aa) and TRBP2-dsRBD2 (154–234) aa] of Human TRBP2 full-length protein used in the study; (B) Sequence alignment of the two constructs mentioned in (A); CS-Rosetta structures of (C) TRBP2-dsRBD2, (D) TRBP2-dsRBD1 (Paithankar et al., 2018), (E) an alignment of core residues of dsRBD1 and dsRBD2.

Table 3.5: Comparison of Amino acid length of different secondary structures observed in TRBP2-dsRBD1 and TRBP2-dsRBD2 CS-ROSSETA structures. α represents an α -helix, L represents a loop, and β represents the β -strand.

Domain Construct	$\alpha 1$	L1	$\beta 1$	L2	$\beta 2$	L3	$\beta 3$	L4	$\alpha 2$
TRBP2-dsRBD1	10	4	8	5	9	2	7	2	17
TRBP2-dsRBD2	10	5	8	6	8	4	6	2	15

3.6. Structure of TRBP2-dsRBD2 using POKY Structure Builder

The structural ensemble of TRBP2-dsRBD2 was determined with PONDEROSA-C/S (Lee, Stark, & Markley, 2014) assisted with AUDANA/AUDASA automation coupled with Xplor-NIH-based structure determination in the POKY Structure Builder suite. The 10 lowest energy structures align with an RMSD of 1.548 Å for backbone atoms across all core residues (Figure 3.6.1). The β -strands have been well defined, whereas the two α -helices require further refinements. Overall, the ensemble shows the presence of the characteristic $\alpha\beta\beta\beta\alpha$ fold, where the two α -helices fold onto the surface of the anti-parallel β -sheet.

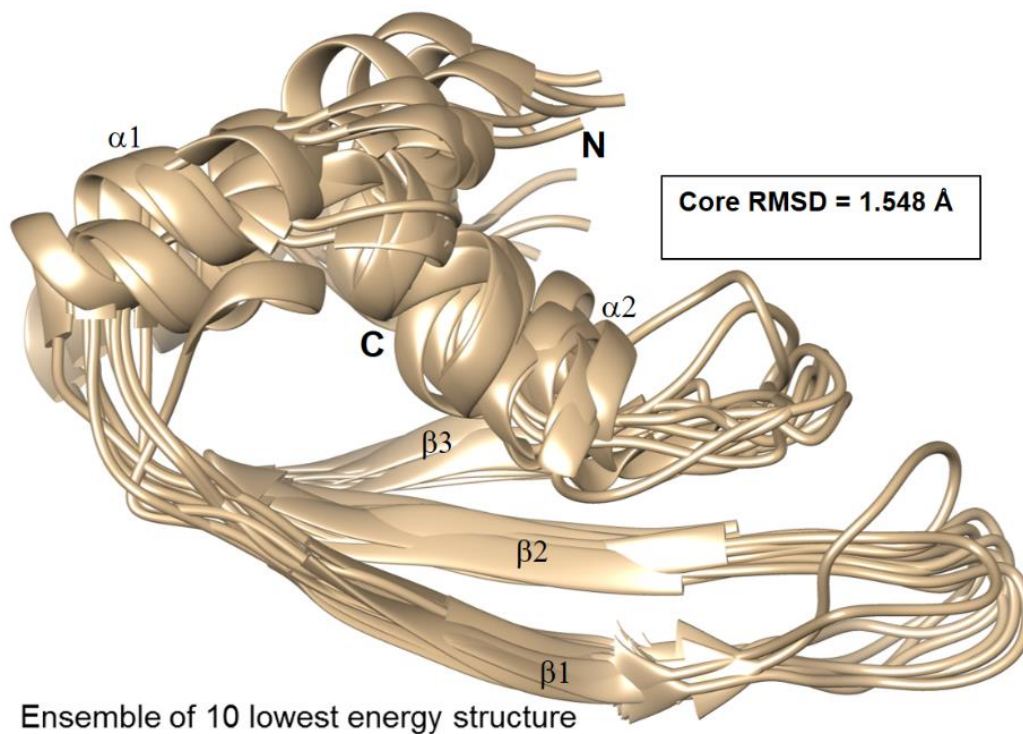


Figure 3.6.1: An ensemble of 10 lowest energy NMR structures of core TRBP2-dsRBD2 using the POKY Structure Builder suite.

The restraints and statistics of the 20 lowest energy structures have been summarized in Table 3.6. On an average, 16.4 distance restraints were obtained for each residue with no angle constraint violations. However, the average number of distance violations per structure were 30.15, which indicated that the structure needed further refinement. The backbone Φ and Ψ torsion angles of 87.68% residues were in the favoured regions of the Ramachandran plot (Ramachandran, Ramakrishnan, & Sasisekharan, 1963) (Figure 3.6.2).

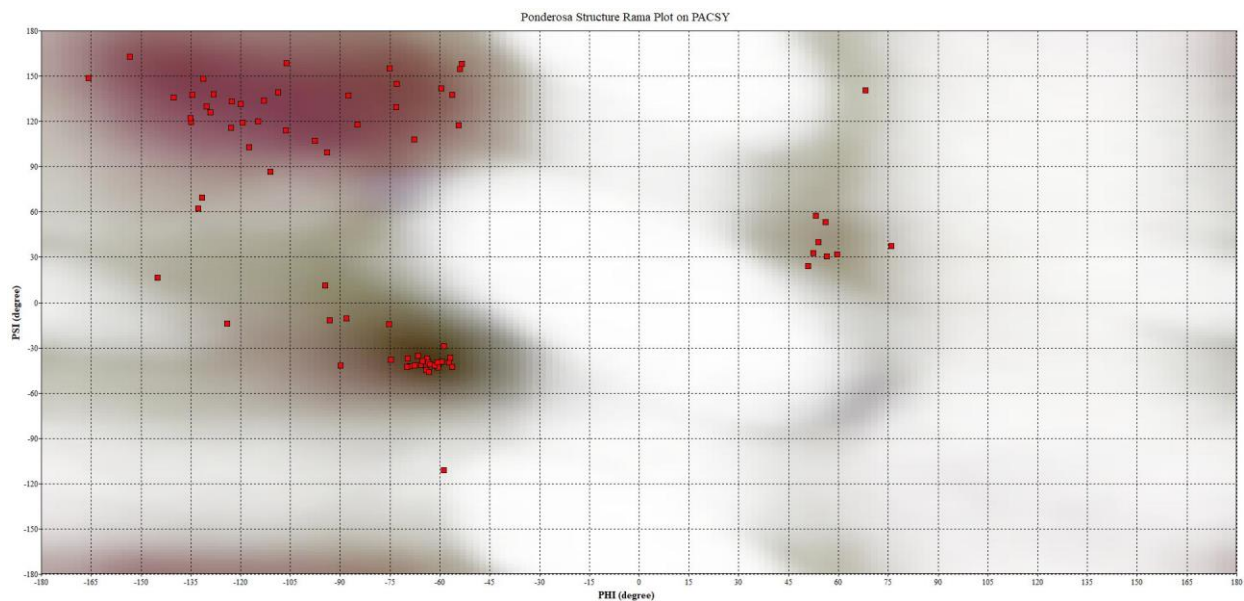


Figure 3.6.2: Ramachandran plot of the Xplor-NIH-based structure of TRBP2-dsRBD2 Model 1 using PODEROSA client in POKY Analyzer.

Table 3.6: Restraints and statistics for 20 best solution NMR structures of TRBP2-dsRBD2.

The structure quality was evaluated using the POKY Analyzer suite.

Parameters	TRBP-dsRBD2 (20 lowest energy conformations)
Total no. of Chemical Shifts	581 [56.918% ¹ H, 45.074% ¹³ C, 58.871% ¹⁵ N]
Backbone Completeness	82.66%
Side-chain Completeness	34.265%
Total Distance Restraints:	1199
Sequential ($ i - j \leq 1$)	530
Medium range ($1 < i - j < 5$)	265
Long range ($ i - j \geq 5$)	404
Average distance restraints/residue	16.4
Total Angle Restraints:	59 (PHI) 59 (PSI)

Backbone RMSD	3.479 Å
Overall RMSD	5.857 Å
Average no. of distance violation/structure	30.15
No. of Angle constraint violations/structure	0
MolProbity Score (Chen et al., 2010, Williams et al., 2018)	2.3978
MolProbity Ramachandran statistics (Favoured region)	87.68%
Ordered Residues	4-5+9-59+64-83
Total no. of Residues	84

Summary

Both unlabeled- and labeled- TRBP2-dsRBD2 were successfully purified in good NMR-experiment measurable concentrations. A total of 73 non-proline residues out of 84 total residues (including 4 prolines in construct) could be successfully assigned using a series of double and triple resonance NMR experiments. The CS-ROSETTA structure was calculated using 581 backbone and side-chain chemical shifts. It matched well with the structure reported earlier with an RMSD of 1.284 Å. The comparison of the two dsRBDs - dsRBD1 and dsRBD2 from the human TRBP isoform 1 shows that the conserved structural $\alpha\beta\beta\beta\alpha$ fold is independent of the primary sequence. This indicates that the structural fold of dsRBDs is more important than the protein sequence and inherits information sufficient for its function i.e., RNA-binding. The β_1 - β_2 loop is equal to the canonical length (6 aa) in dsRBD2, while in dsRBD1, it is shorter by 1 residue, which might affect the RNA-binding of these two domains. Moreover, presence of conserved proline residue in the Loop 2 region of dsRBD2 might have implications in RNA-binding.

References

- Benoit, M. P., Imbert, L., Palencia, A., Perard, J., Ebel, C., Boisbouvier, J., & Plevin, M. J. (2013). The RNA-binding region of human TRBP interacts with microRNA precursors through two independent domains. *Nucleic Acids Res*, *41*(7), 4241-4252. doi:10.1093/nar/gkt086
- Bowers, P. M., Strauss, C. E., & Baker, D. (2000). De novo protein structure determination using sparse NMR data. *J Biomol NMR*, *18*(4), 311-318. doi:10.1023/a:1026744431105
- Chen, V. B., Arendall, W. B., 3rd, Headd, J. J., Keedy, D. A., Immormino, R. M., Kapral, G. J., . . . Richardson, D. C. (2010). MolProbity: all-atom structure validation for macromolecular crystallography. *Acta Crystallogr D Biol Crystallogr*, *66*(Pt 1), 12-21. doi:10.1107/s0907444909042073
- Daviet, L., Erard, M., Dorin, D., Duarte, M., Vaquero, C., & Gatignol, A. (2000). Analysis of a binding difference between the two dsRNA-binding domains in TRBP reveals the modular function of a KR-helix motif. *Eur J Biochem*, *267*(8), 2419-2431. doi:10.1046/j.1432-1327.2000.01256.x
- Fesik, S. W., Zuiderweg, E. R., Olejniczak, E. T., & Gampe, R. T., Jr. (1990). NMR methods for determining the structures of enzyme/inhibitor complexes as an aid in drug design. *Biochem Pharmacol*, *40*(1), 161-167. doi:10.1016/0006-2952(90)90191-m
- Folta-Stogniew, E., & Williams, K. R. (1999). Determination of molecular masses of proteins in solution: Implementation of an HPLC size exclusion chromatography and laser light scattering service in a core laboratory. *J Biomol Tech*, *10*(2), 51-63.
- Imai, K., & Mitaku, S. (2005). Mechanisms of secondary structure breakers in soluble proteins. *Biophysics (Nagoya-shi)*, *1*, 55-65. doi:10.2142/biophysics.1.55
- Krieger, F., Moglich, A., & Kiefhaber, T. (2005). Effect of proline and glycine residues on dynamics and barriers of loop formation in polypeptide chains. *J Am Chem Soc*, *127*(10), 3346-3352. doi:10.1021/ja042798i

Lange, O. F., Rossi, P., Sgourakis, N. G., Song, Y., Lee, H. W., Aramini, J. M., . . . Baker, D. (2012). Determination of solution structures of proteins up to 40 kDa using CS-Rosetta with sparse NMR data from deuterated samples. *Proc Natl Acad Sci U S A*, *109*(27), 10873-10878. doi:10.1073/pnas.1203013109

Lee, W., Petit, C. M., Cornilescu, G., Stark, J. L., & Markley, J. L. (2016). The AUDANA algorithm for automated protein 3D structure determination from NMR NOE data. *J Biomol NMR*, *65*(2), 51-57. doi:10.1007/s10858-016-0036-y

Lee, W., Rahimi, M., Lee, Y., & Chiu, A. (2021). POKY: a software suite for multidimensional NMR and 3D structure calculation of biomolecules. *Bioinformatics*, *37*(18), 3041-3042. doi:10.1093/bioinformatics/btab180

Lee, W., Stark, J. L., & Markley, J. L. (2014). PONDEROSA-C/S: client-server based software package for automated protein 3D structure determination. *J Biomol NMR*, *60*(2-3), 73-75. doi:10.1007/s10858-014-9855-x

Leulliot, N., Quevillon-Cheruel, S., Graille, M., van Tilbeurgh, H., Leeper, T. C., Godin, K. S., . . . Varani, G. (2004). A new alpha-helical extension promotes RNA binding by the dsRBD of Rnt1p RNase III. *EMBO J*, *23*(13), 2468-2477. doi:10.1038/sj.emboj.7600260

Masliyah, G., Barraud, P., & Allain, F. H. (2013). RNA recognition by double-stranded RNA binding domains: a matter of shape and sequence. *Cell Mol Life Sci*, *70*(11), 1875-1895. doi:10.1007/s00018-012-1119-x

Meissner, A., & Sørensen, O. W. (2001). Sequential HNCACB and CBCANH protein NMR pulse sequences. *J Magn Reson*, *151*(2), 328-331. doi:10.1006/jmre.2001.2374

Paithankar, H., Jadhav, P. V., Naglekar, A. S., Sharma, S., & Chugh, J. (2018). (1)H, (13)C and (15)N resonance assignment of domain 1 of trans-activation response element (TAR) RNA binding protein isoform 1 (TRBP2) and its comparison with that of isoform 2 (TRBP1). *Biomol NMR Assign*, *12*(1), 189-194. doi:10.1007/s12104-018-9807-6

Panchal, S. C., Bhavesh, N. S., & Hosur, R. V. (2001). Improved 3D triple resonance experiments, HNN and HN(C)N, for HN and ¹⁵N sequential correlations in (¹³C, ¹⁵N) labeled proteins: application to unfolded proteins. *J Biomol NMR*, 20(2), 135-147. doi:10.1023/a:1011239023422

Ramachandran, G. N., Ramakrishnan, C., & Sasisekharan, V. (1963). Stereochemistry of polypeptide chain configurations. *J Mol Biol*, 7, 95-99. doi:10.1016/s0022-2836(63)80023-6

Schwieters, C. D., Bermejo, G. A., & Clore, G. M. (2018). Xplor-NIH for molecular structure determination from NMR and other data sources. *Protein Sci*, 27(1), 26-40. doi:10.1002/pro.3248

Shen, Y., Bryan, P. N., He, Y., Orban, J., Baker, D., & Bax, A. (2010). De novo structure generation using chemical shifts for proteins with high-sequence identity but different folds. *Protein Sci*, 19(2), 349-356. doi:10.1002/pro.303

Shen, Y., Lange, O., Delaglio, F., Rossi, P., Aramini, J. M., Liu, G., . . . Bax, A. (2008). Consistent blind protein structure generation from NMR chemical shift data. *Proc Natl Acad Sci U S A*, 105(12), 4685-4690. doi:10.1073/pnas.0800256105

Shen, Y., Vernon, R., Baker, D., & Bax, A. (2009). De novo protein structure generation from incomplete chemical shift assignments. *J Biomol NMR*, 43(2), 63-78. doi:10.1007/s10858-008-9288-5

St Johnston, D., Brown, N. H., Gall, J. G., & Jantsch, M. (1992). A conserved double-stranded RNA-binding domain. *Proc Natl Acad Sci U S A*, 89(22), 10979-10983. doi:10.1073/pnas.89.22.10979

Tian, B., Bevilacqua, P. C., Diegelman-Parente, A., & Mathews, M. B. (2004). The double-stranded-RNA-binding motif: interference and much more. *Nat Rev Mol Cell Biol*, 5(12), 1013-1023. doi:10.1038/nrm1528

Williams, C. J., Headd, J. J., Moriarty, N. W., Prisant, M. G., Videau, L. L., Deis, L. N., . . . Richardson, D. C. (2018). MolProbity: More and better reference data for improved all-atom structure validation. *Protein Sci*, 27(1), 293-315. doi:10.1002/pro.3330

Wyatt, P. J. (1993). Light scattering and the absolute characterization of macromolecules. *Analytica Chimica Acta*, 272(1), 1-40. doi:[https://doi.org/10.1016/0003-2670\(93\)80373-S](https://doi.org/10.1016/0003-2670(93)80373-S)

Yamashita, S., Nagata, T., Kawazoe, M., Takemoto, C., Kigawa, T., Guntert, P., . . . Yokoyama, S. (2011). Structures of the first and second double-stranded RNA-binding domains of human TAR RNA-binding protein. *Protein Sci*, 20(1), 118-130. doi:10.1002/pro.543

Zimm, B. H. (2004). Molecular Theory of the Scattering of Light in Fluids. *The Journal of Chemical Physics*, 13(4), 141-145. doi:10.1063/1.1724013 %J The Journal of Chemical Physics

Chapter 4

**Characterization of dsRNA
binding of
TRBP2-dsRBD2**

Introduction

Double stranded RNA binding proteins (dsRBPs) interact with highly structured dsRNAs via dsRBDs (Bevilacqua & Cech, 1996; Masliah, Barraud, & Allain, 2013; Tian, Bevilacqua, Diegelman-Parente, & Mathews, 2004). Their interaction is not sequence-specific, wherein they target the sugar 2'-OH groups (cannot bind dsDNAs) and negatively charged phosphate backbone (Bevilacqua & Cech, 1996). Chemical interactions involve either direct or indirect solvent-mediated interactions like hydrogen bonding, electrostatic, or dipole-dipole interaction, etc. dsRBDs tend to target a particular structural fold, especially the A-form RNA duplex (Masliah et al., 2013).

dsRBDs, both within and across proteins, exhibit significant variations in their binding modes and affinities towards specific RNA targets (Chiliveri, Aute, Rai, & Deshmukh, 2017; Fierro-Monti & Mathews, 2000; Krovat & Jantsch, 1996; Nanduri, Rahman, Williams, & Qin, 2000; Wostenberg et al., 2012). We have recently established that the TRBP2-dsRBD1 is able to recognize a set of topologically different dsRNA structures owing to its high conformational plasticity (Paithankar et al., 2022). In the current study, we have characterized the interaction of TRBP2-dsRBD2 with the same set of topologically different dsRNAs (miR-16-1 mutants) used for dsRBD1 through ^1H - ^{15}N HSQC-based NMR titrations. We have further used a short, perfect duplex A-form RNA (D12 RNA) to investigate the effect of RNA length on TRBP2-dsRBD2 binding. Finally, an Isothermal Titration Calorimetry (ITC) was performed with a 12 bp D12 RNA to compare the RNA-binding affinity (K_d) of the dsRBD1 and dsRBD2 of TRBP2 protein.

Results and Discussion

4.1. NMR-based study of the interaction of TRBP2-dsRBD2 with topologically different dsRNAs

NMR-based investigation of the interaction between the TRBP-dsRBD2 and the four miR-16-1 mutants (22–23 bp) dsRNAs revealed subtle structural perturbations in TRBP2-dsRBD2 (Figures 4.1.1–4.1.4). These changes were indicated by minute chemical shift perturbations (< 0.1 ppm) in the presence of RNA. This indicates that the tertiary structure/fold of the protein remains unperturbed. This observation is consistent with the previous findings reported by Yamashita *et al.*, where authors compared the solution structure of TRBP-dsRBD2 structure with the crystal

structure of GC10RNA-bound TRBP-dsRBD2 (Yamashita et al., 2011; Yang et al., 2010). In addition, there were two other intriguing observations from the ^1H - ^{15}N HSQC-based titrations. First, the amide signals were getting broadened at as low as 0.1 RNA equivalents suggesting the slow-to-intermediate timescale of binding as has also been observed previously by our group and other research groups in TRBP2 dsRBD1 (Paithankar et al., 2022), Staufen dsRBD3 (Yadav et al., 2020), hDus2 dsRBD (Bou-Nader et al., 2019), MLE dsRBD2 (Ankush Jagtap et al., 2019), DBR4 dsRBD1 (Chiliveri et al., 2017), PKR dsRBD (Ucci, Kobayashi, Choi, Alexandrescu, & Cole, 2007), and Dicer dsRBD (Wostenberg et al., 2012). Second, the reported RNA-binding residues and the entire backbone were undergoing line broadening, thereby suggesting the presence of RNA-induced motions in the entire backbone. Since the protein is not saturated with the RNAs at 0.1 RNA equivalents (considering a reported $K_d = 1.7 \mu\text{M}$ for a 22 bp dsRNA (Acevedo, Orench-Rivera, Quarles, & Showalter, 2015), $[\text{protein}] = 50 \mu\text{M}$, $[\text{RNA}] = 5 \mu\text{M}$, fraction bound of protein $< 10\%$), we can rule out an increase in the size due to the formation of a stable protein-RNA complex causing line-broadening. Upon excess addition of RNA (to 2 equivalents of miR-16-1-M), the backbone amide signals were not recovered, which indicated that the RNA-protein interaction does not seem to come out of the local minima of slow-to-intermediate exchange regime (Figure 4.1.4).

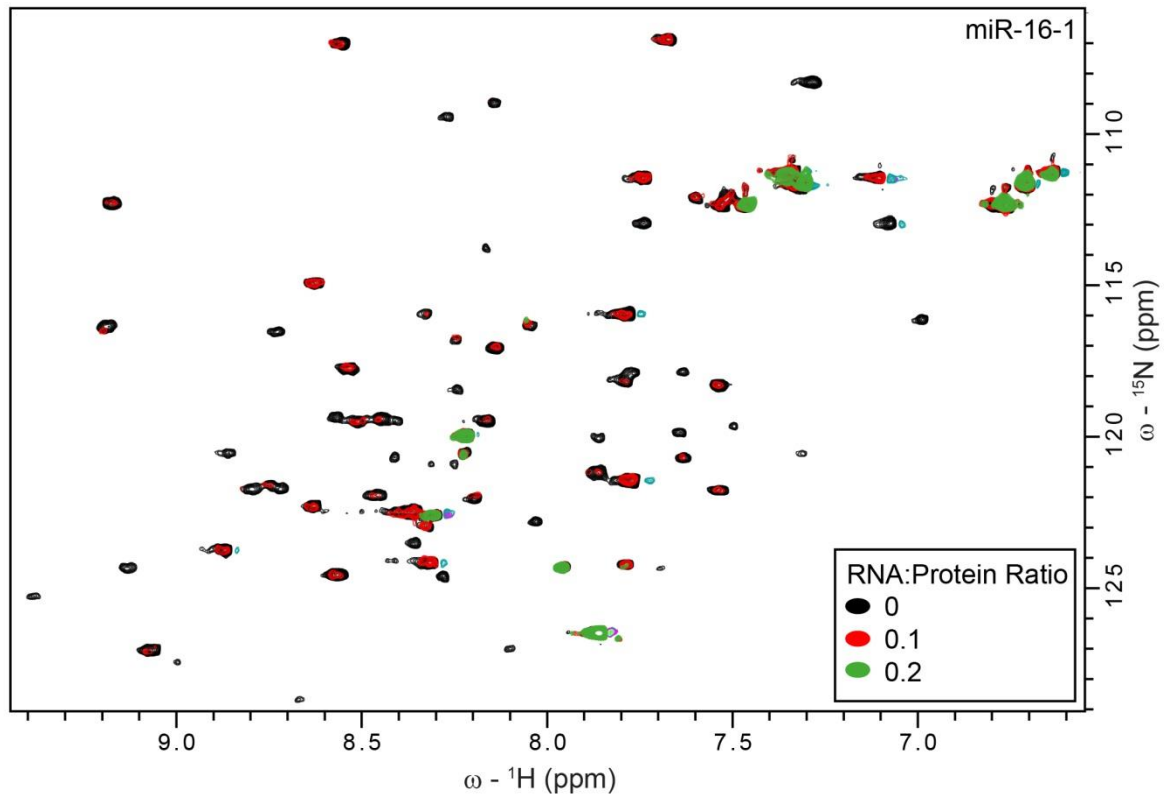


Figure 4.1.1: Titration of ^{15}N -TRBP2-dsRBD2 with different molar equivalents of its reported binder – miR-16-1-A. Representation of the overlay of ^1H - ^{15}N -HSQC spectra of apo-protein (black), (RNA:Protein) = 0.1:1 (red) and (RNA:Protein) = 0.2:1 (green) molar equivalents]. All the data was measured on a 600 MHz NMR spectrometer at 298 K in buffer D, pH 6.4.

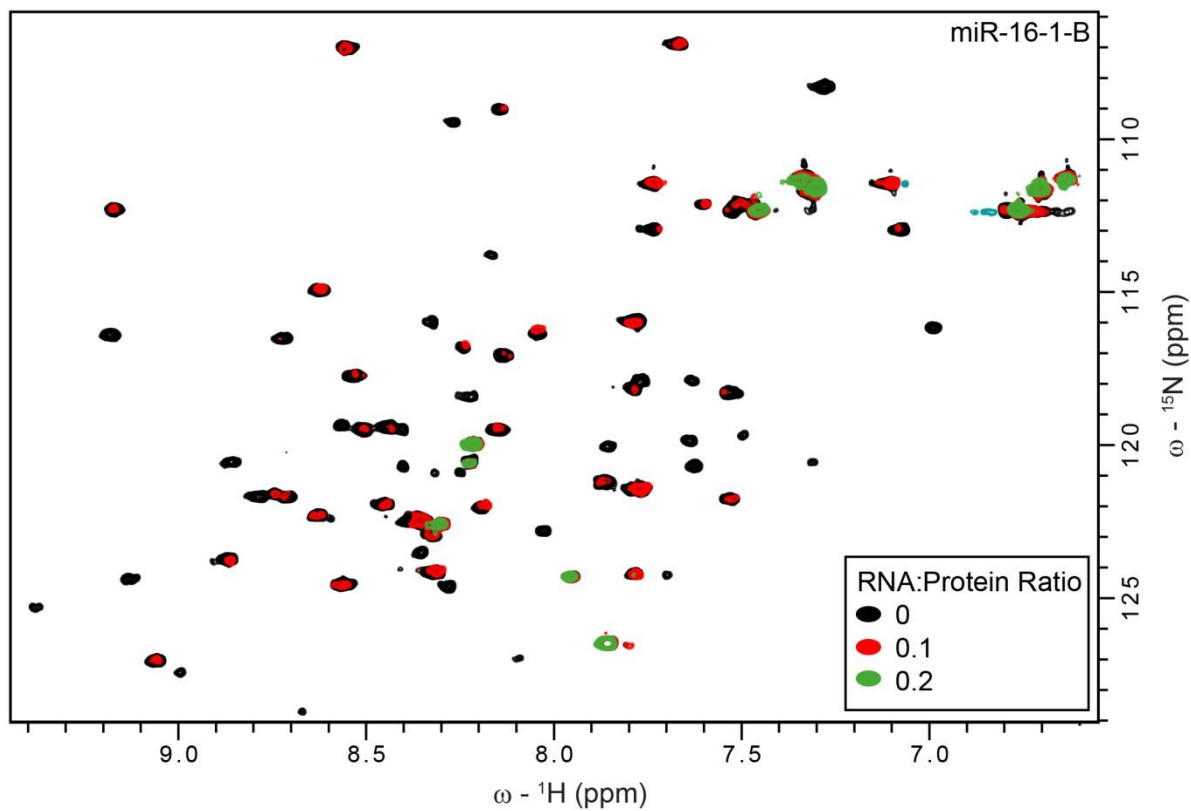


Figure 4.1.2: Titration of ^{15}N -TRBP2-dsRBD2 with different molar equivalents of miR-16-1-B –mutant of miR-16-1 with bulge. Representation of the overlay of the ^1H - ^{15}N -HSQC spectra of apo-protein (black), (RNA:Protein) = 0.1:1 (red) and (RNA:Protein) = 0.2:1 (green) molar equivalents]. All the data was measured on a 600 MHz NMR spectrometer at 298 K in buffer D, pH 6.4.

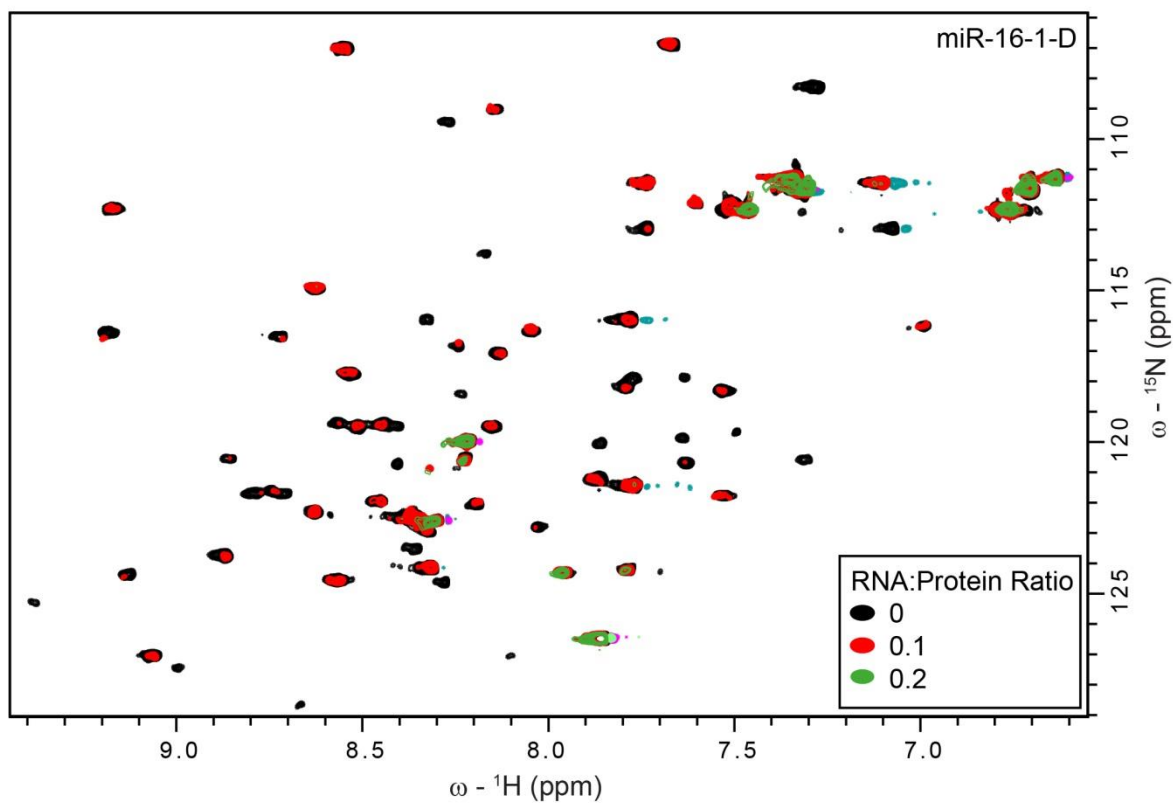


Figure 4.1.3: Titration of ^{15}N -TRBP2-dsRBD2 with different molar equivalents of miR-16-1-D – mutant of miR-16-1 with perfect A-form duplex. Representation of the overlay of the ^1H - ^{15}N -HSQC spectra of apo-protein (black), (RNA:Protein) = 0.1:1 (red) and (RNA:Protein) = 0.2:1 (green) molar equivalents]. All the data was measured on a 600 MHz NMR spectrometer at 298 K in buffer D, pH 6.4.

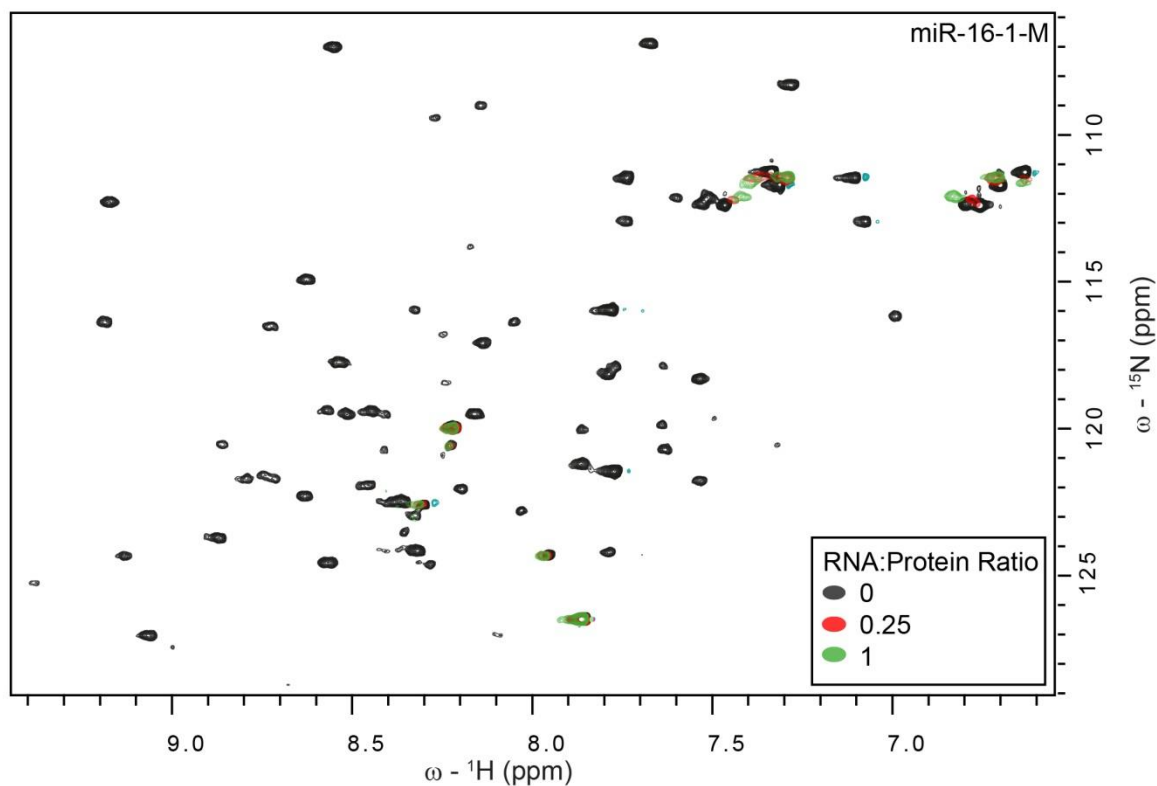


Figure 4.1.4: Titration of ^{15}N -TRBP2-dsRBD2 with the different molar equivalents of miR-16-1-M mutant of miR-16-1 with a mismatch. Representation of the overlay of the ^1H - ^{15}N -HSQC spectra of apo-protein (black), (RNA:Protein) = 0.25:1 (red) and (RNA:Protein) = 1:1 (green) equivalents]. All the data was measured on a 600 MHz NMR spectrometer at 298 K in buffer D, pH 6.4.

Next, to understand the effect of RNA length on the binding, we tested a shorter mutant of miR-16-1-D duplex RNA with 12 base pairs in length (D12 RNA) for binding with the dsRBD. The annealing of D12 RNA was confirmed by analysing the peaks in the imino-region (11-15 ppm) of ^1H NMR spectrum (Figure 4.1.5).

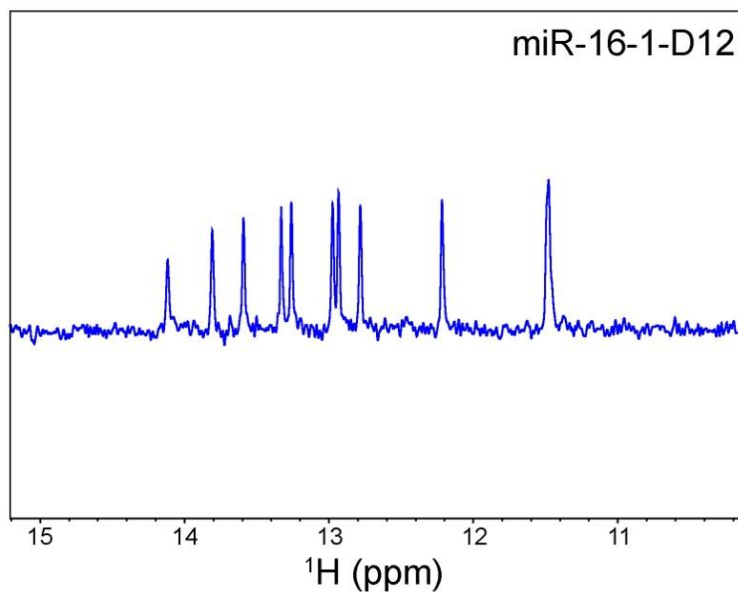


Figure 4.1.5: ^1H -NMR spectrum of the imine-region of the annealed D12 RNA. The peak pattern observed indicated the formation of the RNA duplex.

We repeated the NMR-based titration of TRBP2-dsRBD2 with D12 RNA. The amide NMR signals were partially recovered by shortening the length of the RNA duplex from 22 bp to 12 bp. The line broadening was delayed till 0.35 equivalents of D12 RNA as compared to 0.1 equivalents for the longer RNAs (Figure 4.1.6). The excessive line broadening all along the backbone and recovery of the same by reducing the length of the RNA hints towards the presence of the phenomenon of protein sliding/diffusing over the length of the RNA, as has been reported for TRBP (Koh, Kidwell, Ragunathan, Doudna, & Myong, 2013) earlier along with other dsRBPs like Loqs-PD dsRBD (Tants et al., 2017), MLE dsRBD (Ankush Jagtap et al., 2019), and RDE4 (Chiliveri & Deshmukh, 2014).

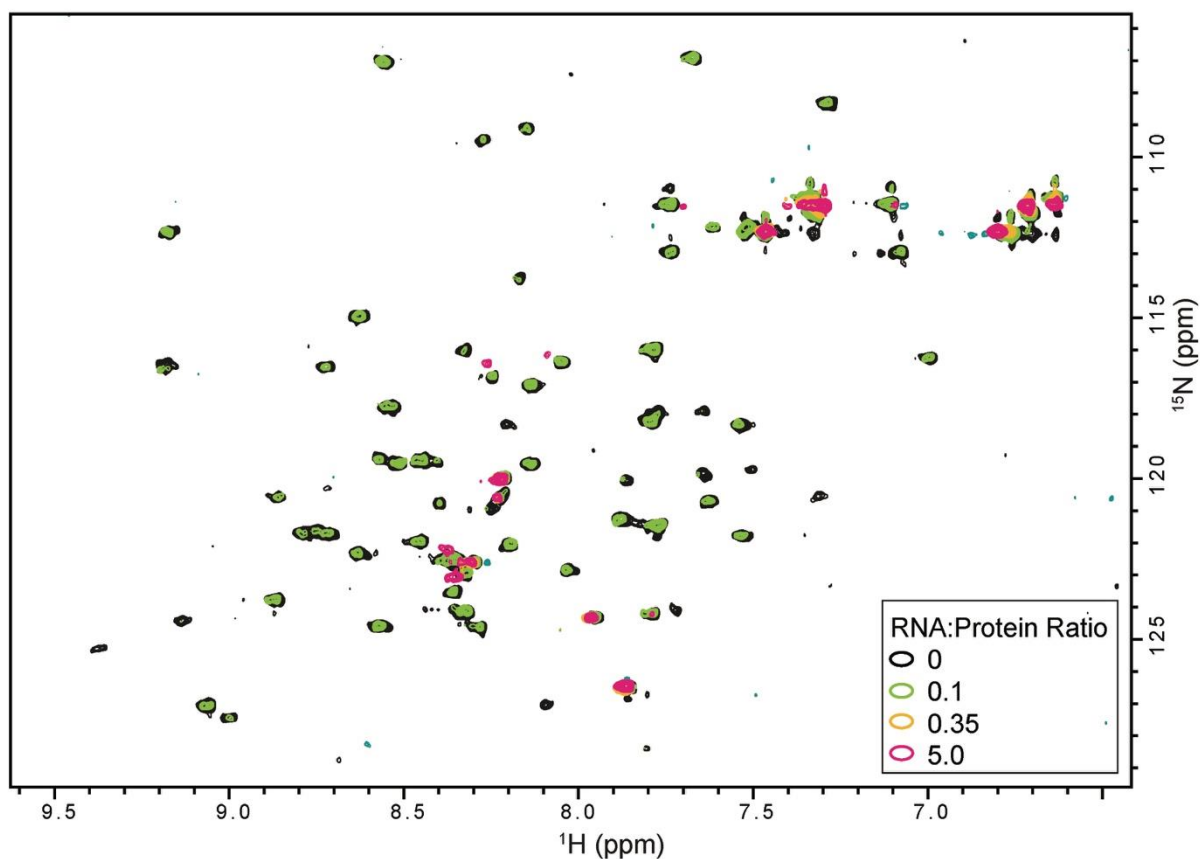


Figure 4.1.6: Titration of ^{15}N -TRBP2-dsRBD2 with D12 RNA, a shorter mutant of miR-16-1-D. An overlay of ^1H - ^{15}N -HSQC spectra of apo-protein (black), (RNA:Protein) = 0.1:1 (green), (RNA:Protein) = 0.35:1 (yellow), and (RNA:Protein) = 5:1 (magenta) molar equivalents, measured on a 600 MHz NMR spectrometer at 298 K in buffer D, pH 6.4.

To extract the binding constant (K_d) for the D12-TRBP-dsRBD2 interaction, residue-wise peak intensities were plotted against the RNA concentration and attempts were made to fit to the binding isotherm for one-site binding (Figure 4.1.7). Due to extensive line broadening, there was a lack of data at the inflection point, affecting the data fitting. Hence, the fitted parameters had large errors and remained inconclusive.

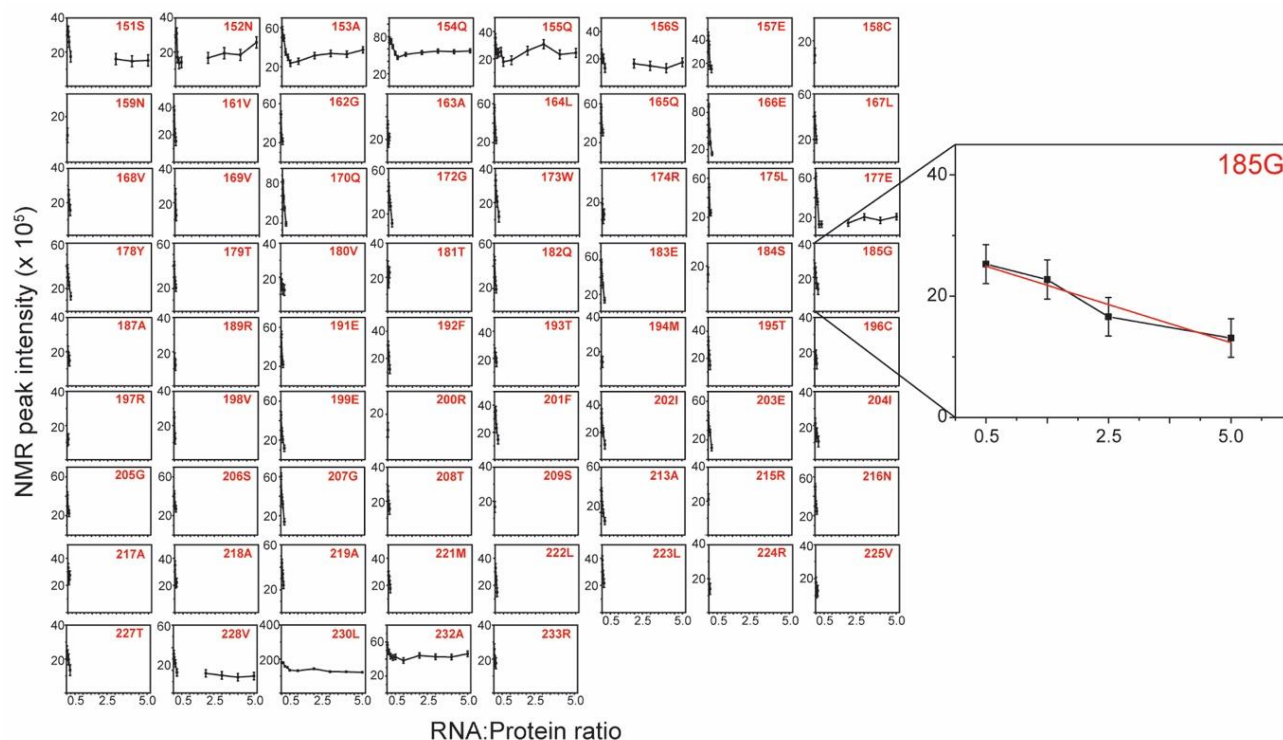


Figure 4.1.7: Normalized NMR peak intensity from ^1H - ^{15}N HSQC spectra of TRBP2-dsRBD2 plotted against protein: D12 RNA ratios depicted here are from the titrations carried out in Figure 4.1.6.

4.2. ITC-based study with D12 RNA

The ITC-based study was performed with D12 RNA to get the apparent RNA-binding affinity (K_d), thermodynamic parameters (ΔH , ΔG , $T\Delta S$), and stoichiometry (n) for the two N-terminal dsRBDs from TRBP2 (Table 4.2). Our studies showed that TRBP2-dsRBD2 binds to D12 RNA relatively strongly with a K_d of $1.1 \pm 0.37 \mu\text{M}$ as compared to TRBP2-dsRBD1 (Figure 4.2.1), which did not show significant heat exchange during the titration, and data could not be fitted to any binding model. The differential potential against the time plot indicates that RNA got saturated with TRBP2-dsRBD2 as early as the eighth injection. The integrated change in injection enthalpy (ΔH) versus the molar ratio of the reactants yielded a ΔH of $-10.15 \pm 0.5 \text{ kcal/mol}$. The negative ΔH means this is an enthalpy-driven binding event, which indicates polar and charge-charge interactions. ITC study was repeated for TRBP2-dsRBD1 with as high as 22 folds excess of protein, but RNA remained unsaturated. These results strongly suggest that TRBP2-dsRBD2 binds more efficiently to a small perfect A-form duplex, D12 RNA, than TRBP2-dsRBD1. The

long, conserved loop 2 and KR-helix motif (refer to Chapter 3, Section 3.5) might help dsRBD2 to establish strong contacts in the minor grooves of dsRNA partners.

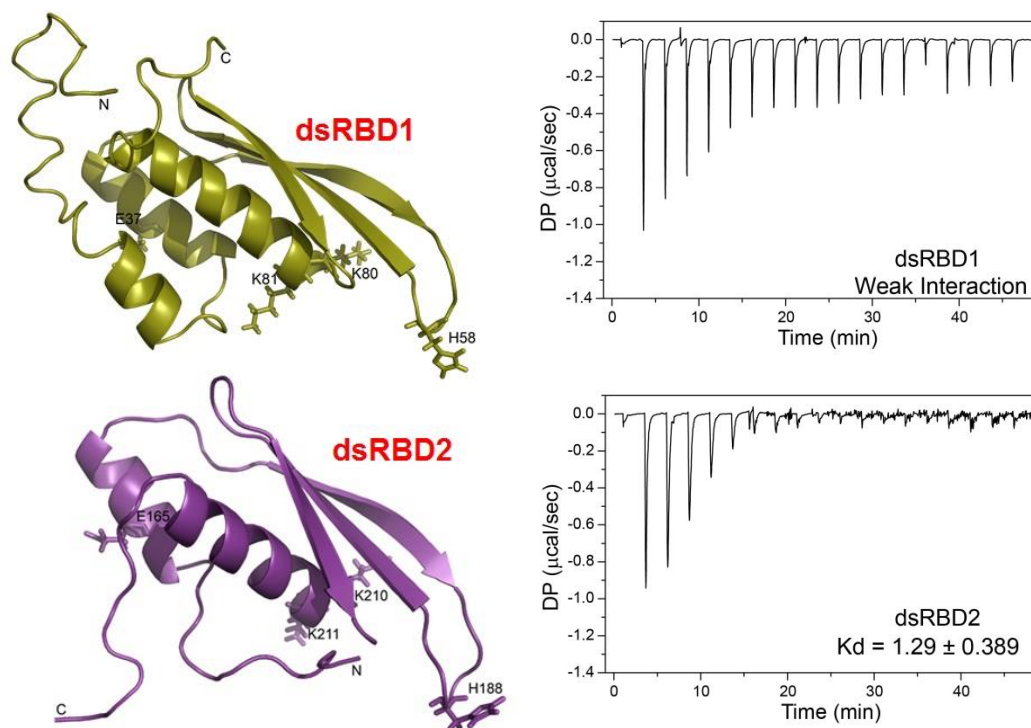


Figure 4.2.1: ITC-based binding study of D12 duplex RNA with TBRP2-dsRBD1 (Upper panel) and TBRP2-dsRBD2 (Lower panel). The CS-ROSETTA structures with conserved RNA binding residues are shown on the left side. The raw differential potential for each injection has been plotted against the titration time on the right side.

Table 4.2: ITC binding study of TBRP2-dsRBD2 and D12 RNA carried out in triplicate.

Experiment No.	[Syr] (mM) TBRP2_dsRBD2	[Cell] (μ M) D12 RNA	N (sites)	k_d (μ M)	ΔH (kcal/mol)	ΔG (kcal/mol)	$-T\Delta S$ (kcal/mol)
1.	1.4	10	3.03 ± 0.09	1.13 ± 0.19	-9.2 ± 0.23	-8.12	1.08
2.	0.8	10	2.84 ± 0.09	0.996 ± 0.30	-9.16 ± 0.39	-8.19	0.97
3.	0.8	10	2.59 ± 1.16	1.61 ± 0.62	-12.1 ± 0.86	-7.90	4.24

Average	-	-	2.82 ± 0.45	1.1 ± 0.37	-10.15 ± 0.5	-8.07	2.1
---------	---	---	----------------	---------------	-----------------	-------	-----

Summary

Our NMR-based studies have unveiled that TRBP2-dsRBD2, like other proteins in the dsRBD family, does not show any significant backbone structural perturbations upon RNA binding. dsRBDs interact with topologically different dsRNAs. The dsRNA binding by TRBP2-dsRBD2 lies in the slow-to-intermediate timescale of binding. Line-broadening in all the core residues, excluding the terminals, and recovery of line-broadening on shortening the length of dsRNA indicate that the protein undergoes diffusion along the length of the RNA. The ITC study unveiled that TRBP2-dsRBD2 binds to D12 RNA more strongly than TRBP2-dsRBD1 with a K_d of $1.1 \pm 0.37 \mu\text{M}$. Negative ΔH suggests that there are polar and charge-charge interactions between the dsRBDs (lysine and arginine-rich protein) and the dsRNA (negatively charged phosphate backbone).

Our previous study showed that dsRBD1 explores and engages topologically different dsRNA owing to its high conformational dynamics (Paithankar et al., 2022). In this study so far, we gather that dsRBD2 firmly adheres to the RNA ligand due to its conserved RNA-binding stretches.

References

- Acevedo, R., Orench-Rivera, N., Quarles, K. A., & Showalter, S. A. (2015). Helical defects in microRNA influence protein binding by TAR RNA binding protein. *PLoS One*, *10*(1), e0116749. doi:10.1371/journal.pone.0116749
- Ankush Jagtap, P. K., Muller, M., Masiewicz, P., von Bulow, S., Hollmann, N. M., Chen, P. C., . . . Hennig, J. (2019). Structure, dynamics and roX2-lncRNA binding of tandem double-stranded RNA binding domains dsRBD1,2 of Drosophila helicase Maleless. *Nucleic Acids Res*, *47*(8), 4319-4333. doi:10.1093/nar/gkz125
- Bevilacqua, P. C., & Cech, T. R. (1996). Minor-groove recognition of double-stranded RNA by the double-stranded RNA-binding domain from the RNA-activated protein kinase PKR. *Biochemistry*, *35*(31), 9983-9994. doi:10.1021/bi9607259
- Bou-Nader, C., Barraud, P., Pecqueur, L., Perez, J., Velours, C., Shepard, W., . . . Hamdane, D. (2019). Molecular basis for transfer RNA recognition by the double-stranded RNA-binding domain of human dihydrouridine synthase 2. *Nucleic Acids Res*, *47*(6), 3117-3126. doi:10.1093/nar/gky1302
- Chiliveri, S. C., Aute, R., Rai, U., & Deshmukh, M. V. (2017). DRB4 dsRBD1 drives dsRNA recognition in Arabidopsis thaliana tasi/siRNA pathway. *Nucleic Acids Res*, *45*(14), 8551-8563. doi:10.1093/nar/gkx481
- Chiliveri, S. C., & Deshmukh, M. V. (2014). Structure of RDE-4 dsRBDs and mutational studies provide insights into dsRNA recognition in the Caenorhabditis elegans RNAi pathway. *Biochem J*, *458*(1), 119-130. doi:10.1042/BJ20131347
- Fierro-Monti, I., & Mathews, M. B. (2000). Proteins binding to duplexed RNA: one motif, multiple functions. *Trends Biochem Sci*, *25*(5), 241-246. doi:10.1016/s0968-0004(00)01580-2
- Koh, H. R., Kidwell, M. A., Raganathan, K., Doudna, J. A., & Myong, S. (2013). ATP-independent diffusion of double-stranded RNA binding proteins. *Proc Natl Acad Sci U S A*, *110*(1), 151-156. doi:10.1073/pnas.1212917110

- Krovat, B. C., & Jantsch, M. F. (1996). Comparative mutational analysis of the double-stranded RNA binding domains of *Xenopus laevis* RNA-binding protein A. *J Biol Chem*, *271*(45), 28112-28119. doi:10.1074/jbc.271.45.28112
- Masliah, G., Barraud, P., & Allain, F. H. (2013). RNA recognition by double-stranded RNA binding domains: a matter of shape and sequence. *Cell Mol Life Sci*, *70*(11), 1875-1895. doi:10.1007/s00018-012-1119-x
- Nanduri, S., Rahman, F., Williams, B. R., & Qin, J. (2000). A dynamically tuned double-stranded RNA binding mechanism for the activation of antiviral kinase PKR. *EMBO J*, *19*(20), 5567-5574. doi:10.1093/emboj/19.20.5567
- Paithankar, H., Tarang, G. S., Parvez, F., Marathe, A., Joshi, M., & Chugh, J. (2022). Inherent conformational plasticity in dsRBDs enables interaction with topologically distinct RNAs. *Biophys J*, *121*(6), 1038-1055. doi:10.1016/j.bpj.2022.02.005
- Tants, J. N., Fesser, S., Kern, T., Stehle, R., Geerlof, A., Wunderlich, C., . . . Sattler, M. (2017). Molecular basis for asymmetry sensing of siRNAs by the *Drosophila* Loqs-PD/Dcr-2 complex in RNA interference. *Nucleic Acids Res*, *45*(21), 12536-12550. doi:10.1093/nar/gkx886
- Tian, B., Bevilacqua, P. C., Diegelman-Parente, A., & Mathews, M. B. (2004). The double-stranded-RNA-binding motif: interference and much more. *Nat Rev Mol Cell Biol*, *5*(12), 1013-1023. doi:10.1038/nrm1528
- Ucci, J. W., Kobayashi, Y., Choi, G., Alexandrescu, A. T., & Cole, J. L. (2007). Mechanism of interaction of the double-stranded RNA (dsRNA) binding domain of protein kinase R with short dsRNA sequences. *Biochemistry*, *46*(1), 55-65. doi:10.1021/bi061531o
- Wostenberg, C., Lary, J. W., Sahu, D., Acevedo, R., Quarles, K. A., Cole, J. L., & Showalter, S. A. (2012). The role of human Dicer-dsRBD in processing small regulatory RNAs. *PLoS One*, *7*(12), e51829. doi:10.1371/journal.pone.0051829
- Yadav, D. K., Zigackova, D., Zlobina, M., Klumpler, T., Beaumont, C., Kubickova, M., . . . Lukavsky, P. J. (2020). Stauf1 reads out structure and sequence features in ARF1 dsRNA for target recognition. *Nucleic Acids Res*, *48*(4), 2091-2106. doi:10.1093/nar/gkz1163

Yamashita, S., Nagata, T., Kawazoe, M., Takemoto, C., Kigawa, T., Guntert, P., . . . Yokoyama, S. (2011). Structures of the first and second double-stranded RNA-binding domains of human TAR RNA-binding protein. *Protein Sci*, 20(1), 118-130. doi:10.1002/pro.543

Yang, S. W., Chen, H. Y., Yang, J., Machida, S., Chua, N. H., & Yuan, Y. A. (2010). Structure of Arabidopsis HYPONASTIC LEAVES1 and its molecular implications for miRNA processing. *Structure*, 18(5), 594-605. doi:10.1016/j.str.2010.02.006

Chapter 5

**Intrinsic and RNA-induced
Conformational dynamics of
TRBP2-dsRBD2**

Introduction

Recent investigations have suggested that the dissimilar RNA-binding behaviour of dsRBDs in Dicer (Wostenberg et al., 2012), DGCR8-dsRBD1 (Wostenberg, Noid, & Showalter, 2010), PKR (Nanduri, Carpick, Yang, Williams, & Qin, 1998; Nanduri, Rahman, Williams, & Qin, 2000), Rnt1p (Hartman et al., 2013) , and double-stranded-RNA-binding protein 4 (DRB4) (Chiliveri, Aute, Rai, & Deshmukh, 2017) might be attributed to the protein dynamics (Chao & Byrd, 2020; Kleckner & Foster, 2011; Palmer, 2004). Along these lines, we have recently established the role of TRBP2-dsRBD1 dynamics in dsRBD-dsRNA interactions and have proposed that it adopts a conformationally dynamic structure to recognize a set of topologically different dsRNA structures (Paithankar et al., 2022). The data suggested that the presence of conformational exchange in the μ s timescale could help TRBP2-dsRBD1 to dynamically tune itself for targeting conformationally distinct dsRNA substrates.

The previous chapters show that TRBP2dsRBD2 binds to D12 RNA with a higher affinity than dsRBD1 despite both the domains having a conserved tertiary fold (with small differences in primary sequence and length of secondary structures). In this chapter, we explore whether the intrinsic protein dynamics plays a key role in the differential RNA-binding of TRBP2 dsRBDs. To achieve this, we have first deciphered the intrinsic protein dynamics of TRBP2-dsRBD2 at ps-ns (using spin relaxation experiments) and μ s-ms timescale (using NMR relaxation dispersion experiments) and then compared it with TRBP2-dsRBD1 which was previously studied in our lab (Paithankar et al., 2022). Further, the interaction between TRBP2-dsRBD2 and the topologically different dsRNAs (described in Chapter 4) hints towards the presence of a slow-to-intermediate timescale of exchange. Only minute structural perturbations have been observed in TRBP2-dsRBD2 upon RNA binding. Thus, an attempt has been made to gain further insights into the RNA-binding mechanism of TRBP2-dsRBD2, wherein protein dynamics have been probed in the presence of D12 RNA (0.05 equivalent of protein) at various timescales. For ps-ns timescales dynamics, nuclear spin relaxation experiments (R_1 , R_2 , and $[^1\text{H}]-^{15}\text{N}$ -nOe) were recorded. Conformational exchange processes in the timescale of 0.3-10 ms were studied by recording CPMG RD experiments, and for 10 μ s–10 ms timescale measurements, HARD NMR experiments were performed. The perturbation of conformational dynamics of TRBP2-dsRBD2 in the presence

of RNA was then compared to dsRBD1 (Paithankar et al., 2022). This helped us understand the dsRNA-recognition and RNA-binding phenomenon in TRBP2 in the light of protein dynamics.

Results and Discussion

5.1. Intrinsic protein dynamics at ps-ns timescales using nuclear relaxation measurements.

To understand the picosecond to nanosecond (ps-ns) timescale motions of apo-dsRBD2, NMR spin relaxation data (R_1 , R_2 , and $[^1\text{H}]-^{15}\text{N}$ nOe) was recorded on 600 and 800 MHz NMR spectrometers. The plots for R_1 , R_2 , and $[^1\text{H}]-^{15}\text{N}$ nOe at 600 and 800 MHz magnetic fields showed the expected trend (Figure 5.1.1). The R_1 of the core residues showed lower values at a higher magnetic field and similar values in the terminal regions at the two magnetic fields.

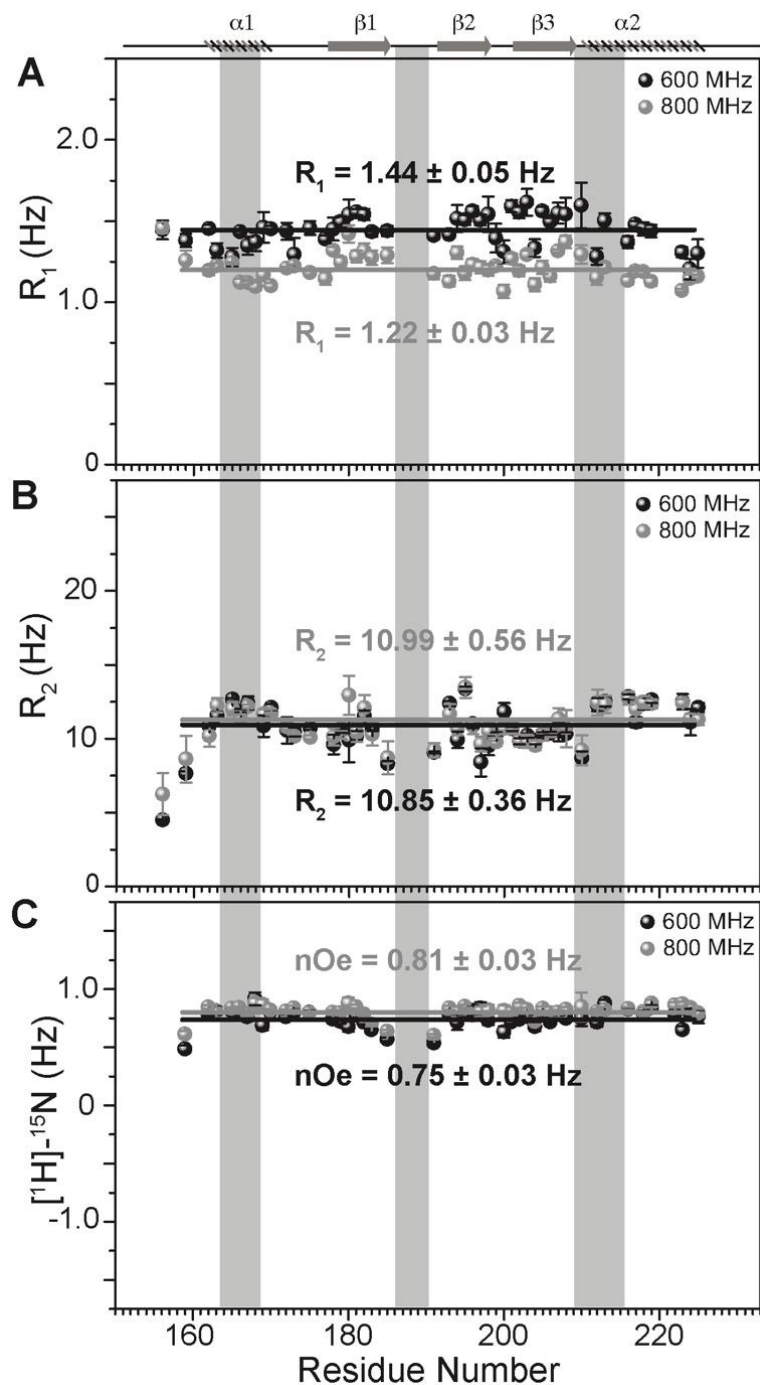


Figure 5.1.1: Intrinsic protein dynamics of TRBP2-dsRBD2 at ps-ns timescale using nuclear relaxation measurements. A) Longitudinal relaxation rates (R_1), B) transverse relaxation rates (R_2), and heteronuclear $[^1\text{H}]-^{15}\text{N}$ -nOe, as measured for common residues of TRBP2-dsRBD2 on 600 MHz (black) and 800 MHz (grey) magnetic fields plotted against residue numbers for both fields. Average R_1 , R_2 , and $[^1\text{H}]-^{15}\text{N}$ -nOe of the core residues at 600 MHz has been depicted in the black bar, and at 800 MHz has been depicted in the grey bar, respectively. The secondary structure

of the protein has been shown on the top, and three RNA-binding regions have been highlighted using vertical grey bars.

The increase of core R_1 rates (decreasing T_1) with increasing magnetic field indicates that most of the core residues lie on the right-hand side of the T_1 minima in the standard plot of T_1 vs. $\omega\tau_c$, where ω is the frequency of motions, and τ_c is rotational correlation time (Figure 5.1.2) (Bloembergen, Purcell, & Pound, 1948)

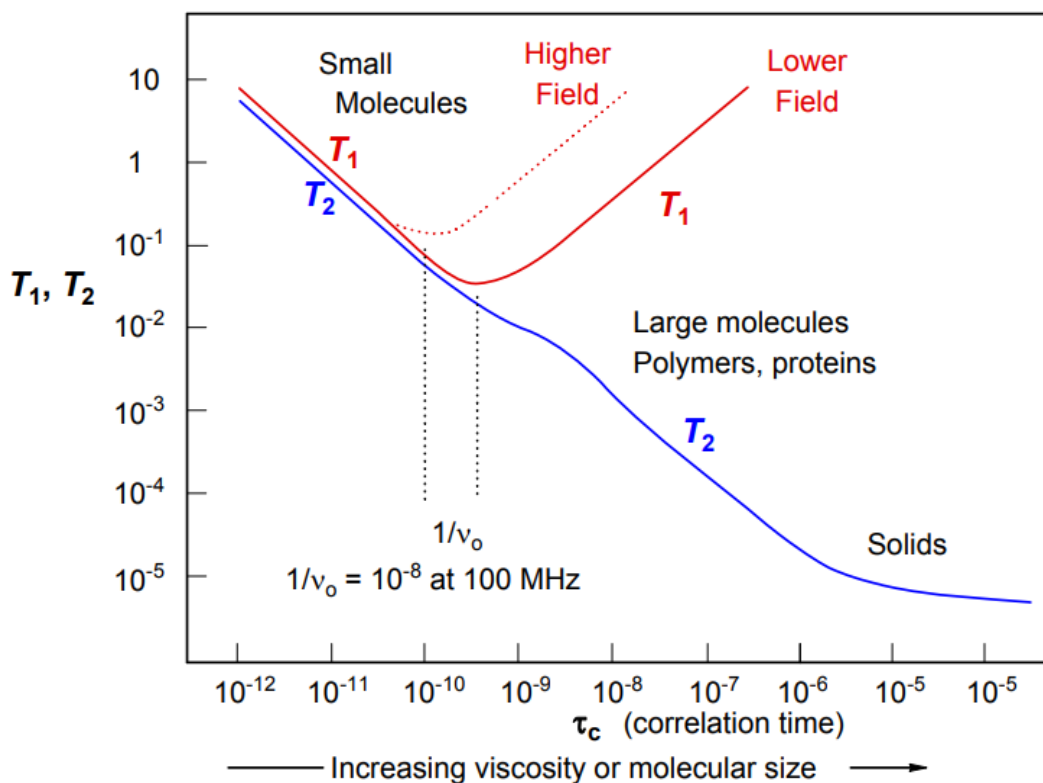


Figure 5.1.2: Standard plot of T_1 vs. $\omega\tau_c$, where ω is the frequency of motions, and τ_c is rotational correlation time (Adapted from (Bloembergen, Purcell, & Pound, 1948).

The core residues had average R_1 rates of 1.44 ± 0.05 Hz (Figure 5.1.1A). The R_2 rates of a few N-terminal (S156, N159) and core residues (V180, M194, R197, V198, G207, and A217) marginally increased (0.7–3 Hz) when measured at 800 MHz than when measured at 600 MHz, suggesting a very insignificant presence of the R_{ex} component in the linewidth of these residues in

the experimental used for the study (Figure 5.1.1B). The terminal (N159, T227) and the loop residues (G185, E191, F200, and K210) exhibited relative flexibility as indicated by lower R_2 and nOe values (Figure 5.1.1C). A few residues lying in different secondary structures, e.g., Q165, L167, and V168 in α_1 ; T193 and T195 in β_2 ; L212, A213, N216, and L223 in α_2 exhibited only slightly higher (> 1 Hz) than the average R_2 rate (11.02 ± 0.39 Hz), indicating a thin conformational exchange in the secondary structured regions (Figure 5.1.1B).

Next, the ps-ns timescales dynamics of TRBP2-dsRBD2 and dsRBD1 were compared. The average R_1 (dsRBD1 = 1.52 ± 0.03 Hz; dsRBD2 = 1.44 ± 0.05 Hz) and R_2 rates (dsRBD1 = 9.83 ± 0.17 Hz; dsRBD2 = 11.02 ± 0.39 Hz) for the two domains were very similar (Figure 5.1.1 for apo TRBP2-dsRBD2 and Figure 5.1.3 for apo TRBP2-dsRBD1 (Paithankar et al., 2022), respectively). In contrast, dsRBD1 had significantly lower average heteronuclear steady-state nOe values (0.63 ± 0.02) than dsRBD2 (0.75 ± 0.029), indicating a more rigid core at the picosecond timescale motions in dsRBD2.

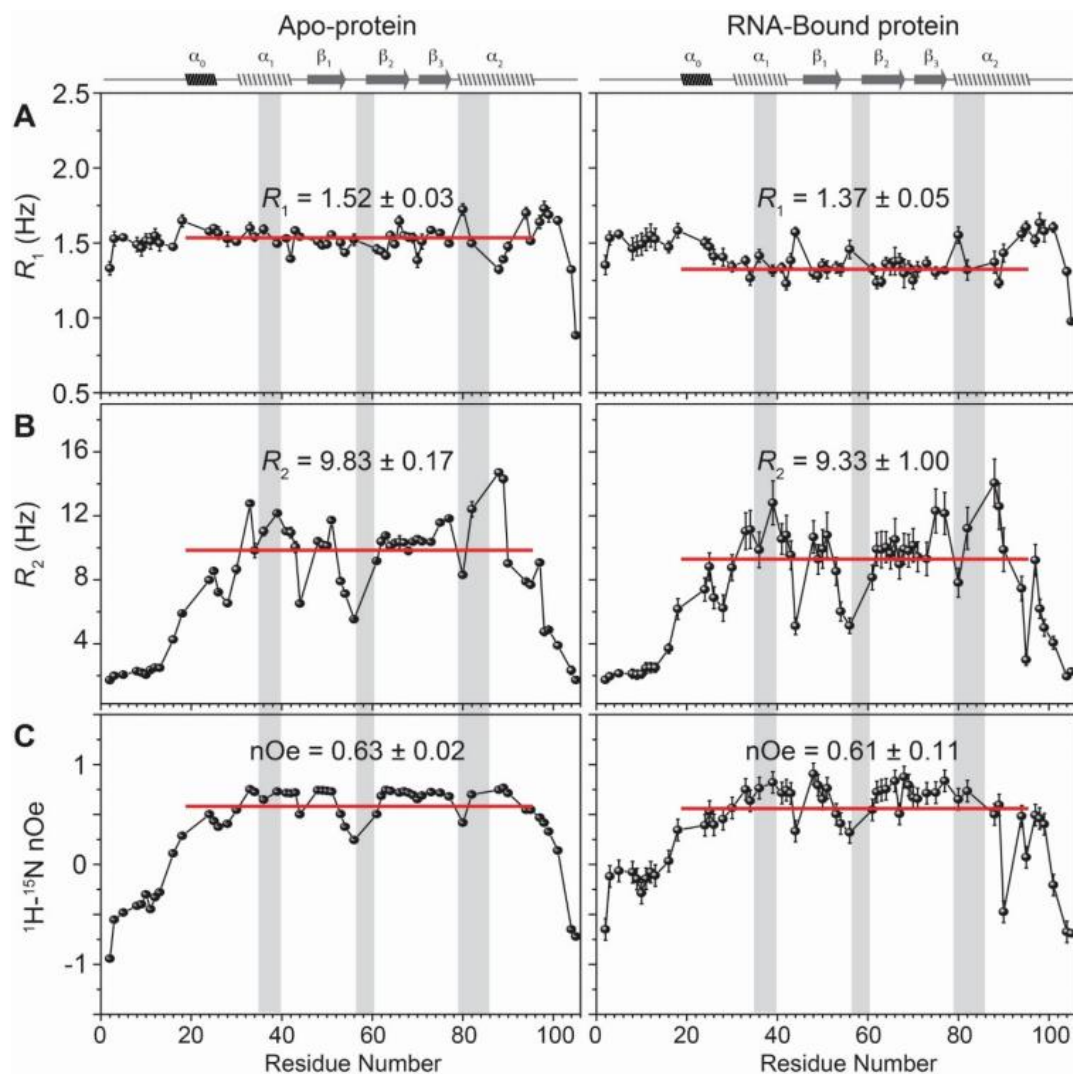


Figure 5.1.3: Relaxation parameters (A) R_1 , (B) R_2 , and (C) $^1\text{H}-^{15}\text{N}$ nOe plotted against the residue numbers for apo-protein (left panel), and D10RNA-bound TRBP2-dsRBD1 (right panel). The secondary structure of TRBP2-dsRBD1 has been mentioned on the top, and the RNA-binding region of the protein has been marked in grey vertical columns. Adapted from (Paithankar et al., 2022).

The extended model-free analysis of the relaxation data for the two core domains allowed us to compare the order parameters S^2 , R_{ex} components, and global tumbling time (τ_c) (Figure 5.1.4). The overall order parameters for dsRBD1 followed the expected trend of higher values in the secondary structured regions and lower values in the terminals and loops (Figure 5.1.4, Top panel). Interestingly, the secondary structural motifs α_1 , loop 2, and α_2 , containing RNA-binding regions of dsRBD2, showed a higher rigidity than dsRBD1. We hypothesize that the absence of

Pro in loop 2 of dsRBD1, despite its shorter length than dsRBD2, might be responsible for the additional observed flexibility in dsRBD1 (refer to section 3.5 of Chapter 3). Loop 1 (W173, L175) of dsRBD2 containing the stabilizing tryptophan (absent in dsRBD1) also showed higher rigidity than dsRBD1. The global tumbling time (τ_c) of dsRBD2 was 6.90 ns, and that of dsRBD1 was 7.64 ns, suggesting a more compact structure of dsRBD2 than dsRBD1. This result corroborates the CD-based determination of the melting point of the two constructs. TRBP2-dsRBD2 exhibits a higher T_m than TRBP2-dsRBD1, thus suggesting a stronger network of interactions in TRBP2-dsRBD2 (Yamashita et al., 2011). Indeed, it has been shown previously that the tryptophan (W173) present in the α_1 - β_1 of dsRBD2 (W is absent in dsRBD1 at this position) induced local hydrophobic and cation- π interactions with K171, E199, R200, F201, and V225, thereby enhancing the overall thermal stability of dsRBD2 (Yamashita et al., 2011).

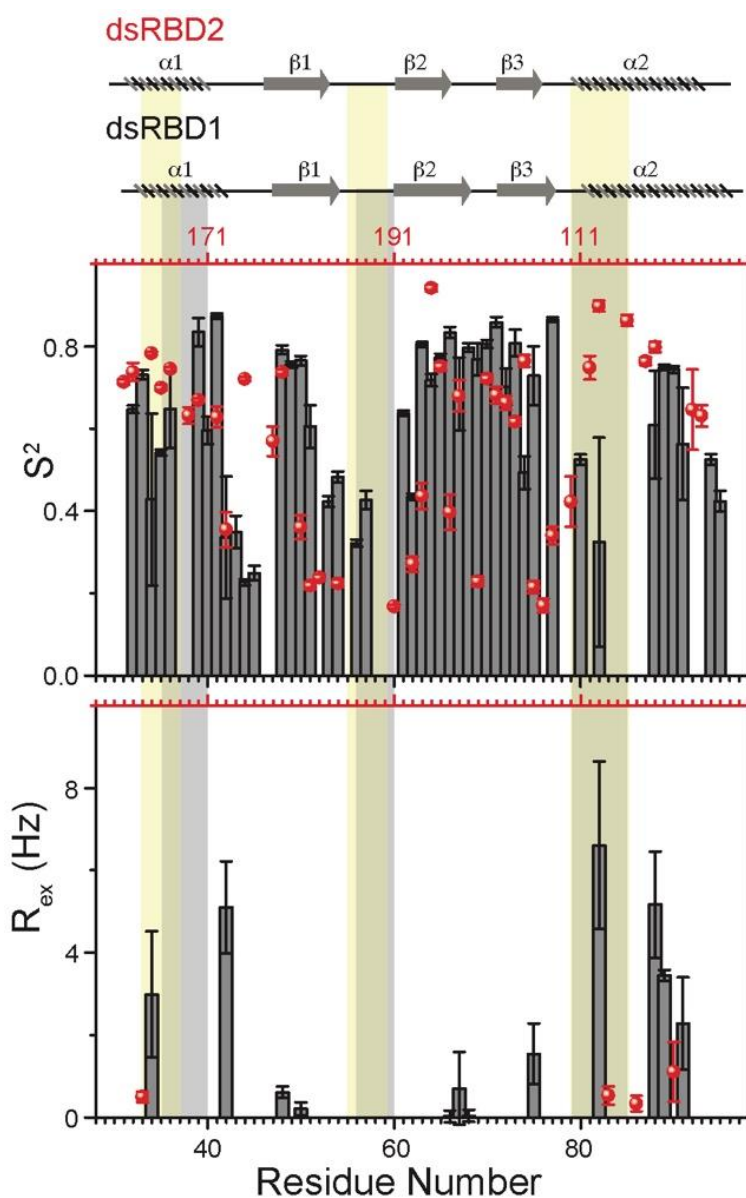


Figure 5.1.4: Order parameters (S^2) (Top panel), and R_{ex} (bottom panel) as calculated using model-free fitting of the fast relaxation data for TRBP2-dsRBD1 (histograms) and TRBP2-dsRBD2 (red scatter) plotted against residue numbers. The secondary structure of both proteins has been shown on the top, and three RNA-binding regions have been highlighted using vertical grey bars (for TRBP2-dsRBD1) and using vertical yellow bars (for TRBP2-dsRBD2).

Only 4 residues of dsRBD2 could fit into the model-free model containing the exchange term (R_{ex}) as opposed to 11 residues in dsRBD1, suggesting that there is significantly lower conformational flexibility at the μ s-ms timescale in dsRBD2 (Figure 5.1.4, bottom panel). While

dsRBD2 depicted a low frequency (< 2 Hz) contribution to the line width of resonances in the RNA-binding regions (E166, N216, A219, and L223), dsRBD1 had a larger contribution (2–8 Hz) to the line width of resonances present all along the backbone (Figure 5.1.4). In summation, the plasticity at the ps-ns timescale is present in both the dsRBDs of TRBP, while the amplitude of motions is found to be largely restricted for the dsRBD2.

5.2. Intrinsic protein dynamics at slower ms timescale using CPMG relaxation dispersion measurements.

Similar to dsRBD1, dsRBD2 does not exhibit motions at a slower ms timescale as probed by the CPMG relaxation dispersion experiments. No dispersion was observed in the $R_{2,\text{eff}}$ rates with increasing ν_{CPMG} , suggesting the absence of motions sensitive to this experiment (Figures 5.2.1 and 5.2.2 for dsRBD2 and dsRBD1, respectively) (Paithankar et al., 2022).

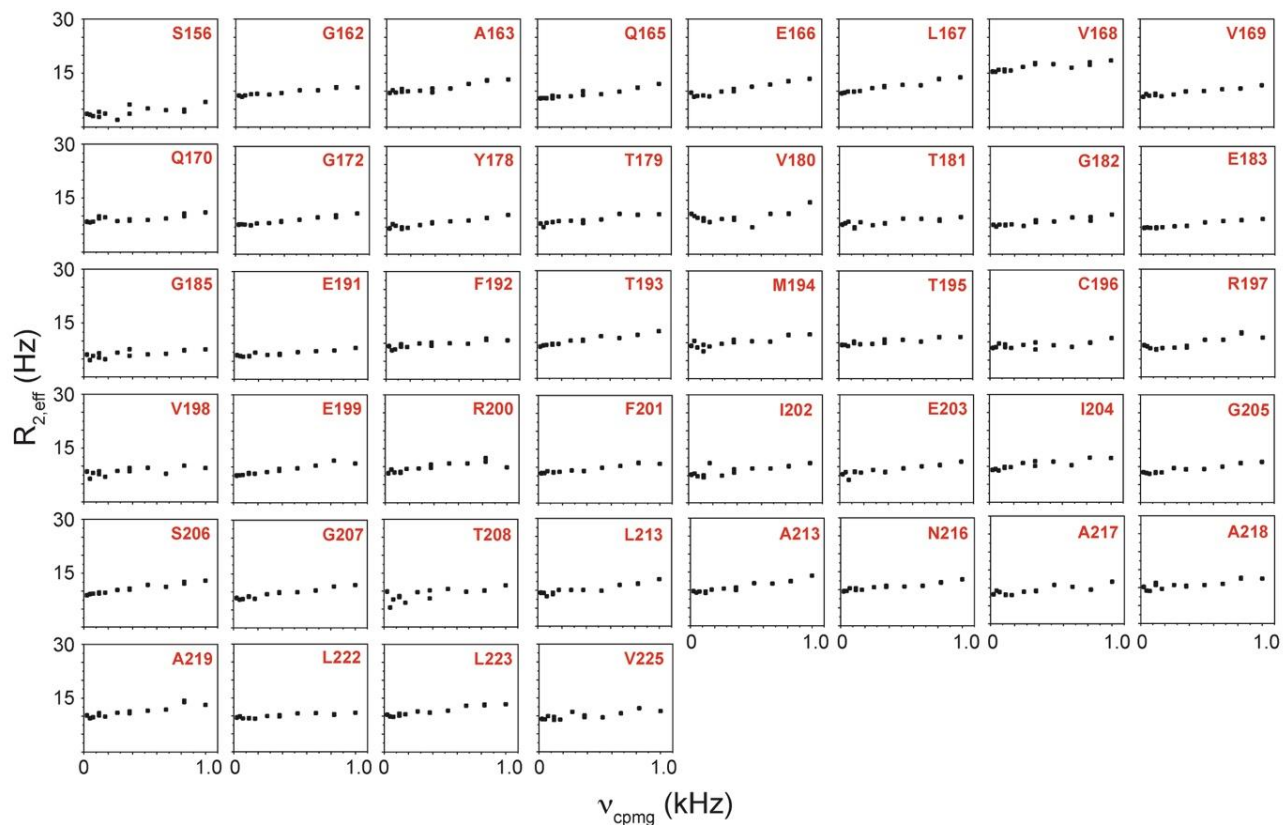


Figure 5.2.1: $R_{2,\text{eff}}$ rates plotted against ν_{CPMG} for the 44 non-overlapping residues of TRBP2-dsRBD2 measured at 600 MHz. The residue names and respective positions in the TRBP2 protein have been mentioned in each plot.

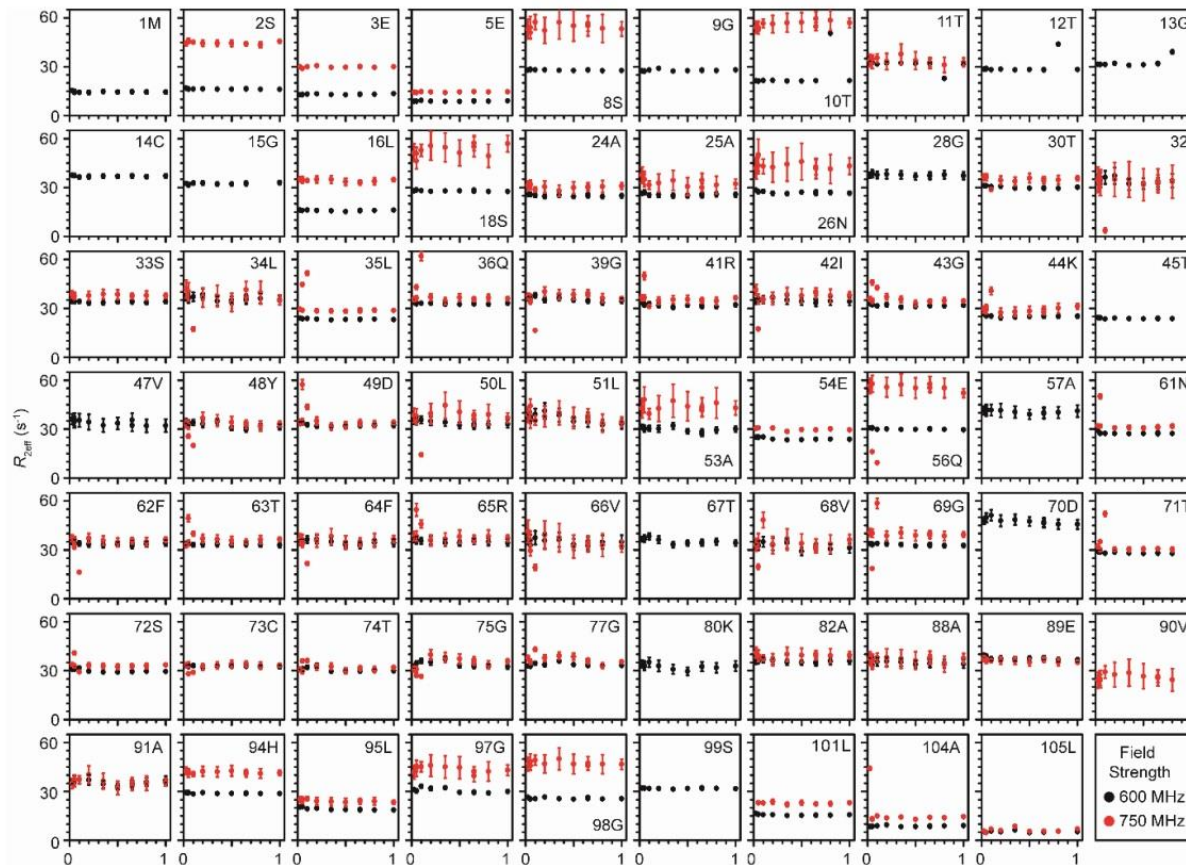


Figure 5.2.2: $R_{2,\text{eff}}$ rates as obtained from CPMG relaxation dispersion experiment plotted against the CPMG frequency for TRBP2-dsRBD1 measured at two magnetic fields 600 MHz (black) and 750 MHz (red). (Adapted from Paithankar *et al.*, Biophys J., 2022) (Paithankar *et al.*, 2022).

5.3. Intrinsic protein dynamics at 10 μs –10 ms timescale using heteronuclear adiabatic relaxation dispersion measurements.

The heteronuclear adiabatic relaxation dispersion (HARD) NMR experiment was used to study NMR spin relaxation in a rotating frame (Chao & Byrd, 2016; Mangia, Traaseth, Veglia, Garwood, & Michaeli, 2010; Traaseth *et al.*, 2012). The dispersion in relaxation rates is created by changing the shape of a hyperbolic secant (HS $_n$, where n = stretching factor) adiabatic pulse that

is used to create the spin-lock. HARD experiments are sensitive to the conformational exchange processes occurring on the 10 μ s–10 ms timescales. The $R_{1\rho}$ and $R_{2\rho}$ relaxation rates showed that with an increase in applied spin-lock field strength from HS1 to HS8, the $R_{1\rho}$ rates increased and the $R_{2\rho}$ rates decreased for both dsRBD1 and dsRBD2 (Figure 5.3.1). The extent of dispersion was much less in the core residues of dsRBD2, indicating the absence of higher conformational dynamics in the dsRBD2 (shown by purple bars on the right side of each of the panels in Figure 5.3.1).

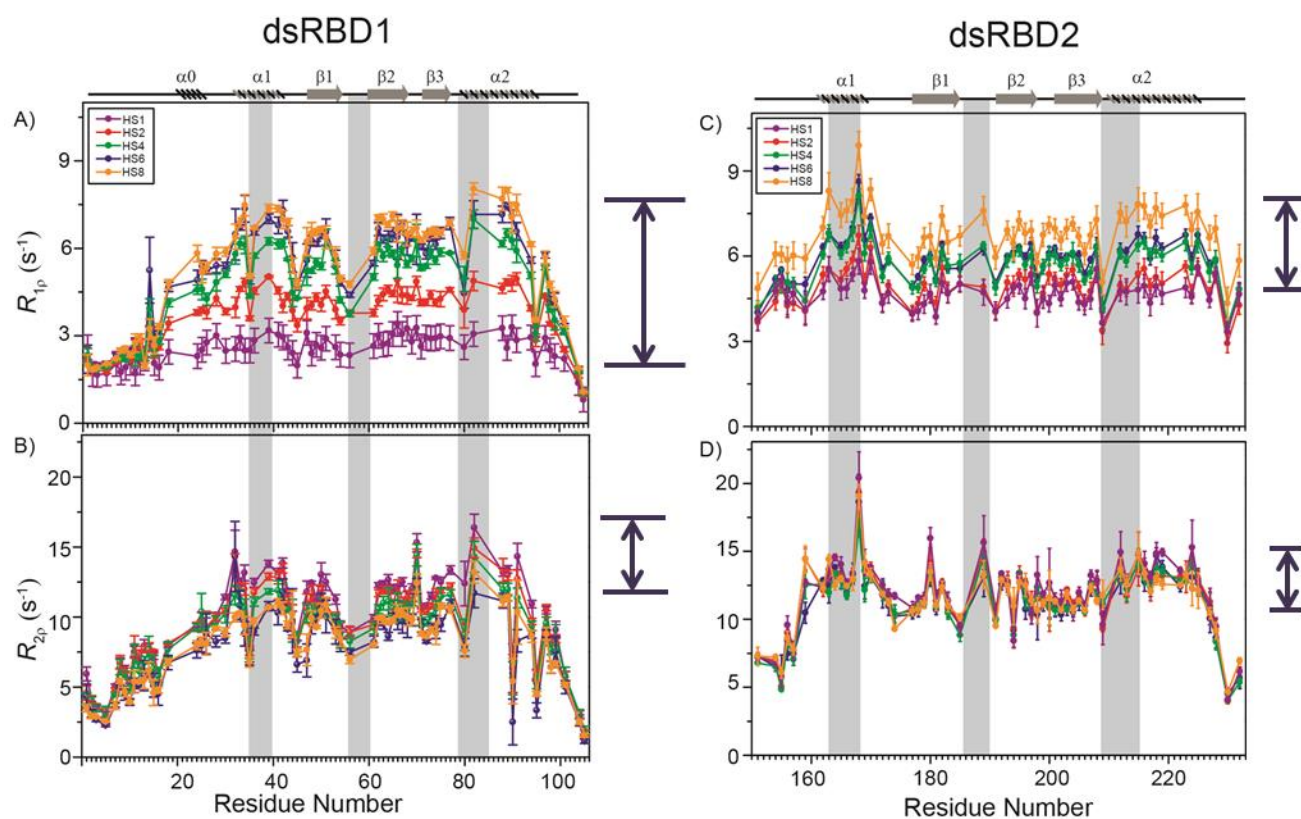


Figure 5.3.1: Representation of Heteronuclear Adiabatic Relaxation Dispersion (HARD) experiments recorded on ^{15}N -TRBP2-dsRBD1 (left) and ^{15}N -TRBP2-dsRBD2 (right) on the 600 MHz NMR spectrometer. Top-panel: $R_{1\rho}$, and Bottom-panel: $R_{2\rho}$ rates plotted against residue numbers. Increasing applied spin-lock field strength has been denoted by increasing the stretching factor, n (in HS n). The secondary structure has been shown on the top, and three RNA-binding regions have been highlighted using vertical grey bars. Different colors indicate different hyperbolic secant family of pulse (HS n) with increasing stretching factors ($n = 1, 2, 4, 6, 8$).

The $R_{1\rho}$ and $R_{2\rho}$ rates were then fit to Block-McConnell equations by using the geometric approximation approach (Chao & Byrd, 2016) to extract the rate of exchange (k_{ex}) and the excited state population (p_B) (Figures 5.3.2).

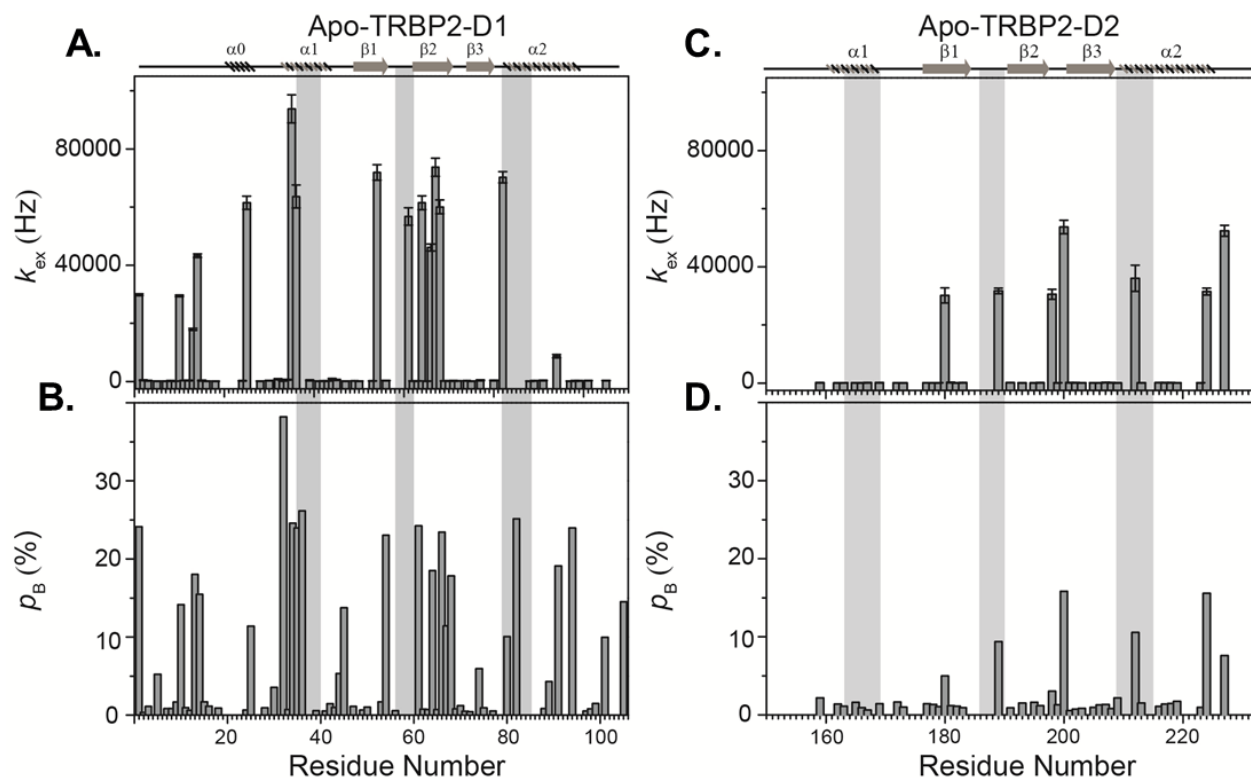


Figure 5.3.2: Conformational exchange in apo- TRBP2-dsRBD1 and TRBP2-dsRBD2. Rate of exchange between the ground state and excited state (k_{ex}) of (A) TRBP2-dsRBD1 and (C) TRBP2-dsRBD2; Excited state population (p_B) as obtained by the geometric approximation method plotted against residue numbers of (B) TRBP2-dsRBD1 and (D) TRBP2-dsRBD2. The secondary structure has been depicted on the top, and three RNA-binding regions have been highlighted using vertical grey bars.

The number of residues with $k_{ex} > 5,000$ Hz and $> 10\%$ p_B (red and green, medium and big spheres) differed vastly between the two domains (Figure 5.3.3). Only 3 residues with such conformational exchange in dsRBD2 were identified: R200 (loop 3), L212 and R224 (α_2); whereas in dsRBD1, the number was 15, distributed along the entire backbone of the protein (Figures 5.3.2 and 5.3.3), similar to what was observed in PKR-dsRBD1, where 75% of the residues from dsRBM1 showed $R_{ex} > 1$ Hz (Nanduri et al., 2000). Interestingly, all three conserved RNA-

binding regions in dsRBD1: α_1 (L35, Q36), β_1 - β_2 loop (E54), and α_2 (N61) were brimming with a $k_{ex} > 50,000$ Hz. To sum it up, most of the dsRBD2 core showed low conformational exchange ($k_{ex} < 5000$ Hz), depicted in blue small spheres, while the dsRBD1 domain was undergoing significantly higher conformational exchange ($k_{ex} > 5000$ Hz) (Figure 5.3.3).

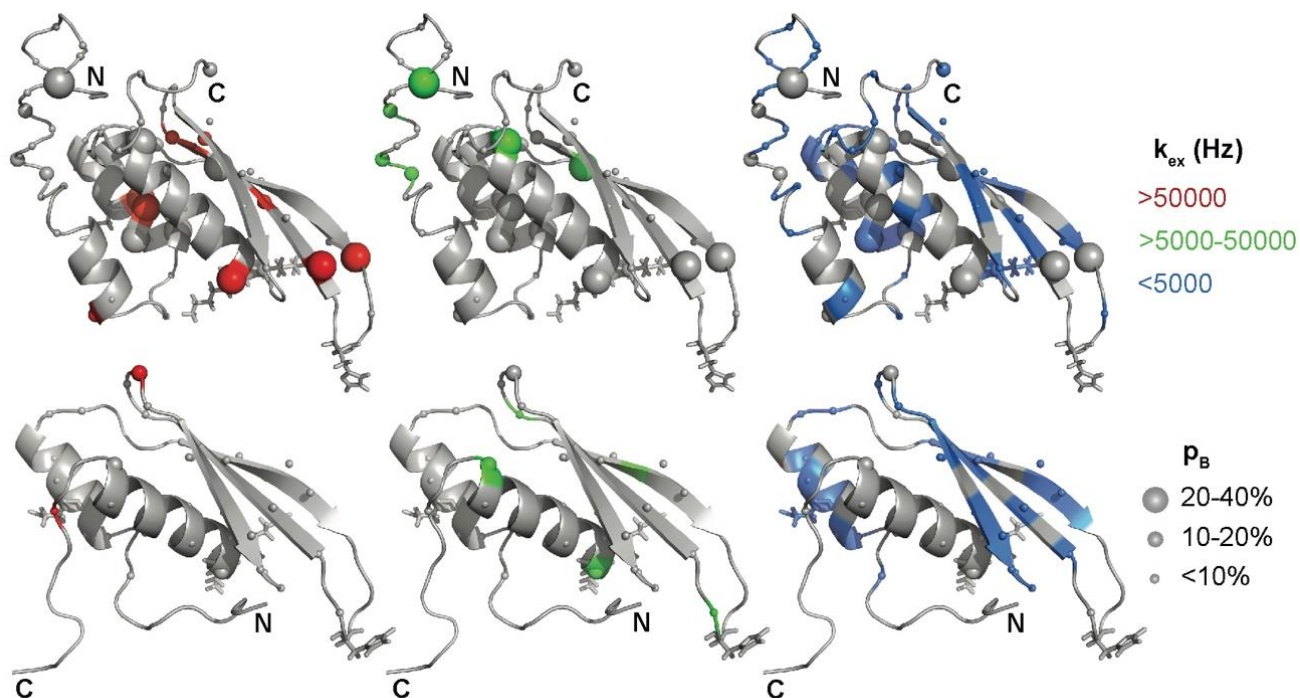


Figure 5.3.3: Mapping of k_{ex} , and p_B , on the CS-Rosetta structure of apo-TRBP2-dsRBD1 (Top Panel) and TRBP2-dsRBD2 (Bottom Panel). Different colors highlight the distribution of k_{ex} values, and the sphere's diameter indicates the extent of p_B along the protein backbone. The residues have been marked in different colors to highlight the distribution of k_{ex} values, and the diameters of the sphere indicate the extent of p_B along the protein backbone. The RNA-binding residues have been depicted in stick mode.

A similar extensive fast and slower timescale conformational dynamics has also been observed for DRB4 protein, where the first domain was found to have a large conformational exchange compared to the second domain (Chiliveri et al., 2017).

5.4. Conformational dynamics perturbations in TRBP2-dsRBD2 at ps-ns timescales in the presence of RNA ligand

Minute structural changes in TRBP2-dsRBD2 in the presence of RNA necessitated a deeper understanding of the conformational dynamics perturbations at multiple timescales. In the presence of D12 RNA, the average R_1 rates (apo = 1.44 ± 0.05 Hz; bound = 1.37 ± 0.07 Hz) and nOe values (apo = 0.75 ± 0.029 ; bound = 0.72 ± 0.076) remained unperturbed, while there was a significant increase in the average R_2 rates (apo = 11.02 ± 0.39 Hz; bound = 20.04 ± 1.11 Hz) (Figure 5.4.1). The apparent increase in the R_2 rates ($= R_2^* + R_{ex}$) indicates a perturbation in the μ s-ms timescale dynamics, to which only R_2 rates are sensitive. This phenomenon occurs either due to an increase in intrinsic R_2^* resulting from an increase in the residence time of the RNA on the protein, or an increase in the R_{ex} component caused by a chemical exchange between apo- and D12-bound state, or RNA-induced conformational exchange in the protein. Interestingly, such a perturbation in R_2 rates was not found for the dsRBD1 upon RNA-binding (Paithankar et al., 2022). The terminal residues (N159, Q154, Q155, S156, E157, V225, V228, L230, A232), a few residues in the vicinity of loop regions (E177, E183, G185, E191, S209) showed a lower than average bound-state R_2 rates than the rest of the core indicating a faster motion induced in these residues. Upon addition of the D12 RNA, the R_2 rates and nOe values of the N- and C-terminal residues (S156, E157, T227, V228, L230, A232), $\beta 1$ (E177), the loop 2 region (E183, G185, 189, E191), and the loop 4 region (S209) decreased, indicating further enhanced flexibility (Figure 5.4.1, right panel).

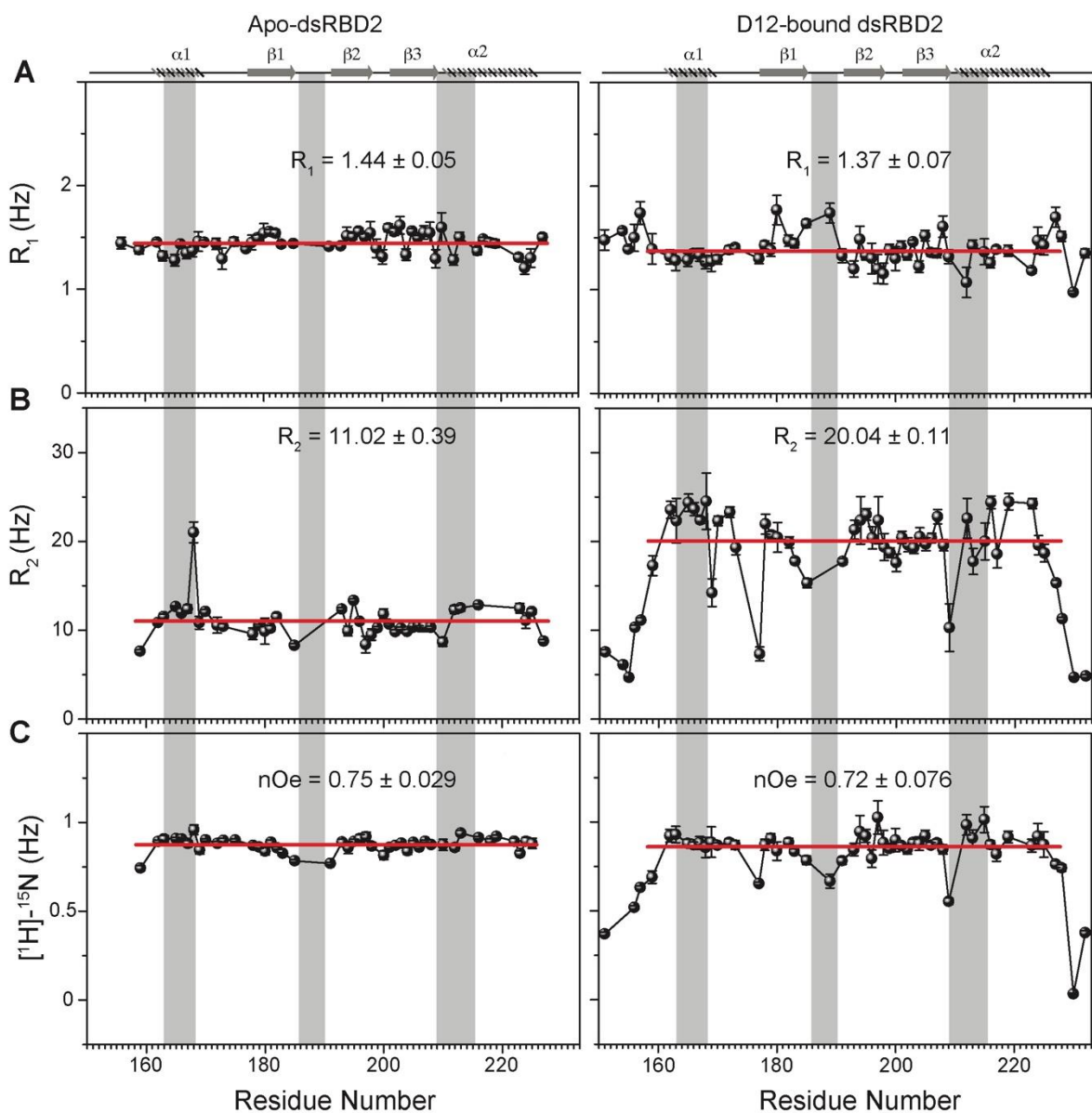


Figure 5.4.1: Spin relaxation parameters (A) R_1 , (B) R_2 , and (C) $[^1\text{H}]-^{15}\text{N}$ nOe plotted against residue numbers for apo-TRBP2-dsRBD2 (left panel) and D12-bound TRBP2-dsRBD2 (right panel) measured on 600 MHz at 298 K. The secondary structure of TRBP2-dsRBD1 and TRBP2-dsRBD2 have been mentioned at the top, and the RNA-binding region of the proteins have been marked using grey vertical bars.

The extended model-free analysis of apo- and RNA-bound TRBP2-dsRBD2 suggested that the anisotropic (ellipsoid) diffusion model was the best fit for the global motion of both (Figure 5.4.2). The global tumbling time (τ_c) of core TRBP2-dsRBD2 in the presence of RNA was 10.9 ns

as against 6.90 for the apo-dsRBD2 core, indicating an apparent increase in molecular weight. The overall higher S^2 values for TRBP2-dsRBD2 indicated a rigidification of the backbone amide vectors in the presence of D12 RNA (Figure 5.4.2, top-panel). A few residues in the $\alpha 1$ (E166) and $\alpha 2$ (N216, A219, L223) regions exhibited a R_{ex} component > 1 Hz, lying in the vicinity of the reported RNA-binding regions 1 and 3. The few number of residues with a significant R_{ex} (> 2 Hz) — implying the presence of μ s-ms timescale motions — increased in the case of bound-state. R_{ex} was found to be induced in the $\alpha 1$ (V168), $\beta 1$ (Y178), $\beta 2$ (T195), $\beta 3$ (I204), and $\alpha 2$ (N216, L223) region (Figure 5.4.2, bottom-panel), thereby indicating that not only the RNA-binding residues but the rest of the core might play a role while interacting with dsRNA substrates. The presence of R_{ex} at multiple sites (in addition to RNA-binding regions) rules out the chemical exchange between apo- and D12-bound state contributes to R_{ex} , thereby implying that RNA-induced conformational exchange is the predominant contributor to R_{ex} and to increased line broadening (or apparent R_2 rates, as also discussed in Chapter 4, Section 4.1).

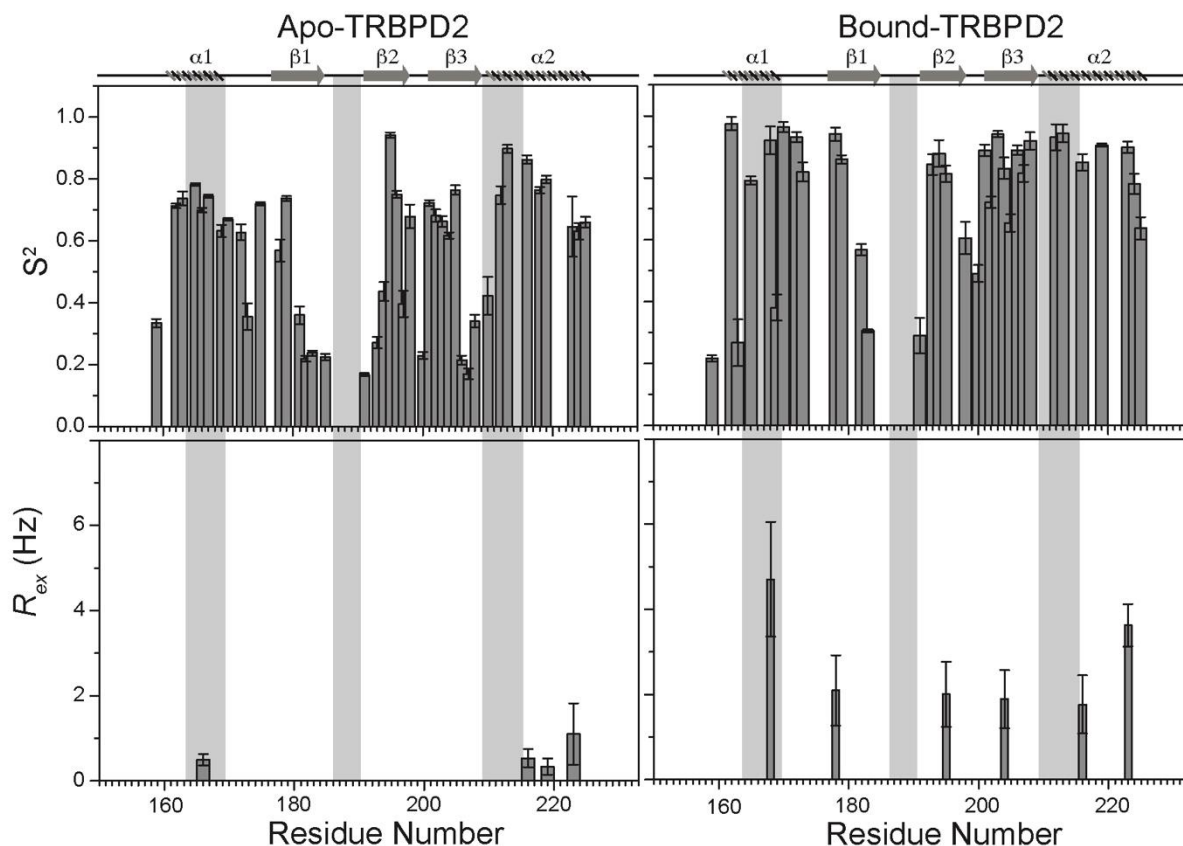


Figure 5.4.2: Extended model-free analysis of apo- and RNA-bound TRBP2-dsRBD2. Order parameters (S^2) (Top-panel), and R_{ex} (bottom-panel) as calculated using model-free fitting of the fast relaxation data for apo-TRBP2-dsRBD2 (left-panel) and D12 RNA-bound-TRBP2-dsRBD2 (right-panel) plotted against residue numbers. The secondary structures for the protein have been shown on the top, and three RNA-binding regions have been highlighted using vertical grey bars.

5.5. Protein dynamics at slower ms timescale (0.3-10 ms) using CPMG relaxation dispersion measurements in presence of RNA

The effective transverse relaxation rates, R_{2eff} , for TRBP2-dsRBD2, were plotted against the CPMG frequencies (ν_{CPMG}) in the presence of D12 RNA (Figure 5.5). None of the residues in either condition showed significant dispersion (> 5 Hz) in the R_{2eff} rates with the increase in ν_{CPMG} , suggesting motions in the 0.3-10 ms timescale sensitive to this experiment remain absent in D12RNA-bound TRBP2-dsRBD2 (Figure 5.5). The same observation was made in case of apo-TRBP2-dsRBD2 CPMG RD experiment (Figure 5.2.1) earlier.

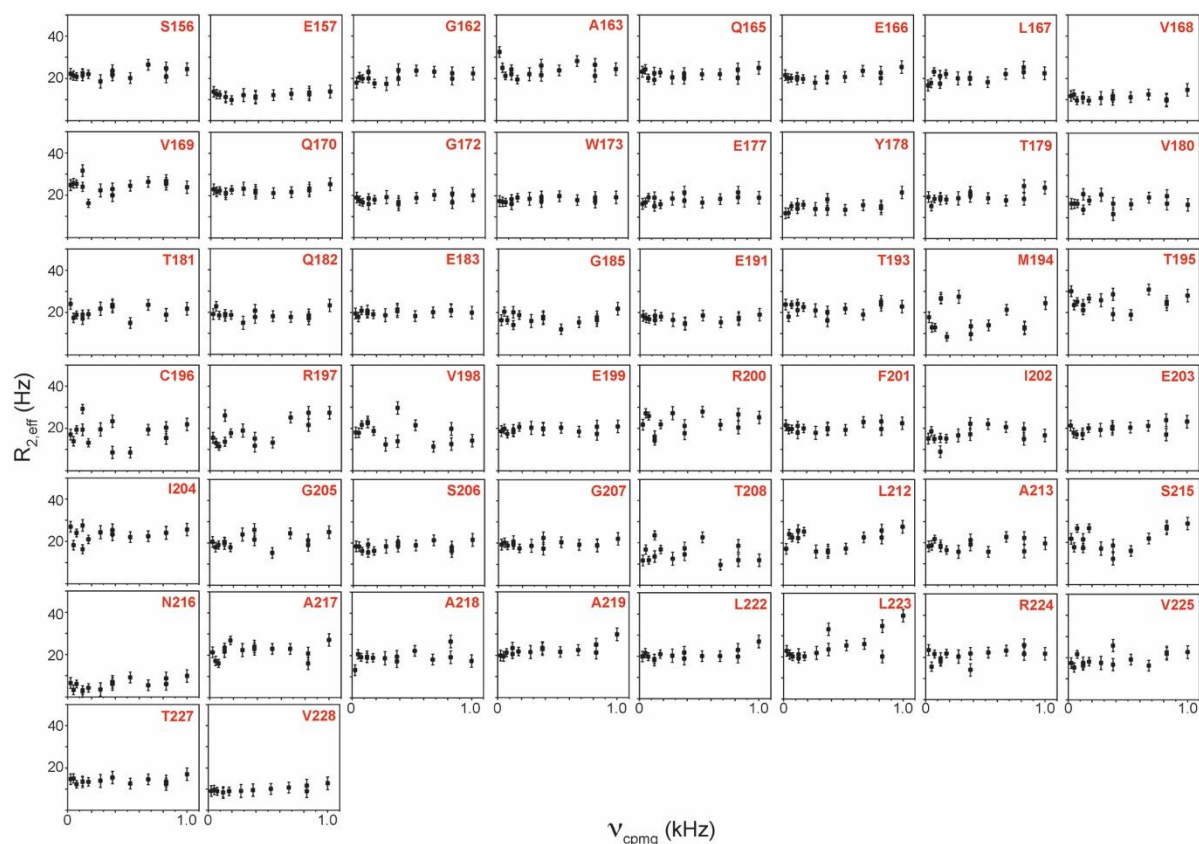


Figure 5.5.1: $R_{2, \text{eff}}$ rates plotted against ν_{CPMG} for the 50 non-overlapping residues of TRBP2-dsRBD2 measured in the presence of D12 RNA on the 600 MHz NMR spectrometer. Residue names and respective positions in the TRBP2 protein have been mentioned in each plot.

5.6. Protein dynamics at the 10 μs –10 ms timescale using HARD relaxation dispersion measurements

The results obtained from the Heteronuclear Adiabatic Relaxation Dispersion (HARD) relaxation dispersion NMR experiments recorded for TRBP2-dsRBD2 in the presence of D12-RNA were quite intriguing. The $R_{1\rho}$ and $R_{2\rho}$ relaxation rates showed that with the increase in applied spin-lock field strength from HS1 to HS8, the $R_{1\rho}$ rates increased and the $R_{2\rho}$ rates decreased for both apo- and RNA-bound protein (Figure 5.6.1). The extent of dispersion increased in the presence of RNA.

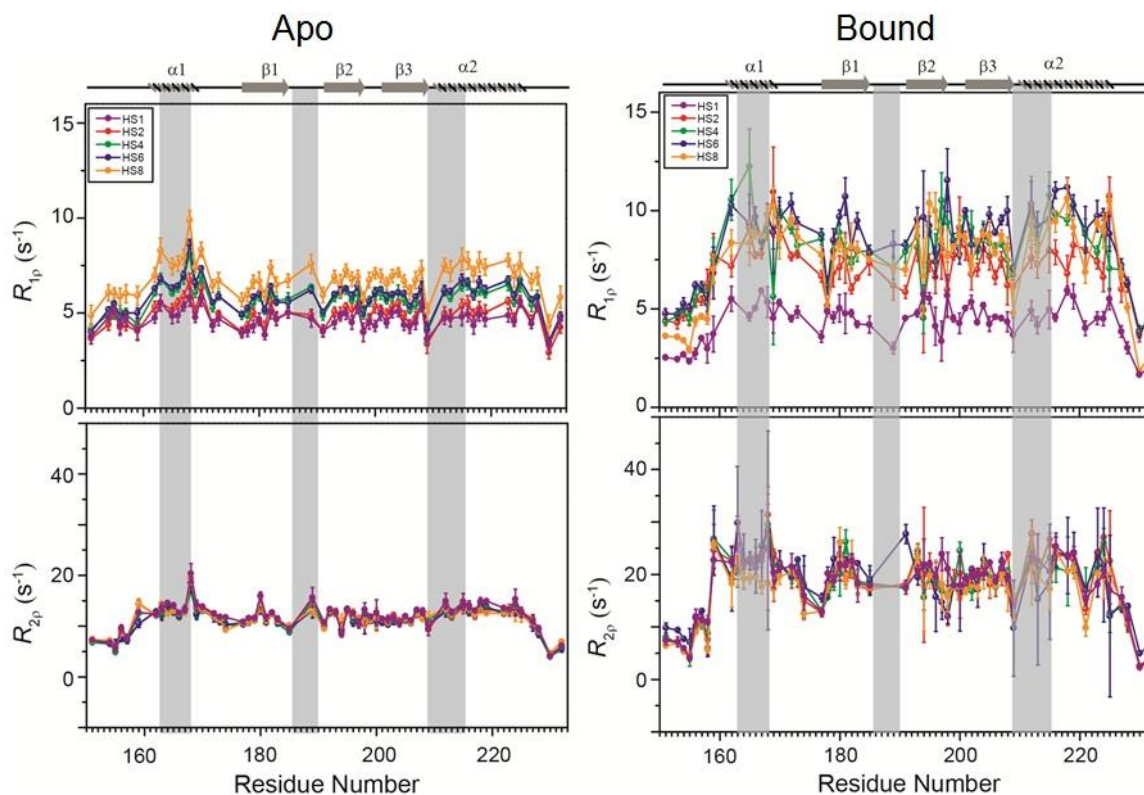


Figure 5.6.1: Heteronuclear Adiabatic Relaxation Dispersion (HARD) experiments recorded on ^{15}N -TRBP2-dsRBD2 in the absence (left Panel) and presence of D12-RNA (right Panel) on the 600 MHz NMR spectrometer. Top-panel: $R_{1\rho}$, and Bottom-panel: $R_{2\rho}$ rates plotted against residue numbers. Increasing applied spin-lock field strength is denoted

by increasing the stretching factor, n (in HS n). The secondary structure has been shown on the top, and three RNA-binding regions have been highlighted using vertical grey bars.

The $R_{1\rho}$ and $R_{2\rho}$ rates were fit to Block-McConnell equations by using the geometric approximation approach (Chao & Byrd, 2016) to extract the rate of exchange (k_{ex}) and the excited state population (p_{B}), as previously done in case of apo-protein.

In the presence of RNA, there was massive induction of 10 μs –10 ms timescale conformational dynamics, as reflected by the increase in the number of residues having significant k_{ex} (Figure 5.6.2). The extent of enhancement in k_{ex} varied along the backbone of the core protein. For example, a k_{ex} of 5000–50,000 kHz with 10–20% p_{B} (green spheres) was observed in α_1 (G162, L167), loop3 (R200), and α_2 (A213, A219) and 20–40% p_{B} in α_1 (V168), and β_3 (E203), depicted by the medium and big green spheres, respectively (Figure 5.6.2B & D). The residues V198 in loop 3 and M221 in the α_2 region exhibited the presence of the highest frequency of motion with a $k_{\text{ex}} > 50,000$ Hz. Intriguingly, among these residues, L167, V168 (α_1), and A213 (α_2) lie in the reported RNA-binding regions 1 and 3, respectively. L167 and V168 are adjacent to the key RNA binding residue E165 (region 1), which interacts directly with the RNA minor groove. A213 precedes the important KR-helix motif in the α_2 region of dsRBD2. The K214 and R215 residues make ionic interactions with the negatively charged phosphate backbone of the RNA major groove. The interaction between the RNA and the RNA-binding residues of the protein might induce conformational exchange within the nearby residues like in the case of G162 (region 1), A219 and M221 (region 2). Additionally, residues like R197 (β_2); V198 and R200 (L3); E203 and G207 (β_3) are further from RNA binding regions with $k_{\text{ex}} > 5000$ Hz. Thus, the ligand affected not only the RNA-binding residues but the entire protein.

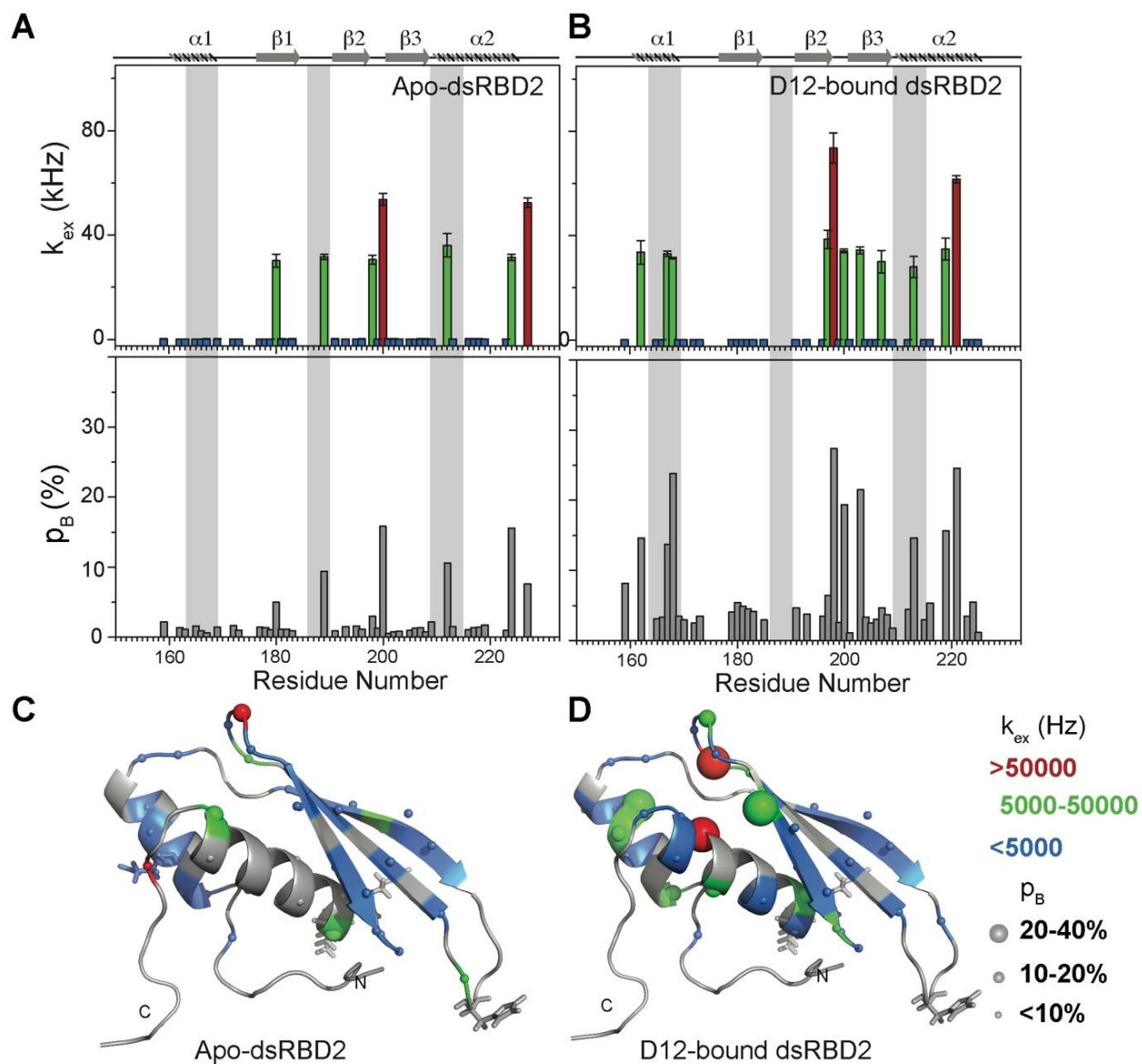


Figure 5.6.2: Conformational exchange in (A) apo- and (B) D12-bound- TRBP2-dsRBD2. Top panel: Rate of exchange between the ground state and excited state (k_{ex}); Bottom panel: excited state population (p_B) as obtained by the geometric approximation method, using the HARD experiment, plotted against residue numbers. Mapping of k_{ex} , and p_B , on the CS-Rosetta structure of apo TRBP2-dsRBD2, as extracted for (C) apo TRBP2-dsRBD2 and (D) D12-bound TRBP2-dsRBD2. Different colors highlight the distribution of k_{ex} values, and the sphere's diameter indicates the extent of p_B along the protein backbone. The RNA-binding residues have been depicted in stick mode.

5.7. Perturbation of 10 μ s–10 ms timescale protein dynamics in presence of RNA of TRBP2-dsRBD2

Significant perturbations in terms of $\Delta k_{\text{ex}} (k_{\text{bound}} - k_{\text{apo}}) > 10,000$ Hz were mapped on the structure of the protein (Figure 5.7). There was an enhancement of k_{ex} in the residues lying in $\alpha 1$ (G162, L167), loop 3 (V198), end of $\beta 3$ (G203), and $\alpha 2$ (A213, A219) region. Concomitantly, a suppression of exchange was observed in $\beta 1$ (V180), loop 3 (R200), and $\alpha 2$ (A212, A224) regions. A tantalizing relay of exchange was seen between two residue pairs in close spatial proximity. For instance, exchange was induced in V198 and quenched in R200 in the loop 3 region. Similarly, in the case of A213 and L212 falling in the N-terminal RNA-binding region 3, and A219 and R224 lying in the C-terminal of $\alpha 2$, the former of the pairs underwent an increase in k_{ex} , while the latter observed a decrease (Figure 5.7). Thus, the enhancement of RNA-induced conformational exchange was accommodated by allosteric quenching of the same. Altogether, there was a significant induction of 10 μs –10 ms timescale motions over the entire backbone of TRBP2-dsRBD2 in the presence of RNA. This induction of motions could be ascribed to either an exchange between the apo- and RNA-bound state of the protein, conformational dynamics in the RNA-bound state of the protein, or the previously reported sliding motion of the protein on the dsRNA (Ankush Jagtap et al., 2019; Chiliveri & Deshmukh, 2014; Koh, Kidwell, Ragunathan, Doudna, & Myong, 2013; Tants et al., 2017).

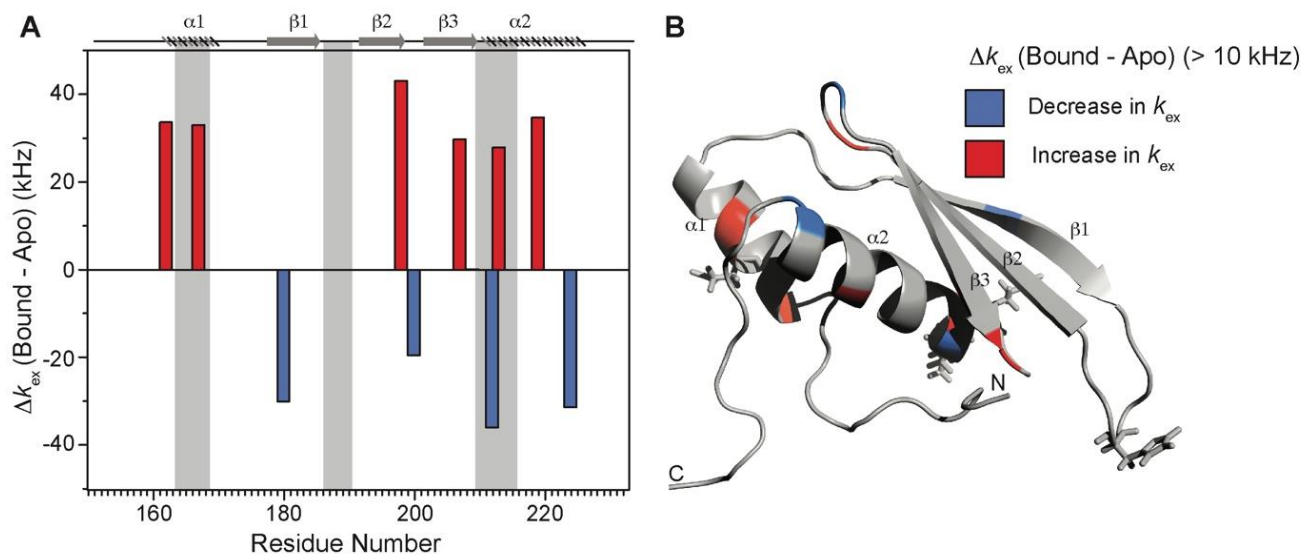


Figure 5.7: Conformational exchange perturbations in TRBP2-dsRBD2 in the presence of D12 RNA. (A) Δk_{ex} (D12-bound – apo) TRBP2-dsRBD2 plotted against residue numbers. The secondary structure has been shown on the top, and three RNA-binding regions have been highlighted using vertical grey bars. Only residues having significant perturbation ($\Delta k_{\text{ex}} > 10$ kHz) have been plotted, where an increase is shown in red, and a decrease is shown in blue,

(B) An increase in k_{ex} (red) and a decrease (blue) in the presence of D12 RNA indicated on the backbone of the CS-Rosetta structure of apo TRBP2-dsRBD2.

Interestingly, in TRBP2-dsRBD2, the extent of dynamics perturbation, in terms of Δk_{ex} , was significantly lower (10–50 kHz) than TRBP-dsRBD1 where at least 10 residues underwent a $\Delta k_{\text{ex}} > 50$ kHz in the presence of small dsRNA (Paithankar et al., 2022). Moreover, a relay of exchange was evident only in loop 3 and α_2 regions of dsRBD2 and not in α_1 region, which was observed earlier in dsRBD1 (Paithankar et al., 2022). Summing up, in the presence of RNA, dsRBD2 undergoes enhanced conformational exchange in the 10 μs –10 ms timescale. When compared to dsRBD1, dsRBD2 samples limited conformational space both in the absence and presence of D12-RNA.

Summary

The intrinsic k_{ex} profile of TRBP2-dsRBD1 and TRBP-dsRBD2 revealed the presence of 10 μs –10 ms timescale conformational dynamics distributed throughout the core dsRBD rather than being localized in the RNA-binding regions; however, the amplitude of motions was found a lot lower in dsRBD2 than that was observed in dsRBD1. dsRBD1, has remarkable flexibility and samples a larger number of conformational states, which allows it to recognize a wide range of structurally and sequentially diverse dsRNAs. Thus, we can conclude that dsRBD2 firmly adheres to the RNA ligand due to its conserved RNA-binding stretches and relatively high rigidity in the core domain. During their interaction with the RNA, both dsRBDs experience enhanced conformational changes on a fast timescale (picoseconds to nanoseconds) and a moderate timescale (microseconds to milliseconds), as observed through nuclear spin relaxation and rotating frame relaxation dispersion measurements. These dynamic changes likely enable the dsRBDs to slide along the length of the RNA, which explains the broadening of the signals observed during titration with longer RNAs. This sliding movement is likely crucial for other associated proteins, such as Dicer (Fareh et al., 2016; Lee & Doudna, 2012; Wilson et al., 2015), to carry out precise microRNA biogenesis. By understanding these processes, detailed insights were obtained into the intricate mechanisms involved in RNA processing, which has major implications in different biological processes.

References

- Ankush Jagtap, P. K., Müller, M., Masiewicz, P., von Bülow, S., Hollmann, N. M., Chen, P. C., . . . Hennig, J. (2019). Structure, dynamics and roX2-lncRNA binding of tandem double-stranded RNA binding domains dsRBD1,2 of *Drosophila* helicase Maleless. *Nucleic Acids Res*, *47*(8), 4319-4333. doi:10.1093/nar/gkz125
- Bloembergen, N., Purcell, E. M., & Pound, R. V. (1948). Relaxation Effects in Nuclear Magnetic Resonance Absorption. *Physical Review*, *73*(7), 679-712. doi:10.1103/PhysRev.73.679
- Chao, F. A., & Byrd, R. A. (2016). Geometric Approximation: A New Computational Approach To Characterize Protein Dynamics from NMR Adiabatic Relaxation Dispersion Experiments. *J Am Chem Soc*, *138*(23), 7337-7345. doi:10.1021/jacs.6b02786
- Chao, F. A., & Byrd, R. A. (2020). Protein Dynamics revealed by NMR Relaxation Methods. *Emerg Top Life Sci*, *2*(1), 93-105. doi:10.1042/etls20170139
- Chiliveri, S. C., Aute, R., Rai, U., & Deshmukh, M. V. (2017). DRB4 dsRBD1 drives dsRNA recognition in *Arabidopsis thaliana* tasi/siRNA pathway. *Nucleic Acids Res*, *45*(14), 8551-8563. doi:10.1093/nar/gkx481
- Chiliveri, S. C., & Deshmukh, M. V. (2014). Structure of RDE-4 dsRBDs and mutational studies provide insights into dsRNA recognition in the *Caenorhabditis elegans* RNAi pathway. *Biochem J*, *458*(1), 119-130. doi:10.1042/bj20131347
- Fareh, M., Yeom, K. H., Haagsma, A. C., Chauhan, S., Heo, I., & Joo, C. (2016). TRBP ensures efficient Dicer processing of precursor microRNA in RNA-crowded environments. *Nat Commun*, *7*, 13694. doi:10.1038/ncomms13694
- Hartman, E., Wang, Z., Zhang, Q., Roy, K., Chanfreau, G., & Feigon, J. (2013). Intrinsic dynamics of an extended hydrophobic core in the *S. cerevisiae* RNase III dsRBD contributes to recognition of specific RNA binding sites. *J Mol Biol*, *425*(3), 546-562. doi:10.1016/j.jmb.2012.11.025
- Kleckner, I. R., & Foster, M. P. (2011). An introduction to NMR-based approaches for measuring protein dynamics. *Biochim Biophys Acta*, *1814*(8), 942-968. doi:10.1016/j.bbapap.2010.10.012

- Koh, H. R., Kidwell, M. A., Rangunathan, K., Doudna, J. A., & Myong, S. (2013). ATP-independent diffusion of double-stranded RNA binding proteins. *Proc Natl Acad Sci U S A*, *110*(1), 151-156. doi:10.1073/pnas.1212917110
- Lee, H. Y., & Doudna, J. A. (2012). TRBP alters human precursor microRNA processing in vitro. *Rna*, *18*(11), 2012-2019. doi:10.1261/rna.035501.112
- Mangia, S., Traaseth, N. J., Veglia, G., Garwood, M., & Michaeli, S. (2010). Probing slow protein dynamics by adiabatic R(1rho) and R(2rho) NMR experiments. *J Am Chem Soc*, *132*(29), 9979-9981. doi:10.1021/ja1038787
- Nanduri, S., Carpick, B. W., Yang, Y., Williams, B. R., & Qin, J. (1998). Structure of the double-stranded RNA-binding domain of the protein kinase PKR reveals the molecular basis of its dsRNA-mediated activation. *Embo j*, *17*(18), 5458-5465. doi:10.1093/emboj/17.18.5458
- Nanduri, S., Rahman, F., Williams, B. R., & Qin, J. (2000). A dynamically tuned double-stranded RNA binding mechanism for the activation of antiviral kinase PKR. *Embo j*, *19*(20), 5567-5574. doi:10.1093/emboj/19.20.5567
- Paithankar, H., Tarang, G. S., Parvez, F., Marathe, A., Joshi, M., & Chugh, J. (2022). Inherent conformational plasticity in dsRBDs enables interaction with topologically distinct RNAs. *Biophys J*, *121*(6), 1038-1055. doi:10.1016/j.bpj.2022.02.005
- Palmer, A. G., 3rd. (2004). NMR characterization of the dynamics of biomacromolecules. *Chem Rev*, *104*(8), 3623-3640. doi:10.1021/cr030413t
- Tants, J. N., Fesser, S., Kern, T., Stehle, R., Geerlof, A., Wunderlich, C., . . . Sattler, M. (2017). Molecular basis for asymmetry sensing of siRNAs by the Drosophila Loqs-PD/Dcr-2 complex in RNA interference. *Nucleic Acids Res*, *45*(21), 12536-12550. doi:10.1093/nar/gkx886
- Traaseth, N. J., Chao, F. A., Masterson, L. R., Mangia, S., Garwood, M., Michaeli, S., . . . Veglia, G. (2012). Heteronuclear Adiabatic Relaxation Dispersion (HARD) for quantitative analysis of conformational dynamics in proteins. *J Magn Reson*, *219*, 75-82. doi:10.1016/j.jmr.2012.03.024

Wilson, R. C., Tambe, A., Kidwell, M. A., Noland, C. L., Schneider, C. P., & Doudna, J. A. (2015). Dicer-TRBP complex formation ensures accurate mammalian microRNA biogenesis. *Mol Cell*, 57(3), 397-407. doi:10.1016/j.molcel.2014.11.030

Wostenberg, C., Lary, J. W., Sahu, D., Acevedo, R., Quarles, K. A., Cole, J. L., & Showalter, S. A. (2012). The role of human Dicer-dsRBD in processing small regulatory RNAs. *PLoS One*, 7(12), e51829. doi:10.1371/journal.pone.0051829

Wostenberg, C., Noid, W. G., & Showalter, S. A. (2010). MD simulations of the dsRBP DGCR8 reveal correlated motions that may aid pri-miRNA binding. *Biophys J*, 99(1), 248-256. doi:10.1016/j.bpj.2010.04.010

Yamashita, S., Nagata, T., Kawazoe, M., Takemoto, C., Kigawa, T., Güntert, P., . . . Yokoyama, S. (2011). Structures of the first and second double-stranded RNA-binding domains of human TAR RNA-binding protein. *Protein Sci*, 20(1), 118-130. doi:10.1002/pro.543

Chapter 6

Conclusions

Conclusions

dsRNA-binding proteins (dsRBPs) play a vital role in maintaining the homeostasis of the cell. One of the vital regulatory pathways involving a battery of dsRBPs is the RNAi pathway, which is involved in post-transcriptional gene regulation. Among these dsRBPs, though the RNA-binding variation and function of TRBP2 was studied but the mechanism of RNA recognition remained to be deciphered. Here, in our study we have characterized the RNA-binding function and mechanism of TRBP2 protein and compared it with TRBP-dsRBD1 based on various biophysical techniques. From this work we could gather the following informations. TRBP2-dsRBD2 protein was successfully purified to conduct various biochemical and biophysical experiments. From the SEC-MALS study, dsRBD2 was found to be monomeric in solution (NMR buffer: pH 6.4, 298 K) with a molecular mass of 9.2 kDa. Of the total 84 residues (including the 4 Pro in construct), 73 residues could be successfully assigned using a battery of double and triple resonance NMR experiments. The CS-ROSETTA structure calculated from the 581 backbone and side-chain chemical shifts matched very well with the canonical structure of dsRBDs, with an RMSD of 1.28 Å when compared to a reported solution structure (2CPN). The comparison of the primary and tertiary structures of dsRBD1 and dsRBD2 of TRBP2 indicated that the structural fold is conserved despite having significant differences in the primary sequence (only 30% identity and 38% similarity). On comparing the secondary structures of the two dsRBDs, we found that the β_1 - β_2 loop (one of the important RNA-binding regions in the dsRBDs) is equal to the canonical length (6 aa) in dsRBD2, but in dsRBD1, it was one residue shorter. Moreover, the β_1 - β_2 loop has a conserved Pro residue (P186) in dsRBD2, which imparts vital flexibility and makes it easily available to the incoming RNA partner. dsRBD2 has an additional KR-helix motif in α_2 -helix, which is known to increase the RNA-binding affinity. Thus, all these differences between the two A-type dsRBDs of TRBP2 might have implications for the RNA-binding by the protein in the RNAi pathway.

NMR-based titration of TRBP2-dsRBD2 with miR16-1 mutants showed minute backbone structural perturbations. The dsRNA binding by TRBP2-dsRBD2 is suspected to lie in the slow-to-intermediate timescale. Extensive line-broadening and its recovery on shortening the length of dsRNA suggests the phenomenon of diffusion/sliding along the length of the RNA. ITC-based experiments revealed that TRBP2-dsRBD2 bound the 12 bp perfect A-form D12 RNA more strongly than dsRBD1 with a K_d of $1.1 \pm 0.37 \mu\text{M}$. It was found to be an enthalpy-driven reaction;

thus, polar and charge-charge interactions might be the key forces between the interacting RNA and the protein.

A comparison of the intrinsic conformational dynamics of TRBP2-dsRBD1 and TRBP2-dsRBD2 indicated dsRBD2 was relatively rigid and samples lesser conformational states than dsRBD1. The thermal stability and rigidity of the core can be attributed to the presence of the W173 in the α_1 - β_1 loop region. It was observed that the conformational dynamics was distributed throughout the core dsRBD and not limited to the RNA-binding regions in both the domains. However, the amplitude of such motions was significantly lower in dsRBD2 than in dsRBD1. This detailed comparison of conformational dynamics measured at multiple timescales in the two domains led us to propose that the dsRBD1, with its remarkable flexibility and accessibility to a larger number of conformational states, is able to recognize a wide range of structurally and sequentially diverse dsRNAs in the cellular pool. On the other hand, dsRBD2 firmly binds to the incoming RNA ligand (recognized by dsRBD1) due to its conserved RNA-binding residues and relatively high rigidity in the core domain.

While interacting with the RNAs, both dsRBDs undergo significant conformational exchange on a fast timescale (picoseconds to nanoseconds) and a moderate timescale (microseconds to milliseconds). The induced motions in the presence of RNA might enable the dsRBDs to diffuse/slide along the length of the RNA. This underlying phenomenon explains the broadening of the NH signals in the HSQC spectra observed during titration. The diffusion phenomenon helps the co-complex proteins of TRBP2, like Dicer, to carry out critical functions in the microRNA biogenesis pathway.

Model Proposed

It has been long established that despite engaging with a wide array of dsRNA molecules exhibiting diverse structures and sequences, dsRBDs remain unaffected in their own structural conformation during their involvement in critical cellular pathways. However, the more significant question that persisted was whether the protein dynamics plays a crucial role in these intriguing interactions. Though variability in the binding affinity for the two type-A dsRBDs of TRBP (pivotal protein in the RNAi pathway) has been reported, the specific contribution of conformational dynamics has remained unexplored until now. In this study, we have exclusively probed into the role of conformational dynamics of the two type-A dsRBDs of TRBP2 in RNA

recognition and binding. Our findings have unveiled that TRBP2-dsRBD2 samples a limiting conformational space in solution, and it is dsRBD1 that is the key player in recognizing sequentially and structurally diverse RNA substrates through its high conformational plasticity. While dsRBD1 explores and engages dsRNA via its dynamically interactive RNA-binding surface, dsRBD2 holds the RNA in position via stronger canonical contacts. Once bound to the RNA, the ensuing conformational exchange in both dsRBD1 and dsRBD2 might facilitate the domains to diffuse over the length of the RNA freely, thus playing a pivotal role in assisting Dicer-mediated differential cleavage of RNA (Figure 6.1). Thus, this study not only adds valuable insights into the mechanics of RNA-protein interactions but also underscores the significance of conformational dynamics in dictating the functional outcome in such intricate biological processes as the RNAi pathway.

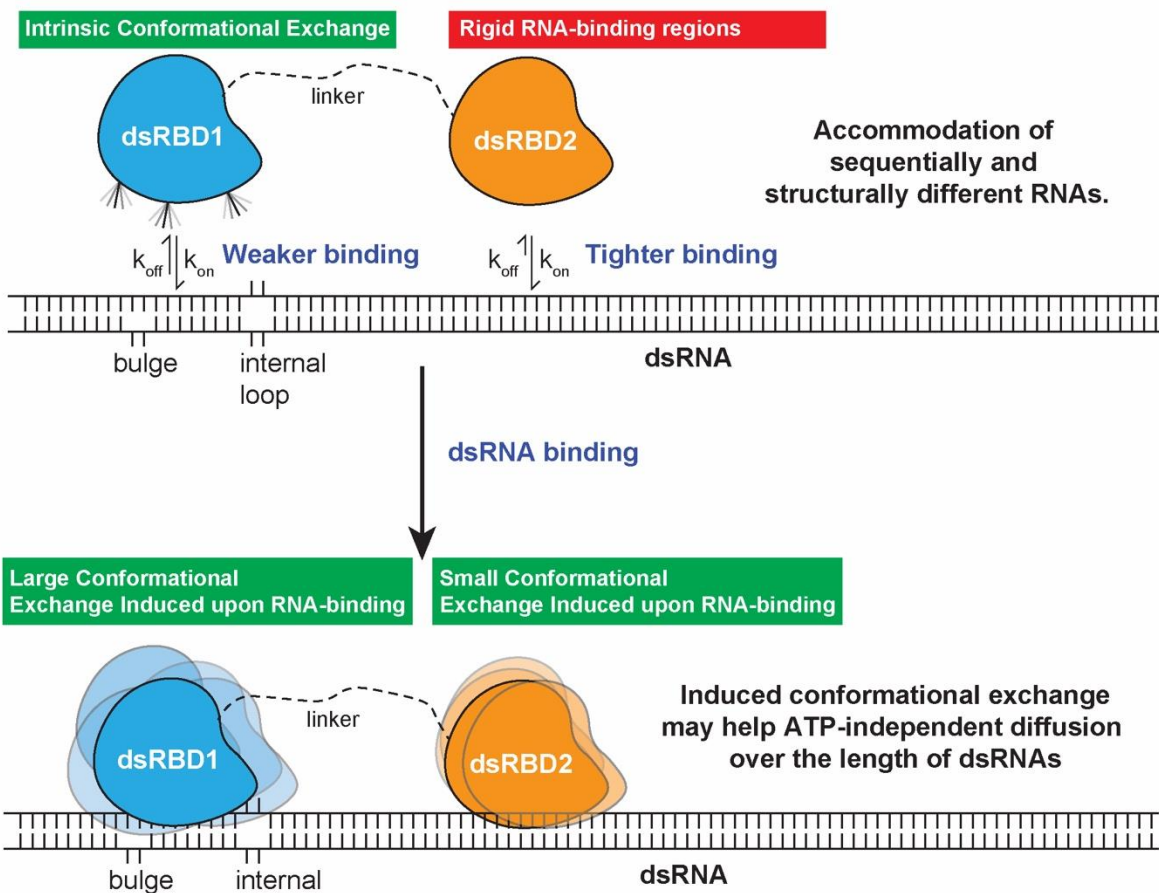


Figure 6.1: The model proposed for the two type-A dsRBDs in TRBP2 protein interacting with a target dsRNA. dsRBD2, with rigid and conserved RNA-binding regions, is able to bind the RNA tightly, whereas dsRBD1, with high intrinsic conformational exchange in the RNA-binding regions, is able to recognize different RNA structures (often with bulges and internal loops). Following this, the two dsRBDs, upon contacting the RNA, undergo enhanced conformational exchange to different extents. This enhanced conformational exchange, coupled with a differential binding affinity towards dsRNA, might enable the tandem dsRBDs to move along the backbone of the RNA molecule, leading to ATP-independent diffusion.

Appendix I

Supporting Tables

Table A.1: Nuclear spin relaxation data for apo TRBP2-dsRBD2 recorded at 600 MHz and 800 MHz NMR spectrometer.

Residue Number	600 MHz						800 MHz					
	R_1 (Hz)		R_2 (Hz)		NOE		R_1 (Hz)		R_2 (Hz)		NOE	
	Value	Error	Value	Error	Value	Error	Value	Error	Value	Error	Value	Error
S156	1.45	0.06	0.69	0.03			1.46	0.03	6.24	1.42	0.25	0.01
N159	1.38	0.04	0.73	0.02	0.48	0.03	1.26	0.06	8.61	1.59	0.61	0.03
G162	1.45	0.02	0.69	0.01	0.78	0.02	1.20	0.03	10.20	0.74	0.84	0.02
A163	1.32	0.04	0.76	0.03	0.81	0.04	1.22	0.02	12.27	0.47	0.82	0.02
Q165	1.28	0.06	0.78	0.03	0.82	0.02	1.24	0.01	12.03	0.46	0.84	0.01
E166	1.43	0.02	0.70	0.01	0.81	0.01	1.12	0.02	11.40	0.24	0.84	0.01
L167	1.35	0.06	0.74	0.03	0.76	0.04	1.12	0.01	12.18	0.11	0.79	0.02
V168	1.37	0.06	0.73	0.03	0.92	0.06	1.10	0.03			0.88	0.04
V169	1.46	0.09	0.68	0.04	0.69	0.04	1.17	0.02	11.68	0.31	0.87	0.04
Q170	1.45	0.02	0.69	0.01	0.80	0.01	1.10	0.02	11.69	0.10	0.82	0.01
G172	1.44	0.05	0.70	0.03	0.76	0.02	1.21	0.01	10.80	0.32	0.81	0.02
W173	1.29	0.10	0.77	0.06	0.80	0.03	1.22	0.01	10.15	0.16	0.84	0.02
L175	1.46	0.04	0.69	0.02	0.80	0.02	1.18	0.02	10.09	0.13	0.80	0.02
E177	1.39	0.02	0.72	0.01			1.15	0.04	9.65	0.56	0.59	0.01
Y178	1.45	0.07	0.69	0.03	0.74	0.03	1.32	0.02	10.13	0.60	0.80	0.02
T179	1.50	0.03	0.67	0.01	0.72	0.02	1.25	0.03	10.69	0.69	0.80	0.02
V180	1.54	0.09	0.65	0.04	0.68	0.04	1.42	0.05	12.93	1.34	0.88	0.05
T181	1.56	0.02	0.64	0.01	0.78	0.02	1.28	0.04	10.42	0.64	0.85	0.02
Q182	1.54	0.03	0.65	0.01	0.71	0.02	1.32	0.04	12.09	0.85	0.79	0.02
E183	1.43	0.03	0.70	0.01	0.65	0.01	1.28	0.04	10.30	0.76	0.70	0.01
G185	1.44	0.03	0.69	0.01	0.57	0.02	1.29	0.05	8.71	1.11	0.64	0.02
E191	1.41	0.02	0.71	0.01	0.54	0.01	1.18	0.03	9.23	0.49	0.60	0.01
F192							1.22	0.03	12.16	0.53	0.79	0.02
T193	1.42	0.02	0.71	0.01	0.78	0.03	1.13	0.03	11.67	0.67	0.84	0.02
M194	1.52	0.08	0.66	0.04	0.72	0.07	1.31	0.04	10.71	0.50	0.80	0.06
T195	1.51	0.03	0.66	0.01	0.78	0.03	1.18	0.04	13.47	0.70	0.85	0.02
C196	1.56	0.03	0.64	0.01	0.82	0.04	1.23	0.04	10.85	0.52	0.78	0.02
R197	1.51	0.03	0.66	0.02	0.84	0.05	1.22	0.04	9.64	0.50	0.81	0.04
V198	1.54	0.11	0.65	0.05	0.73	0.04	1.20	0.03	10.49	0.61	0.82	0.05
E199	1.39	0.09	0.72	0.05			1.22	0.02	9.77	0.29	0.76	0.01
R200	1.31	0.07	0.76	0.04	0.63	0.05	1.07	0.04	10.69	0.38	0.82	0.05
F201	1.59	0.04	0.63	0.02	0.72	0.01	1.27	0.03	10.73	0.38	0.79	0.02
I202	1.55	0.04	0.64	0.02	0.74	0.02	1.19	0.03	9.86	0.41	0.86	0.02
E203	1.62	0.08	0.62	0.03	0.77	0.01	1.29	0.02	9.83	0.44	0.82	0.02

I204	1.33	0.05	0.75	0.03	0.68	0.04	1.11	0.04	9.54	0.33	0.72	0.03
G205	1.56	0.03	0.64	0.01	0.77	0.02	1.22	0.04	10.27	0.39	0.83	0.02
S206	1.50	0.02	0.67	0.01	0.72	0.01	1.16	0.03	10.55	0.43	0.80	0.02
G207	1.55	0.07	0.65	0.03	0.79	0.01	1.32	0.01	11.35	0.72	0.80	0.02
T208	1.54	0.10	0.65	0.04	0.75	0.02	1.37	0.04	10.68	1.25	0.83	0.02
S209	1.29	0.09										
K210	1.60	0.14	0.77	0.05	0.75	0.06	1.30	0.06	9.23	1.02	0.85	0.12
L212	1.28	0.05	0.63	0.06	0.72	0.04	1.15	0.04	12.44	0.88	0.81	0.02
A213	1.50	0.05	0.78	0.03	0.88	0.03	1.22	0.03	12.33	0.59	0.82	0.03
N216	1.37	0.04	0.67	0.02	0.83	0.01	1.13	0.02	12.74	0.44	0.83	0.01
A217	1.48	0.02	0.73	0.02			1.19	0.03	12.01	0.73	0.88	0.03
A218	1.45	0.04	0.68	0.01	0.79	0.02	1.19	0.02	12.47	0.40	0.81	0.04
A219	1.44	0.04	0.69	0.02	0.84	0.02	1.13	0.03	12.36	0.31	0.88	0.03
L222					0.79	0.03	1.13	0.02	12.70	0.26	0.86	0.02
L223	1.31	0.03	0.69	0.02	0.65	0.03	1.07	0.01	12.44	0.24	0.87	0.02
R224	1.20	0.06	0.76	0.02	0.79	0.05	1.15	0.03	11.33	0.36	0.84	0.03
V225	1.30	0.09	0.83	0.04	0.76	0.05	1.16	0.01	11.29	0.38	0.79	0.04
T227	1.50	0.04	0.77	0.05								

Table A.2: R_{2eff} values measured at different CPMG frequencies from CPMG relaxation dispersion experiment for apo TRBP2-dsRBD2 at 600 MHz NMR spectrometer.

Residue Number	R_{2eff} at CPMG frequency (Hz)												Repeat		
	25	50	75	125	175	275	375	525	675	825	1000	125	375	825	
error	0.52	0.48	0.43	0.44	0.33	0.33	0.30	0.30	0.25	0.25	0.28	0.38	0.28	0.28	
S156	3.67	3.40	3.02	4.22	3.73	1.97	3.67	5.16	4.67	4.29	6.94	2.80	6.27	4.81	
G162	8.75	8.40	8.77	9.07	9.22	9.00	9.42	10.20	10.20	10.90	11.00	9.09	9.46	11.10	
A163	9.48	10.20	9.58	9.76	9.92	10.10	10.70	10.70	12.00	13.00	13.20	10.60	9.64	12.90	
Q165	7.97	8.05	8.00	8.69	8.46	8.53	8.89	9.12	9.81	10.90	12.00	7.94	9.96	11.00	
E166	9.56	8.40	8.63	66.30	8.50	9.83	9.94	11.20	11.80	12.70	13.40	8.76	10.60	12.80	
L167	9.37	9.58	9.83	9.79	9.98	10.80	11.40	11.70	11.60	13.30	13.80	9.82	11.10	13.40	
V168	15.40	15.40	15.90	16.00	15.70	16.70	17.50	17.50	16.50	18.00	18.50	15.50	17.80	17.30	
V169	8.40	9.12	8.68	9.27	8.55	9.03	9.91	10.00	10.50	10.70	11.60	8.85	9.84	10.70	
Q170	8.42	8.27	8.42	9.89	9.64	8.62	9.11	8.90	9.31	9.95	11.00	9.33	8.70	10.70	
G172	8.20	8.31	8.22	7.95	8.52	8.64	8.97	9.56	10.20	10.30	11.30	8.04	9.18	10.80	
W173	7.12	8.34	7.89	7.02	7.31	8.09	8.59	9.11	9.34	10.00	10.90	7.42	8.84	10.10	
Y178	7.78	6.44	7.96	7.64	7.72	8.28	7.62	84.20	8.77	11.50	11.20	8.04	9.44	11.20	
T179	8.50	7.54	8.68	8.93	9.16	9.30	9.41	9.64	11.20	11.00	11.10	8.91	8.63	10.90	
V180	11.20	10.60	10.10	9.96	8.91	9.77	10.10	7.47	11.20	11.20	14.40	9.25	9.55	11.30	
T181	8.24	8.59	9.01	7.14	8.89	8.04	8.63	9.86	9.81	9.64	10.30	7.46	8.48	9.27	
Q182	8.16	7.68	8.23	8.21	8.27	7.83	9.46	9.08	10.20	9.32	11.00	8.00	8.86	10.30	
E183	7.30	7.43	7.30	7.44	7.49	7.74	7.89	8.82	9.20	9.42	9.78	7.18	7.80	9.49	
G185	6.24	4.69	5.88	6.62	4.94	6.76	7.73	6.29	6.47	7.35	7.69	5.37	5.90	7.49	
E191	6.67	6.48	6.26	6.47	7.39	6.75	7.04	7.52	7.78	7.98	8.69	6.38	6.74	7.99	
F192	9.20	8.03	8.28	9.72	8.96	9.93	10.20	10.00	9.87	10.90	10.80	9.05	9.29	11.30	
T193	8.84	9.17	9.26	9.33	9.55	10.50	10.70	11.70	11.20	12.10	13.10	9.62	10.40	12.10	
M194	9.13	10.50	8.68	9.42	8.96	9.68	10.80	10.40	10.30	12.10	12.30	7.61	10.10	12.20	
T195	9.39	9.39	9.06	10.30	9.57	9.66	9.94	10.80	10.30	11.50	11.60	9.90	10.90	11.60	
C196	8.38	8.57	9.57	8.55	8.33	9.19	9.86	9.08	8.63	9.77	11.10	9.33	7.91	9.86	
R197	8.81	8.49	7.95	7.72	8.00	8.13	8.61	10.30	10.30	12.10	10.90	7.54	8.15	12.40	
V198	8.49	6.46	8.07	7.74	7.01	8.63	8.56	9.51	7.88	10.10	9.46	8.57	9.46	10.10	
E199	7.56	7.65	7.70	8.07	8.07	8.54	8.86	9.56	10.30	11.70	10.90	8.26	9.45	11.70	
R200	8.18	9.23	8.39	8.31	9.41	9.50	9.71	10.90	10.90	11.40	9.85	8.59	10.60	12.40	
F201	8.27	8.35	8.87	8.58	8.67	9.06	8.87	9.82	10.30	11.10	10.90	8.49	8.94	11.20	
I202	7.81	8.12	7.34	7.02	11.00	7.51	8.35	9.49	9.50	10.10	11.00	7.61	9.28	10.20	
E203	7.90	8.48	6.33	8.48	8.35	9.09	8.56	9.52	10.10	10.40	11.40	8.69	8.45	10.50	
I204	9.02	9.29	8.84	9.87	9.76	10.90	10.10	11.30	10.30	12.40	12.30	9.58	11.40	12.40	
G205	8.43	8.20	8.01	8.21	8.36	9.58	9.18	9.32	9.99	10.90	11.30	8.41	9.27	11.00	
S206	8.84	9.17	9.26	9.33	9.55	10.30	10.70	11.70	11.20	12.10	12.90	9.62	10.40	12.60	
G207	8.30	7.89	8.00	8.60	8.09	9.37	9.90	9.92	10.40	11.50	11.90	8.80	9.72	11.50	

T208	9.89	5.44	7.69	8.33	6.76	9.71	7.99	10.60	9.83	10.10	11.60	8.63	10.20	10.20
L212	9.36	9.27	8.34	9.36	10.10	10.10	10.10	9.88	11.50	11.90	13.10	8.94	10.10	11.80
A213	9.71	9.31	9.59	9.19	10.10	10.40	9.98	11.90	11.80	12.40	14.00	9.57	10.70	12.50
N216	9.56	9.68	10.40	10.40	9.96	10.70	11.10	10.90	11.10	12.00	12.90	9.93	10.80	12.10
A217	8.19	9.23	8.85	7.99	7.99	8.92	9.23	10.80	10.30	9.47	11.70	8.14	9.08	9.52
A218	10.20	9.14	9.03	11.30	9.65	10.70	10.50	10.70	11.00	12.50	12.50	10.70	10.30	12.70
A219	10.20	9.39	9.66	10.80	9.85	10.90	11.30	11.50	11.80	13.90	13.10	10.20	10.80	14.30
L222	9.58	9.89	9.35	9.40	9.27	10.00	10.20	10.70	10.80	10.30	10.90	9.33	9.90	10.50
L223	10.40	9.88	9.78	10.70	10.50	11.30	11.00	11.50	12.90	13.00	13.30	10.10	10.90	13.20
V225	9.13	9.04	9.91	8.86	8.92	11.10	10.10	9.56	10.70	12.10	11.30	9.69	9.63	12.10

Table A.3: $R_{1\rho}$ relaxation rates measured using HS $_n$ pulses ($n=1,2,4,6,8$) from HARD experiment for apo TRBP2-dsRBD2 at 600 MHz NMR spectrometer.

Residue Number	$R_{1\rho}$ (Hz)									
	HS1		HS2		HS4		HS6		HS8	
	Value	Error	Value	Error	Value	Error	Value	Error	Value	Error
S151	3.76	0.39	3.67	0.29	4.18	0.25	4.01	0.12	4.86	0.54
154	4.78	0.30	4.40	0.30	4.93	0.36	5.19	0.13	6.07	0.42
Q155	5.14	0.23	5.02	0.32	5.13	0.43	5.51	0.10	6.06	0.28
S156	4.37	0.53	4.26	0.33	5.08	0.32	4.78	0.18	5.87	0.44
E157	4.68	0.38	4.34	0.25	4.94	0.31	5.02	0.11	6.02	0.48
N159	4.12	0.56	4.06	0.45	4.42	0.19	5.01	0.25	5.92	0.50
G162	4.75	0.27	5.34	0.29	6.05	0.14	6.31	0.13	7.00	0.39
A163	5.54	0.44	5.55	0.42	6.81	0.29	6.80	0.16	8.30	0.64
Q165	4.84	0.39	5.16	0.32	6.06	0.16	6.32	0.15	7.44	0.43
E166	4.86	0.34	5.54	0.24	6.35	0.23	6.44	0.10	7.60	0.40
L167	5.35	0.23	5.87	0.29	6.88	0.35	6.99	0.19	7.95	0.43
V168	5.82	0.46	6.73	0.35	8.11	0.27	8.62	0.25	9.90	0.49
V169	4.79	0.28	5.05	0.34	6.09	0.27	6.57	0.21	7.40	0.29
Q170	5.78	0.42	6.29	0.23	6.94	0.33	7.34	0.15	8.34	0.39
G172	4.34	0.32	4.35	0.31	5.27	0.21	5.57	0.09	6.42	0.34
W173	4.70	0.35	4.97	0.17	5.91	0.23	5.88	0.13	6.71	0.43
E177	3.96	0.25	4.01	0.25	4.89	0.22	4.92	0.10	5.70	0.36
Y178	4.05	0.29	4.33	0.23	4.88	0.16	5.27	0.11	5.95	0.37
T179	4.31	0.32	5.02	0.25	5.53	0.14	5.86	0.13	6.65	0.35
V180	4.67	0.33	4.57	0.19	5.94	0.29	6.00	0.15	6.69	0.47
T181	3.86	0.26	4.35	0.22	5.09	0.17	5.18	0.11	5.91	0.29
Q182	5.05	0.34	5.59	0.24	6.12	0.27	6.42	0.10	7.41	0.36
E183	4.67	0.32	4.72	0.36	5.66	0.26	5.57	0.11	6.49	0.41
G185	5.01	0.25	5.02	0.30	5.75	0.32	5.56	0.27	6.71	0.35
R189	4.72	0.45	4.91	0.27	6.38	0.13	6.23	0.18	7.60	0.50
E191	4.06	0.32	4.03	0.26	4.88	0.25	5.07	0.10	5.95	0.40
T193	4.49	0.31	5.08	0.23	5.85	0.24	5.99	0.11	6.91	0.33
M194	4.88	0.18	4.94	0.36	6.04	0.26	6.12	0.26	6.44	0.58
T195	4.96	0.29	5.35	0.19	6.21	0.21	6.31	0.07	7.24	0.34
C196	4.51	0.36	5.17	0.33	5.68	0.14	5.93	0.18	6.79	0.37
R197	5.29	0.32	5.36	0.20	6.01	0.36	6.43	0.22	6.90	0.34
V198	3.99	0.48	4.03	0.10	4.92	0.22	5.12	0.24	5.77	0.33
E199	4.53	0.37	4.68	0.28	5.62	0.26	5.62	0.12	6.74	0.41
R200	4.33	0.29	5.36	0.36	6.01	0.35	6.09	0.23	7.10	0.29
F201	4.96	0.35	5.18	0.25	6.02	0.28	6.26	0.13	6.96	0.35
I202	4.49	0.24	4.98	0.23	5.67	0.19	5.89	0.20	6.54	0.32

E203	5.04	0.29	5.33	0.24	5.89	0.22	6.00	0.12	6.95	0.34
I204	5.08	0.27	5.51	0.17	6.11	0.37	6.07	0.11	7.13	0.24
G205	4.37	0.27	4.91	0.19	5.68	0.25	6.04	0.14	6.68	0.32
S206	4.29	0.36	4.36	0.27	5.13	0.14	5.37	0.12	6.08	0.38
G207	4.48	0.34	4.76	0.32	5.42	0.20	5.87	0.11	6.73	0.45
T208	5.53	0.47	5.54	0.46	6.29	0.27	6.33	0.33	7.28	0.49
S209	3.64	0.36	3.38	0.50	4.04	0.59	4.15	0.46	5.07	0.44
L212	4.76	0.34	4.97	0.35	6.13	0.23	6.20	0.26	7.52	0.35
A213	4.74	0.46	4.83	0.26	5.81	0.19	6.16	0.14	7.21	0.54
R215	4.81	0.46	5.38	0.35	6.39	0.21	6.76	0.29	7.82	0.58
N216	4.95	0.40	5.55	0.36	6.48	0.24	6.64	0.19	7.76	0.46
A217	4.34	0.44	4.93	0.27	6.06	0.22	5.91	0.22	7.05	0.40
A218	4.93	0.36	5.26	0.35	6.16	0.21	6.64	0.29	7.68	0.54
A219	4.67	0.36	5.03	0.41	6.01	0.20	6.26	0.19	7.42	0.44
L223	4.88	0.35	5.64	0.18	6.50	0.31	6.74	0.20	7.79	0.34
R224	4.56	0.22	4.66	0.34	5.56	0.21	5.91	0.21	6.93	0.58
V225	5.57	0.24	5.62	0.32	6.48	0.36	6.74	0.21	7.56	0.63
T227	4.44	0.25	4.70	0.19	5.44	0.34	5.72	0.14	6.65	0.44
V228	5.38	0.24	5.29	0.24	5.89	0.31	5.83	0.08	6.96	0.46
L230	3.33	0.43	2.93	0.33	3.54	0.19	3.51	0.18	4.33	0.57
A232	4.65	0.40	4.27	0.31	4.83	0.25	4.83	0.17	5.84	0.57

Table A.4: $R_{2\rho}$ relaxation rates measured using HS $_n$ pulses ($n=1,2,4,6,8$) from HARD experiment for apo TRBP2-dsRBD2 at 600 MHz NMR spectrometer.

Residue Number	$R_{2\rho}$ (Hz)									
	HS1		HS2		HS4		HS6		HS8	
	Value	Error	Value	Error	Value	Error	Value	Error	Value	Error
S151	7.22	0.25	7.20	0.35	6.78	0.07	7.27	0.19	7.30	0.64
Q154	6.78	0.24	6.98	0.15	6.55	0.36	6.54	0.35	7.20	0.22
Q155	5.75	0.74	5.06	0.11	4.86	0.18	6.35	1.02	6.09	0.41
S156	9.58	0.68	9.00	0.63	8.43	0.51	7.46	0.45	8.63	0.49
E157	7.68	0.72	7.75	0.13	7.05	0.45	7.44	0.81	7.78	0.40
N159	12.73	0.23	14.44	0.79	12.52	1.01	10.49	0.77	14.41	0.99
G162	12.32	0.37	12.14	0.46	12.59	0.03	12.88	0.09	12.30	0.35
A163	13.65	0.91	13.41	0.62	11.97	0.31	12.47	1.28	14.41	0.35
L164	14.55	0.24	13.28	0.30	13.33	0.16	13.83	0.03	12.48	0.32
Q165	14.05	0.55	13.32	0.41	12.93	0.65	13.00	0.78	13.00	0.18
E166	12.61	0.35	12.51	0.03	11.74	0.28	12.00	0.51	12.45	0.12
L167	13.39	0.76	12.91	0.35	12.96	0.25	13.32	0.41	12.99	0.86
V168	20.39	1.92	19.34	0.25	16.87	0.79	18.63	2.04	19.05	0.87
V169	14.19	0.95	13.55	0.54	12.16	0.88	12.45	0.95	14.13	0.70
Q170	13.85	0.07	13.71	0.50	13.03	0.30	13.10	0.39	13.28	0.49
G172	12.51	0.49	11.90	0.31	12.13	0.76	11.81	0.96	11.88	0.14
W173	11.85	0.39	11.63	0.59	11.42	0.25	10.98	0.69	11.25	0.26
R174	11.73	0.24	10.27	0.78	10.40	0.68	10.23	0.49	9.29	0.15
E177	10.83	0.46	10.81	0.18	10.60	0.31	10.36	0.32	10.61	0.33
Y178	11.61	0.04	10.91	0.37	10.97	0.47	10.72	0.55	10.75	0.39
T179	11.63	0.34	11.39	0.59	11.19	0.21	11.14	0.27	11.19	0.37
V180	15.96	0.78	14.19	1.10	13.22	0.40	13.27	0.85	13.50	0.63
T181	11.86	0.29	11.37	0.22	10.92	0.12	10.72	0.37	11.02	0.37
Q182	12.69	0.18	12.46	0.52	12.48	0.22	12.44	0.27	12.36	0.44
E183	11.39	0.60	10.75	0.20	10.48	0.48	10.83	0.68	10.99	0.46
G185	9.43	0.58	9.59	0.34	8.82	0.46	9.58	0.32	10.15	0.25
R189	15.64	1.98	14.98	0.94	14.67	0.66	13.13	1.48	13.28	1.04
E191	10.71	0.42	9.96	0.37	9.94	0.21	10.04	0.31	9.51	0.12
F192	13.38	0.07	12.92	0.36	13.11	0.10	12.54	0.36	12.90	0.12
T193	12.72	0.50	12.80	0.72	12.45	0.48	12.58	0.32	12.45	0.66
M194	8.43	0.49	9.32	1.43	8.84	0.51	9.21	0.28	10.98	1.37
T195	13.09	0.38	13.14	0.79	13.18	0.39	13.38	0.18	12.72	0.47
C196	12.58	0.35	12.68	0.32	11.60	0.80	10.74	0.74	12.52	0.86
R197	10.37	0.70	11.05	1.01	10.43	0.25	10.60	0.96	11.38	0.36
V198	13.26	1.36	11.51	1.40	12.37	1.02	10.36	1.86	10.64	0.94
E199	11.88	0.19	11.36	0.19	11.15	0.13	11.10	0.51	11.18	0.29

R200	12.68	2.54	10.82	1.71	10.99	1.47	11.10	1.08	11.60	2.00
F201	11.48	0.45	11.38	0.11	10.67	0.38	10.77	0.58	11.34	0.09
I202	11.36	0.79	11.19	0.64	10.99	0.51	10.34	0.47	10.68	0.16
E203	11.67	0.56	12.18	0.20	10.82	0.26	10.92	0.62	11.83	0.32
I204	10.53	0.64	11.15	0.29	10.62	0.32	10.66	0.48	10.75	0.29
G205	11.98	0.40	11.92	0.21	11.30	0.23	11.16	0.48	11.37	0.07
S206	11.12	0.13	10.59	0.33	10.53	0.05	11.01	0.14	10.66	0.15
G207	13.23	0.39	12.35	0.42	12.69	0.53	12.58	0.86	12.33	0.29
T208	12.86	0.74	12.63	0.55	11.74	0.46	12.86	0.66	11.34	0.23
S209	9.60	1.46	9.31	0.23	11.16	0.32	10.41	0.63	11.80	1.09
L212	14.93	1.52	14.22	0.75	13.55	0.97	12.83	0.96	13.68	0.85
A213	12.78	0.53	11.71	0.50	12.23	0.90	12.87	0.12	12.54	0.72
R215	14.78	1.64	13.74	1.27	14.28	0.93	13.86	0.40	14.89	1.57
N216	14.09	0.92	14.09	0.39	12.96	0.44	12.77	0.70	13.37	0.41
A217	13.10	0.42	12.05	0.69	12.37	0.47	12.54	0.89	12.05	0.10
A218	14.84	0.80	13.03	0.29	13.80	0.43	14.71	0.56	13.03	0.47
A219	14.93	0.28	13.18	0.34	13.53	0.40	13.84	0.49	12.58	0.37
L222	13.60	0.24	13.10	0.38	12.83	0.05	12.41	0.37	12.52	0.13
L223	13.32	0.20	13.13	1.16	12.79	0.21	13.05	0.35	13.32	0.69
R224	15.29	2.02	14.00	1.41	14.32	0.30	13.10	0.98	12.28	1.27
V225	12.72	1.02	12.95	0.62	12.63	0.80	12.77	0.43	12.13	1.31
T227	10.96	1.32	11.29	0.74	10.76	1.18	10.05	1.02	10.45	0.41
V228	9.46	0.64	9.48	0.49	8.37	0.61	8.64	0.76	9.16	0.61
L230	4.07	0.15	3.97	0.17	4.03	0.18	4.51	0.46	4.65	0.14
A232	6.18	0.31	6.18	0.21	5.37	0.30	5.70	0.80	6.94	0.23

Table A.5: R_1 relaxation rates measured from HARD experiment for apo TRBP2-dsRBD2 at 600 MHz NMR spectrometer.

Residue Number	R_1 (Hz)	
	Value	Error
S151	1.50	0.04
Q154	1.57	0.07
Q155	1.41	0.06
S156	1.60	0.05
E157	1.65	0.04
N159	1.54	0.11
G162	1.54	0.05
A163	1.49	0.08
Q165	1.50	0.05
E166	1.49	0.05
L167	1.44	0.07
V168	1.42	0.08
V169	1.51	0.05
Q170	1.48	0.06
G172	1.50	0.06
W173	1.50	0.06
E177	1.46	0.06
Y178	1.55	0.05
T179	1.56	0.04
V180	1.71	0.08
T181	1.62	0.04
Q182	1.63	0.05
E183	1.57	0.07
G185	1.57	0.05
R189	1.72	0.07
E191	1.46	0.05
T193	1.49	0.04
M194	1.58	0.07
T195	1.57	0.04
C196	1.62	0.04
R197	1.63	0.09
V198	1.55	0.08
E199	1.56	0.06
R200	1.44	0.05
F201	1.60	0.05
I202	1.52	0.07
E203	1.61	0.04

I204	1.47	0.07
G205	1.62	0.04
S206	1.50	0.04
G207	1.55	0.04
T208	1.71	0.04
S209	1.35	0.05
L212	1.42	0.04
A213	1.53	0.06
R215	1.42	0.08
N216	1.44	0.06
A217	1.53	0.09
A218	1.45	0.06
A219	1.42	0.05
L223	1.35	0.06
R224	1.45	0.08
V225	1.33	0.10
T227	1.63	0.05
V228	1.67	0.07
L230	1.06	0.06
A232	1.47	0.06

Table A.6: Nuclear spin relaxation data for RNA bound TRBP2-dsRBD2 recorded at 600 MHz and 800 MHz NMR spectrometer.

Residue Number	600 MHz						800 MHz					
	R_1 (Hz)		R_2 (Hz)		NOE		R_1 (Hz)		R_2 (Hz)		NOE	
	Value	Error	Value	Error	Value	Error	Value	Error	Value	Error	Value	Error
S151	1.48	0.10	7.55	0.29	-0.26	-0.02	1.32	0.25	7.24	0.30	0.10	0.03
Q154	1.57	0.02	6.12	0.06			1.40	0.13	5.76	0.25	0.38	0.01
Q155	1.39	0.03	4.68	0.10			1.25	0.14	5.54	0.09		
S156	1.50	0.13	10.32	0.26	0.04	0.02	1.39	0.27	11.19	0.26	0.33	0.03
E157	1.74	0.11	11.13	0.28	0.26	0.02	1.45	0.22	11.59	0.41	0.39	0.03
N159	1.39	0.15	17.27	1.13	0.38	0.07	1.54	0.27	21.17	1.04	0.55	0.14
G162	1.32	0.07	23.58	0.97	0.85	0.07	1.19	0.10	24.71	2.09	0.81	0.15
A163	1.28	0.10	22.33	2.50	0.86	0.09	0.88	0.12	25.06	2.61	1.01	0.16
Q165	1.29	0.06	24.36	0.97	0.76	0.05	1.02	0.10	24.87	0.54	0.85	0.07
E166	1.35	0.04	23.64	0.74	0.74	0.03	1.04	0.09	24.39	0.35	0.77	0.06
L167	1.34	0.06	22.40	0.39	0.76	0.07	0.86	0.07	26.05	0.62	0.73	0.13
V168	1.27	0.07	24.52	3.18	0.71	0.11	0.96	0.17	33.08	2.23	0.63	0.22
V169	1.27	0.10	14.23	1.55	0.77	0.17	1.16	0.10	12.32	1.64	0.69	0.22
Q170	1.29	0.05	22.32	0.55	0.74	0.03	1.01	0.07	23.28	0.82	0.76	0.06
G172	1.38	0.04	23.28	0.60	0.77	0.04	1.00	0.09	27.34	1.36	0.68	0.07
W173	1.41	0.03	19.33	0.84	0.74	0.05	1.01	0.07	21.83	0.84	0.82	0.07
E177	1.30	0.05	7.35	0.79	0.31	0.02	1.11	0.15	8.38	0.93	0.66	0.05
Y178	1.43	0.04	21.96	1.13	0.74	0.06	0.89	0.08	22.49	2.11	0.93	0.11
T179	1.38	0.06	20.72	0.42	0.82	0.05	0.90	0.17	23.41	0.64	0.68	0.09
V180	1.77	0.14	20.46	1.68	0.67	0.10	1.16	0.30	25.52	2.19	1.22	0.30
Q182	1.47	0.05	19.91	0.63	0.77	0.04	1.26	0.12	25.21	1.67	0.74	0.09
E183	1.45	0.04	17.79	0.36	0.67	0.03	1.24	0.14	20.92	0.40	0.71	0.05
G185	1.64	0.04	15.33	0.53	0.57	0.05	1.20	0.19	20.94	0.54	0.68	0.07
R189	1.74	0.10			0.34	0.08	1.41	0.09	26.32	1.69	0.90	0.25
E191	1.33	0.07	17.75	0.33	0.56	0.04	0.94	0.14	19.38	0.68	0.52	0.06
T193	1.20	0.08	21.32	1.07	0.69	0.07	1.05	0.15	22.19	0.95	0.67	0.10
M194	1.49	0.13	22.38	2.67	0.89	0.18	1.28	0.06	21.07	4.10	0.77	0.26
T195	1.33	0.05	23.04	0.64	0.84	0.07	1.06	0.15	27.43	1.58	0.87	0.14
C196	1.30	0.15	20.41	1.26	0.59	0.10	1.20	0.14	25.47	1.26	0.55	0.11
R197	1.20	0.14	22.37	2.66	1.05	0.19	1.38	0.13	26.97	1.80	0.76	0.21
V198	1.15	0.10	19.37	1.51	0.77	0.14	1.03	0.20	24.74	3.10	1.08	0.29
E199	1.39	0.05	18.73	0.55	0.70	0.04	1.02	0.07	20.50	0.76	0.78	0.08
R200	1.30	0.11	17.60	0.98	0.80	0.13	1.16	0.10	20.62	2.50	0.59	0.18
F201	1.41	0.06	20.46	0.67	0.74	0.04	1.00	0.08	22.79	0.92	0.76	0.06
I202	1.33	0.05	19.62	0.78	0.69	0.05	1.00	0.09	20.53	0.59	0.84	0.10
E203	1.46	0.02	19.29	0.65	0.77	0.04	0.99	0.10	24.02	0.46	0.77	0.08

I204	1.22	0.05	20.52	1.00	0.76	0.08	0.86	0.09	22.86	0.81	0.87	0.15
G205	1.52	0.05	19.70	0.73	0.85	0.06	1.11	0.16	19.37	0.87	1.02	0.13
S206	1.36	0.04	20.38	0.54	0.74	0.03	0.95	0.13	20.90	0.65	0.80	0.06
G207	1.35	0.04	22.78	0.80	0.77	0.04	1.00	0.12	22.56	0.79	0.97	0.10
T208	1.61	0.10	19.56	0.63	0.69	0.05	1.31	0.24	22.45	1.75	0.94	0.12
S209	1.32	0.07	10.29	2.68	0.11	0.04	1.06	0.15	7.85	5.43	0.49	0.17
L212	1.07	0.14	22.60	2.24	0.97	0.11	0.76	0.22	23.43	1.98	0.86	0.17
A213	1.43	0.05	17.74	1.45	0.82	0.09	0.98	0.11	20.26	1.86	0.95	0.17
R215	1.37	0.12	20.01	2.07	1.03	0.15	0.92	0.05	25.59	1.33	0.77	0.15
N216	1.26	0.05	24.39	0.72	0.75	0.04	0.87	0.10	24.44	0.92	0.77	0.07
A217	1.39	0.03	18.58	1.56	0.64	0.08	1.06	0.10	23.62	1.23	1.08	0.21
A219	1.37	0.05	24.46	0.93	0.83	0.06	1.01	0.01	27.16	0.21	0.72	0.13
L223	1.18	0.03	24.26	0.56	0.74	0.07	0.92	0.06	27.62	0.81	0.85	0.10
R224	1.47	0.13	19.59	1.09	0.84	0.14	0.95	0.16	25.31	2.80	0.74	0.18
V225	1.43	0.09	18.70	1.00	0.75	0.14	0.95	0.14	23.69	2.26	0.81	0.22
T227	1.70	0.10	15.33	0.31	0.53	0.03	1.36	0.18	16.08	0.24	0.64	0.05
V228	1.52	0.05	11.29	0.20	0.48	0.04	1.31	0.12	13.59	0.38	0.63	0.06
L230	0.97	0.01	4.70	0.09	-0.93	-0.01	1.02	0.04	2.33	0.60	-0.63	-0.01
A232	1.35	0.04	4.85	0.19	-0.25	-0.02	1.29	0.14	5.94	0.37	0.29	0.03

Table A.7: R_{2eff} values measured at different CPMG frequencies from CPMG relaxation dispersion experiment for bound TRBP2-dsRBD2 at 600 MHz NMR spectrometer.

Residue Number	R_{2eff} at CPMG frequency (Hz)											Repeat		
	25	50	75	125	175	275	375	525	675	825	1000	125	375	825
error	2.52	2.21	1.84	2.15	1.98	3.09	2.93	2.52	2.52	2.93	2.97	2.73	2.90	2.99
S156	22.20	21.30	20.80	22.50	22.00	18.60	23.50	20.20	26.50	20.80	24.40	21.60	21.80	24.80
G162	18.00	20.60	19.90	20.00	17.60	17.40	19.80	23.70	23.20	19.90	22.30	23.10	24.00	22.40
E157	13.70	12.60	12.20	11.20	9.84	12.10	11.40	12.10	12.70	12.40	13.80	11.20	10.90	13.30
A163	32.50	25.00	21.20	24.20	19.50	22.00	26.10	23.80	28.20	21.20	24.40	22.00	21.60	26.40
Q165	23.20	24.30	20.20	19.30	22.80	20.50	20.30	21.90	22.00	20.20	25.00	22.50	22.10	24.20
E166	21.50	20.10	20.20	20.70	19.80	18.00	20.30	20.70	23.60	20.20	25.40	19.80	20.80	22.70
L167	16.70	17.80	23.20	17.50	22.10	20.00	20.30	18.20	22.10	23.00	22.40	21.10	19.70	25.20
V168	11.70	12.40	9.58	11.00	9.46	10.70	10.30	11.10	12.40	9.58	14.60	10.80	11.70	9.98
V169	24.80	25.70	25.40	24.00	16.20	22.30	20.00	24.50	26.30	25.40	23.80	31.60	22.90	26.70
Q170	23.00	21.80	22.40	21.30	22.70	23.30	21.40	21.20	21.70	22.40	25.40	20.90	22.40	23.40
G172	19.00	17.50	16.70	18.60	18.00	19.20	15.80	18.80	20.20	16.70	20.00	15.90	16.90	20.80
W173	17.40	17.10	16.90	18.30	19.10	18.50	19.20	19.80	17.90	17.20	19.20	16.10	17.40	18.90
E177	16.30	17.00	19.40	15.10	16.10	18.80	21.70	16.90	18.60	19.40	19.20	19.20	17.70	21.70
Y178	11.60	11.70	14.90	13.70	15.60	13.60	13.60	13.20	15.40	14.90	21.40	15.80	18.10	14.00
T179	19.60	15.30	18.70	19.50	18.40	19.00	20.20	19.00	18.00	18.70	24.00	18.70	21.70	24.80
V180	16.60	16.60	16.60	13.80	18.10	20.90	16.60	16.30	19.50	16.60	16.10	21.10	11.70	20.20
T181	24.10	17.50	18.90	19.00	19.20	21.80	22.80	15.10	23.60	18.90	21.80	17.10	23.60	19.00
Q182	19.10	22.80	18.50	19.10	18.70	15.00	17.70	18.10	17.70	18.50	23.20	18.50	20.70	17.10
E183	19.50	17.80	20.80	19.50	19.10	18.70	21.40	18.30	20.10	20.80	19.90	20.70	20.60	21.10
G185	16.40	20.40	16.40	14.10	18.80	16.00	17.20	12.10	15.40	16.40	21.80	20.10	17.90	17.70
E191	18.40	17.40	16.80	16.40	18.00	16.50	14.60	18.60	15.40	16.80	19.00	18.50	14.90	17.50
T193	23.80	18.00	23.70	24.10	22.60	21.00	16.20	21.80	19.00	23.70	22.80	21.10	20.20	25.10
M194	17.80	13.00	13.00	26.50	8.49	27.50	13.50	14.00	21.30	13.00	24.40	26.80	9.79	12.50
T195	30.10	23.50	25.10	21.10	26.60	25.80	19.20	18.90	30.90	25.10	28.00	23.50	28.60	24.00
C196	17.10	13.90	19.40	29.20	13.20	19.50	23.40	8.60	19.40	20.30	21.90	19.40	8.65	15.50
R197	15.60	13.10	11.50	13.70	17.80	19.00	15.20	13.30	25.10	21.60	27.40	26.10	11.80	27.40
V198	18.10	17.90	21.70	22.50	18.80	12.40	13.90	21.50	11.40	12.60	14.20	23.00	29.70	19.80
E199	18.70	19.80	17.40	18.20	20.70	20.30	19.60	20.30	18.50	17.40	20.90	19.10	20.00	20.80
R200	21.80	27.10	25.80	14.30	21.90	27.20	17.70	27.90	21.70	26.60	25.20	16.10	21.20	20.40
F201	21.50	19.60	19.70	21.20	20.00	17.90	19.50	19.30	23.00	19.70	22.40	17.90	20.10	23.30
I202	15.20	18.60	15.00	15.50	15.20	16.70	17.20	22.00	20.60	15.00	16.70	8.95	22.20	19.80
E203	21.30	17.90	17.10	17.10	20.10	19.30	20.80	20.40	21.20	17.10	23.20	17.40	19.80	23.90
I204	26.90	18.20	24.00	16.30	21.00	24.30	23.30	22.00	22.40	24.00	25.60	27.50	25.30	24.10
G205	20.50	18.00	19.00	20.50	17.90	24.00	21.60	15.30	24.50	19.00	25.10	19.70	26.20	21.20
S206	18.40	18.30	16.20	15.50	16.30	18.40	18.70	18.90	21.30	16.20	21.50	19.20	20.30	17.80

G207	19.30	20.20	18.80	19.30	17.50	18.70	17.40	20.40	19.20	18.80	22.00	20.70	22.40	19.00
T208	11.70	16.80	11.80	23.50	16.90	12.50	14.50	22.60	9.57	11.80	11.80	13.50	17.40	18.60
L212	17.20	24.10	22.50	22.30	25.30	15.90	16.40	17.30	22.60	22.50	27.60	25.80	15.60	25.80
A213	18.30	18.70	21.70	18.00	16.50	15.70	21.20	15.70	22.70	22.20	19.60	18.50	19.10	15.90
R215	21.70	17.70	26.60	17.30	26.70	17.10	18.50	16.00	21.80	26.60	28.90	21.40	12.20	27.40
N216	6.54	3.31	6.10	3.17	4.25	3.50	7.14	9.19	5.51	6.10	9.90	2.60	6.06	8.75
A217	21.40	17.30	16.10	23.50	27.00	22.40	24.10	23.00	23.00	16.10	27.20	21.70	22.90	20.80
A218	13.10	20.60	19.20	19.00	18.90	18.70	19.40	22.20	18.10	19.20	17.40	19.40	17.20	26.60
A219	19.90	19.50	21.30	20.60	21.80	21.50	22.90	21.60	22.50	21.30	29.90	23.40	23.50	25.00
L222	19.90	21.50	19.80	18.70	21.00	20.30	18.90	20.10	20.10	19.80	27.00	18.20	21.80	23.00
R224	23.50	15.60	21.60	18.10	21.80	20.40	14.10	22.30	23.20	21.60	21.70	19.50	21.80	25.80
L223	22.80	21.10	20.10	19.30	20.20	21.80	23.50	25.30	26.00	20.10	39.40	21.10	33.00	34.50
V225	17.40	15.30	21.60	16.20	18.10	17.50	25.70	19.10	16.20	21.80	22.60	17.50	16.70	22.50
T227	14.70	15.00	12.30	13.60	13.40	13.90	15.50	12.60	14.60	12.30	17.00	13.40	15.40	13.60
V228	9.09	9.59	8.98	8.41	9.01	9.09	9.48	10.10	10.70	8.98	12.70	8.36	9.54	11.60

Table A.8: $R_{1\rho}$ relaxation rates measured using HS n pulses ($n=1,2,4,6,8$) from HARD experiment for RNA-bound TRBP2-dsRBD2 at 600 MHz NMR spectrometer.

Residue Number	$R_{1\rho}$ (Hz)									
	HS1		HS2		HS4		HS6		HS8	
	Value	Error	Value	Error	Value	Error	Value	Error	Value	Error
A153	2.45	0.11	4.29	0.30	4.62	0.18	4.73	0.28	3.58	0.11
Q154	2.68	0.03	4.68	0.28	4.94	0.14	5.27	0.30	3.41	0.09
Q155	2.35	0.12	4.54	0.39	4.48	0.27	5.06	0.20	2.93	0.16
S156	2.73	0.28	5.41	0.32	5.56	0.38	6.20	0.17	4.38	0.23
E157	3.52	0.10	5.42	0.23	6.00	0.15	6.14	0.25	4.62	0.13
C158	2.99	0.74	6.28	0.74	5.45	0.56	5.27	0.56	4.47	0.25
N159	3.72	0.91	7.78	1.05	7.49	1.12	6.83	1.32	7.02	0.73
G162	5.52	0.64	7.17	0.55	10.55	1.03	10.27	0.49	8.35	0.67
Q165	4.61	0.22	9.11	1.27	12.24	1.89	9.34	1.48	8.33	1.12
E166	5.04	0.08	7.73	0.16	9.16	0.45	9.67	0.51	8.88	0.31
L167	5.93	0.04	7.80	0.25	8.47	0.19	8.43	0.39	8.74	0.13
V168	5.34	0.77	8.95	0.46	9.29	0.81	9.78	0.58	9.73	0.50
V169	4.53	0.76	10.95	2.28	5.62	2.43	8.88	2.08	10.24	0.97
Q170	5.32	0.17	9.17	1.07	9.96	0.50	9.62	1.06	8.55	1.00
G172	4.52	0.17	7.66	0.21	9.12	0.29	10.36	0.53	9.55	0.29
W173	4.85	0.29	7.79	0.19	8.23	0.38	9.37	0.31	8.66	0.61
E177	3.59	0.28	6.66	0.29	8.56	0.29	8.78	0.30	7.75	0.39
Y178	4.88	0.12	5.15	0.39	6.02	0.24	6.20	0.47	4.98	0.37
T179	4.57	0.28	6.85	0.72	7.93	0.34	8.49	0.59	7.59	0.62
V180	5.04	0.70	7.11	0.60	8.87	0.39	9.68	0.35	8.34	0.42
T181	4.77	1.02	7.60	1.28	7.97	0.38	10.72	0.94	7.86	0.76
Q182	4.78	0.19	6.02	0.25	7.32	0.26	8.07	0.43	8.15	1.22
E183	4.23	0.17	6.58	0.13	7.93	0.52	9.48	0.41	8.03	0.41
G185	4.20	0.42	7.33	0.59	7.93	0.31	7.82	0.41	7.52	0.07
R189	3.01	0.30	6.19	0.73	7.10	0.62	8.28	0.69	7.09	0.29
E191	4.53	0.05	5.86	0.32	7.91	0.54	8.25	0.23	6.99	0.30
T193	4.78	0.19	8.12	0.68	8.69	0.68	9.54	0.61	9.16	0.54
M194	5.75	0.46	4.95	2.17	4.54	0.79	9.66	2.35	6.67	1.91
T195	5.53	0.28	7.36	0.45	8.92	0.23	9.22	0.50	10.38	0.52
C196	4.12	0.96	6.61	0.82	7.87	0.95	7.39	0.77	9.97	0.94
R197	3.37	1.01	8.05	1.54	10.52	1.42	8.28	0.30	8.51	0.67
V198	5.68	1.05	5.97	1.41	9.38	1.48	11.55	1.59	7.68	1.36
E199	4.52	0.18	7.68	0.20	8.30	0.29	8.48	0.36	8.16	0.12
200	4.27	0.52	9.13	1.56	8.82	0.70	7.76	0.48	8.73	1.00
F201	5.03	0.12	8.21	0.73	9.68	0.11	9.98	0.17	8.59	0.24
I202	5.35	0.34	6.76	0.79	9.12	0.87	8.26	0.70	7.22	0.51

E203	4.32	0.11	7.00	0.33	7.90	0.37	8.19	0.27	8.46	0.13
I204	5.17	0.15	8.06	0.71	8.92	0.52	8.63	0.69	8.78	0.33
G205	4.24	0.37	7.66	0.67	8.34	0.57	9.79	0.38	8.71	0.78
S206	4.59	0.10	6.61	0.35	8.13	0.22	8.90	0.14	7.85	0.16
G207	4.53	0.12	7.51	0.40	8.30	0.15	9.52	0.25	8.73	0.29
T208	4.35	0.51	6.20	0.98	7.47	0.85	9.98	0.72	8.05	0.59
S209	3.69	0.89	6.11	0.96	6.73	0.25	7.06	0.17	4.79	1.26
L212	4.91	0.50	7.60	0.51	10.10	1.63	10.33	1.17	9.31	1.06
A213	4.17	0.43	7.24	0.67	8.28	0.65	9.23	0.71	7.89	0.70
R215	4.97	0.97	7.98	1.13	10.78	1.19	9.56	1.69	9.36	1.12
N216	4.56	0.19	7.88	0.63	9.82	0.16	11.03	0.42	9.44	0.56
A218	5.93	0.22	6.79	0.93	9.53	0.27	11.19	0.49	10.61	1.04
A219	5.63	0.63	8.24	0.59	10.28	0.22	10.26	0.54	9.15	0.41
M221	4.02	0.37	8.04	0.77	8.79	0.78	9.02	1.18	6.86	0.56
L223	4.53	0.32	7.39	0.36	7.90	0.31	9.71	0.80	9.38	0.22
R224	4.50	0.36	6.61	0.73	9.11	0.44	9.80	0.29	8.96	0.87
V225	5.51	0.54	10.74	0.96	7.06	1.11	8.82	0.89	10.48	0.44
T227	3.86	0.29	5.99	0.65	7.00	0.26	7.24	0.31	6.81	0.40
V228	3.02	0.30	6.23	0.37	6.32	0.18	6.30	0.19	5.06	0.22
L230	1.66	0.03	3.69	0.36	3.90	0.11	3.84	0.31	1.85	0.05
A232	2.09	0.09	4.69	0.37	4.64	0.12	4.49	0.28	2.68	0.13

Table A.9: R_{2p} relaxation rates measured using HS $_n$ pulses ($n=1,2,4,6,8$) from HARD experiment for RNA bound TRBP2-dsRBD2 at 600 MHz NMR spectrometer.

Residue Number	R_{2p} (Hz)									
	HS1		HS2		HS4		HS6		HS8	
	Value	Error	Value	Error	Value	Error	Value	Error	Value	Error
S151	7.52	0.88	7.36	0.08	8.09	0.39	9.85	0.93	6.44	0.17
A153	7.20	0.93	7.03	0.12	6.90	0.66	9.42	0.20	6.89	0.38
Q154	5.95	0.19	5.43	0.29	5.39	0.12	7.74	0.00	5.41	0.54
Q155	4.06	0.56	4.54	0.50	4.69	2.13	7.14	2.55	4.43	0.96
S156	11.98	1.44	10.14	0.77	9.29	0.40	11.78	0.66	8.98	0.10
E157	11.42	0.63	11.44	0.90	10.55	0.93	13.03	0.04	11.13	0.32
C158	10.99	0.56	7.60	2.88	8.80	3.36	5.86	1.50	5.66	0.04
N159	22.76	1.58	24.66	4.86	26.77	5.51	26.46	6.61	25.79	0.72
G162	22.34	0.84	22.53	2.55	22.89	2.43	19.21	6.19	18.27	4.48
A163	25.68	5.44	20.88	0.59	20.24	2.68	29.83	10.75	23.13	5.24
L164	22.11	1.08	21.66	1.43	21.37	2.58	22.51	5.18	19.30	2.13
Q165	22.98	0.15	22.62	1.66	22.82	1.03	22.58	1.74	19.23	0.98
E166	21.15	0.97	23.39	1.79	21.98	0.91	21.58	5.12	19.53	0.44
L167	23.56	1.19	22.80	0.47	22.95	1.58	25.44	6.71	17.64	1.41
V168	24.93	11.77	31.39	3.93	29.52	3.91	28.40	18.94	18.46	0.43
V169	20.39	2.98	23.93	0.90	21.70	0.94	17.28	2.39	17.25	2.25
Q170	21.15	0.74	22.25	0.06	21.78	0.45	22.11	2.39	19.74	1.63
G172	21.47	2.52	19.56	2.17	19.37	1.05	19.66	0.29	20.35	0.38
W173	20.46	1.15	19.23	1.52	19.90	2.37	22.82	0.06	19.05	0.04
R174	15.98	2.78	15.03	0.86	18.07	3.56	17.64	5.95	12.51	1.18
E177	12.92	0.77	12.70	0.80	13.02	0.65	15.59	0.79	12.96	0.30
Y178	20.19	0.27	16.56	0.74	15.63	0.37	18.41	3.01	17.56	0.94
T179	18.75	1.11	19.94	0.53	18.82	1.83	22.96	4.09	18.83	0.36
V180	22.01	3.27	21.46	2.48	20.08	4.19	23.91	0.50	26.12	2.81
T181	21.68	1.07	18.85	0.86	26.22	2.28	22.72	0.69	18.85	1.54
Q182	22.61	1.38	20.11	0.82	20.71	0.04	22.64	1.13	23.06	3.42
E183	18.22	3.48	17.77	1.30	18.62	2.35	22.15	0.40	17.84	1.83
G185	17.93	0.46	17.18	0.71	18.36	2.42	18.95	2.71	17.48	0.21
E191	17.60	1.33	18.25	0.17	17.37	1.06	27.71	1.83	17.71	0.94
T193	20.75	1.00	24.53	1.32	23.89	1.95	19.42	1.43	23.31	2.38
M194	21.64	5.16	19.92	12.84	15.64	2.44	21.92	0.14	17.78	8.54
T195	22.00	0.70	21.89	2.18	20.70	0.25	20.08	1.54	19.74	2.44
C196	19.54	1.76	17.44	0.32	18.67	0.14	15.72	6.59	20.17	2.55
R197	23.88	3.14	18.10	5.39	16.82	0.17	14.73	3.25	18.00	4.74
V198	21.00	3.24	15.94	5.64	15.97	2.03	12.01	1.39	15.78	2.91
E199	17.92	0.09	19.06	1.85	18.11	1.08	17.92	0.24	17.62	0.03

200	17.91	6.24	20.25	1.94	24.53	1.66	16.34	7.13	15.38	0.16
F201	19.22	0.12	17.94	0.24	18.44	1.67	18.23	1.48	16.84	0.65
I202	20.00	1.61	19.45	0.39	16.81	1.66	20.95	0.46	17.96	0.02
E203	19.80	1.40	20.52	0.20	18.91	1.30	17.10	3.39	17.46	1.94
I204	20.08	1.11	21.68	0.27	21.36	1.32	22.82	3.02	20.50	3.25
G205	22.26	0.40	18.03	0.24	19.48	0.28	18.40	2.92	18.65	3.01
S206	18.69	0.50	17.92	2.08	17.61	0.08	18.80	0.02	17.81	0.10
G207	22.45	1.73	20.50	2.59	21.27	1.82	21.01	2.15	20.08	1.31
T208	19.50	0.64	23.86	0.48	20.49	0.79	17.94	0.23	16.75	3.78
S209	14.26	0.66	12.31	0.20	14.55	1.79	9.77	9.13	14.36	3.10
L212	23.28	1.15	27.70	2.68	24.48	0.90	23.33	5.02	21.71	7.43
A213	22.66	4.90	20.19	1.04	20.21	0.53	15.27	12.49	19.65	1.12
R215	20.61	1.26	26.71	1.26	23.27	4.53	18.58	11.00	17.22	3.91
N216	25.37	2.54	23.62	0.11	21.27	2.74	24.28	2.86	24.34	0.35
A218	23.38	0.51	23.58	0.66	20.59	6.55	23.59	7.26	20.66	0.21
A219	24.02	1.34	22.84	0.63	21.45	1.20	24.16	3.88	21.11	1.95
M221	15.46	1.37	13.39	1.01	17.72	3.58	16.92	0.88	9.83	1.58
L223	18.21	0.54	23.29	1.03	21.64	0.76	24.19	8.45	20.25	0.39
R224	20.78	1.38	27.11	0.01	26.05	2.72	21.81	10.88	19.37	3.91
V225	17.02	2.64	22.54	9.64	12.75	3.81	12.07	15.39	19.89	1.51
T227	15.66	1.96	13.51	0.75	13.80	0.66	14.58	1.57	14.46	0.17
V228	11.44	2.07	10.40	1.40	11.43	1.75	13.93	0.57	10.89	0.65
L230	2.51	0.23	2.28	0.13	2.56	0.51	5.01	0.36	2.66	0.00
A232	4.35	0.21	3.89	0.21	4.25	0.55	6.80	0.24	4.39	0.47

Table A.10: R_1 relaxation rates measured from HARD experiment for RNA bound TRBP2-dsRBD2 at 600 MHz NMR spectrometer.

Residue Number	R_1 (Hz)	
	Value	Error
S151	1.36	0.10
A153	1.48	0.02
Q154	1.47	0.03
Q155	1.17	0.04
S156	1.41	0.13
E157	1.55	0.11
C158	1.51	0.17
N159	1.67	0.24
G162	1.21	0.21
A163	1.28	0.11
Q165	1.30	0.15
E166	1.35	0.10
L167	1.15	0.18
V168	1.36	0.30
V169	1.40	0.12
Q170	1.29	0.05
G172	1.35	0.05
W173	1.33	0.11
E177	1.26	0.08
Y178	1.43	0.08
T179	1.39	0.09
V180	1.50	0.23
T181	1.46	0.13
Q182	1.56	0.08
E183	1.41	0.10
G185	1.46	0.14
R189	1.51	0.22
E191	1.41	0.07
T193	1.44	0.18
M194	1.37	0.42
T195	1.34	0.18
C196	1.61	0.09
R197	1.36	0.19
V198	1.54	0.38
E199	1.46	0.08
R200	0.96	0.23
F201	1.45	0.04

I202	1.35	0.10
E203	1.52	0.06
I204	1.22	0.11
G205	1.52	0.07
S206	1.38	0.03
G207	1.35	0.04
T208	1.51	0.15
S209	1.25	0.10
L212	1.35	0.20
A213	1.14	0.19
R215	1.07	0.12
N216	1.37	0.07
A218	1.36	0.16
A219	1.25	0.10
M221	1.27	0.15
L223	1.31	0.14
R224	1.40	0.09
V225	1.27	0.33
T227	1.56	0.10
V228	1.57	0.06
L230	0.96	0.02

Table A.11: Order parameter (S^2) extracted from Model-free analysis of the Nuclear Spin Relaxation data for apo TRBP2-dsRBD2 recorded at 600 MHz and 800 MHz NMR spectrometer.

Residue Number	S^2	
	Value	Error
N159	0.34	0.01
G162	0.71	0.01
A163	0.74	0.02
Q165	0.78	0.00
E166	0.70	0.01
L167	0.74	0.00
V169	0.63	0.02
Q170	0.67	0.00
G172	0.63	0.03
W173	0.36	0.04
L175	0.72	0.00
Y178	0.57	0.04
T179	0.74	0.01
T181	0.36	0.03
Q182	0.22	0.01
E183	0.24	0.01
G185	0.22	0.01
E191	0.17	0.00
T193	0.27	0.02
M194	0.44	0.03
T195	0.94	0.01
C196	0.75	0.01
R197	0.40	0.04
V198	0.68	0.04
R200	0.23	0.01
F201	0.72	0.01
I202	0.68	0.02
E203	0.66	0.02
I204	0.62	0.01
G205	0.76	0.01
S206	0.22	0.01
G207	0.17	0.02
T208	0.34	0.02
K210	0.42	0.06
L212	0.75	0.03
A213	0.90	0.01
N216	0.86	0.01

A218	0.76	0.01
A219	0.80	0.01
L223	0.65	0.10
R224	0.63	0.03
V225	0.66	0.02

Table A.12: Order parameter (S^2) extracted from Model-free analysis of the Nuclear Spin Relaxation data for RNA bound TRBP2-dsRBD2 recorded at 600 MHz and 800 MHz NMR spectrometer.

Residue Number	S^2	
	Value	Error
N159	0.22	0.01
G162	0.98	0.02
A163	0.27	0.08
Q165	0.79	0.01
V168	0.92	0.04
V169	0.38	0.04
Q170	0.96	0.02
G172	0.93	0.02
W173	0.82	0.03
Y178	0.94	0.02
T179	0.86	0.01
Q182	0.57	0.02
E183	0.31	0.01
E191	0.29	0.06
T193	0.84	0.03
M194	0.88	0.04
T195	0.81	0.03
V198	0.61	0.05
R200	0.49	0.03
F201	0.89	0.02
I202	0.72	0.02
E203	0.94	0.01
I204	0.83	0.03
G205	0.65	0.03
S206	0.89	0.02
G207	0.81	0.03
T208	0.92	0.03
L212	0.93	0.04
A213	0.94	0.03
N216	0.85	0.03
A219	0.91	0.01
L223	0.90	0.02
R224	0.78	0.03
V225	0.64	0.04

Table A.13: R_{ex} of residues extracted from Model-free analysis of the Nuclear Spin Relaxation data for apo TRBP2-dsRBD2 recorded at 600 MHz and 800 MHz NMR spectrometer.

Residue Number	R_{ex} (Hz)	
	Value	Error
E166	0.50	0.13
V180	4.31	2.09
N216	0.53	0.21
A219	0.34	0.19
L223	1.10	0.72

Table A.14: R_{ex} of residues extracted from Model-free analysis of Nuclear Spin Relaxation data for RNA bound TRBP2-dsRBD2 recorded at 600 MHz and 800 MHz NMR spectrometer.

Residue Number	R_{ex} (Hz)	
	Value	Error
V168	4.70	1.35
Y178	2.10	0.83
T195	2.01	0.77
I204	1.89	0.69
N216	1.77	0.68
L223	3.62	0.50

Table A.15: Dynamics parameters extracted from HARD experimental data from geoHARD method for apo TRBP2-dsRBD2.

Residue Number	k_{ex} (Hz)		p_B (%)
	Value	Error	
N159	193.02	74.20	2.18
G162	108.91	9.01	1.39
A163	143.20	40.06	1.10
Q165	145.51	32.02	1.60
E166	113.27	11.37	0.94
L167	153.11	78.02	0.63
V169	181.02	63.29	1.41
G172	149.65	32.10	1.64
W173	111.43	13.12	0.99
E177	144.32	24.23	1.43
Y178	149.17	45.08	1.34
T179	116.90	6.58	1.05
V180	30162.81	2556.08	4.98
T181	225.86	113.77	1.16
Q182	104.47	6.91	1.12
E183	151.01	54.24	0.92
R189	31748.72	955.20	9.37
E191	185.94	58.22	0.89
T193	113.50	14.73	1.51
T195	110.02	13.94	1.60
C196	164.04	75.77	1.18
V198	30554.87	1687.74	3.05
E199	115.53	14.31	1.31
R200	53667.71	2331.35	15.82
F201	148.85	63.15	0.56
I202	153.01	64.86	0.74
E203	129.64	34.33	0.84
205	153.79	40.99	0.96
S206	137.90	32.54	1.26
G207	204.01	64.95	1.34
T208	173.36	69.90	0.81
S209	110.46	12.18	2.16
L212	36081.01	4503.77	10.56
A213	121.17	17.10	1.53
N216	195.81	71.97	1.07
A217	160.24	74.26	1.40
A218	162.39	53.99	1.45

A219	138.44	43.89	1.74
L223	107.89	13.48	0.95
R224	31519.02	1155.44	15.57
T227	52411.81	1883.58	7.57

Table A.16: Dynamics parameters extracted from HARD experimental data from geoHARD method for RNA bound TRBP2-dsRBD2.

Residue Number	k_{ex} (Hz)		p_B (%)
	Value	Error	
N159	109.84	6.09	8.18
G162	33694.84	4498.63	14.58
Q165	144.71	39.88	3.07
E166	117.25	18.81	3.31
L167	33136.76	1028.77	13.75
V168	31361.87	381.57	23.84
V169	157.41	44.83	3.44
Q170	116.96	11.92	2.92
G172	175.47	86.44	2.47
W173	114.07	8.10	3.51
T179	109.72	7.08	4.01
V180	143.37	29.57	5.40
T181	114.44	6.67	4.89
Q182	137.39	19.91	4.48
E183	119.61	13.26	4.15
G185	130.95	25.10	2.92
E191	110.37	8.93	4.66
T193	111.15	9.42	3.73
C196	117.34	15.76	3.48
R197	38548.93	3434.10	6.46
V198	73599.49	5723.40	27.41
E199	114.28	11.25	2.60
R200	34143.21	678.61	19.36
F201	171.94	65.01	1.11
E203	34467.84	1310.56	21.48
I204	111.56	15.16	3.32
G205	154.09	34.56	2.51
S206	120.58	16.23	3.03
G207	29981.15	4358.72	4.63
T208	148.23	48.27	3.66
S209	125.06	16.57	1.77
L212	120.49	18.57	4.42
A213	27995.83	4031.29	14.63
R215	136.63	33.31	2.96
N216	111.11	5.78	5.34
A219	34874.65	4100.95	15.65
M221	61676.83	1371.30	24.59

L223	101.90	2.14	3.50
R224	109.67	9.36	5.47
V225	125.89	18.09	1.15

Appendix II

Assignment Report of TRBP2-dsRBD2
(as obtained from CARA in NMR-STAR 3.1 format)

```

data_starch_output
#####
#           Chemical Shift Ambiguity Index Value Definitions           #
#                                                                 #
# The values other than 1 are used for those atoms with different #
# chemical shifts that cannot be assigned to stereospecific atoms #
# or to specific residues or chains.                                #
#                                                                 #
#   Index Value           Definition                                #
#                                                                 #
#     1           Unique (including isolated methyl protons, #
#                 geminal atoms, and geminal methyl #
#                 groups with identical chemical shifts) #
#                 (e.g. ILE HD11, HD12, HD13 protons) #
#     2           Ambiguity of geminal atoms or geminal methyl #
#                 proton groups (e.g. ASP HB2 and HB3 #
#                 protons, LEU CD1 and CD2 carbons, or #
#                 LEU HD11, HD12, HD13 and HD21, HD22, #
#                 HD23 methyl protons) #
#     3           Aromatic atoms on opposite sides of #
#                 symmetrical rings (e.g. TYR HE1 and HE2 #
#                 protons) #
#     4           Intraresidue ambiguities (e.g. LYS HG and #
#                 HD protons or TRP HZ2 and HZ3 protons) #
#     5           Interresidue ambiguities (LYS 12 vs. LYS 27) #
#     6           Intermolecular ambiguities (e.g. ASP 31 CA #
#                 in monomer 1 and ASP 31 CA in monomer 2 #
#                 of an asymmetrical homodimer, duplex #
#                 DNA assignments, or other assignments #
#                 that may apply to atoms in one or more #
#                 molecule in the molecular assembly) #
#     9           Ambiguous, specific ambiguity not defined #
#                                                                 #
#####
loop_
  _Atom_chem_shift.Atom_ID
  _Atom_chem_shift.Comp_index_ID
  _Atom_chem_shift.Comp_ID
  _Atom_chem_shift.Atom_ID
  _Atom_chem_shift.Atom_type
  _Atom_chem_shift.Val
  _Atom_chem_shift.Val_err
  _Atom_chem_shift.Ambiguity_code

C           1           SER           C           C
171.651    0.3
CA          1           SER           CA          C
59.107     0.3           1

```

CB	1	SER	CB	C
66.892	0.3	1		
H	1	SER	H	H
8.050	0.020	1		
HA	1	SER	HA	H
4.658	0.020	1		
HB2	1	SER	HB2	H
4.128	0.020	1		
HB3	1	SER	HB3	H
4.128	0.020	1		
N	1	SER	N	N
116.264	0.3	1		
C	2	ASN	C	C
173.474	0.3	1		
CA	2	ASN	CA	C
53.594	0.3	1		
CB	2	ASN	CB	C
26.344	0.3	1		
H	2	ASN	H	H
8.316	0.020	1		
HA	2	ASN	HA	H
4.660	0.020	1		
HB2	2	ASN	HB2	H
2.282	0.020	1		
HB3	2	ASN	HB3	H
2.282	0.020	2		
N	2	ASN	N	N
122.883	0.3	1		
C	3	ALA	C	C
174.311	0.3	1		
CA	3	ALA	CA	C
60.321	0.3	1		
CB	3	ALA	CB	C
29.395	0.3	1		
H	3	ALA	H	H
8.289	0.020	1		
HA	3	ALA	HA	H
4.188	0.020	1		
HB	3	ALA	HB	H
1.548	0.020	1		
N	3	ALA	N	N
122.526	0.3	1		
C	4	GLN	C	C
172.965	0.3	1		
CA	4	GLN	CA	C
51.009	0.3	1		
CB	4	GLN	CB	C
38.197	0.3	1		
H	4	GLN	H	H
8.212	0.020	1		
HA	4	GLN	HA	H
4.700	0.020	1		
HB2	4	GLN	HB2	H
1.669	0.020	1		

HB3	4	GLN	HB3	H
1.577	0.020	2		
HG2	4	GLN	HG2	H
2.586	0.020	1		
HG3	4	GLN	HG3	H
2.817	0.020	2		
N	4	GLN	N	N
119.927	0.3	1		
C	5	GLN	C	C
173.494	0.3	1		
CA	5	GLN	CA	C
53.100	0.3	1		
CB	5	GLN	CB	C
26.290	0.3	1		
H	5	GLN	H	H
8.214	0.020	1		
HA	5	GLN	HA	H
4.687	0.020	1		
HB2	5	GLN	HB2	H
1.585	0.020	1		
HB3	5	GLN	HB3	H
1.585	0.020	2		
HG2	5	GLN	HG2	H
2.551	0.020	1		
HG3	5	GLN	HG3	H
2.831	0.020	2		
N	5	GLN	N	N
120.433	0.3	1		
C	6	SER	C	C
171.706	0.3	1		
CA	6	SER	CA	C
56.270	0.3	1		
CB	6	SER	CB	C
60.665	0.3	1		
H	6	SER	H	H
8.241	0.020	1		
HA	6	SER	HA	H
4.690	0.020	1		
HB2	6	SER	HB2	H
3.730	0.020	1		
HB3	6	SER	HB3	H
4.196	0.020	2		
N	6	SER	N	N
116.723	0.3	1		
C	7	GLU	C	C
173.718	0.3	1		
CA	7	GLU	CA	C
53.829	0.3	1		
CB	7	GLU	CB	C
27.232	0.3	1		
H	7	GLU	H	H
8.197	0.020	1		
HA	7	GLU	HA	H
4.676	0.020	1		

HB2	7	GLU	HB2	H
1.905	0.020	1		
HB3	7	GLU	HB3	H
1.905	0.020	1		
HG2	7	GLU	HG2	H
2.083	0.020	1		
HG3	7	GLU	HG3	H
2.083	0.020	1		
N	7	GLU	N	N
121.958	0.3	1		
CA	8	CYS	CA	C
50.998	0.3	1		
CB	8	CYS	CB	C
38.589	0.3	1		
H	8	CYS	H	H
8.291	0.020	1		
HA	8	CYS	HA	H
4.550	0.020	1		
HB2	8	CYS	HB2	H
2.578	0.020	1		
HB3	8	CYS	HB3	H
2.578	0.020	1		
N	8	CYS	N	N
120.809	0.3	1		
C	9	ASN	C	C
170.017	0.3	1		
CA	9	ASN	CA	C
47.594	0.3	1		
CB	9	ASN	CB	C
35.659	0.3	1		
H	9	ASN	H	H
8.703	0.020	1		
HA	9	ASN	HA	H
4.679	0.020	1		
HB2	9	ASN	HB2	H
2.704	0.020	2		
HB3	9	ASN	HB3	H
2.991	0.020	2		
N	9	ASN	N	N
120.150	0.3	1		
C	11	VAL	C	C
177.012	0.3	1		
CA	11	VAL	CA	C
63.640	0.3	1		
CB	11	VAL	CB	C
28.907	0.3	1		
H	11	VAL	H	H
7.731	0.020	1		
HA	11	VAL	HA	H
4.516	0.020	1		
HB	11	VAL	HB	H
3.104	0.020	1		
HG1	11	VAL	HG1	H
1.968	0.020	1		

HG2	11	VAL	HG2	H
1.968	0.020	1		
N	11	VAL	N	N
117.949	0.3	1		
C	12	GLY	C	C
173.359	0.3	1		
CA	12	GLY	CA	C
44.424	0.3	1		
H	12	GLY	H	H
7.285	0.020	1		
HA2	12	GLY	HA2	H
3.763	0.020	1		
HA3	12	GLY	HA3	H
3.763	0.020	1		
N	12	GLY	N	N
108.233	0.3	1		
C	13	ALA	C	C
178.136	0.3	1		
CA	13	ALA	CA	C
52.023	0.3	1		
CB	13	ALA	CB	C
15.946	0.3	1		
H	13	ALA	H	H
8.273	0.020	1		
HA	13	ALA	HA	H
4.023	0.020	1		
HB	13	ALA	HB	H
1.339	0.020	1		
N	13	ALA	N	N
124.528	0.3	1		
C	14	LEU	C	C
178.136	0.3	1		
CA	14	LEU	CA	C
51.916	0.3	1		
CB	14	LEU	CB	C
15.823	0.3	1		
H	14	LEU	H	H
8.436	0.020	1		
HA	14	LEU	HA	H
4.016	0.020	1		
HB2	14	LEU	HB2	H
2.000	0.020	1		
HB3	14	LEU	HB3	H
2.000	0.020	1		
N	14	LEU	N	N
119.386	0.3	1		
C	15	GLN	C	C
174.032	0.3	1		
CA	15	GLN	CA	C
57.538	0.3	1		
CB	15	GLN	CB	C
25.246	0.3	1		
H	15	GLN	H	H
7.540	0.020	1		

HA	15	GLN	HA	H
3.634	0.020	1		
HB2	15	GLN	HB2	H
2.154	0.020	1		
HB3	15	GLN	HB3	H
2.154	0.020	1		
HG2	15	GLN	HG2	H
2.397	0.020	1		
HG3	15	GLN	HG3	H
2.397	0.020	1		
N	15	GLN	N	N
118.263	0.3	1		
C	16	GLU	C	C
176.016	0.3	1		
CA	16	GLU	CA	C
56.389	0.3	1		
CB	16	GLU	CB	C
26.832	0.3	1		
H	16	GLU	H	H
7.775	0.020	1		
HA	16	GLU	HA	H
3.866	0.020	1		
HB2	16	GLU	HB2	H
1.967	0.020	1		
HB3	16	GLU	HB3	H
1.967	0.020	1		
N	16	GLU	N	N
115.882	0.3	1		
CA	17	LEU	CA	C
56.442	0.3	1		
H	17	LEU	H	H
7.622	0.020	1		
HA	17	LEU	HA	H
3.946	0.020	1		
HB2	17	LEU	HB2	H
1.726	0.020	1		
HB3	17	LEU	HB3	H
1.726	0.020	1		
N	17	LEU	N	N
120.591	0.3	1		
C	18	VAL	C	C
175.377	0.3	1		
CA	18	VAL	CA	C
63.745	0.3	1		
CB	18	VAL	CB	C
28.297	0.3	1		
H	18	VAL	H	H
8.318	0.020	1		
HA	18	VAL	HA	H
3.397	0.020	1		
HB	18	VAL	HB	H
2.322	0.020	1		
N	18	VAL	N	N
115.936	0.3	1		

C	19	VAL	C	C
177.933	0.3	1		
CA	19	VAL	CA	C
63.494	0.3	1		
CB	19	VAL	CB	C
28.541	0.3	1		
H	19	VAL	H	H
7.863	0.020	1		
HA	19	VAL	HA	H
3.762	0.020	1		
HB	19	VAL	HB	H
2.055	0.020	1		
HG1	19	VAL	HG1	H
0.911	0.020	2		
HG2	19	VAL	HG2	H
0.911	0.020	1		
N	19	VAL	N	N
119.974	0.3	1		
C	20	GLN	C	C
175.579	0.3	1		
CA	20	GLN	CA	C
55.967	0.3	1		
CB	20	GLN	CB	C
25.238	0.3	1		
H	20	GLN	H	H
7.766	0.020	1		
HA	20	GLN	HA	H
3.883	0.020	1		
HB2	20	GLN	HB2	H
2.198	0.020	1		
HB3	20	GLN	HB3	H
2.198	0.020	1		
HG2	20	GLN	HG2	H
2.389	0.020	1		
HG3	20	GLN	HG3	H
2.389	0.020	1		
N	20	GLN	N	N
121.355	0.3	1		
C	22	GLY	C	C
172.249	0.3	1		
CA	22	GLY	CA	C
42.640	0.3	1		
H	22	GLY	H	H
7.670	0.020	1		
HA2	22	GLY	HA2	H
3.988	0.020	1		
HA3	22	GLY	HA3	H
3.988	0.020	2		
N	22	GLY	N	N
106.857	0.3	1		
C	23	TRP	C	C
172.485	0.3	1		
CA	23	TRP	CA	C
50.567	0.3	1		

CB	23	TRP	CB	C
28.907	0.3	1		
H	23	TRP	H	H
7.536	0.020	1		
HA	23	TRP	HA	H
4.968	0.020	1		
HB2	23	TRP	HB2	H
3.277	0.020	1		
HB3	23	TRP	HB3	H
3.223	0.020	2		
HD1	23	TRP	HD1	H
7.195	0.020	1		
HE1	23	TRP	HE1	H
9.950	0.020	1		
HZ2	23	TRP	HZ2	H
6.757	0.020	1		
N	23	TRP	N	N
121.648	0.3	1		
C	24	ARG	C	C
173.124	0.3	1		
CA	24	ARG	CA	C
53.780	0.3	1		
CB	24	ARG	CB	C
27.809	0.3	1		
H	24	ARG	H	H
8.401	0.020	1		
HA	24	ARG	HA	H
4.056	0.020	1		
HB2	24	ARG	HB2	H
1.761	0.020	1		
HB3	24	ARG	HB3	H
1.761	0.020	1		
HE	24	ARG	HE	H
3.174	0.020	1		
N	24	ARG	N	N
119.407	0.3	1		
CA	25	LEU	CA	C
53.728	0.3	1		
CB	25	LEU	CB	C
27.813	0.3	1		
H	25	LEU	H	H
7.786	0.020	1		
HA	25	LEU	HA	H
4.222	0.020	1		
N	25	LEU	N	N
118.119	0.3	1		
C	27	GLU	C	C
172.956	0.3	1		
CA	27	GLU	CA	C
51.604	0.3	1		
CB	27	GLU	CB	C
29.883	0.3	1		
H	27	GLU	H	H
8.353	0.020	1		

HA	27	GLU	HA	H
4.674	0.020	1		
HB2	27	GLU	HB2	H
1.936	0.020	1		
HB3	27	GLU	HB3	H
2.181	0.020	2		
HG2	27	GLU	HG2	H
3.006	0.020	1		
HG3	27	GLU	HG3	H
3.006	0.020	2		
N	27	GLU	N	N
122.417	0.3	1		
CA	28	TYR	CA	C
51.602	0.3	1		
H	28	TYR	H	H
9.065	0.020	1		
HA	28	TYR	HA	H
5.594	0.020	1		
HB2	28	TYR	HB2	H
2.720	0.020	1		
HB3	28	TYR	HB3	H
2.720	0.020	2		
HD1	28	TYR	HD1	H
6.900	0.020	1		
HE1	28	TYR	HE1	H
6.545	0.020	1		
N	28	TYR	N	N
126.987	0.3	1		
C	29	THR	C	C
170.601	0.3	1		
CA	29	THR	CA	C
58.160	0.3	1		
CB	29	THR	CB	C
68.776	0.3	1		
H	29	THR	H	H
8.531	0.020	1		
HA	29	THR	HA	H
4.540	0.020	1		
HB	29	THR	HB	H
3.840	0.020	1		
HG2	29	THR	HG2	H
1.073	0.020	1		
N	29	THR	N	N
117.650	0.3	1		
C	30	VAL	C	C
173.258	0.3	1		
CA	30	VAL	CA	C
60.094	0.3	1		
CB	30	VAL	CB	C
29.319	0.3	1		
H	30	VAL	H	H
8.990	0.020	1		
HA	30	VAL	HA	H
4.595	0.020	1		

HB	30	VAL	HB	H
2.116	0.020	1		
HG1	30	VAL	HG1	H
1.068	0.020	1		
HG2	30	VAL	HG2	H
1.068	0.020	1		
N	30	VAL	N	N
127.369	0.3	1		
C	31	THR	C	C
172.047	0.3	1		
CA	31	THR	CA	C
59.394	0.3	1		
CB	31	THR	CB	C
66.291	0.3	1		
H	31	THR	H	H
8.705	0.020	1		
HA	31	THR	HA	H
4.349	0.020	1		
HB	31	THR	HB	H
4.074	0.020	1		
HG1	31	THR	HG1	H
1.087	0.020	1		
N	31	THR	N	N
121.646	0.3	1		
C	32	GLN	C	C
170.904	0.3	1		
CA	32	GLN	CA	C
53.471	0.3	1		
CB	32	GLN	CB	C
28.907	0.3	1		
H	32	GLN	H	H
7.885	0.020	1		
HA	32	GLN	HA	H
4.685	0.020	1		
HB2	32	GLN	HB2	H
1.935	0.020	1		
HB3	32	GLN	HB3	H
1.935	0.020	1		
HG2	32	GLN	HG2	H
2.201	0.020	1		
HG3	32	GLN	HG3	H
2.201	0.020	1		
HE21	32	GLN	HE21	H
7.261	0.020	1		
HE22	32	GLN	HE22	H
6.888	0.020	1		
N	32	GLN	N	N
121.190	0.3	1		
C	33	GLU	C	C
172.417	0.3	1		
CA	33	GLU	CA	C
52.370	0.3	1		
CB	33	GLU	CB	C
28.769	0.3	1		

H	33	GLU	H	H
8.316	0.020	1		
HA	33	GLU	HA	H
4.685	0.020	1		
HB2	33	GLU	HB2	H
1.781	0.020	1		
N	33	GLU	N	N
124.085	0.3	1		
C	34	SER	C	C
170.904	0.3	1		
CA	34	SER	CA	C
54.725	0.3	1		
CB	34	SER	CB	C
62.221	0.3	1		
H	34	SER	H	H
8.197	0.020	1		
HA	34	SER	HA	H
4.687	0.020	1		
HB2	34	SER	HB2	H
3.635	0.020	1		
HB3	34	SER	HB3	H
3.635	0.020	1		
HG	34	SER	HG	H
2.603	0.020	1		
N	34	SER	N	N
118.212	0.3	1		
C	35	GLY	C	C
169.424	0.3	1		
CA	35	GLY	CA	C
41.480	0.3	1		
H	35	GLY	H	H
8.147	0.020	1		
HA2	35	GLY	HA2	H
3.837	0.020	2		
HA3	35	GLY	HA3	H
4.692	0.020	2		
N	35	GLY	N	N
109.048	0.3	1		
H	37	ALA	H	H
8.246	0.020	1		
HA	37	ALA	HA	H
4.254	0.020	1		
HB	37	ALA	HB	H
1.673	0.020	1		
N	37	ALA	N	N
120.862	0.3	1		
C	39	ARG	C	C
171.442	0.3	1		
CA	39	ARG	CA	C
52.850	0.3	1		
CB	39	ARG	CB	C
27.564	0.3	1		
H	39	ARG	H	H
7.719	0.020	1		

HA	39	ARG	HA	H
4.660	0.020	1		
HB2	39	ARG	HB2	H
1.568	0.020	1		
HB3	39	ARG	HB3	H
1.568	0.020	1		
HG2	39	ARG	HG2	H
1.353	0.020	1		
HG3	39	ARG	HG3	H
1.353	0.020	1		
HD2	39	ARG	HD2	H
2.093	0.020	1		
HD3	39	ARG	HD3	H
2.093	0.020	1		
HE	39	ARG	HE	H
3.053	0.020	1		
N	39	ARG	N	N
123.947	0.3	1		
C	41	GLU	C	C
172.384	0.3	1		
CA	41	GLU	CA	C
52.842	0.3	1		
CB	41	GLU	CB	C
29.395	0.3	1		
H	41	GLU	H	H
8.128	0.020	1		
HA	41	GLU	HA	H
4.367	0.020	1		
HB2	41	GLU	HB2	H
1.943	0.020	1		
HB3	41	GLU	HB3	H
1.943	0.020	1		
HG2	41	GLU	HG2	H
1.642	0.020	1		
HG3	41	GLU	HG3	H
1.642	0.020	1		
N	41	GLU	N	N
119.493	0.3	1		
C	42	PHE	C	C
172.384	0.3	1		
CA	42	PHE	CA	C
52.842	0.3	1		
CB	42	PHE	CB	C
29.395	0.3	1		
H	42	PHE	H	H
8.775	0.020	1		
HA	42	PHE	HA	H
4.880	0.020	1		
HB2	42	PHE	HB2	H
2.553	0.020	1		
HB3	42	PHE	HB3	H
2.553	0.020	1		
HD1	42	PHE	HD1	H
6.881	0.020	1		

HE1	42	PHE	HE1	H
7.236	0.020	1		
N	42	PHE	N	N
121.600	0.3	1		
C	43	THR	C	C
170.803	0.3	1		
CA	43	THR	CA	C
58.772	0.3	1		
CB	43	THR	CB	C
67.826	0.3	1		
H	43	THR	H	H
8.717	0.020	1		
HA	43	THR	HA	H
5.105	0.020	1		
HB	43	THR	HB	H
3.836	0.020	1		
HG2	43	THR	HG2	H
1.068	0.020	1		
N	43	THR	N	N
116.346	0.3	1		
CA	44	MET	CA	C
58.782	0.3	1		
H	44	MET	H	H
9.360	0.020	1		
HA	44	MET	HA	H
5.392	0.020	1		
HB2	44	MET	HB2	H
1.896	0.020	1		
HB3	44	MET	HB3	H
1.896	0.020	2		
HG2	44	MET	HG2	H
2.327	0.020	1		
HG3	44	MET	HG3	H
2.327	0.020	1		
N	44	MET	N	N
125.128	0.3	1		
C	45	THR	C	C
170.904	0.3	1		
CA	45	THR	CA	C
58.162	0.3	1		
CB	45	THR	CB	C
67.634	0.3	1		
H	45	THR	H	H
9.190	0.020	1		
HA	45	THR	HA	H
4.937	0.020	1		
HB	45	THR	HB	H
3.910	0.020	1		
HG1	45	THR	HG1	H
1.032	0.020	1		
N	45	THR	N	N
116.395	0.3	1		
C	46	CYS	C	C
169.350	0.3	1		

CA	46	CYS	CA	C
54.079	0.3	1		
CB	46	CYS	CB	C
26.896	0.3	1		
H	46	CYS	H	H
9.124	0.020	1		
HA	46	CYS	HA	H
4.566	0.020	1		
HB2	46	CYS	HB2	H
2.260	0.020	1		
HB3	46	CYS	HB3	H
2.260	0.020	1		
N	46	CYS	N	N
124.254	0.3	1		
C	47	ARG	C	C
173.314	0.3	1		
CA	47	ARG	CA	C
51.588	0.3	1		
CB	47	ARG	CB	C
30.648	0.3	1		
H	47	ARG	H	H
8.671	0.020	1		
HA	47	ARG	HA	H
5.201	0.020	1		
HB2	47	ARG	HB2	H
1.416	0.020	1		
HB3	47	ARG	HB3	H
1.416	0.020	1		
HG2	47	ARG	HG2	H
1.232	0.020	1		
HG3	47	ARG	HG3	H
1.232	0.020	1		
HD2	47	ARG	HD2	H
1.658	0.020	1		
HD3	47	ARG	HD3	H
1.658	0.020	1		
N	47	ARG	N	N
128.627	0.3	1		
C	48	VAL	C	C
170.805	0.3	1		
CA	48	VAL	CA	C
58.397	0.3	1		
CB	48	VAL	CB	C
32.934	0.3	1		
H	48	VAL	H	H
8.096	0.020	1		
HA	48	VAL	HA	H
4.080	0.020	1		
HB	48	VAL	HB	H
2.224	0.020	1		
HG1	48	VAL	HG1	H
0.975	0.020	1		
HG2	48	VAL	HG2	H
0.975	0.020	1		

N	48	VAL	N	N
126.933	0.3	1		
C	49	GLU	C	C
173.140	0.3	1		
CA	49	GLU	CA	C
55.357	0.3	1		
CB	49	GLU	CB	C
23.782	0.3	1		
H	49	GLU	H	H
8.859	0.020	1		
HA	49	GLU	HA	H
3.259	0.020	1		
HB2	49	GLU	HB2	H
1.237	0.020	1		
HB3	49	GLU	HB3	H
1.237	0.020	1		
HG2	49	GLU	HG2	H
1.493	0.020	1		
HG3	49	GLU	HG3	H
1.493	0.020	1		
N	49	GLU	N	N
123.705	0.3	1		
C	50	ARG	C	C
173.133	0.3	1		
CA	50	ARG	CA	C
53.146	0.3	1		
CB	50	ARG	CB	C
26.588	0.3	1		
H	50	ARG	H	H
7.312	0.020	1		
HA	50	ARG	HA	H
4.135	0.020	1		
HB2	50	ARG	HB2	H
1.300	0.020	1		
HG2	50	ARG	HG2	H
1.011	0.020	1		
N	50	ARG	N	N
120.474	0.3	1		
C	51	PHE	C	C
173.133	0.3	1		
CA	51	PHE	CA	C
53.146	0.3	1		
H	51	PHE	H	H
8.628	0.020	1		
HA	51	PHE	HA	H
4.660	0.020	1		
HB2	51	PHE	HB2	H
2.811	0.020	1		
HB3	51	PHE	HB3	H
3.153	0.020	2		
HD1	51	PHE	HD1	H
7.068	0.020	1		
N	51	PHE	N	N
122.221	0.3	1		

CA	52	ILE	CA	C
53.634	0.3	1		
H	52	ILE	H	H
8.452	0.020	1		
HA	52	ILE	HA	H
4.943	0.020	1		
HB	52	ILE	HB	H
0.701	0.020	1		
HG12	52	ILE	HG12	H
1.545	0.020	1		
HG13	52	ILE	HG13	H
1.545	0.020	1		
N	52	ILE	N	N
121.877	0.3	1		
C	53	GLU	C	C
171.777	0.3	1		
CA	53	GLU	CA	C
51.238	0.3	1		
CB	53	GLU	CB	C
32.080	0.3	1		
H	53	GLU	H	H
8.561	0.020	1		
HA	53	GLU	HA	H
4.697	0.020	1		
HB2	53	GLU	HB2	H
1.365	0.020	1		
HB3	53	GLU	HB3	H
1.365	0.020	1		
HG2	53	GLU	HG2	H
2.132	0.020	1		
HG3	53	GLU	HG3	H
2.132	0.020	1		
N	53	GLU	N	N
124.418	0.3	1		
CB	54	ILE	CB	C
32.080	0.3	1		
H	54	ILE	H	H
8.845	0.020	1		
HA	54	ILE	HA	H
4.898	0.020	1		
HB	54	ILE	HB	H
0.738	0.020	1		
HG2	54	ILE	HG2	H
1.545	0.020	1		
HD1	54	ILE	HD1	H
0.940	0.020	1		
N	54	ILE	N	N
120.479	0.3	1		
C	55	GLY	C	C
169.020	0.3	1		
CA	55	GLY	CA	C
40.943	0.3	1		
H	55	GLY	H	H
9.177	0.020	1		

HA2	55	GLY	HA2	H
3.672	0.020	1		
HA3	55	GLY	HA3	H
4.678	0.020	2		
N	55	GLY	N	N
112.301	0.3	1		
C	56	SER	C	C
171.341	0.3	1		
CA	56	SER	CA	C
53.780	0.3	1		
CB	56	SER	CB	C
63.810	0.3	1		
H	56	SER	H	H
8.625	0.020	1		
HA	56	SER	HA	H
5.910	0.020	1		
HG	56	SER	HG	H
3.727	0.020	1		
N	56	SER	N	N
114.811	0.3	1		
C	57	GLY	C	C
169.928	0.3	1		
CA	57	GLY	CA	C
42.860	0.3	1		
H	57	GLY	H	H
8.552	0.020	1		
HA2	57	GLY	HA2	H
3.948	0.020	1		
HA3	57	GLY	HA3	H
4.440	0.020	2		
N	57	GLY	N	N
106.946	0.3	1		
C	58	THR	C	C
170.467	0.3	1		
CA	58	THR	CA	C
59.902	0.3	1		
CB	58	THR	CB	C
66.004	0.3	1		
H	58	THR	H	H
8.273	0.020	1		
HA	58	THR	HA	H
4.638	0.020	1		
N	58	THR	N	N
109.376	0.3	1		
CA	59	SER	CA	C
39.410	0.3	1		
CB	59	SER	CB	C
22.842	0.3	1		
H	59	SER	H	H
7.322	0.020	1		
HA	59	SER	HA	H
4.699	0.020	1		
HB2	59	SER	HB2	H
2.920	0.020	1		

HB3	59	SER	HB3	H
2.920	0.020	1		
N	59	SER	N	N
112.329	0.3	1		
C	60	LYS	C	C
172.956	0.3	1		
CB	60	LYS	CB	C
28.348	0.3	1		
H	60	LYS	H	H
8.408	0.020	1		
HA	60	LYS	HA	H
4.695	0.020	1		
HB2	60	LYS	HB2	H
1.948	0.020	1		
HB3	60	LYS	HB3	H
1.948	0.020	1		
N	60	LYS	N	N
123.979	0.3	1		
C	62	LEU	C	C
172.014	0.3	1		
CA	62	LEU	CA	C
52.846	0.3	1		
CB	62	LEU	CB	C
29.395	0.3	1		
H	62	LEU	H	H
7.693	0.020	1		
HA	62	LEU	HA	H
4.331	0.020	1		
HB2	62	LEU	HB2	H
1.985	0.020	1		
HB3	62	LEU	HB3	H
1.985	0.020	1		
HG	62	LEU	HG	H
1.728	0.020	1		
N	62	LEU	N	N
119.625	0.3	1		
C	63	ALA	C	C
175.882	0.3	1		
CA	63	ALA	CA	C
52.846	0.3	1		
CB	63	ALA	CB	C
15.348	0.3	1		
H	63	ALA	H	H
8.034	0.020	1		
HA	63	ALA	HA	H
3.636	0.020	1		
HB	63	ALA	HB	H
1.233	0.020	1		
N	63	ALA	N	N
122.781	0.3	1		
C	65	ARG	C	C
175.007	0.3	1		
CA	65	ARG	CA	C
57.215	0.3	1		

CB	65	ARG	CB	C
27.516	0.3	1		
H	65	ARG	H	H
7.639	0.020	1		
HA	65	ARG	HA	H
3.708	0.020	1		
HB2	65	ARG	HB2	H
1.874	0.020	1		
HB3	65	ARG	HB3	H
1.874	0.020	1		
N	65	ARG	N	N
117.798	0.3	1		
C	66	ASN	C	C
175.007	0.3	1		
CA	66	ASN	CA	C
53.435	0.3	1		
CB	66	ASN	CB	C
35.946	0.3	1		
H	66	ASN	H	H
8.132	0.020	1		
HA	66	ASN	HA	H
4.532	0.020	1		
HB2	66	ASN	HB2	H
2.880	0.020	1		
HB3	66	ASN	HB3	H
2.880	0.020	1		
HD21	66	ASN	HD21	H
7.094	0.020	1		
N	66	ASN	N	N
117.005	0.3	1		
C	67	ALA	C	C
176.184	0.3	1		
CA	67	ALA	CA	C
52.533	0.3	1		
CB	67	ALA	CB	C
15.362	0.3	1		
H	67	ALA	H	H
8.345	0.020	1		
HA	67	ALA	HA	H
4.660	0.020	1		
HB	67	ALA	HB	H
1.435	0.020	1		
N	67	ALA	N	N
123.376	0.3	1		
C	68	ALA	C	C
176.891	0.3	1		
CA	68	ALA	CA	C
52.223	0.3	1		
CB	68	ALA	CB	C
15.664	0.3	1		
H	68	ALA	H	H
8.568	0.020	1		
HA	68	ALA	HA	H
4.058	0.020	1		

HB	68	ALA	HB	H
1.527	0.020	1		
N	68	ALA	N	N
119.272	0.3	1		
C	69	ALA	C	C
178.438	0.3	1		
CA	69	ALA	CA	C
52.524	0.3	1		
CB	69	ALA	CB	C
15.365	0.3	1		
H	69	ALA	H	H
8.514	0.020	1		
HA	69	ALA	HA	H
3.966	0.020	1		
HB	69	ALA	HB	H
1.527	0.020	1		
N	69	ALA	N	N
119.440	0.3	1		
C	71	MET	C	C
175.310	0.3	1		
CA	71	MET	CA	C
51.659	0.3	1		
CB	71	MET	CB	C
15.670	0.3	1		
H	71	MET	H	H
8.387	0.020	1		
HA	71	MET	HA	H
4.660	0.020	1		
HB2	71	MET	HB2	H
1.292	0.020	1		
HB3	71	MET	HB3	H
1.292	0.020	1		
N	71	MET	N	N
120.698	0.3	1		
CB	72	LEU	CB	C
29.395	0.3	1		
H	72	LEU	H	H
8.751	0.020	1		
HA	72	LEU	HA	H
3.709	0.020	1		
N	72	LEU	N	N
121.565	0.3	1		
H	73	LEU	H	H
6.998	0.020	1		
HA	73	LEU	HA	H
4.001	0.020	1		
HB2	73	LEU	HB2	H
1.703	0.020	1		
HB3	73	LEU	HB3	H
1.703	0.020	1		
HG	73	LEU	HG	H
1.543	0.020	1		
N	73	LEU	N	N
116.181	0.3	1		

C	74	ARG	C	C
176.004	0.3	1		
CA	74	ARG	CA	C
54.952	0.3	1		
CB	74	ARG	CB	C
26.605	0.3	1		
H	74	ARG	H	H
7.504	0.020	1		
HA	74	ARG	HA	H
3.865	0.020	1		
HB2	74	ARG	HB2	H
1.864	0.020	1		
HB3	74	ARG	HB3	H
1.864	0.020	1		
N	74	ARG	N	N
119.653	0.3	1		
C	75	VAL	C	C
174.368	0.3	1		
CA	75	VAL	CA	C
61.297	0.3	1		
CB	75	VAL	CB	C
28.785	0.3	1		
H	75	VAL	H	H
8.172	0.020	1		
HA	75	VAL	HA	H
3.764	0.020	1		
HB	75	VAL	HB	H
2.058	0.020	1		
HG1	75	VAL	HG1	H
0.830	0.020	1		
HG2	75	VAL	HG2	H
0.830	0.020	1		
N	75	VAL	N	N
113.698	0.3	1		
C	77	THR	C	C
171.543	0.3	1		
CA	77	THR	CA	C
59.712	0.3	1		
CB	77	THR	CB	C
67.226	0.3	1		
H	77	THR	H	H
7.614	0.020	1		
HA	77	THR	HA	H
4.667	0.020	1		
HB	77	THR	HB	H
4.219	0.020	1		
HG2	77	THR	HG2	H
1.160	0.020	1		
N	77	THR	N	N
112.134	0.3	1		
C	78	VAL	C	C
175.982	0.3	1		
CA	78	VAL	CA	C
57.525	0.3	1		

CB	78	VAL	CB	C
29.720	0.3	1		
H	78	VAL	H	H
7.783	0.020	1		
HA	78	VAL	HA	H
4.312	0.020	1		
HB	78	VAL	HB	H
2.079	0.020	1		
HG1	78	VAL	HG1	H
0.976	0.020	1		
HG2	78	VAL	HG2	H
0.976	0.020	1		
N	78	VAL	N	N
124.088	0.3	1		
C	80	LEU	C	C
178.080	0.3	1		
CA	80	LEU	CA	C
52.947	0.3	1		
CB	80	LEU	CB	C
39.401	0.3	1		
H	80	LEU	H	H
7.851	0.020	1		
HA	80	LEU	HA	H
4.267	0.020	1		
HB2	80	LEU	HB2	H
2.538	0.020	1		
HB3	80	LEU	HB3	H
2.538	0.020	1		
N	80	LEU	N	N
126.412	0.3	1		
H	81	ASP	H	H
7.999	0.020	1		
HA	81	ASP	HA	H
4.643	0.020	1		
HB2	81	ASP	HB2	H
2.895	0.020	1		
HB3	81	ASP	HB3	H
2.895	0.020	1		
N	81	ASP	N	N
120.618	0.3	1		
C	82	ALA	C	C
174.606	0.3	1		
CA	82	ALA	CA	C
49.694	0.3	1		
CB	82	ALA	CB	C
16.460	0.3	1		
H	82	ALA	H	H
7.960	0.020	1		
HA	82	ALA	HA	H
4.193	0.020	1		
HB	82	ALA	HB	H
1.255	0.020	1		
N	82	ALA	N	N
124.204	0.3	1		

H	83	ARG	H	H
7.639	0.020	1		
HA	83	ARG	HA	H
3.965	0.020	1		
HB2	83	ARG	HB2	H
1.603	0.020	1		
HB3	83	ARG	HB3	H
1.603	0.020	1		
HE	83	ARG	HE	H
2.572	0.020	1		
N	83	ARG	N	N
119.956	0.3	1		
CB	84	ASP	CB	C
39.157	0.3	1		
H	84	ASP	H	H
7.807	0.020	1		
HA	84	ASP	HA	H
4.241	0.020	1		
HB2	84	ASP	HB2	H
2.517	0.020	1		
HB3	84	ASP	HB3	H
2.517	0.020	1		
N	84	ASP	N	N
126.487	0.3	1		

stop_
